



**NATIONAL TECHNICAL UNIVERSITY OF ATHENS**  
FACULTY OF NAVAL ARCHITECTURE AND MARINE ENGINEERING

**INTER-DEPARTMENTAL POSTGRADUATE PROGRAM**  
**«MARINE TECHNOLOGY AND SCIENCE»**

**ULTIMATE HULL GIRDER STRENGTH ASSESSMENT USING**  
**SEMI-ANALYTICAL AND COMPUTATIONAL METHODS**

Dissertation

**Eftyhia Dalma**

**Athens – June 2009**

## LIST OF CONTENTS

<b>CONTENTS</b>	<b>1</b>
LIST OF CONTENTS	1
LIST OF FIGURES	5
LIST OF TABLES	11
<b>SUMMARY</b>	<b>13</b>
<b>CHAPTER 1</b>	<b>14</b>
<b>INTRODUCTION</b>	<b>14</b>
1.1. General	14
1.2. Previous work in this area	16
1.3. Structure of Dissertation Thesis	17
<b>CHAPTER 2</b>	<b>19</b>
<b>HULL GIRDER ULTIMATE STRENGTH</b>	<b>19</b>
2.1. General	19
2.2. Hull Loading and Structural Response	19
2.3. Modes of Structural Failure	21
2.4. Hull girder structural analysis	22
2.4.1. Limit State Design Approaches	23
2.5. Ultimate Limit State Approach (ULS)	23
2.5.1. Ultimate Limit strength of Plates and Stiffened Plates	24
2.5.1.1. Failure modes of plates and stiffened plates	25
2.5.1.2. Factors affecting the behaviour of plates and stiffened plates	28
2.5.1.3. Elastic Buckling Strength	31
2.5.1.4. Plasticity Correction to Euler Buckling Strength	32
2.5.1.5. Ultimate Strength of Un-Stiffened Plates	33
2.5.1.6. Ultimate Lateral-Torsional Strength of Stiffened Plates	35
2.5.1.7. Ultimate Web Local Buckling Strength of Stiffened Plates	35
<b>CHAPTER 3</b>	<b>36</b>
<b>CSR HULL GIRDER STRENGTH ASSESSMENT</b>	<b>36</b>
3.1. General	36
3.2. Partial Safety Factor Method	36
3.3. Hull Girder Assessment	37
3.4. Hull Girder Ultimate Bending Capacity	39
3.4.1. General	39
3.4.2. Assumptions of CSR Hull Girder Ultimate Bending Capacity Methods	40

3.4.3. Single Step Ultimate Capacity Method	41
3.4.4. Simplified Method Based on an Incremental-iterative Approach	41
3.4.4.1. Assumptions of Incremental-Iterative Approach	41
3.4.4.2. Procedure of Incremental-Iterative Approach	42
3.4.4.3. Load End Shortening Curves for Incremental-Iterative Approach	46
3.4.5. Alternatives methods	51
3.4.5.1. Incremental-iterative procedure	51
3.4.5.2. Non-linear finite element analysis	52
3.5. Net Thickness Approach	52

---

## **CHAPTER 4** **54**

### **FINITE ELEMENT ANALYSIS** **54**

4.1. General	54
4.2. Finite Element Analysis Procedure	54
4.3. The Finite Element Code ABAQUS	56
4.4. Finite Elements issues in the ABAQUS code	56
4.4.1. Finite Elements in general	56
4.4.2 Shell Elements	58
4.5. Linear Buckling Analysis in ABAQUS	59
4.6. Non Linear FE Analysis in ABAQUS	60
4.6.1. Static Non Linear Analysis	61
4.6.2. Riks Non Linear Analysis	63

---

## **CHAPTER 5** **65**

### **DETAILS OF THE VESSEL USED IN THIS STUDY** **65**

5.1. General	65
5.2. Vessel's particulars	65
5.3. Midship Section	66
5.3.1. Bottom Plating Panels	69
5.3.2. Side Shell Panels	70
5.3.3. Inner Bulkhead Panels	71
5.3.4. CL Bulkhead Plating	73
5.3.5. Main Deck Plating	74
5.3.6. Inner Bottom Plating Panels	75
5.3.7. Remaining panels	76
5.4. Design bending moments	77

---

## **CHAPTER 6** **79**

### **APPLICATION OF THE CSR INCREMENTAL-ITERATIVE APPROACH** **79**

6.1. General	79
6.2. Steps of Incremental – Iterative Approach	79
6.2.1. Step 1 - Division of the Section into Structural Elements	80
6.2.2. Step 2 - Calculation of the Load-end Shortening Curves	81

6.2.3. Step 3 - Estimation of the curvature step size and initial position of the neutral axis	89
6.2.4. Steps 4 to 5 - Calculation of the neutral axis at each step	93
6.2.5. Step 6 - Calculation of the bending moment at each step	94
6.2.6. Step 7 - Construction of the M-k Curve and the Ultimate Bending Capacity estimate	94
6.3. Predominant Buckling modes obtained by CSR Approach	94
6.4. Load End Shortening Curves of the Structural Elements	97
6.5. Position of neutral axis versus imposed curvature	102
6.6. Hull girder ultimate bending capacity	102

---

## **CHAPTER 7** **107**

### **FINITE ELEMENT APPROACH** **107**

7.1. General	107
7.2. Procedure of Finite Element Approach	107
7.3. Preprocessing of the Finite Element Models	108
7.3.1. Finite Element Structural Modeling	108
7.3.2. Type and Size of Finite Element	113
7.3.3. Boundary Conditions	115
7.3.3.1. Boundary Conditions along the unloaded edge of the panels	116
7.3.3.2. Boundary Conditions along the panels' loaded edge	118
7.3.3.3. Boundary Conditions of panels that require special consideration	120
7.3.4. Initial Imperfections	122
7.3.5. Loading conditions	128
7.3.6. Materials properties	129
7.3.7. Net Thickness Approach	130
7.4. Simulation	130
7.5. Postprocessing	131
7.5.1. Stress-Strain Curves Calculation	131
7.5.2. Stress-strain curves of Structural Elements	133
7.5.3. Ultimate Limit State Collapse of Panels under compression	135
7.5.3.1. Ultimate Limit State of Main Deck Panel M1	136
7.5.3.2. Ultimate Limit State of Main Deck Panel M2	139
7.5.3.3. CL Bulkhead Panel CL2	143
7.5.3.4. Ultimate Limit State of Side Shell Panel S5	147
7.5.3.5. Inner Bulkhead Panel I2 and Side Shell Panel S3	149
7.5.3.6. Ultimate Limit State of remaining compressed Panels	151
7.5.4. Deformed shape of Panels under Tension	160
7.5.5. Panels in the region of the neutral axis	165
7.5.6. Position of the neutral axis	167
7.5.7. Ultimate Hull Girder Limit State	168

---

## **CHAPTER 8** **170**

### **COMPARISON OF THE APPROACHES** **170**

8.1. General	170
8.2. Load End Shortening Curves of structural elements	170



---

8.2.1. Longitudinal Stiffeners under uniaxial compression	171
8.2.2. Longitudinal Stiffeners/Hard Corners under uniaxial tension	179
8.2.3. Hard Corners under uniaxial compression	181
8.3. Position of Neutral Axis	181
8.4. Vertical Bending Moment versus Imposed Curvature	182
8.5. The Tanker Ultimate Hull Girder Capacity as per the CSR and other methods reported in the literature	188
<b>CHAPTER 9</b>	<b>189</b>
<b>DISCUSSION</b>	<b>189</b>
<b>CHAPTER 10</b>	<b>192</b>
<b>CONCLUDING REMARKS</b>	<b>192</b>
<b>REFERENCES</b>	<b>194</b>
<b>APPENDIX A</b>	<b>196</b>

## LIST OF FIGURES

<b>CHAPTER 2</b>	<b>19</b>
<b>HULL GIRDER ULTIMATE STRENGTH</b>	<b>19</b>
Fig.2.1. (a) Uneven distribution of vessel's loading, (b) Sagging and Hogging condition.	20
Fig.2.2. Structural design based on Ultimate Strength	22
Fig.2.3. Hull Girder comprising of plates and stiffened plates	25
Fig.2.4. Overall collapse of plating and stiffener as a unit : (a) Cross-stiffened panel, (b) Uniaxial stiffened panel	25
Fig.2.5. Biaxial compressive collapse	26
Fig.2.6. Beam Column Type Collapse	26
Fig.2.7. Web Local Buckling	27
Fig.2.8. Tripping or Torsional Buckling	27
Fig.2.9. Definition of plates' geometric properties	28
Fig.2.10. Load end shortening curves of stiffened plates for a range of $\lambda$ and $\beta$ combinations	29
Fig.2.11. Typical initial deflection patterns in steel plating between stiffeners	30
Fig.2.12. Typical initial deflection pattern in steel plating between stiffeners	31
Fig.2.13. Euler Elastic Buckling Stress	31
Fig.2.14. Effect of Johnson-Osterfeld plasticity correction	33
Fig.2.15. Actual Stress Distribution in a Compressed Stiffened Plate	34
<b>CHAPTER 3</b>	<b>36</b>
<b>CSR HULL GIRDER STRENGTH ASSESSMENT</b>	<b>36</b>
Fig.3.1. Partial Safety Factors for Hull Girder Assessment	38
Fig.3.2. Bending Moment-curvature relationship (M-k)	40
Fig.3.3. Interframe buckling failure of a tanker under sagging condition	40
Fig.3.4. Elements considered to form the hull girder cross section	42
Fig.3.5. Flowchart of the Incremental-Iterative Approach	45
Fig.3.6.(a) Elastic perfectly plastic failure of all elements under tension and of hard corners both tensioned or compressed, (b) Elasto-plastic failure of stiffeners	47
Fig.3.7. Net Thickness Approach	52
Fig.3.8. Corrosion addition considered for double hull oil tankers	53
<b>CHAPTER 4</b>	<b>54</b>
<b>FINITE ELEMENT ANALYSIS</b>	<b>54</b>
Fig.4.1. Illustration of the Finite Element Analysis Procedure	55

Fig.4.2. Abaqus/Standard Analysis Stages	56
Fig.4.3. Abaqus elements	58
Fig.4.4. Integration of shell elements	58
Fig.4.5. Linear and Non-Linear Analysis	60
Fig.4.6. Linear and Non-Linear Analysis	61
Fig.4.7. Linear and Non-Linear Analysis	62
Fig.4.8. Non Linear analysis - Newton-Raphson method	62
Fig.4.9. Non Linear analysis – Procedure for iterations	63
Fig.4.10. Non Linear analysis – Riks Method	64

---

## **CHAPTER 5** **65**

### **DETAILS OF THE VESSEL USED IN THIS STUDY** **65**

Fig.5.1. Vessel's profile view and tank top view	67
Fig.5.2. Nomenclature of considered midship section panels	68
Fig.5.3. Nomenclature of Stiffeners' dimensions	69
Fig.5.4. Bottom Plating Panels	70
Fig.5.5. Side Shell Panels	71
Fig.5.6. Inner Bulkhead Panels	72
Fig.5.7. CL Bulkhead Panels	73
Fig.5.8. Main Deck Plating Panels	75
Fig.5.9. Inner Bottom Plating Panels	75
Fig.5.10. Remaining panels. (a) Hopper and Bilge Panel, (b) Stringers	76

---

## **CHAPTER 6** **79**

### **APPLICATION OF THE CSR INCREMENTAL-ITERATIVE APPROACH** **79**

Fig.6.1. Midship section area of the tanker between the web frames	80
Fig.6.2. Division of the Double Hull Tanker into structural elements	81
Fig.6.3. Corrosion addition accounted for the determination of the net scantlings	82
Fig.6.4. Side Shell Structural Element 34 (290x10/100x16) – Beam Column Buckling	87
Fig.6.5. Side Shell Structural Element 37 (200x90x8/14) - Beam Column Buckling	88
Fig.6.6. Inner Shell Structural Element 29 (370x10/125x16) - Torsional Buckling	88
Fig.6.7. Calculation of the Midship Section Modulus	90
Fig.6.8. Feature "Goal seek" of software Excel	93
Fig.6.9. Load end shortening curves of Main Deck longitudinal stiffeners (L 250x90x9/15) under compression	98
Fig.6.10. Load end shortening curves of Inner Shell Longitudinal Stiffener 33 (T 320x10/100x16) under compression	99
Fig.6.11. Load end shortening curves of CL Bulkhead Longitudinal Stiffener 37 (L 250x90x9/14) under compression	99

Fig.6.12. Load end shortening curves of CL Bulkhead Longitudinal Stiffener 36 (L 300x90x10/16) under compression	100
Fig.6.13. Load end shortening curves of Inner Bottom Longitudinal Stiffener 13 (T 400x10/125x22) under tension	100
Fig.6.14. Load end shortening curves of Hard Corner Main Deck - CL Bulkhead under compression	101
Fig.6.15. Load end shortening curves of Hard Corner Inner Bottom - CL Bulkhead under tension	101
Fig.6.16. Position of neutral axis at each imposed curvature	102
Fig.6.17. CSR Hull Girder Vertical Bending Moment - Imposed Curvature Curve	103
Fig.6.18. Hull Girder Vertical Bending Moment - Imposed Curvature Curve as per all alternative approaches	105
Fig.6.19. Applied Strain versus distance from Base Line and imposed curvature	106

---

**CHAPTER 7** **107**

**FINITE ELEMENT APPROACH** **107**

Fig.7.1. Stiffened and/or Unstiffened panels required by the CSR Rules for the modelling of the longitudinally effective hull girder structure and the buckling strength assessment	109
Fig.7.2. Extent of panels considered by Finite Element Approach	110
Fig.7.3. Buckling Mode of I3 Symmetric Panel: (a) one-bay, (b) two-bays	111
Fig.7.4. Normalised $U_y$ displacement of the symmetric I3 Panel along a transverse edge	111
Fig.7.5. Normalised $U_y$ displacement of the symmetric I3 Panel along a longitudinal edge	112
Fig.7.6. Load end shortening curves of I3 symmetric panel	112
Fig.7.7. Panel M-1: (a) 50mm element mesh, (b) Path used for plotting of $U_z$	114
Fig.7.8. Panel M-1: Plot of $U_z$ displacement along the path shown in Fig.7.7 (b).	114
Fig.7.9. Boundary Conditions in way of unloaded edges	116
Fig.7.10. Panel for Illustration of simply support conditions	117
Fig.7.11. Boundary Conditions of hull girder section horizontal panels	119
Fig.7.12. Boundary Conditions of hull girder section perpendicular panels	120
Fig.7.13. Boundary conditions of the hopper plating panel	121
Fig.7.14. Buckling Mode of Panel M1. Normalised $U_z$ displacement along (a) its length (mid breadth), (b) its breadth (mid span)	125
Fig.7.15. Panel M1: Plot of plate normalized $U_z$ displacement along the plate's length (at mid-breadth)	125
Fig.7.16. Panel M1: Plot of plate normalized $U_z$ displacement along the plate's breadth (at mid span)	126
Fig.7.17. Panel M1: Plot of stiffener's web normalized $U_y$ displacement along its length (at mid web height)	126
Fig.7.18. Panel M1: Plot of stiffener's flange normalized $U_z$ displacement along its length (at mid flange breadth)	127
Fig.7.19. Elastic-perfectly plastic material behavior	129

Fig.7.20. Stress components used to compute the axial stress intensity in the case of a shell element with 7 through thickness integration (section) points	132
Fig.7.21. Hard Corner between Stringer 36 and Inner Bulkhead	133
Fig.7.22. Axial compressive stress versus strain relationship of Panel M-1 obtained by FEA	137
Fig.7.23. Deformed shape of Panel M-1 at its Ultimate Limit State– Magnitude of Displacement	137
Fig.7.24. Deformed shape of Panel M-1 at its Ultimate Limit State, (a) $U_y$ Displacement, (b) $U_z$ Displacement	138
Fig.7.25. Von Mises Stress of Panel M-1 at (a) $0.571 \epsilon_{M1ur}$ , (b) $0.679 \epsilon_{M1ur}$ , (c) $\sigma_{M1ur}$ , (d) at Hull Girder Ultimate Limit State, $1.987 \epsilon_{M1u}$	139
Fig.7.26. Axial compressive stress versus strain relationship of Panel M-2 obtained by FEA	140
Fig.7.27. Deformed shape of Panel M-2 at its Ultimate Limit State, $\sigma_{M2u}$ – Magnitude of Displacement	140
Fig.7.28. Deformed shape of Panel M-2 at its Ultimate Limit State, (a) $U_y$ Displacement, (b) Plot of Stiffener’s 16 web $U_y$ Displacement	141
Fig.7.29. Von Mises Stress of Panel M-2 at (a) $0.876 \epsilon_{M2ur}$ , (b) $0.931 \epsilon_{M2ur}$ , (c) $\sigma_{M2ur}$ , (d) at Hull Girder Ultimate Limit State, $2.405 \epsilon_{M2u}$	142
Fig.7.30. Panel CL2 above stiffener 27 at the time of the Hull Girder Collapse, $\epsilon_{HullColl}/\epsilon_{ydequivCL2}=1.08$ . (a) Illustration of Elements’ yield stress, (b) Von Mises Stress.	143
Fig.7.31. Plot of plate’s $U_y$ Displacement along its length at the time of the hull girder collapse	144
Fig.7.32. Displacement Magnitude of Panel CL2 above stiffener 27 at the time of (a) the Stiffeners’ 37-39 Collapse, $\epsilon_{CL2}/\epsilon_{HullColl}=0.40$ , (b) the Hull Girder Collapse, $\epsilon_{CL2}/\epsilon_{HullColl}=1.00$	145
Fig.7.33. Von Mises Stress of Panel CL2 above stiffener 27 at the time of the Stiffeners’ 37-39 Collapse, $\epsilon_{CL2}/\epsilon_{HullColl}=0.40$	146
Fig.7.34. Plot of stiffener’s 39 $U_z$ Displacement along its length at the time of (a) the stiffener’s collapse, (b) the hull girder collapse	146
Fig.7.35. Axial compressive stress versus strain relationship of Panel S-5 obtained by FEA	147
Fig.7.36. Deformed shape of Panel S-5 at its Ultimate Limit State– Magnitude of Displacement	148
Fig.7.37. Deformed shape of Panel S-5 at its Ultimate Limit State, (a) $U_z$ Displacement, (b) Plot of Stiffener’s 39 web $U_z$ Displacement along its length	148
Fig.7.38. Von Mises Stress of Panel S-5 at (a) $0.786 \epsilon_{S5ur}$ , (b) $1.0 \epsilon_{S5ur}$ , (c) at Hull Girder Ultimate Limit State, $1.573 \epsilon_{S5u}$	149
Fig.7.39. Panel I2 at the time of its structural elements’ collapse (a) Magnitude of Displacement, (b) Von Mises Stress Distribution	150
Fig.7.40. Panel S3 at the time of its structural elements’ collapse (a) Magnitude of Displacement, (b) Von Mises Stress Distribution	150
Fig.7.41. Axial compressive stress versus strain relationship of Panel I-4 obtained by FEA	151

Fig.7.42. Axial compressive stress versus strain relationship of Panel I-3 obtained by FEA.	152
Fig.7.43. Axial compressive stress versus strain relationship of Panel S-4 by FEA	152
Fig.7.44. Axial compressive stress versus strain relationship of Panel ST-4 by FEA	153
Fig.7.45. Axial compressive stress versus strain relationship of Panel ST-3 by FEA	153
Fig.7.46. Deformed shape of Panel I4 - Magnitude of Displacement : (a) at its Ultimate Limit State, $\epsilon_{I4u}$ , (b) at Hull Girder Collapse, 1.391 $\epsilon_{I4u}$	154
Fig.7.47. Deformed shape of Panel I3 - Magnitude of Displacement : (a) at its Ultimate Limit State, $\epsilon_{I3u}$ , (b) at Hull Girder Collapse, 1.369 $\epsilon_{I3u}$	154
Fig.7.48. Deformed shape of Panel S4 - Magnitude of Displacement : (a) at its Ultimate Limit State, $\epsilon_{S4u}$ , (b) at Hull Girder Collapse, 1.098 $\epsilon_{S4u}$	155
Fig.7.49. Deformed shape of Panel ST4 - Magnitude of Displacement : (a) at its Ultimate Limit State, $\epsilon_{ST4u}$ , (b) at Hull Girder Collapse, 1.703 $\epsilon_{ST4u}$	155
Fig.7.50. Deformed shape of Panel ST3 - Magnitude of Displacement : (a) at its Ultimate Limit State, $\epsilon_{ST3u}$ , (b) at Hull Girder Collapse, 1.099 $\epsilon_{ST3u}$	156
Fig.7.51. Von Mises Stress of Panel I4 : (a) at its Ultimate Limit State, $\epsilon_{I4u}$ , (b) at Hull Girder Collapse, 1.391 $\epsilon_{I4u}$	156
Fig.7.52. Von Mises Stress of Panel I3 : (a) at its Ultimate Limit State, $\epsilon_{I3u}$ , (b) at Hull Girder Collapse, 1.369 $\epsilon_{I3u}$	157
Fig.7.53. Von Mises Stress of Panel S4 : (a) at its Ultimate Limit State, $\epsilon_{S4u}$ , (b) at Hull Girder Collapse, 1.098 $\epsilon_{S4u}$	157
Fig.7.54. Von Mises Stress of Panel ST4 : (a) at its Ultimate Limit State, $\epsilon_{ST4u}$ , (b) at Hull Girder Collapse, 1.703 $\epsilon_{ST4u}$	158
Fig.7.55. Von Mises Stress of Panel ST3 : (a) at its Ultimate Limit State, $\epsilon_{ST3u}$ , (b) at Hull Girder Collapse, 1.099 $\epsilon_{ST3u}$	158
Fig.7.56. Panel B1 : (a) Displacement Magnitude, (b) Von Mises Stress Distribution at the time of the Hull Girder Collapse, $\epsilon_{B1ap} = \epsilon_{Hullu}$	162
Fig.7.57. Panel B2 : (a) Displacement Magnitude, (b) Von Mises Stress Distribution at the time of the Hull Girder Collapse, $\epsilon_{B2ap} = \epsilon_{Hullu}$	162
Fig.7.58. Panel BLG : (a) Displacement Magnitude, (b) Von Mises Stress Distribution at the time of the Hull Girder Collapse, $\epsilon_{BLGap} = \epsilon_{Hullu}$	163
Fig.7.59. Panel CL1 : (a) Displacement Magnitude, (b) Von Mises Stress Distribution at the time of the Hull Girder Collapse, $\epsilon_{CL1ap} = \epsilon_{Hullu}$	163
Fig.7.60. Panel SG : (a) Displacement Magnitude, (b) Von Mises Stress Distribution at the time of the Hull Girder Collapse, $\epsilon_{SGap} = \epsilon_{Hullu}$	163
Fig.7.61. Panel HP : (a) Displacement Magnitude, (b) Von Mises Stress Distribution at the time of the Hull Girder Collapse, $\epsilon_{HPap} = \epsilon_{Hullu}$	164
Fig.7.62. Panel IB1: (a) Displacement Magnitude, (b) Von Mises Stress Distribution at the time of the Hull Girder Collapse, $\epsilon_{HPap} = \epsilon_{Hullu}$	164
Fig.7.63. Panel S1: (a) Displacement Magnitude, (b) Von Mises Stress Distribution at the time of the Hull Girder Collapse, $\epsilon_{S1ap} = \epsilon_{Hullu}$	165
Fig.7.64. Panel ST1 : (a) Displacement Magnitude, (b) Von Mises Stress Distribution at the time of the Hull Girder Collapse, $\epsilon_{ST1ap} = \epsilon_{Hullu}$	165
Fig.7.65. Applied strain/yield strain ration versus position of neutral axis	166
Fig.7.66. Illustration of initial and final position of the neutral axis	167
Fig.7.67. Position of neutral axis at each imposed curvature	168

Fig.7.68. FEA Hull Girder Vertical Bending Moment - Imposed Curvature Curve 168

---

**CHAPTER 8 170**

**COMPARISON OF THE APPROACHES 170**

Fig.8.1. Load end Shortening Curves Comparison of Longitudinal Stiffener, I2-29 176

Fig.8.2. Load end Shortening Curves Comparison of Longitudinal Stiffener, I3-33 177

Fig.8.3. Load end Shortening Curves Comparison of Longitudinal Stiffener, S4-30 177

Fig.8.4. Load end Shortening Curves Comparison of Longitudinal Stiffener, CL2-38 178

Fig.8.5. Load end Shortening Curves Comparison of Longitudinal Stiffener, M2-7 178

Fig.8.6. Bottom Longitudinals B1-3/ B1-4/ B1-5 under tension 179

Fig.8.7. Side Girder Longitudinal SG-2 under tension 180

Fig.8.8. Hard corner connecting the side shell to stringer 23 under tension 180

Fig.8.9. Hard corner connecting the main deck to CL Bulkhead under compression 181

Fig.8.10. Position of neutral axis at each imposed curvature 182

Fig.8.11. Comparison of M-k Curves of all applied approaches 183

Fig.8.12. Percentage of absolute difference in stress response of structural elements under compression at Increment 45 and Increment 103 185

## LIST OF TABLES

<b>CHAPTER 2</b>	<b>19</b>
<b>HULL GIRDER ULTIMATE STRENGTH</b>	<b>19</b>
Table 2.1. Euler Buckling Stress-Parameters for all possible Boundary Conditions	32 32
<b>CHAPTER 3</b>	<b>36</b>
<b>CSR HULL GIRDER STRENGTH ASSESSMENT</b>	<b>36</b>
Table 3.1. Modes of failure of each element considered by CSR	46
Table 3.2. Abbreviations used for the load-end shortening curves formulas	49
<b>CHAPTER 5</b>	<b>65</b>
<b>DETAILS OF THE VESSEL USED IN THIS STUDY</b>	<b>65</b>
Table 5.1. Vessel's Main Particulars	66
Table 5.2. Geometry properties of Bottom Plating Panels	69
Table 5.3. Geometry properties of Side Shell panels	70
Table 5.4. Geometry properties of Inner Bulkhead Panels	72
Table 5.5. Geometry properties of CL Bulkhead Plating Panels	74
Table 5.6. Geometry properties of Main Deck Plating Panels	75
Table 5.7. Geometry properties of Inner Bottom Plating Panels	76
Table 5.8. Geometry properties of remaining panels	77
Table 5.9. Maximum expected still water Bending Moments as per CSR	77 77
Table 5.10. Permissible still water Bending Moments as per vessel's Loading Manual	78 78
<b>CHAPTER 6</b>	<b>79</b>
<b>APPLICATION OF THE CSR INCREMENTAL-ITERATIVE APPROACH</b>	<b>79</b>
Table 6.1. Geometric properties of structural elements based on net scantlings	84
Table 6.2. Predominant Buckling Modes as per CSR Formulas	95
<b>CHAPTER 7</b>	<b>107</b>
<b>FINITE ELEMENT APPROACH</b>	<b>107</b>
Table 7.1. Stiffened and/or Unstiffened panels required by CSR Rules for the modelling of the longitudinally effective hull girder structure and the buckling strength assessment	109



---

Table 7.2. Computational time/ Ultimate limit state /Plate $U_z$ displacement of panel M1 for 25mm and 50mm element size	115
Table 7.3. Simply Support Conditions at the unloaded edge of the panels	117
Table 7.4. Additional Boundary Support Conditions at unloaded edge	118
Table 7.5. Boundary Conditions in way of loaded edge of panels	119
Table 7.6. Boundary condition in case of transverse edges not extending up to the primary support members	121
Table 7.7. Plate deflection tolerances between stiffeners as per IACS Shipbuilding and Quality Repair Standard	123
Table 7.8. Initial Deflections accounted for the Finite Element Approach	124
Table 7.9. Maximum Initial Deflections of Panel M1	127
Table 7.10. Material properties	129
Table 7.11. Ultimate Limit State characteristics of all structural elements under compression	134
Table 7.12. Ultimate Limit State Characteristics of Panels constantly under Compression	159
Table 7.13. Applied Strain to Panels' structural elements constantly under Tension at the time of the Hull Girder Collapse	161
Table 7.14. Structural elements in way of the position of the neutral axis	166
<b>CHAPTER 8</b>	<b>170</b>
<b>COMPARISON OF THE APPROACHES</b>	<b>170</b>
Table 8.1. Comparison of the buckling failure and ULS modes of longitudinal stiffeners constantly under compression	172
Table 8.2. Comparison of the ultimate strength characteristics of longitudinal stiffeners constantly under compression	174
Table 8.3. Comparison of Hull Girder's Ultimate Limit State Characteristics of all Approaches	187

## **SUMMARY**

As Common Structural Rules (CSR) come into effect, the ultimate limit state assessment is being recognized as an important aspect of a ship's structural analysis. The work reported in the present Dissertation aims to verify the IACS CSR Incremental – Iterative Approach which is a method adopted by the IACS for the estimation of the Hull Girder Ultimate Bending Capacity. For this purpose, a double hull oil tanker is used as a case study.

The vessel's Hull Girder Ultimate Capacity is computed by applying the CSR proposed Incremental – Iterative Approach as well as by introducing an alternative approach based on Finite Element Analysis. The finite element code used is ABAQUS/Standard.

The load end shortening curves, failure modes and ultimate limit states of the hull girder's stiffened plate elements, as derived by both methods, are analyzed and detailed results and comparisons are presented.

Moreover, the hull girder bending moment capacity, as determined using the bending moment curvature relationship computed by both approaches, is compared and the found differences discussed.

# CHAPTER 1

## INTRODUCTION

### 1.1. General

One of the main challenges in naval architecture and ship structural design that requires special consideration is the estimation of the Hull Girder Ultimate Bending Strength. Taking into account the complexity of the vessel's structure in combination with the complexity of the sea environment in which it operates, it becomes self-explanatory that the determination of the Hull Girder Ultimate Strength is a particularly challenging engineering problem.

Traditionally, the determination of the hull girder strength has been based on estimates of the buckling strength of its structural components derived from their elastic buckling strength and adjusted by a simple plasticity correction. Nevertheless, during the recent years, substantial efforts have been made by the shipbuilding industry for the development of limit state design approaches, rather than the traditional allowable stress approaches for the design and strength assessment of ship structures. The limit state is defined as the condition at which a particular structural member or an entire structure fails to perform its function. More specifically, Ultimate Limit Strength refers to the collapse of the structure due to loss of structural stiffness and strength.

Nowadays, the ultimate limit state approach is recognised to be a more rational basis for design and strength assessment as opposed to the traditional design which did not necessarily lead to the most cost effective designs. With the aim of harmonisation, the International Association of Classification Societies (IACS) has revised the Classification Rules concerning the structural design by developing the Common Structural Rules for Double Oil Tankers and Bulk Carriers. Simultaneously, the need for a coherent limit state design approach has been addressed since the CSR Rules also include limit state design approaches for the assessment of the hull girder strength.

For the purpose of estimating the Hull Girder Ultimate Capacity, the CSR Rules have adopted two alternative methods, the Single Step and the Multi-Step Method. The latter is referred to as the ***Incremental-Iterative Approach***. The ultimate hull girder sagging capacity of tankers in accordance with the Single Step Method, is the point at which the ultimate capacity of the stiffened deck panels is reached, whereas as per the Incremental Iterative Approach same is defined as the peak value of the static non-linear bending moment-curvature ( $M-\kappa$ ) relationship.

Recognising that each longitudinal component of the hull girder plays its unique role to the overall strength and stiffness of the hull girder structure under longitudinal bending loads, the Incremental Iterative Approach is based on the division of the hull girder transverse section into individual structural elements and the determination of their collapse behavior, that is a load-end shortening curve, or stress-strain  $\epsilon$ - $\sigma$  curve, for each structural element. For this purpose, the CSR Rules use simplified design formulas that consider all relevant failure modes for the individual structural elements, such as plate buckling, beam column buckling, torsional stiffener buckling and stiffener web buckling. It should be noted that each structural element is considered to act independently of the other.

The present dissertation has two main objectives. The first is the detailed application of the CSR Incremental-Iterative Approach to a double hull oil tanker of 47326 dwt. The second is the verification of this approach by introducing an alternative procedure based on Finite Element (FE) Analysis. According to this procedure, referred to here as the ***Finite Element Approach***, the hull girder transverse section is divided into a series of stiffened panels which are taken to extend transversely between the adjacent primary support members and longitudinally between the vessel's web frames. Subsequently, the load-end shortening response of each panel, and therefore of each constituent plate-stiffener element, is determined through nonlinear FE analysis, here using the commercially available FE code ABAQUS. The Finite Element Approach is however based on the CSR Incremental-Iterative Approach since the individual structural element stress-strain curves computed through the FE analysis are used to replace the corresponding curves constructed through the application of the CSR formulas. In general, it is expected that the Finite Element analysis, as opposed to the CSR formulas, will provide a more accurate estimate of the stress-strain response of the individual structural elements and therefore will predict more accurately the Hull

Girder Ultimate Capacity. In this respect, the usage of the Finite Element Approach aims to verify the simplified design formulas adopted by CSR for the collapse prediction of the hull girder structural elements as well as of the resultant hull girder ultimate capacity. Moreover, it will be possible to ascertain whether the increased accuracy obtained through the application of the FE Method justifies the significant increase in the effort and time involved due to the development of detailed FE models and the subsequent simulation with the FE code.

## **1.2. Previous work in this area**

Upon the development and prior to the release of the CSR Rules, which include the new feature of Hull Girder Limit State Strength Assessment, it is likely that a number of studies were carried out for the verification of the CSR Methods and especially the Incremental-Iterative Approach. However, there are only a limited number of relevant studies for tankers in the open literature and these were published by Paik and his co-workers.

The method often used in these studies for the Ultimate Hull Girder Assessment is the Idealized Structural Unit Method (ISUM) which is a simplified nonlinear FE Method [1,3]. Unlike the conventional nonlinear FE methods the ISUM idealizes each structural component of the structure as one ISUM unit with only a few nodal points. In the case of ship structures the most commonly ISUM units used is the ISUM beam column unit without attached plating (with two nodal points) and the ISUM plate unit (with four nodal points) for the idealisation of the stiffeners and the attached plating respectively. Each nodal point has 6 degrees of freedom. The authors of these studies claim that compared to a conventional FE method, the ISUM Method reduces significantly both the modelling and computational effort, while it provides results in better agreement with those obtained with more refined non linear FE analysis. Moreover, the authors claim that this method, contrary to the CSR assessment methodology, can better simulate the progressive failures of the individual components and their interaction effects. The ISUM method in the case of ship or ship-based offshore structures can be applied using the software ALPS/HULL.

Another method used in these studies but for the assessment of the ultimate limit state of stiffened and or unstiffened plate structures is the ALPS/ULSAP (Ultimate Limit State Assessment of Plates) Method [1,2,3]. For APLS/ULSAP calculations, it is considered that a stiffened panel collapses if one of the collapse

modes described in Chapter 2 takes place as the applied actions increase. The minimum value of the ultimate strengths calculated for each of these collapse modes is considered as the ultimate limit state value. It should be noted that the ALPS/ULSAP method requires an equivalent plate thickness to be defined over the whole plate structure. This method can presumably be used instead of the CSR simplified design formulas, however this is not reported as such in the available literature.

For comparison reasons some of the above mentioned studies [1,3] have also used FE Analysis (FE Code ANSYS) for the Hull Girder Ultimate Strength assessment and/or Stiffened Panels Ultimate Strength Assessment.

These studies aim mainly to compare the resultant Hull Girder Bending Capacity calculated by CSR, ISUM and FE methods without giving reference to the effectiveness of the CSR Formulas for the estimation of the individual structural elements collapse mode, ultimate limit state and pre-post buckling behaviour.

The present study aims not only to compare the Hull Girder Ultimate Capacity, as estimated by the CSR Incremental-Iterative Approach and the FE Approach introduced here, but also the buckling mode, ultimate limit state and pre/post buckling behaviour of the individual structural elements.

### **1.3. Structure of Dissertation Thesis**

In order to fully explain the term Hull Girder Strength, Chapter 2 includes a short introduction of the stresses and loads to which the hull is subjected, summarises the possible modes of failure of stiffened plates and panels, presents the factors affecting these modes and outlines the approaches used for the stiffened plates' and hull girder ultimate strength analysis and assessment.

In Chapter 3, reference is made to the Common Structural Rules and in particular to its new features related to Hull Girder Ultimate Limit State Assessment. The chapter summarizes the design principles of the new rules and presents the methods adopted here for the hull girder assessment of the candidate vessel.

Chapter 4 describes the finite element procedure used for the simulation/analysis of a structure in general, introduces the ABAQUS finite element code used in this study and outlines the code's features and theory which are relevant to the work reported here.

Chapter 5 describes the vessel used as a case study, including its particulars and structure amidships. In addition, details regarding the steel material and the scantlings of the midship section are reported. Moreover, the design still water and wave bending moments are presented.

The application of the CSR Incremental-Iterative Approach used in the context of this study is described in Chapter 6. All stages of the procedure are presented including, but not limited to, the division of the midship-section into structural elements, the determination of the net scantlings, the calculation of the load end shortening curves and any considerations/assumptions made.

The procedure of the Finite Element Approach introduced in this work is detailed in Chapter 7. This chapter outlines all the assumptions made concerning the development of the FE models, such as the prescribed boundary conditions, mesh refinement issues, the FE procedure used in the simulations and, ultimately, gives a full account of the results obtained.

The comparison of the two approaches takes place in Chapter 8. It includes a comparison of the failure modes and the ultimate strength of stiffened panels and, finally, the computed hull girder bending moment- curvature relationship.

Discussion is included in Chapter 9, whereas concluding remarks are summarized in Chapter 10.

## **CHAPTER 2**

# **HULL GIRDER ULTIMATE STRENGTH**

### **2.1. General**

It is beyond doubt that the task of assessing the adequacy of the hull girder strength is one of the most challenging engineering problems. The complexity of the vessel's structure in combination with the complexity of the sea environment in which it operates poses fundamental difficulties in determining the vessel's loading and identifying its response to that loading. The objectives of this chapter is to make a short introduction to the stresses and loads to which the hull is subjected, to discuss the possible modes of the structure's failure and to outline the approaches used for the hull girder strength analysis and assessment.

### **2.2. Hull Loading and Structural Response**

The different loads acting on the hull during its lifetime can be classified to the following groups:

- The body forces such as weight and inertia
- The dynamic pressure on the ship's hull due to the incident and diffracted waves
- The inertial forces arising from the acceleration of the fluid (referring to both the sea and the liquids carried in tanks on the ship)
- The inertial and damping forces arising due to wave radiation from the ship.

Excluding the inertial forces, the loading of the ship derives from the two dominant loads, gravity and water pressure. The uneven distribution of such loads along the vessel's length (refer to image 2.1), causes its bending. Assuming that the vessel acts as a beam, the hull girder response can be determined by calculating the longitudinal bending moment which is considered separately for still water (Still Water Bending Moment) and when at sea (Wave Bending Moment). It is useful to separate the two, as whilst the still water bending moment depends on the mass



distribution (weight minus buoyancy), the bending moment due to waves depends on the hull's geometry and wave characteristics. Two conditions are considered, one with the wave crests at the end of the ship where the buoyancy forces tend to sag the vessel (sagging condition) and one with the wave crests at the mid of the ship where the buoyancy forces tend to hog the vessel (hogging condition).

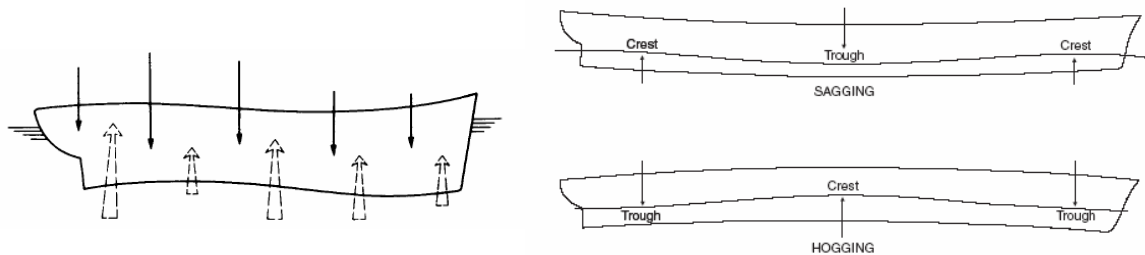


**Fig.2.1. (a)** Uneven distribution of vessel's loading, **(b)** Sagging and Hogging condition.

For the computation of the axial stresses applied due to the longitudinal bending moments, the elementary Bernoulli-Euler beam theory is used. At this point, it would be useful to state the assumptions under which this theory is applied to ship structures:

- The beam is prismatic, i.e. all cross sections are uniform.
- Plane cross sections remain plane and merely rotate as the beam deflects.
- Transverse (Poisson) effects on the strain are neglected.
- The material behaves elastically.
- Shear effects can be separated from and not influence bending stresses or strains.

This gives the following well-known formula for derived axial stresses:

$$\sigma = \frac{M}{SM} = \frac{M_s + M_w}{SM}$$

where,  $M_s$  and  $M_w$  is the still water and wave bending moment respectively and  $SM$  is the section modulus of the ship. When the beam section bends for example in sagging condition, the structural elements in way of the main deck are in

compression and in tension in way of the bottom. There is a position called the neutral axis, where the structural elements are neither in tension nor in compression.

These stresses generated in the ship's structure and the resulting deformations must be kept within acceptable limits by careful design. For this purpose, each longitudinal element of the structure must play its role.

### **2.3. Modes of Structural Failure**

Failure of the structure occurs when the structure cannot withstand the loads imposed on it and as a result cannot longer carry out its intended function. Failure of a structure may mean permanent strain, cracking, unacceptable deflection, instability, etc. If in failing one element merely sheds its load on to another which can withstand it, then there is usually no safety problem, although remedial measures may be needed. In opposite case, however, a domino effect takes place and the surrounding elements fail in turn, resulting to a possible loss of the ship. Specifically for the ship girder, structural failure can occur due to one or a combination of the following:

- **Direct Failure** may be caused when a part of the structure becomes distorted due to being strained beyond the ultimate yield stress.
- **Fatigue Failure.** The elastic fatigue lives of structures are not definable except by test as opposed to the elastic fatigue lives of materials which are well documented. Corrosion fatigue is a special case of accelerated failure under when the material is in a corrosive environment.
- **Cracking.** This occurs when the material can no longer sustain the load applied and its parts. The loading may exceed the ultimate strength of the material or more likely failure is due to the fatigue of material.
- **Instability.** Very large deflections may occur under relatively light loads. In effect the structure behaves like a cripples strut. In a plating stiffener it may cause torsional tripping. Instability can be regarded as failure only if related to the whole structure. Where only part of the structure shrinks its load, overall failure does not necessarily occur.

## 2.4. Hull girder structural analysis

During the recent years, substantial efforts have been made by the shipbuilding industry for the development of limit state design approaches rather than the traditional allowable stress approaches for the design and strength assessment of ship structures. Traditionally, the design of ship structures had been based on estimates of the buckling strength (refer to point A of Figure 2.2) of the structural components derived from their elastic buckling strength and adjusted by a simple plasticity correction.

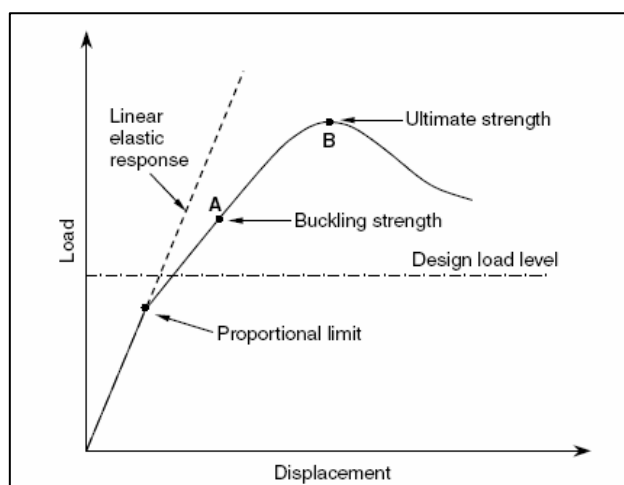


**Fig.2.2.** Structural design based on Ultimate Strength

The aim of the Classification Societies was to keep the stresses resulting from the design loads under a certain working stress level that was usually based on many years of accumulated knowledge, research, expertise and of course successful similar past experience. The allowable stress was expressed as a fraction of the mechanical properties of materials such as uniaxial yield or ultimate tensile strength. As a result, neither the post-buckling behaviour nor the actual ultimate limit strength (refer to point B) of the components was not taken into account.

Nowadays, the ultimate limit state approach is recognised to be a more rational basis for design and strength assessment as opposed to the traditional design which did not necessarily lead to the most cost effective designs.

In this respect the International Association of Classification Societies (IACS) has revised the Classification Rules by developing the Common Structural Rules for

Double Oil Tankers and Bulk Carriers which include limit state design approaches for the assessment of the hull girder strength. Prior to presenting the Common Structural Rules for Hull Girder Strength Design and Assessment it is essential to make a reference to the concept of Limit State Design Approaches, giving particular attention to the ultimate limit state design.

### **2.4.1. Limit State Design Approaches**

The limit state is defined as the condition at which a particular structural member or an entire structure fails to perform its function. From the scope of the structural engineer four types of limit states are taken into account for steel structures:

- **Serviceability Limit State (SLS) - Displacements and deflections.** SLS represents failure under normal operating conditions due to deterioration of routine functionality.
- **Fatigue Limit State (FLS) - Fatigue and fracture behavior.** Fatigue is the cumulative material damage caused by cyclic loading. Examples of this type of loading in marine structures include alternating stresses associated with the wave induced loading, vortex-induced-vibration (VIV) and load fluctuations due to the wind and other environmental effects.
- **Accidental Limit State (ALS) - Collision, fire, blast, dropped object, etc.** ALS represents excessive structural damage as a consequence of accidents, collisions, fire, explosion, etc.
- **Ultimate Limit State (ULS) - Ultimate strength behavior.** ULS refers to the collapse of the structure due to loss of structural stiffness and strength.

## **2.5. Ultimate Limit State Approach (ULS)**

The scope of the ultimate limit state design is to assess the ultimate load carrying-capacity of the structure and to evaluate its true safety margins by comparing its ultimate strength to the extreme loading condition to which the structure is subjected.

This is expressed by the following formula:

**Design Demand ( $D_d$ )  $\leq$  Design Capacity ( $C_d$ )**

$$\gamma_o \cdot \sum D_{ki} (F_{ki}, \gamma_{fi}) \leq C_k / \gamma_M \quad \text{or}$$

$$\gamma_o \cdot \sum D_{ki} (F_{ki}, \gamma_{fi}) \leq C_k / (\gamma_m \cdot \gamma_c)$$

where,

$\gamma_o$  : partial safety factors taking into account the degree of seriousness of the particular limit state with regards to safety and serviceability. Economical and social consequences as well as any other special circumstance, such as the mission of the ship, the type of cargo etc are counterbalanced.

$C_k$  : characteristic measure of capacity

$\gamma_M$  : capacity-related safety factor

$\gamma_m$  : partial safety factor taking account of the uncertainties due to material properties

$\gamma_c$  : partial safety factor taking account of the uncertainties on the capacity of the structure, such as quality of the construction, corrosion, method considered for determination of the capacity.

### **2.5.1. Ultimate Limit strength of Plates and Stiffened Plates**

It is well recognised that each longitudinal component of the hull girder plays its unique role to the overall strength and stiffness of the hull girder structure under longitudinal bending loads. Structural members that are considered to contribute to the longitudinal strength of the hull girder comprise of the main deck, the side shell, the bottom, the inner bottom, the inner longitudinal bulkheads including hopper, bilge plate, double bottom girders and horizontal girders.

As the main structural components of the vessel's hull girder are plates and stiffened plates (refer to Figure 2.3), the assessment of their ultimate capacity is imperative for the assessment of the whole hull girder ultimate strength.

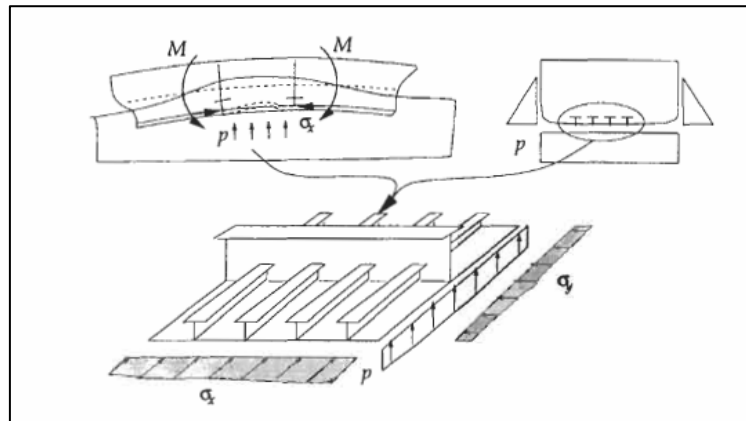


**Fig.2.3.** Hull Girder comprising of plates and stiffened plates

The ultimate strength of unstiffened plates, stiffeners and stiffened plates has been the subject of study of many researchers for many years. The following paragraphs aim at the presentation of stiffened plates' failure modes, the factors affecting these modes and the methods suggested for the stiffened plates' ultimate strength assessment.

### 2.5.1.1. Failure modes of plates and stiffened plates

The potential failure modes of plates and stiffened plates under predominantly compressive loads can be summarized to the following six types:

- **Mode 1 - Overall Collapse of the plating and the stiffener as a unit.** This mode takes place when the stiffeners are relatively weak. Even if the overall buckling of the plating and the stiffener as a unit occurs in the elastic regime, the stiffened plate may be able to sustain further loading and as a result the ultimate strength is reached by the formation of a large yield region inside the panel and/or along the panel edges. It should be noted that the overall collapse of a uniaxial stiffened panel is initiated by the beam-column mode.

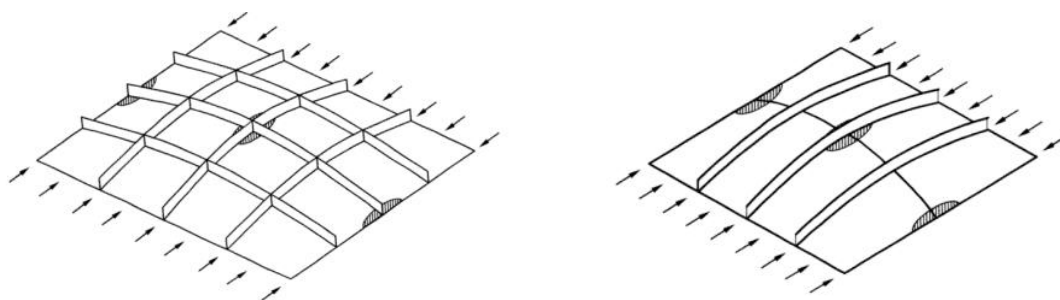


**Fig.2.4.** Overall collapse of plating and stiffener as a unit : **(a)** Cross-stiffened panel, **(b)** Uniaxial stiffened panel

- **Mode 2 - Biaxial Compressive Collapse.** At this mode the panel collapses by yielding along the plate-stiffener intersection at the panel edges with no stiffener failure. This type of collapse takes place when the panel is predominantly subjected to biaxial compressive loads and/or the plating is stocky.

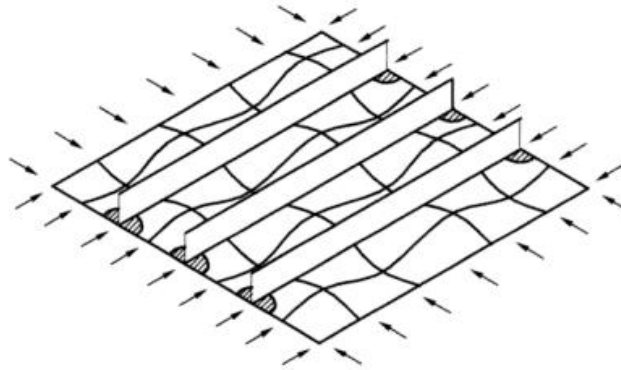


**Fig.2.5.** Biaxial compressive collapse

- **Mode 3 - Beam Column Type Collapse.** This mode refers to a failure pattern in which the ultimate strength is reached by yielding of the plate-stiffener at mid-span. This failure typically occurs when the dimensions of the stiffeners are intermediate, neither too weak nor very strong.

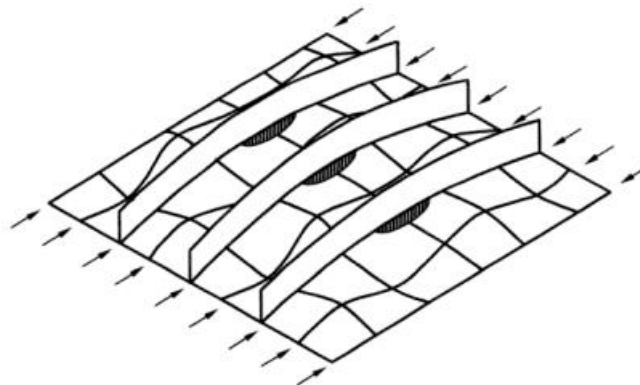


**Fig.2.6.** Beam Column Type Collapse

- **Mode 4 - Web Local Buckling.** This type of failure typically arises when the ratio of stiffener web height to stiffener web thickness is large or/and when the stiffener flange is inadequate to remain straight. As a result the stiffener web buckles or twists sideways.

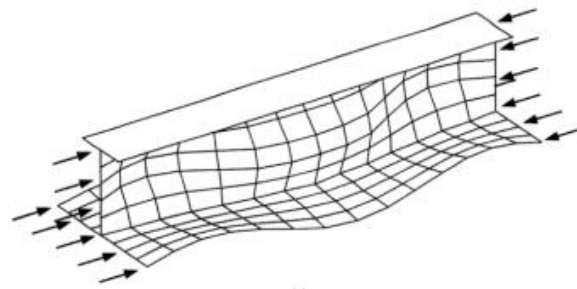


**Fig.2.7.** Web Local Buckling

- **Mode 5 - Tripping or Torsional Buckling of Stiffener.** This mode derives from stiffener-induced failure when the stiffener flange is inadequate to remain straight. As a result the stiffener web buckles or twists sideways. This mode happens suddenly and leaves the plating with essentially no stiffening leading to a possible overall collapse mode.

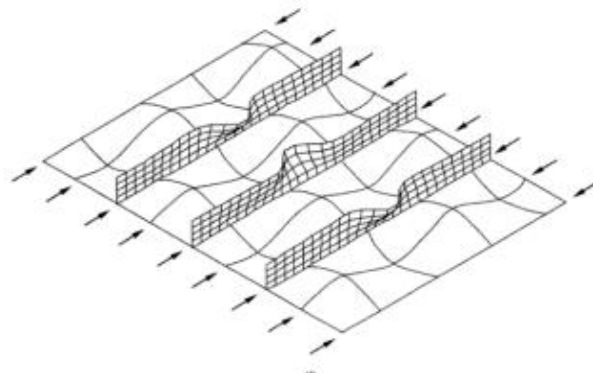


**Fig.2.8.** Tripping or Torsional Buckling

- **Mode 6 - Gross yielding.** This mode takes place when the panel slenderness is very small and/or when the panel is predominantly subjected to axial tensile loading, so that neither local nor overall buckling occurs.

It should be highlighted that the possible failure modes which above have been presented to act separately, in fact interact or act simultaneously. Besides, the assessment of stiffened plates' ultimate strength is not straightforward as there are many affecting factors such as geometric and material properties, loading conditions, initial imperfections, etc. Some of these factors will be presented at the next paragraph.



### 2.5.1.2. Factors affecting the behaviour of plates and stiffened plates

Material and Geometric Factors affecting the buckling behaviour and therefore the load shortening curves of plates and stiffened plates include the following:

- Plate slenderness ratio,  $b_p$
- Ratio of stiffener cross section  $A_s$  to the overall cross section  $A$  ( $A_s/A$ )
- Web slenderness ratio ( $b_w$ )
- Column slenderness ratio ( $\lambda$ )
- Material Yield Stress ( $\sigma_{yd}$ )

These geometric properties are defined as follows:

Property	Expression
Cross-sectional area	$A = A_p + A_w + A_f, A_e = A_{pe} + A_w + A_f$ where $A_p = bt, A_{pe} = b_e t, A_w = h_w t_w, A_f = b_f t_f$
Equivalent yield strength over the cross-section	$\sigma_{yeq} = \frac{A_p \sigma_{yp} + A_w \sigma_{yw} + A_f \sigma_{yf}}{A}$
Distance from outer surface of attached plating to elastic horizontal neutral axis	$z_0 = \frac{0.5bt^2 + A_w(t + 0.5h_w) + A_f(t + h_w + 0.5t_f)}{A}$ $z_p = \frac{0.5b_e t^2 + A_w(t + 0.5h_w) + A_f(t + h_w + 0.5t_f)}{A_e}$
Moment of inertia	$I = \frac{bt^3}{12} + A_p \left(z_0 - \frac{t}{2}\right)^2 + \frac{h_w^3 t_w}{12} + A_w \left(z_0 - t - \frac{h_w}{2}\right)^2$ $+ \frac{b_f t_f^3}{12} + A_f \left(t + h_w + \frac{t_f}{2} - z_0\right)^2$ $I_e = \frac{b_e t^3}{12} + A_{pe} \left(z_p - \frac{t}{2}\right)^2 + \frac{h_w^3 t_w}{12} + A_w \left(z_p - t - \frac{h_w}{2}\right)^2$ $+ \frac{b_f t_f^3}{12} + A_f \left(t + h_w + \frac{t_f}{2} - z_p\right)^2$
Radius of gyration	$r = \sqrt{\frac{I}{A}}, r_e = \sqrt{\frac{I_e}{A}}$
Column slenderness ratio	$\lambda = \frac{L}{\pi r} \sqrt{\frac{\sigma_{yeq}}{E}}, \lambda_e = \frac{L}{\pi r_e} \sqrt{\frac{\sigma_{yeq}}{E}}$
Plate slenderness ratio	$\beta = \frac{b}{t} \sqrt{\frac{\sigma_{yp}}{E}}$

*Note:* The subscript 'e' represents the effective cross-section.

**Fig.2.9.** Definition of plates' geometric properties

Following figure depicts the load end shortening curves for a range of Plate Slenderness Ratio ( $\beta$ ) and Column Slenderness Ratio ( $\lambda$ ) combinations. Establishing the load end shortening curves of the structural elements is of uppermost importance as they allow the designer to determine the buckling and post buckling collapse of the plate-stiffener combinations and hence the collapse of the ship section as a whole. Although in general, elements can withstand some additional stress even after collapse, the load end shortening curves for plate-stiffener combinations of  $\lambda \geq 0.6$  of below figure show a dramatic reduction in strength post collapse. For that reason it is recommended design to be based on values of  $\lambda$  of 0.4 or less.

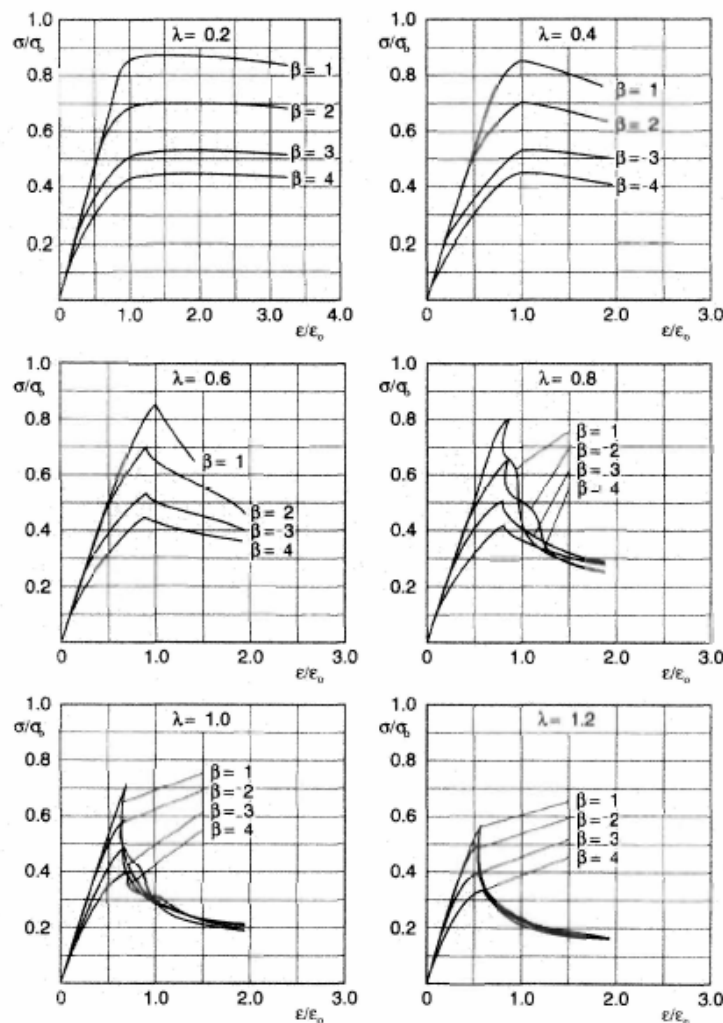


**Fig.2.10.** Load end shortening curves of stiffened plates for a range of  $\lambda$  and  $\beta$  combinations

In addition, initial imperfections, boundary conditions and types of loading also affect the behaviour of stiffened plates.

Initial imperfections relate to initial distortions and residual stresses which may develop during the fabrication of steel structures resulting to reduced structural capacity. These initial imperfections affect the structure's behaviour and should be taken into account in structural design. For this purpose efforts have been made to develop approximate methods based on insights from measurements in order to simulate these initial imperfections. Some typical initial deflection patterns in steel plating between stiffeners in the long (plate length) direction are depicted in Figure 2.11.

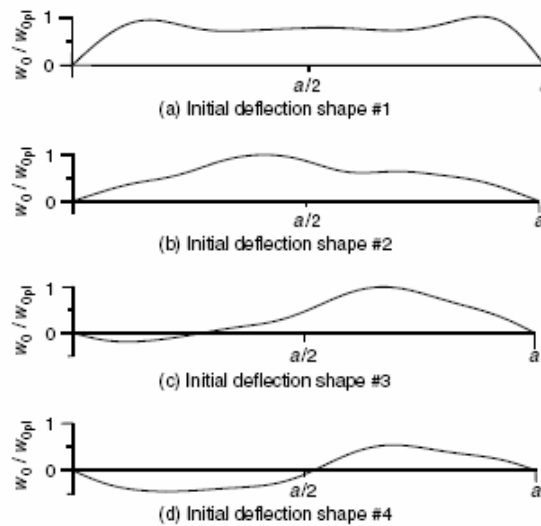


**Fig.2.11.** Typical initial deflection patterns in steel plating between stiffeners

When relevant initial deflection measurements are not available, the initial deflection amplitudes may be approximately defined by empirical formulations. The most widely used formulas for the prediction of the maximum plate initial deflection for steel plates between stiffeners are the Smith formulas which account for slight, average and severe initial imperfections as follows:

$$\frac{w_{opl}}{t} = \begin{cases} 0.025\beta^2 & \text{for slight level} \\ 0.1\beta^2 & \text{for average level} \\ 0.3\beta^2 & \text{for severe level} \end{cases}$$

where  $w_{opl}$  is the maximum initial deflection of the plate between the stiffeners, as shown in Figure 2.12.

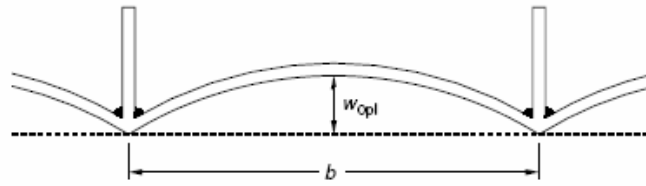


**Fig.2.12.** Typical initial deflection pattern in steel plating between stiffeners

It should be noted that the Classification societies specify construction tolerances of strength members as related to the maximum initial deflection with the intention that the initial distortions in the fabricated structure must be less than the corresponding specified values.

### 2.5.1.3. Elastic Buckling Strength

When an initially straight and of perfect geometry bar is subjected to the action of a compressive force without eccentricity, the bar is characterised as an ideal column. As per the Euler Theory, a mathematically straight, prismatic, pin-ended (simply supported), perfectly centrally loaded column that is able to buckle without the stress extending the proportional limit at any point of the column's cross section, has a buckling or critical load defined as follows:

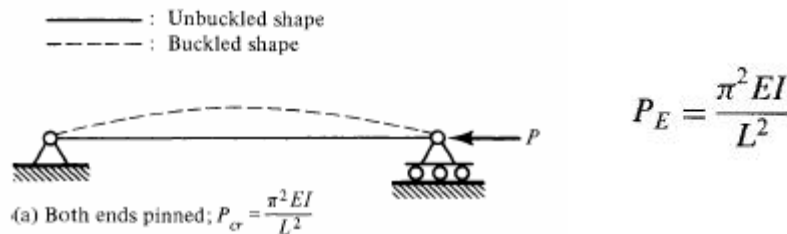


**Fig.2.13.** Euler Elastic Buckling Stress

where,  $E \cdot I$  is the elastic stiffness and  $L$  is the column's length. This is known as the Euler Buckling Stress and represents the buckling strength of an Euler column that collapses in the elastic region. For all possible boundary conditions the buckling or critical load can be expressed as follows:

$$P_{cr} = C \frac{\pi^2 EI}{L^2}$$

where C and L' shall be regarded as per below table dependent on the boundary conditions.

Boundary Conditions	C	L'
Both ends simply supported	1	L
One end fixed, the other free	$\frac{1}{4}$	2L
Both ends fixed	4	$\frac{L}{2}$
One end fixed, the other simply supported	$\left(\frac{4.493}{\pi}\right)^2$	0.699L

**Table 2.1.** Euler Buckling Stress-Parameters for all possible Boundary Conditions

In practice though, a stocky stiffened panel will buckle in the inelastic region with a certain degree of plasticity. For this reason, a plasticity correction to the Euler Buckling Stress is taken into account.

#### 2.5.1.4. Plasticity Correction to Euler Buckling Strength

Various methods exist to account for plasticity effects. A convenient technique for modifying the elastic critical stress due to plasticity is the  $\phi$ -method, as per which the elastic-plastic buckling stress is given by,

$$\sigma_{cr} = \phi \cdot \sigma_Y$$

where,  $\phi$  is an empirical function related to the structural slenderness. Several parameters may be used, but the most general measure is the reduced slenderness ratio:

$$\bar{\lambda} = \sqrt{\frac{\sigma_Y}{\sigma_E}}$$

where  $\sigma_E$  is the Euler Buckling Stress. Various expressions for  $\phi$ , exist. One method is to account for elasto-plastic effects by means of an elliptical interaction equation.

It is seen that,

$$\begin{aligned} \sigma_{cr} &\rightarrow \sigma_Y \text{ when } \sigma_E \rightarrow \infty \\ \sigma_{cr} &\rightarrow \sigma_E \text{ when } \sigma_E \ll \sigma_Y \end{aligned}$$

Hence, the formula converges to the correct solution for both stocky members and slender members. Solving for  $\sigma_{cr}$ , we obtain,

$$\sigma_{cr} = \frac{\sigma_Y}{\sqrt{1 + \bar{\lambda}^4}} \Rightarrow \phi = \frac{1}{\sqrt{1 + \bar{\lambda}^4}}$$

Another well-known solution which is widely used is the Johnson-Ostenfeld formula :

$$\phi = \begin{cases} 1 - \frac{\bar{\lambda}^2}{4}, & \bar{\lambda}^2 \leq 2 \\ \frac{1}{\bar{\lambda}^2}, & \bar{\lambda}^2 \geq 2 \end{cases}$$

Solving for  $\sigma_{cr} = \sigma_{ULT}$ , we obtain,

$$\begin{aligned} \sigma_{ULT} &= \sigma_E && \text{for } \sigma_E / \sigma_Y \leq 0.5 \\ \sigma_{ULT} &= \sigma_Y \left( 1 - \frac{1}{4\sigma_E / \sigma_Y} \right) && \text{for } \sigma_E / \sigma_Y \geq 0.5 \end{aligned}$$

The effect of the Johnson-Ostenfeld plasticity correction is shown in Figure 2.14.

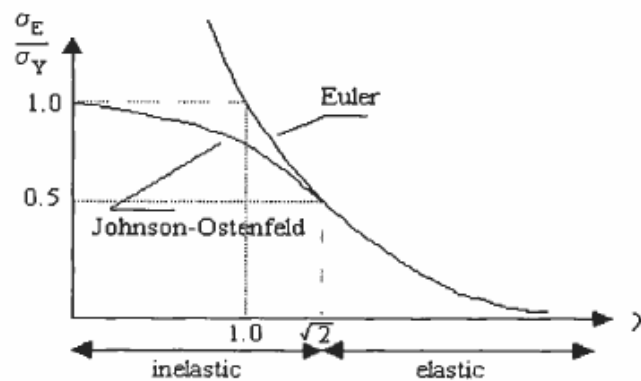


**Fig.2.14.** Effect of Johnson-Osterfeld plasticity correction

### 2.5.1.5. Ultimate Strength of Un-Stiffened Plates

Slender plates can carry loads larger than what is predicted by elastic theory if their unloaded edges are constrained to remain straight. Because of large lateral

deflections, membrane stresses develop in the transverse direction, which tend to stabilize the plates. At this stage, the distribution of stresses along the unloaded edges is no longer uniform but rather, it increases towards the stiffeners. According to the effective width method, the ultimate strength is obtained when the edge stress, approaches the yield stress. The following formula has been suggested by Faulkner and has been widely used for simply supported plates under longitudinal compression alone where the unloaded edges are constrained to remain straight:

$$\frac{b_e}{b} = \frac{\sigma_{xm}}{\sigma_y} = \begin{cases} \frac{2}{\beta} - \frac{1}{\beta^2} & \beta \geq 1 \\ 1 & \beta \leq 1 \end{cases}$$

where,  $b$  is the plate slenderness ratio.

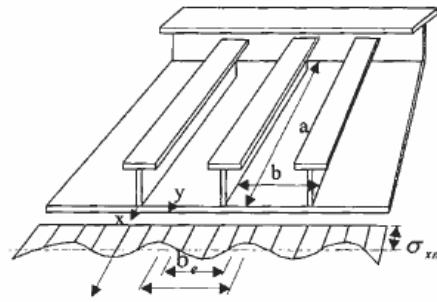


**Fig.2.15.** Actual Stress Distribution in a Compressed Stiffened Plate

Mansour suggested the following effective width formula which may be used for compressive loads acting in line with the long edge,  $a / b \geq 1.0$  or short edge,  $a / b < 1.0$  (Mansour, 1997):

$$b_e = \begin{cases} C_b & \text{for } \frac{a}{b} \geq 1.0 \\ \frac{a}{b} C_b + 0.08 \left( 1 - \frac{a}{b} \right) \left( 1 - \frac{1}{\beta^2} \right)^2 \leq 1.0 & \text{for } \frac{a}{b} < 1.0 \end{cases}$$

$$C_b = \begin{cases} 1 & \text{for } \beta < 1.25 \\ \frac{2.25}{\beta} - \frac{1.25}{\beta^2} & \text{for } 1.25 \leq \beta < 3.5 \\ \frac{1}{\sqrt{12(1-\nu^2)} \beta^2} & \text{for } \beta \geq 3.5 \end{cases}$$

### **2.5.1.6. Ultimate Lateral-Torsional Strength of Stiffened Plates**

In a plate-stiffener combination under axial compression where the web height to thickness ratio is large or the flange is weak and inadequate to remain straight, the stiffener may twist sideways leading to a tripping failure mode. This phenomenon occurs suddenly and results in subsequent unloading of the support member. For this reason it may be regarded as a collapse mode of the stiffened plate since once the stiffeners twist sideways the plating is left with essentially no stiffening and global buckling mode may follow immediately.

In view of the above, the ultimate strength of the stiffened panel may be approximated as a weighed average of the ultimate strengths of the plating and the tripping strength of the stiffener. The intention behind the average proposed is to avoid a pessimistic estimate of the stiffened panel ultimate strength. The tripping strength may be predicted by using the elastic buckling stress equation corrected by the Johnson-Ostenfeld formula:

$$\sigma_{el} = n \cdot E \frac{I_A}{Al^2}$$

The ultimate strength of the plating can be calculated as mentioned in above paragraph.

### **2.5.1.7. Ultimate Web Local Buckling Strength of Stiffened Plates**

Local web buckling of stiffened plates is likely to take place when the height of stiffener web compared to its thickness is relatively high. Once web buckling occurs, the plating, as in the case of torsional buckling, is left with no stiffening leading to overall collapse mode. At this mode though, it is considered that the plate reaches the ULS immediately after the local buckling of the stiffener web.

In this respect the ultimate strength of this mode can be calculated by the local buckling strength of the stiffener web taking into account the influence of rotational restraints along the plate-stiffener and stiffener web-flange combinations. As an approximation in such cases, the effective width of the plating likely to buckle is used for calculating the torsion constraints supplied by the plating.



## **CHAPTER 3**

# **CSR HULL GIRDER STRENGTH ASSESSMENT**

### **3.1. General**

The Common Structural Rules have been developed by the International Association of Classification Societies with an aim to harmonize the different Rules and Regulations of the members on a common basis. The first draft of the CSR Rules, which was available in public in June 2004, was reissued upon comments from the shipbuilding industry until its final adoption and entry into force on the 1<sup>st</sup> April 2006.

One of the new features of the CSR Rules is the assessment of the Hull Girder Strength by using the Ultimate Limit State Approach. This chapter summarizes the design principles of the new rules and presents the methods adopted for the hull girder assessment.

### **3.2. Partial Safety Factor Method**

For the assessment of a structures' strength it is imperative to identify the loads to be applied on the structure, to define the acceptance criteria and to determine the characteristic structural capacity.

The CSR criteria for the hull girder strength assessment are based on the Partial Safety Factor (PF) method, also known as Load and Resistance Factor Design (LRFD). Two design assessment conditions and corresponding acceptance criteria are taken into account. These conditions are associated with the probability level of the combined loads, A and B:

- Condition A is applicable to design load combinations based on 'expected' characteristic load values, typically covered by the static design load combinations.

- Condition B is applicable to design load combinations based on 'extreme' characteristic load values, typically covered by the static and dynamic load combinations.

The Partial Safety Factor (PF) Method has the following composition:

where,

$$\gamma_{stat-1}W_{stat} + \gamma_{dyn-1}W_{dyn} \leq \frac{R}{\gamma_R} \quad \text{for condition A}$$

$$\gamma_{stat-2}W_{stat} + \gamma_{dyn-2}W_{dyn} \leq \frac{R}{\gamma_R} \quad \text{for condition B}$$

$\gamma_{stat-i}$  partial safety factor that accounts for the uncertainties related to static loads

$W_{stat}$  simultaneously occurring static loads (or load effects in terms of stresses)

$\gamma_{dyn-i}$  partial safety factor that accounts for the uncertainties related to dynamic loads

$W_{dyn}$  simultaneously occurring dynamic loads. The dynamic loads are typically a combination of local and global load components

$R$  characteristic structural capacity. In case of the Hull Girder Assessment this is the Ultimate hull girder moment.

$\gamma_R$  partial safety factor that accounts for the uncertainties related to structural capacity

### 3.3. Hull Girder Assessment

For the assessment of the hull girder of Double Oil Tankers, as per the CSR Rules, the ultimate bending capacity in sagging is to be evaluated and checked to ensure that it satisfies the following criteria:

$$\gamma_S M_{sw} + \gamma_W M_{sw-sag} \leq \frac{M_{U}}{\gamma_R}$$

- **$M_{sw}$  sagging still water bending moment** is to be regarded either as the permissible sagging still water bending moment as defined by the rules or the maximum still water bending moment of the subject ship at full load condition. (refer to figure 3.1.)

The permissible sagging still water bending moment,  $M_{sw-perm-sea}$  in way of the midship region is given by:

$$M_{sw-min-sea-mid} = 0.01 C_{ww} L^2 B (11.97 - 1.9C_b)$$

where,  $C_{ww}$  wave coefficient computed as follows:

$$C_{ww} = \begin{cases} 10.75 - \left(\frac{300-L}{100}\right)^{\frac{3}{2}} & \text{for } 150 \leq L \leq 300 \\ 10.75 & \text{for } 300 < L \leq 350 \\ 10.75 - \left(\frac{L-350}{150}\right)^{\frac{3}{2}} & \text{for } 350 < L \leq 500 \end{cases}$$

- **$M_{wv-sag}$  midship sagging vertical wave bending moment**, defined as:

$$M_{wv-sag} = -f_{prob} 0.11 f_{wv-v} C_{ww} L^2 B (C_b + 0.7)$$

where,

$f_{prob}$  is regarded as 1.0

$f_{wv-v}$  is a distribution factor for the vertical wave bending moment along the vessel's length. For the midship region it equals to 1.

- **$\gamma_s, \gamma_w, \gamma_R$  are the partial safety factors** dependent on the design loading condition considered. Such design load combinations are depicted in Figure 3.1.

Design load combination	Definition of Still Water Bending Moment, $M_{sw}$	$\gamma_s$	$\gamma_w$	$\gamma_R$
a)	Permissible sagging still water bending moment, $M_{sw-perm-sea}$ , in kNm, see Section 7.2.1.1	1.0	1.2	1.1
b)	Maximum sagging still water bending moment for homogenous full load condition, $M_{sw-full}$ , in kNm, see note 1	1.0	1.3	1.1
Where:				
$\gamma_s$ partial safety factor for the sagging still water bending moment				
$\gamma_w$ partial safety factor for the sagging vertical wave bending moment covering environmental and wave load prediction uncertainties				
$\gamma_R$ partial safety factor for the sagging vertical hull girder bending capacity covering material, geometric and strength prediction uncertainties				
Notes				
1 The maximum sagging still water bending moment is to be taken from the departure, arrival or any mid-voyage condition with the ship homogeneously loaded at maximum draught in the departure condition.				

**Fig.3.1.** Partial Safety Factors for Hull Girder Assessment

- **$M_U$  sagging vertical hull girder ultimate bending capacity.** CSR propose following alternatives for the Ultimate Hull Girder Bending Capacity estimation:
  - a) Single Step Ultimate Capacity Method
  - b) Simplified Method Based on an Incremental-Iterative Approach
  - c) Alternatives methods

These methods are summarised at the next paragraphs giving emphasis on the Incremental - Iterative Approach which is in the scope of subject study.

### **3.4. Hull Girder Ultimate Bending Capacity**

#### **3.4.1. General**

The hull girder ultimate bending moment capacity,  $M_U$ , is defined as the maximum bending capacity of the hull girder beyond which the hull will collapse. During the last years many mathematical models have been developed for the estimation of the longitudinal strength analysis of ship hulls. Among these, we should distinguish the Smith Method which is the origin of the Incremental-Iterative Approach adopted by the CSR Rules.

In the Smith method, the hull section is divided into stiffened panels and corner elements. It is considered that the ultimate hull girder strength is dependent on the collapse behaviour of each of its structural elements. The progressive collapse of each stiffened plate and corner element due to buckling and yielding is taken into account by deriving the stress-strain relationships, while also considering post-buckling behaviour. The sagging hull girder ultimate capacity of a hull girder section, is defined as the maximum value on the static non-linear bending moment-curvature relationship  $M-\kappa$  (refer to image 3.2) which represents the progressive collapse behaviour of hull girder under vertical bending. The prediction of load-shortening behaviour of stiffened panels up to the post collapse region is of uppermost importance.

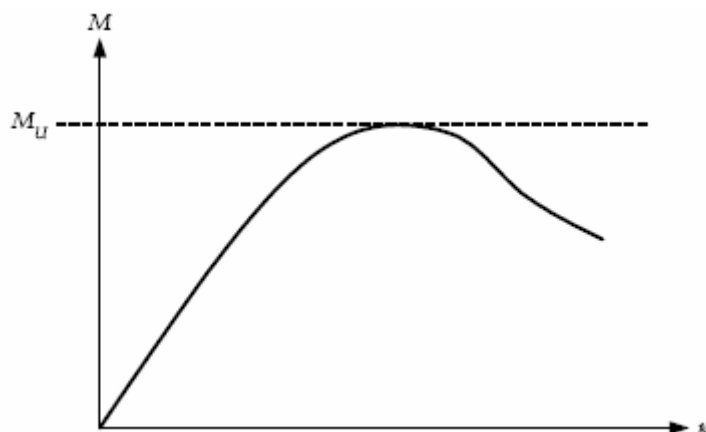


**Fig.3.2.** Bending Moment-curvature relationship (M-κ)

### 3.4.2. Assumptions of CSR Hull Girder Ultimate Bending Capacity Methods

Common Structural Rules as mentioned above have adopted two alternative methods for the Ultimate Hull Girder Capacity estimation. Both methods take into account following assumptions:

- In order to estimate the ultimate hull girder capacity the critical failure modes of all main longitudinal structural elements need to be identified. For tankers, in sagging condition, the critical mode is generally the inter-frame buckling of deck structures, as shown in Figure 3.3.

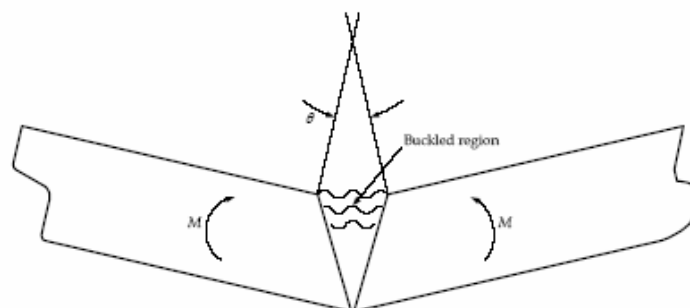


**Fig.3.3.** Interframe buckling failure of a tanker under sagging condition

- Structures compressed beyond their buckling limit have reduced load carrying capacity. All relevant failure modes for individual structural elements, such as plate buckling, torsional stiffener buckling, stiffener web buckling, lateral or global stiffener buckling; and their interactions, are to be considered in order to identify the weakest inter-frame failure mode.

- For tankers in the sagging condition, only vertical bending is considered. The effects of shear force, torsional loading, horizontal bending moment and lateral pressure are neglected.
- At both methods the net thickness approach is considered.

### **3.4.3. Single Step Ultimate Capacity Method**

The assumption behind this procedure is that the ultimate sagging capacity of tankers is the point at which the ultimate capacity of the stiffened deck panels is reached. The calculation is based on a reduced hull girder bending stiffness accounting for buckling of the deck.

### **3.4.4. Simplified Method Based on an Incremental-iterative Approach**

In this method the vertical bending moment  $M$  versus the curvature  $k$  of the vessel's cross section is obtained by means of an incremental-iterative approach which steps are summarized herewith. Prior to this though it would be useful to highlight the assumptions on which this method has been based.

#### **3.4.4.1. Assumptions of Incremental-Iterative Approach**

In adopting this approach following assumptions have been considered:

- The ultimate strength is calculated at a hull girder transverse section between two adjacent transverse webs.
- The hull girder transverse section remains plane during each curvature increment.
- The material properties of steel are assumed to be elastic, perfectly plastic.
- The hull girder transverse section can be divided into a set of elements which act independently of each other. The elements making up the hull girder transverse section are considered to be:
  - **Longitudinal Stiffeners** with attached plating,
  - **Transversely Stiffened Plate Panels**

- **Hard Corners.** As hard corners following structural elements have been defined:
  - a) the plating area adjacent to intersecting plates
  - b) the plating area adjacent to knuckles in the plating with an angle greater than 30 degrees.
  - c) plating comprising of rounded gunwales.

An illustration of hard corner definition for girders on longitudinal bulkheads is given in Figure 3.4.

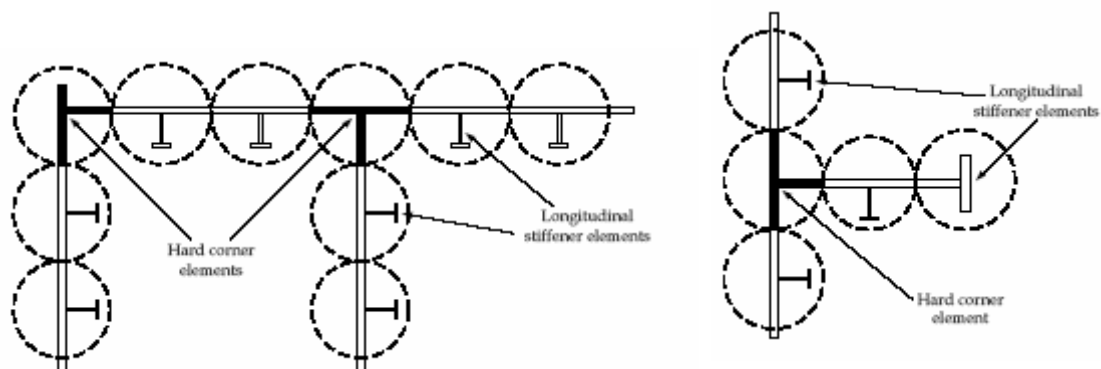


**Fig.3.4.** Elements considered to form the hull girder cross section

### 3.4.4.2. Procedure of Incremental-Iterative Approach

In this approach, as mentioned above, the curve  $M-\kappa$  is obtained by means of an incremental-iterative approach.

The bending moment  $\mathbf{M}_i$  which acts on the hull girder transverse section due to the imposed curvature  $\mathbf{k}_i$  is calculated for each step of the incremental procedure. This imposed curvature corresponds to an angle of rotation of the hull girder transverse section about its effective horizontal neutral axis, which induces an axial strain  $\boldsymbol{\varepsilon}$  in each hull structural element. In the sagging condition, the structural elements below the neutral axis are lengthened, whilst elements above the neutral axis are shortened.

The stress  $\boldsymbol{\sigma}$  induced in each structural element by the strain  $\boldsymbol{\varepsilon}$  is obtained from the stress-strain curve  $\boldsymbol{\sigma}-\boldsymbol{\varepsilon}$  of the element, which takes into account the behaviour of the structural element in the non-linear elasto-plastic domain.

The force in each structural element is obtained from its area times the stress and these force are summated to derive the total axial force on the transverse section. Note the element area is taken as the total net area of the structural element. This total force may not be zero as the effective neutral axis may have moved due to the non linear response. Hence it is necessary to adjust the neutral axis position, recalculate the element strains, forces and total sectional force and iterate until the total force is zero.

Once the position of the new neutral axis is known, then the correct stress distribution in the structural elements is obtained. The bending moment  $\mathbf{M}_i$  about the new neutral axis due to the imposed curvature  $\mathbf{k}_i$  is then obtained by summing the moment contribution given by the force in each structural element.

The main steps of the incremental-iterative approach as described below are illustrated in the flow chart shown in Figure 3.5.

**Step 1.** The hull girder transverse section is divided in structural elements which comprise of longitudinal stiffened panels (one stiffener per element), hard corners and transversely stiffened panels as shown in Figure 3.4.

**Step 2.** For all structural elements the stress-strain curves (or so called load-end shortening curves) are derived. CSR Rules propose specific formulas for the estimation of the load end shortening curves which are to be presented at the next paragraph.

**Step 3.** For the estimation of the curvature step size at each step, the expected maximum required curvature  $\mathbf{k}_F$ , is estimated as follows:

$$\kappa_F = 3 \frac{M_{yd}}{EI_{v-net50}} 10^{-3} \text{ m}^{-1}$$

where,

- $\mathbf{M}_{yd}$  vertical bending moment given by a linear elastic bending stress of yield in the deck or keel. To be taken as the greater of  $Z_{v-net50-dk} \sigma_{yd} 10^3$  or  $Z_{v-net50-kl} \sigma_{yd} 10^3$
- $\mathbf{Z}_{v-net50-dk}$  section modulus at deck
- $\mathbf{Z}_{v-net50-kl}$  section modulus at bottom
- $\mathbf{E}$  modulus of elasticity



- $\sigma_{yd}$  specified minimum yield stress of the material
- $I_{v-net50}$  hull girder moment of inertia

The curvature step size  $\Delta\kappa$  at each step is regarded as  $\kappa_F/300$ . For the first incremental step ( $i=1$ ) the curvature,  $\kappa_1$  is regarded as  $\Delta\kappa$  while the initial position of the neutral axis  $z_{NA-i}$  is computed with the value of the elastic hull girder section modulus,  $Z_{v-net50}$ .

**Step 4.** For each element (index  $j$ ), the strain corresponding to curvature  $\kappa_i$ , is calculated as  $\epsilon_{ij} = \kappa_i (z_j - z_{NA-i})$ . The corresponding stress is derived by the end shortening curves obtained during step 2, while the force acting on the element is calculated as  $\sigma_j \cdot A_j$ . It should be noted that for each structural element, the stress  $\sigma_j$  corresponding to the element strain  $\epsilon_{ij}$  is to be taken as the minimum stress value from all applicable stress-strain curves  $\sigma$ - $\epsilon$  for that element.

**Step 5.** Having calculated the forces acting on each element, the new neutral axis position  $z_{NA-i}$  can be determined by checking the longitudinal force equilibrium over the whole transverse section. For each step, adjustment of the neutral axis takes place and therefore steps 4 and 5 are repeated until equilibrium is achieved:

$$F_i = 0.1 \cdot \sum A_j \sigma_j = 0$$

Equilibrium is satisfied when the change in neutral axis position is less than 0.0001m.

**Step 6.** Having satisfied the equilibrium at a specific step, the moment is calculating by summing the force contributions of all elements as follows:

$$M_i = 0.1 \sum \sigma_j A_j \left| (z_j - z_{NA-i}) \right|$$

**Step 7.** At each step the curvature is being increased by  $\Delta\kappa$ . The neutral axis position of each step is regarded as the initial value for the next curvature increment. Steps 4 to 6 are repeated until the maximum required curvature is reached. The ultimate capacity is the peak value  $M_u$  from the M- $\kappa$  curve. If the peak does not occur in the curve, then  $\kappa_F$  is to be increased until the peak is reached.



### 3.4.4.3. Load End Shortening Curves for Incremental-Iterative Approach

CSR have adopted certain formulas for the evaluation of the elements' load end shortening curves. Following failure modes of stiffened panels are taken into account:

- Elastic perfectly plastic failure
- Beam Column buckling
- Torsional buckling
- Web local buckling

The modes of failure applicable for each type of element are presented in Table 3.1.

Element	Mode of failure
Lengthened transversely framed plate panels or stiffeners	Elastic, perfectly plastic failure
Shortened stiffeners	Beam column buckling Torsional buckling Web local buckling of flanged profiles Web local buckling of flat bars
Shortened transversely framed plate panels	Plate buckling

**Table 3.1.** Modes of failure of each element considered by CSR

Following paragraphs summarize the calculation of the load shortening curves adopted by CSR to the extent that are relevant for subject study. For an easiest reference, the nomenclature used at following paragraphs is summarised in Table 3.2.

#### **Elasto-plastic failure**

The equation describing the stress-strain curve  $\sigma$ - $\varepsilon$  or the elasto-plastic failure of structural elements is obtained by the following formula, valid for both positive (compression or shortening) of hard corners and negative (tension or lengthening) strains of all elements (refer to Figure 3.6):

$$\sigma = \Phi \cdot \sigma_{yd} \tag{3.1}$$

where,

$\Phi$  is an edge function defined as:

$$\begin{aligned} \Phi &= -1 \quad \text{for} \quad \varepsilon < -1 \\ \Phi &= \varepsilon \quad \text{for} \quad -1 < \varepsilon < 1 \\ \Phi &= 1 \quad \text{for} \quad \varepsilon > 1 \end{aligned} \quad (3.2)$$

$\varepsilon$  is the relative strain equal to  $\varepsilon_E/\varepsilon_{yd}$

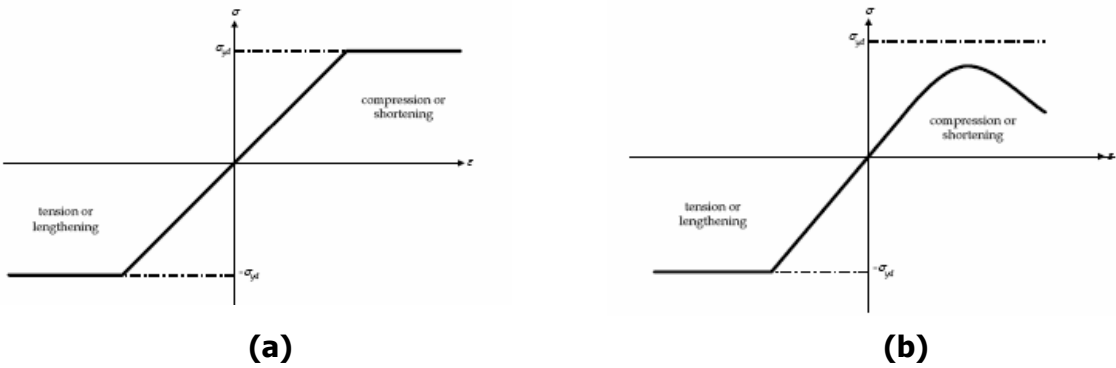


**Fig.3.6.(a)** Elastic perfectly plastic failure of all elements under tension and of hard corners both tensioned or compressed, **(b)** Elasto-plastic failure of stiffeners

### Beam Column Buckling

The equation describing the shortening portion of the stress strain curve  $\sigma_{CR1}-\varepsilon$  for the beam column buckling of stiffeners is obtained by the following formula:

$$\sigma_{CR1} = \Phi \sigma_{C1} \left( \frac{A_{s-net50} + 10^{-2} b_{off-p} t_{net50}}{A_{s-net50} + 10^{-2} s t_{net50}} \right) \quad (3.3)$$

where,

- $\sigma_{C1}$  is the critical stress defined as:

$$\begin{aligned} \sigma_{C1} &= \frac{\sigma_{E1}}{\varepsilon} \quad \text{for} \quad \sigma_{E1} \leq \frac{\sigma_{yd}}{2} \varepsilon \\ \sigma_{C1} &= \sigma_{yd} \left( 1 - \frac{\Phi \sigma_{yd} \varepsilon}{4 \sigma_{E1}} \right) \quad \text{for} \quad \sigma_{E1} > \frac{\sigma_{yd}}{2} \varepsilon \end{aligned} \quad (3.4)$$

- $\sigma_{E1}$  is the Euler Buckling stress defined as:

$$\sigma_{E1} = \pi^2 E \frac{I_{E-net50}}{A_{E-net50} l_{stf}^2} 10^{-4} \quad (3.5)$$

- $\Phi$  edge function defined in the previous paragraph
- $I_{E-net50}$  net moment of inertia of stiffeners with attached plating of width  $b_{eff-s}$
- $b_{eff-s}$  effective width of the attached plating for the stiffener

$$\begin{aligned} b_{eff-s} &= \frac{s}{\beta_p} & \text{for } \beta_p > 1.0 \\ b_{eff-s} &= s & \text{for } \beta_p \leq 1.0 \end{aligned} \quad (3.6)$$

- Plate slenderness ratio

$$\beta_p = \frac{s}{t_{net50}} \sqrt{\frac{\epsilon \sigma_{yd}}{E}} \quad (3.7)$$

Remaining abbreviations are explained at Table 3.2.

<b>Symbol</b>	<b>Description</b>	<b>Calculation</b>
$\epsilon_{yd}$	Strain corresponding to yield stress in the element	$\epsilon_{yd} = \frac{\sigma_{yd}}{E}$
$\sigma_{yd}$	Specified minimum yield stress of the material	-
<b>E</b>	Modulus of elasticity	-
$t_{net50}$	Net thickness of attached plating	-
<b>s</b>	Plate breadth	Spacing between the stiffeners
$A_{s-net50}$	Net area of the stiffener without attached plating	-
$t_{f-net50}$	Net thickness of the flange	-
$b_f$	Breadth of the flange	-
$t_{w-net50}$	Net thickness of the web	-
$d_w$	Depth of the web	-
$l_{stif}$	Span of stiffeners	Spacing between primary support members
$I_{p-net}$	Net polar moment of inertia of the stiffener	$\left( \frac{A_{w-net} (e_f - 0.5t_{f-net})^2}{3} + A_{f-net} e_f^2 \right) 10^{-4}$
$I_{T-net}$	Net St. Venant's moment of inertia of the stiffener	$\frac{(e_f - 0.5t_{f-net}) t_{w-net}^3}{3 \times 10^4} \left( 1 - 0.63 \frac{t_{f-net}}{e_f - 0.5t_{f-net}} \right)$ $+ \frac{b_f t_{f-net}^3}{3 \times 10^4} \left( 1 - 0.63 \frac{t_{f-net}}{b_f} \right)$
$I_{\omega-net}$	Net sectorial moment of inertia of the stiffener	for bulb flats and angles: $\frac{A_{f-net} e_f^2 b_f^2}{12 \times 10^6} \left( \frac{A_{f-net} + 2.6 A_{w-net}}{A_{f-net} + A_{w-net}} \right)$ for T bars: $\frac{b_f^3 t_{f-net} e_f^2}{12 \times 10^6}$
$l_t$	Torsional buckling length	Distance between tripping supports

**Table 3.2.** Abbreviations used for the load-end shortening curves formulas

## Torsional buckling of stiffeners

The equation describing the shortening portion of the stress-strain curve  $\sigma_{CR2-\varepsilon}$  for the lateral-flexural buckling of stiffeners is obtained according to the following formula:

$$\sigma_{CR2} = \Phi \frac{A_{s-net50} \sigma_{C2} + 10^{-2} s t_{net50} \sigma_{CP}}{A_{s-net50} + 10^{-2} s t_{net50}} \quad (3.8)$$

where,

- $\sigma_{C2}$  is the critical stress defined as:

$$\begin{aligned} \sigma_{C2} &= \frac{\sigma_{E2}}{\varepsilon} & \text{for } \sigma_{E2} \leq \frac{\sigma_{yd}}{2} \varepsilon \\ \sigma_{C2} &= \sigma_{yd} \left( 1 - \frac{\Phi \sigma_{yd} \varepsilon}{4 \sigma_{E2}} \right) & \text{for } \sigma_{E2} > \frac{\sigma_{yd}}{2} \varepsilon \end{aligned} \quad (3.9)$$

- $\sigma_{E2}$  is the Euler Buckling stress defined as:

$$\frac{E}{I_{p-net}} \left( \frac{\varepsilon \pi^2 I_{\omega-net} 10^{-4}}{l_i^2} + 0.385 I_{T-net} \right) \quad (3.10)$$

- $\sigma_{CP}$  is the ultimate strength of the attached plating for the stiffener defined as:

$$\begin{aligned} \sigma_{CP} &= \left( \frac{2.25}{\beta_p} - \frac{1.25}{\beta_p^2} \right) \sigma_{yd} & \text{for } \beta_p > 1.25 \\ \sigma_{CP} &= \sigma_{yd} & \text{for } \beta_p \leq 1.25 \end{aligned} \quad (3.11)$$

## Web local buckling of stiffeners with flanged profiles

The equation describing the shortening portion of the stress strain curve  $\sigma_{CR3-\varepsilon}$  for the web local buckling of flanged stiffeners is obtained from the following formula:

$$\sigma_{CR3} = \Phi \sigma_{yd} \left( \frac{b_{off-s} t_{net50} + d_{w-off} t_{w-net50} + b_f t_{f-net50}}{s t_{net50} + d_w t_{w-net50} + b_f t_{f-net50}} \right) \quad (3.12)$$

where,

- $d_{w\text{-eff}}$  is the effective depth of the web

$$\begin{aligned} d_{w\text{-eff}} &= \left( \frac{2.25}{\beta_w} - \frac{1.25}{\beta_w^2} \right) d_w \quad \text{for } \beta_w > 1.25 \\ d_{w\text{-eff}} &= d_w \quad \text{for } \beta_w \leq 1.25 \end{aligned} \quad (3.13)$$

- $\beta_w$  is the web slenderness ratio

$$\beta_w = \frac{d_w}{t_w} \sqrt{\frac{\varepsilon \sigma_{yd}}{E}} \quad (3.14)$$

### 3.4.5. Alternatives methods

The CSR Rules account for alternative methods to the ones adopted by the rules for the evaluation of the ultimate hull girder capacity subject that all the relevant effects important to the non-linear response with due considerations of the following are taken into account:

- non-linear geometrical behavior
- inelastic material behavior
- geometrical imperfections and residual stresses (geometrical out-of flatness of plate and stiffeners)
- simultaneously acting loads such as bi-axial compression, bi-axial tension, shear and lateral pressure
- boundary conditions
- interactions between buckling modes
- interactions between structural elements such as plates, stiffeners, girders etc.
- post-buckling capacity

These methods are described below.

#### 3.4.5.1. Incremental-iterative procedure

The most generally used method to assess the hull girder ultimate moment capacity is to derive the non-linear moment-curvature relationship,  $M-\kappa$ , by incrementally increasing the bending curvature,  $\kappa$ , of the hull section between two



adjacent transverse frames and then identifying the maximum moment along this curve as the ultimate bending capacity,  $M_U$ .

As per CSR Rules the M- $\kappa$  curve is to be based on the axial non-linear P- $\epsilon$  (load/strain) load shortening curves for individual structural component in the cross-section considering all relevant structural effects as listed above.

### 3.4.5.2. Non-linear finite element analysis

CSR Rules allow for advanced non-linear finite element analyses models to be used for the assessment of the hull girder ultimate capacity provided that such models consider the relevant effects important to the non-linear responses as listed above. Particular attention is required to be given to modelling the shape and size of geometrical imperfections. It is to be ensured that the shape and size of geometrical imperfections trigger the most critical failure modes.

## 3.5. Net Thickness Approach

The philosophy behind the net thickness approach is to:

- provide a direct link between the thickness used for strength calculations during the new building stage and the minimum thickness accepted during the operational phase
- enable the status of the structure with respect to corrosion to be clearly ascertained throughout the life of the ship.

This philosophy is illustrated in Figure 3.7.

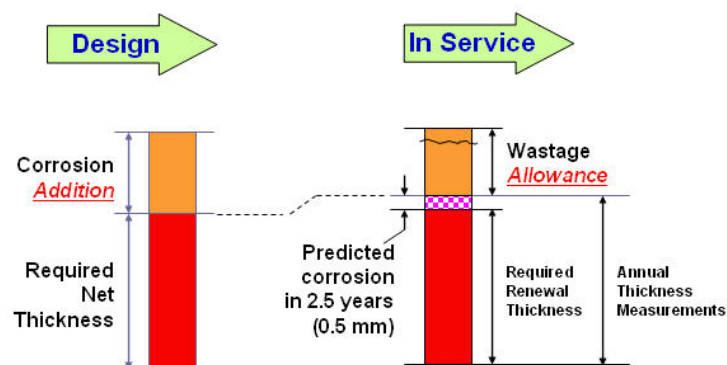
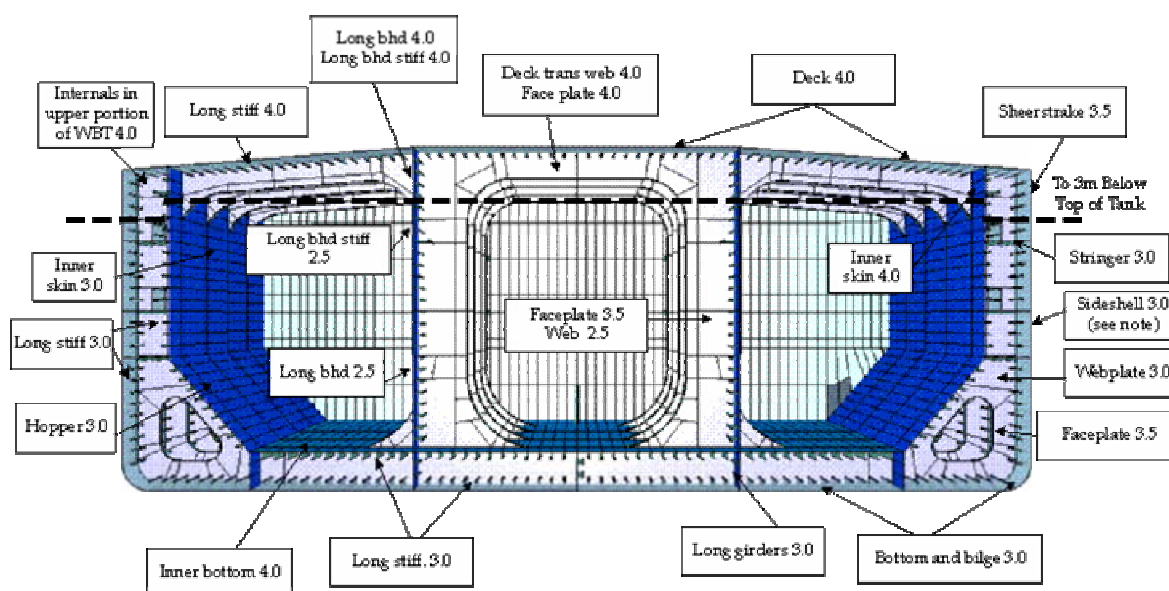


Fig.3.7. Net Thickness Approach

The required gross thickness of a structural element is given by adding the corrosion addition ( $t_{corr}$ ) to the required rounded net thickness as defined by the rules. The thickness at which annual surveys are required is obtained by subtracting the total wastage allowance from the as-built thickness. The thickness at which renewal is required is obtained by subtracting the total wastage allowance and the thickness  $t_{corr-2.5}$  from the as-built thickness. The thickness  $t_{corr-2.5}$  is the wastage allowance in reserve for corrosion occurring in the two and half years between Intermediate and Special surveys.

The assessment of hull girder scantlings is based on the overall global corrosion, by deducting half the local corrosion addition for all structural members simultaneously. The assumption is that the full local corrosion will not occur globally and hence a lesser average value of assumed corrosion is appropriate. Individual structural elements may corrode to the maximum corrosion addition and this is taken into account in the buckling assessment.

The corrosion addition considered for the structural elements of a double oil tanker is depicted in Figure 3.8.



**Fig.3.8.** Corrosion addition considered for double hull oil tankers

## **CHAPTER 4**

### **FINITE ELEMENT ANALYSIS**

#### **4.1. General**

As already mentioned, the present study aims to verify the CSR Incremental-Iterative Approach for the estimation of the Hull Girder's Ultimate Capacity. For this purpose, a finite element analysis is carried out by using the software ABAQUS while a double hull oil tanker has been used as a case study. This Chapter describes in general the finite element procedure for the simulation/analysis of a structure, introduces the finite element code used and presents the code's relevant features and theory.

#### **4.2. Finite Element Analysis Procedure**

The finite element method (FEM), sometimes referred to as finite element analysis (FEA), is a computational technique used to obtain approximate solutions of physical problems in engineering. More specifically, FEM is a numerical method seeking an approximated solution of the distribution of field variables in the problem domain that is difficult to obtain analytically. It is done by dividing the problem domain into several elements, which usually have a very simple geometry, and then introducing approximate functions to describe the response of each element in terms of variables evaluated at selected positions on its boundary, referred to as the nodes. In brief, the procedure of a finite element analysis is shown in Figure 4.1.

The physical problem typically involves an actual structure or structural component subject to certain loads. This physical problem under certain assumptions is idealised to a mathematical model governed by differential equations. It is self explanatory that the finite element method will solve only the mathematical problem and that any assumptions made to the idealisation of the physical problem will affect the solution of the mathematical model. In this respect the choice of a mathematical problem is crucial, determines the accuracy of the results and the extent of insight into the actual physical problem. The assumptions that have to be made during the

idealisation of the mathematical problem include but, are not limited to, the geometry or domain of the system, the properties of the material or medium, the boundary, loading initial and conditions.

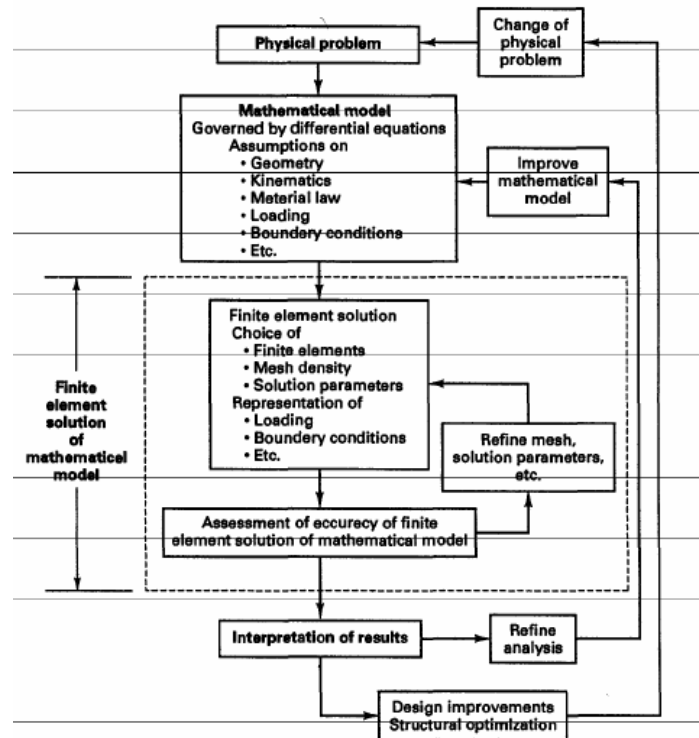


**Fig.4.1.** Illustration of the Finite Element Analysis Procedure

In the next step the mathematical model is turned into a finite element model. For this purpose the modelled geometry is discretized into finite elements, any initial imperfections in the structure are introduced into the model, and the boundary/loading conditions are specified at the nodes or element faces.

Upon the solution of the equations, which are obtained when the mathematical model is divided into finite elements, a decision has to be made on whether the analysis needs to be refined, for example using an alternative type of element or reducing the element size (i.e. a mesh refinement), in order to improve the accuracy of the results and hence the insight into the physical problem, or alternatively, whether the assumptions built into the mathematical model need to be altered.

The following paragraphs introduce the features of the finite element code (ABAQUS) used in this study for the processing/definition of the Finite Element Model

and in particular features related to buckling prediction, element selection, and non linear static analysis.

### 4.3. The Finite Element Code ABAQUS

The finite element code used is ABAQUS/Standard which is a general-purpose analysis module that can solve a wide range of linear and nonlinear problems involving the static, dynamic, thermal, and electrical response of components.

A complete ABAQUS/Standard analysis, as shown in Figure 4.2, consists of three distinct stages: pre-processing, simulation, and post-processing.

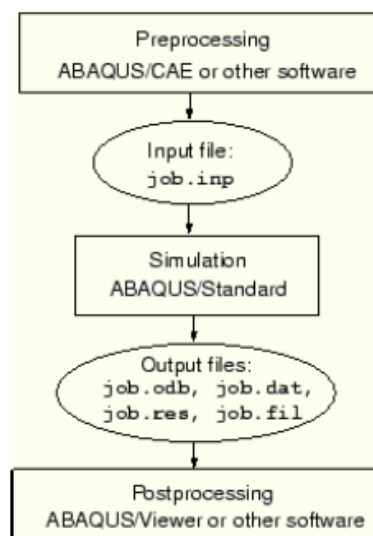


**Fig.4.2.** Abaqus/Standard Analysis Stages

The pre-processing relates to the development of the FE model of the physical problem, the simulation refers to the solution of the mathematical problem, whereas the post-processing is the display/evaluation process of the results obtained from a solution of the FE equations.

## 4.4. Finite Elements issues in the ABAQUS code

### 4.4.1. Finite Elements in general

A crucial part of the finite element model definition is the meshing of the geometry and in particular the selection of the elements size and type. The selected finite elements not only define the basic geometry of the physical structure but also affect the results obtained by the simulation. The greater the mesh density, the more

accurate are the results and thus the response of the mathematical model. It should be noted that a simulation is considered successful if beyond a certain mesh density the analysis converges to a unique solution.

In the ABAQUS FE Code each element type is characterised by the following:

- **Family.** The family of each element mainly characterizes the geometry type of the element. ABAQUS range of element families most commonly used in stress analyses is shown in Figure 4.3.
- **Degrees of freedom (directly related to the element family).** The degrees of freedom (dof) are the fundamental variables calculated during the analysis. For a stress/displacement simulation the degrees of freedom are the translations as well as, for shell and beam elements, the rotations at each node.
- **Number of nodes.** The fundamental variables are calculated only at the nodes of the element. At any other point in the element, the variables are obtained by interpolating from the nodal variables. The interpolation order is determined by the number of nodes used in the element. Elements that have nodes only at their corners, use linear interpolation in each direction (linear elements or first-order elements) whereas elements with midside nodes use quadratic interpolation (quadratic elements or second-order elements).
- **Formulation.** An element's formulation refers to the mathematical theory used to define the element's behaviour. All of the stress/displacement elements in ABAQUS are based on the Lagrangian or material description of behaviour: the material associated with an element remains associated with the element throughout the analysis, and material cannot move among elements.
- **Integration.** ABAQUS uses numerical techniques to integrate various quantities over the volume of each element. Using Gaussian quadrature for most elements, ABAQUS evaluates the material response at each integration point in each element.

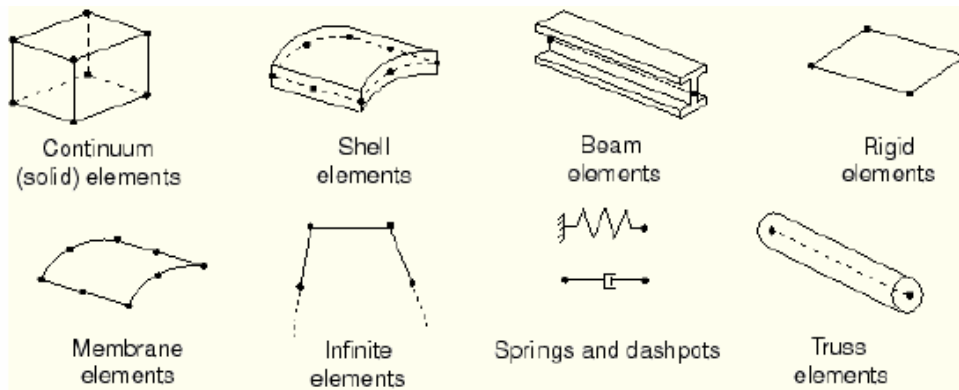


**Fig.4.3.** Abaqus elements

#### 4.4.2. Shell Elements

Shell elements are used to model structures in which one dimension (the thickness) is significantly smaller than the other dimensions, and the stresses normal to the thickness direction are negligible.

When using shell elements the user can choose numerical integration to be carried out independently at each section point (integration point) through the thickness of the shell, thus allowing for nonlinear material behaviour or linear elastic material behaviour. The location of the single integration point in an S4R (4-node, reduced integration) element and the configuration of the section points through the shell thickness are shown in Figure 4.4.

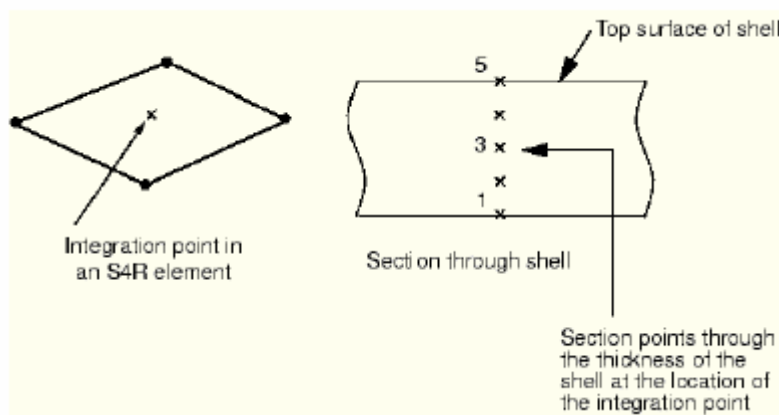


**Fig.4.4.** Integration of shell elements

There are three different classes of shell elements, thin-only shell elements, thick-only shell elements and general-purpose shell elements which are valid for use with both thick & thin shell problems and allow finite membrane strains. Thick-only shell elements apply to problems at which the effects of transverse shear deformation are important for the solution. Thin-only shell elements, on the other hand, apply to problems at which that transverse shear deformation is small enough and can be neglected.

In the present study the **S4** element has been used, which is a general purpose, fully integrated, 4-node shell element. Through thickness integration is carried out using either a Simpson or Gauss integration. The element formulation accounts for both large displacements/rotations and finite membrane strains. Despite it's higher computational cost, due to the full integration, it is expected to give greater accuracy for the highly nonlinear response of a stiffened panel.

## **4.5. Linear Buckling Analysis in ABAQUS**

Buckling Analysis is usually performed prior to a non-linear static analysis in order to determine the buckling modes and therefore to define candidate initial geometric imperfections in the structure in accordance with these buckling modes. This was the procedure also adopted at present study to introduce appropriate initial imperfections into the FE model. For further information, reference is made to Chapter 7.

The buckling modes are normalized vectors so that the maximum displacement component has a magnitude of 1.0. They do not represent actual magnitudes of deformation but they predict the likely buckling mode of the structure.

The resulting eigenvalue problem is expressed by the following formula:

$$(K_0^{NM} + \lambda_i K_{\Delta}^{NM}) v_i^M = 0,$$

where,



$K_0^{N, M}$  is the stiffness matrix corresponding to the base state, which includes the effects of the preloads  $P^N$ , if any

$K_{\Delta}^{N, M}$  is the differential initial stress and load stiffness matrix due to the applied loading pattern,  $Q^N$

$\lambda_i$  are the eigenvalues

$u_i^M$  are the buckling mode shapes (eigenvectors)

M and N refer to degrees of freedom M and N of the whole model

i refers to the  $i^{\text{th}}$  buckling mode.

The critical buckling loads are then  $P^N + \lambda_i \cdot Q^N$ .

## 4.6. Non Linear FE Analysis in ABAQUS

Taking into account that during the collapse of a stiffened panel its response is highly nonlinear, the ABAQUS nonlinear analysis algorithms are relevant here. In a non linear analysis the structure's stiffness changes as it deforms and as a result the stiffness matrix of the structure has to be assembled and inverted many times during the course of the analysis. This is not the case for the linear analysis where there is a linear relationship between the applied loads and the response of the system (refer to figure 4.5).

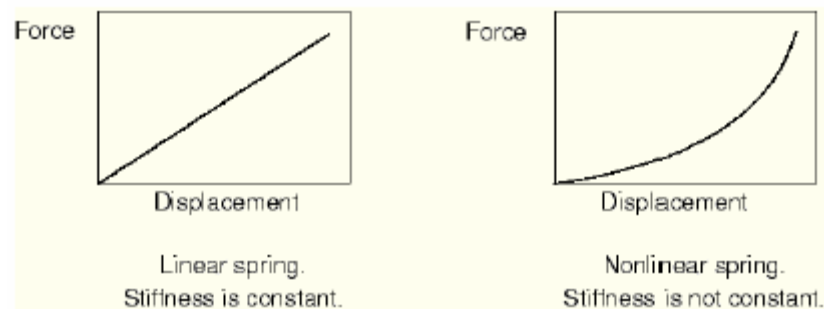


**Fig.4.5.** Linear and Non-Linear Analysis

There are three sources of nonlinearity in structural mechanics simulations:

- **Material nonlinearity.** Most metals have a fairly linear stress/strain relationship at low strain values, but at higher strains the material yields, and the response becomes nonlinear and irreversible.

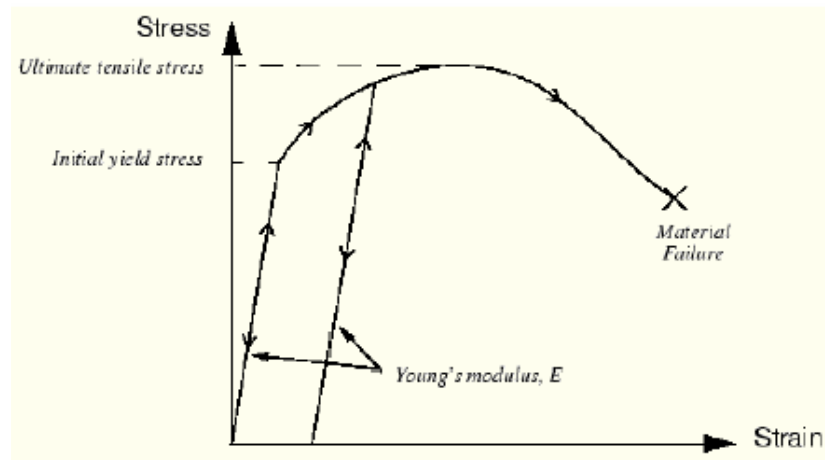


**Fig.4.6.** Linear and Non-Linear Analysis

- **Boundary nonlinearity.** Boundary nonlinearity occurs if the boundary conditions change during the analysis, for example due to changes in contact.
- **Geometric nonlinearity.** Geometric nonlinearity occurs whenever the magnitude of the displacements affects the response of the structure. This may be caused by large deflections or rotations, snap through, initial stresses or load stiffening.

ABAQUS can solve both linear and non linear problems. At this point, it would be useful to briefly discuss the procedure that ABAQUS uses for the solution of non linear problems.

#### 4.6.1. Static Non Linear Analysis

ABAQUS uses the Newton-Raphson method to obtain iteratively the solution of the nonlinear equations resulting due to the nonlinearities mentioned above. In a nonlinear analysis the solution cannot be calculated by solving a single system of equations, as would be done in a linear problem. Instead, the solution is found by applying the specified loads gradually and incrementally working towards the final solution. In this respect, the simulation is divided into a number of load increments at the end of each an approximate equilibrium configuration is found.

Let us consider the internal nodal forces caused by the element's stresses  $I$ , and the external forces  $P$ , acting on a body (refer to figure 4.7). Equilibrium is achieved when the forces acting at every node equals to zero:  $P - I = 0$ .

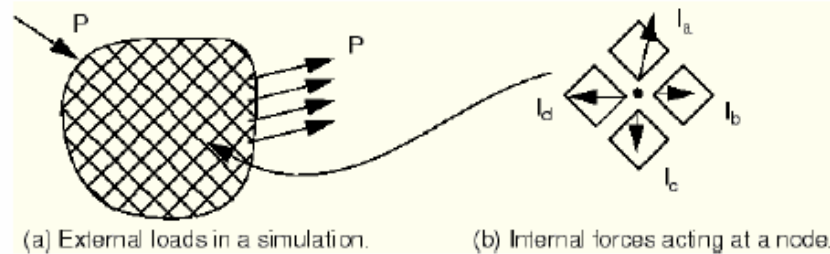


**Fig.4.7.** Linear and Non-Linear Analysis

The total load applied is broken into smaller increments for each of which the FE Code searches for a solution that converges. Let us consider the non linear response of figure 4.8.

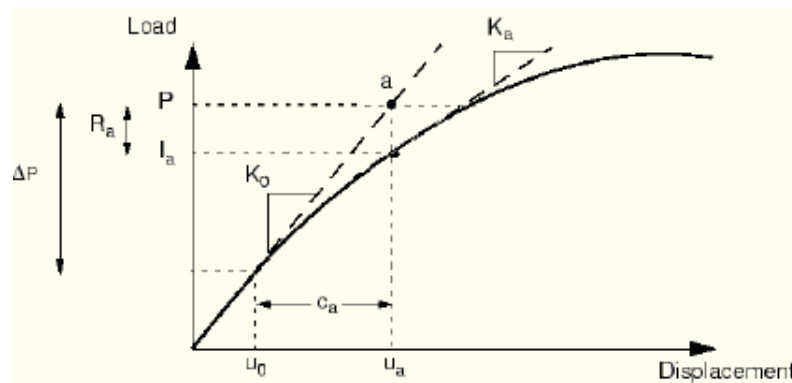


**Fig.4.8.** Non Linear analysis - Newton-Raphson method

ABAQUS uses the structure's initial stiffness,  $\mathbf{K}_0$ , which is based on its configuration at  $\mathbf{u}_0$ , and the increment in load  $\Delta \mathbf{P}$  to calculate a displacement correction,  $\mathbf{c}_a$ , for the structure. Using  $\mathbf{c}_a$ , the structure's configuration is updated to  $\mathbf{u}_a$ , a new stiffness  $\mathbf{K}_a$ , for the structure is formed, and the structure's internal forces,  $\mathbf{I}_a$ , are calculated. Then the difference between the total applied load,  $\mathbf{P}$ , and  $\mathbf{I}_a$  is calculated, giving  $\mathbf{R}_a$  which is the force residual for the iteration.

When the residual force vector  $\mathbf{R}_a$  is zero at every degree of freedom in the model, the structure is in equilibrium and point  $\mathbf{a}$  lies on the load-deflection curve.

Since in practice  $\mathbf{R}_a$  is almost impossible to be equal to zero, it is compared to a tolerance value. If, following a number of iterations,  $\mathbf{R}_a$  is found to be less than this tolerance value, an additional check is being performed prior to accepting the updated configuration as the equilibrium solution. More specifically, the displacement correction,  $\mathbf{c}_a$ , is also checked to be relatively small to the total incremental displacement,  $\Delta \mathbf{u}_a = \mathbf{u}_a - \mathbf{u}_0$ .

If  $\mathbf{c}_a$  is greater than 1% of the incremental displacement, another iteration is performed until both convergence checks are satisfied. Only then the solution is said to have fully converged for that load increment. It should be noted that, by default, the tolerance value of the residual force is set to 0.5% of a spatially and over time average force in the structure.

If the solution from an iteration has not converged, another iteration is performed to try to bring the internal and external forces into balance. This second iteration uses the stiffness  $\mathbf{K}_a$ , calculated at the end of the previous iteration together with  $\mathbf{R}_a$  to determine another displacement correction  $\mathbf{c}_b$ , that brings the system closer to equilibrium (refer to point b in Figure 4.9).

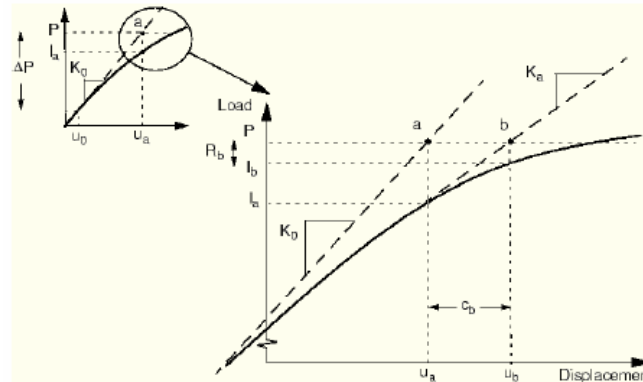


**Fig.4.9.** Non Linear analysis – Procedure for iterations

It often takes ABAQUS several iterations to determine an acceptable solution to a given load increment. The sum of all the incremental responses is the approximate solution of the nonlinear analysis.

#### 4.6.2. Riks Non Linear Analysis

It is often necessary to obtain nonlinear static equilibrium solutions for unstable problems, where the load displacement response may exhibit the type of

behaviour sketched in Figure 4.10 at which the load and/or the displacement decreases as the solution evolves. In such cases Abaqus uses the modified Riks method in order to find the solution.

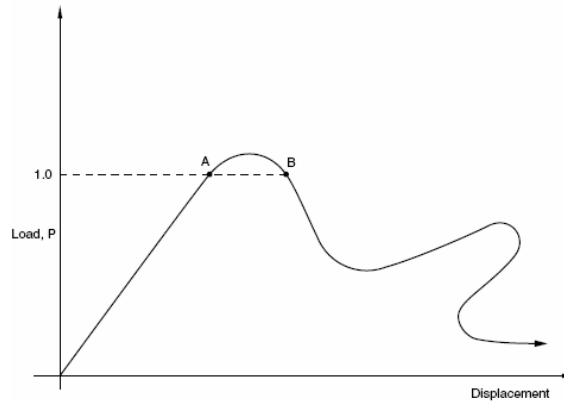


**Fig.4.10.** Non Linear analysis – Riks Method

The Riks method uses the load magnitude as an additional unknown while the progress of the solution is measured by the “arc length,”  $l$ , along the static equilibrium path of the load-displacement curve.

The loading during a Riks step is always proportional. The current load magnitude is defined by:

$$P_{\text{total}} = P_0 + \lambda(P_{\text{ref}} - P_0).$$

where,  $P_0$  is the “dead load,”  $P_{\text{ref}}$  is the reference (applied) load vector, and  $\lambda_f$  is the “load proportionality factor” which is found as part of the solution. Dead loads are any loads that exist at the beginning of the step and are not redefined. The Riks algorithm has been used here in cases where the static nonlinear analysis algorithm failed to converge, as discussed in Chapter 7.

## **CHAPTER 5**

### **DETAILS OF THE VESSEL USED IN THIS STUDY**

#### **5.1. General**

As already mentioned, subject study aims to calculate the ultimate hull girder strength assessment of a vessel by using both semi-analytical and computational approaches. For this purpose, the computation of the ultimate hull girder capacity of a double hull oil tanker is carried out as a case study. The scope of this chapter is the presentation of the vessel's particulars and the description of its structure amidships. In particular, details regarding the steel material and the scantlings of the midship section are reported. Moreover, design still water and wave bending moments are presented.

#### **5.2. Vessel's particulars**

The vessel used in subject study is a double hull Product Tanker of 47.326 tn deadweight tonnage carrying crude oil as well as clean & dirty petroleum in bulk. It has a continuous freeboard deck without forecastle or poop deck while the main hull under the main deck is divided in six pairs of cargo oil tanks. Hull construction is of mild steel of minimum yield stress  $245 \text{ Nt/mm}^2$  and of high tensile steel of minimum yield stress  $315 \text{ Nt/mm}^2$ .

It should be highlighted that the keel was laid on 2004 prior to the entry into force of the Common Structural Rules (1<sup>st</sup> April 2006) and under the supervision of a well recognized Classification Society, American Bureau of Shipping (ABS), member of the IACS Community.

Table 5.1 summarizes vessel's main particulars whereas Figure 5.1 depicts its profile and tank top view.

Length between perpendiculars	$L_{BP}=172.00$ m
Length Overall	$L_{OA}=182.50$ m
Scantling Length (0,97 LWL)	$L_{SC}=171.69$ m
Moulded Breadth	$B=32.20$ m
Moulded Depth	$D=18.10$ m
Design Draft	$T= 11.30$ m
Scantling Draft	$T_{SC}=12.60$ m
Deadweight at design draft	$DWT=40854$ tn
Deadweight at scantling draft	$DWT=47326$ tn

**Table 5.1.** Vessel's Main Particulars

### 5.3. Midship Section

The vessel which in way of the midship section area is longitudinally stiffened, as shown in Figure 5.2, comprises of a Double Bottom, Side Ballast Tanks and a Centre Line Bulkhead. Inner Bottom and Bottom plating are stiffened by the longitudinals and the transverse floors whereas Inner Bulkhead Plating and Shell plating are stiffened by the longitudinals and the web transverses. The spacing of the transverse frames is 4050mm while the spacing of the stiffeners varies, dependent on the stiffened panel considered, from 825mm (inner bottom, bottom, main deck) to 850mm (side shell, inner bulkhead, CL bulkhead). Smaller stiffener spacing is accounted for the stingers (702.5mm) and the girders (677.5mm and 725mm).

For the purpose of the present study and for the more efficient presentation of the results, the midship section has been divided in nineteen (19) major stiffened panels for each of which the results are presented separately in Chapter 7. The nomenclature of the panels is defined in Figure 5.2. All panels are considered to extend between the vessel's web frames (4050mm) and the adjacent primary support members (stringers, decks, girders, bulkheads whichever applicable).

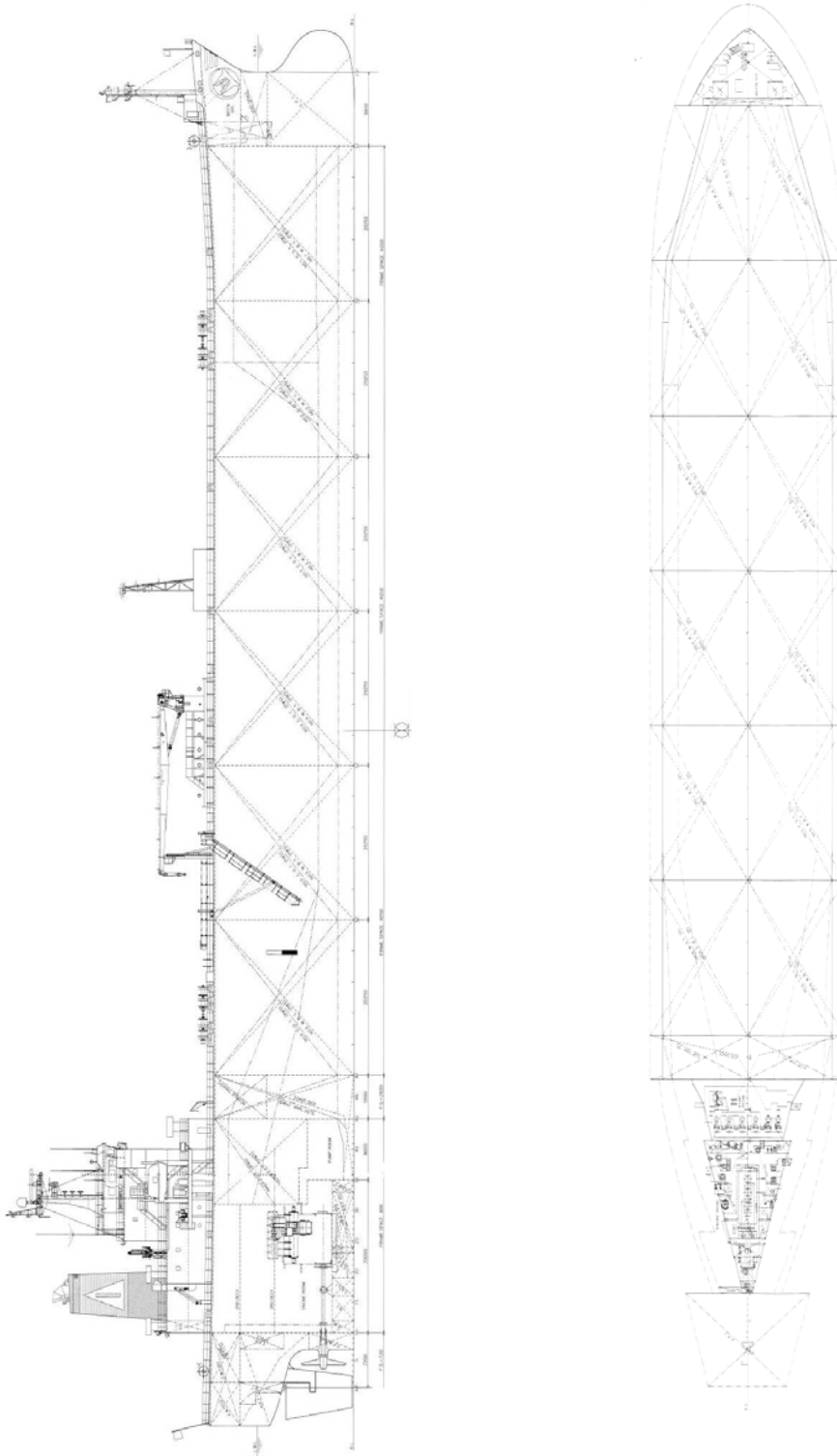


**Fig.5.1.** Vessel's profile view and tank top view



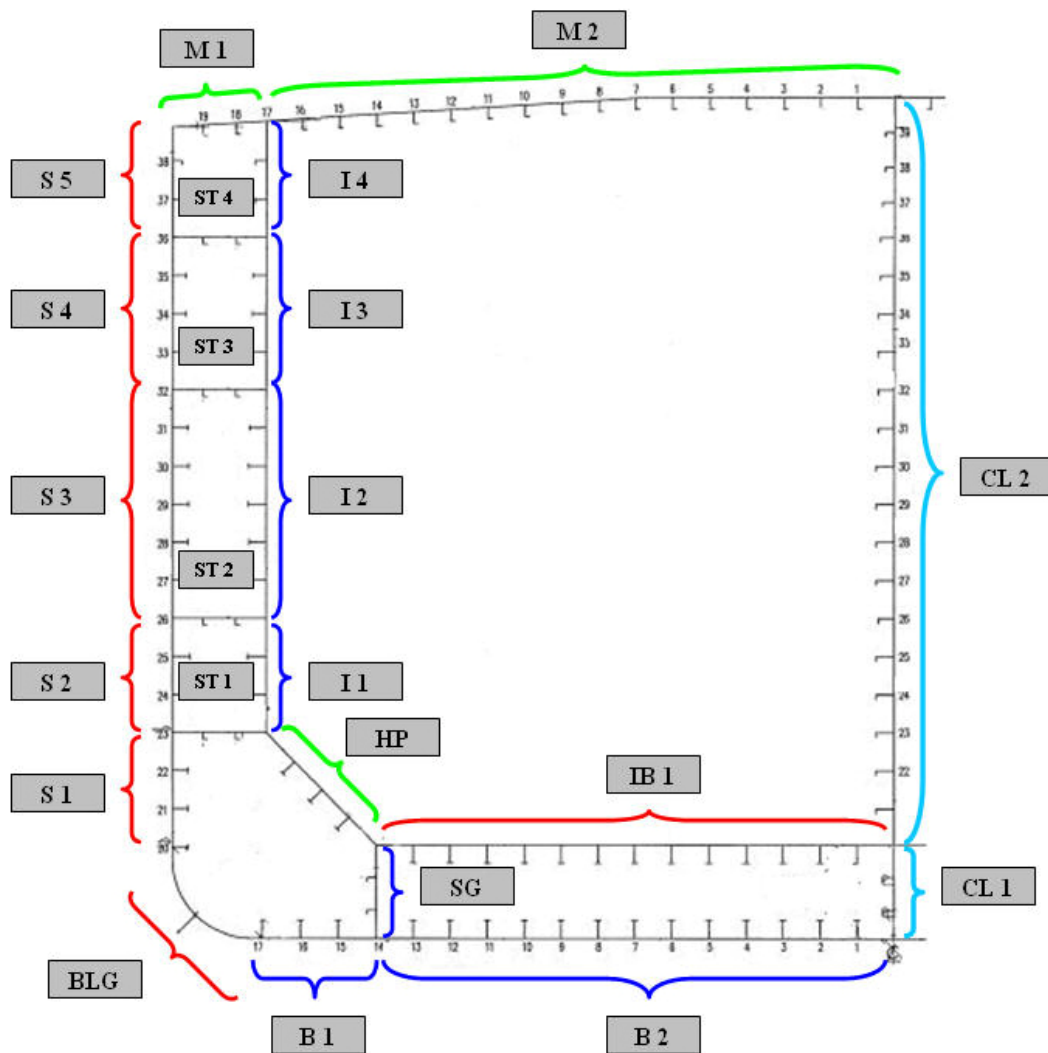


**Fig.5.2.** Nomenclature of considered midship section panels

The breadth ( $b$ ), span ( $a$ ), aspect ratio ( $a/b$ ), plate slenderness ratio  $\{(b/t) \cdot (\sigma_{yd}/E)^{1/2}\}$  and web slenderness ratio  $\{(d_w/t_w) \cdot (\sigma_{yd}/E)^{1/2}\}$  of all structural elements per stiffened panel is indicated in the following paragraphs. The nomenclature of the stiffener's dimensions are as per Figure 2.3. It should be noted that the geometric properties summarized herewith correspond to the gross thickness of the panels without taking into account the deduction due to corrosion addition. The plate slenderness ratio is in the range of 2.25-2.37 for the bottom and side shell plating, 2.31-2.83 for Inner Bulkhead, 2.22-2.76 for CL Bulkhead and 1.86-2.22 for Main Deck and Inner Bottom. The web slenderness ratio is in the range 0.8-1.34 for Side Shell, Inner Bulkhead and CL Bulkhead, 0.898 for Main Deck, 1.475 for Inner Bottom Plating and 1.486 for Bottom Plating.

At appendix A of the present dissertation a copy of the midship section plan is attached.

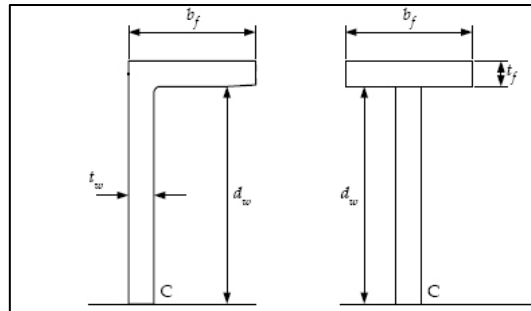


**Fig.5.3.** Nomenclature of Stiffeners' dimensions

### 5.3.1. Bottom Plating Panels

The bottom plating comprises of panels B1 and B2 divided by the side girder. The thickness of the bottom plating is not identical along the panel B-2 as indicated in bellow figure. Dimensions and geometry properties of the bottom plating panels are shown in Figure 5.4 and Table 5.2 respectively. The numbering of each stiffener along the panels follows the numbering shown in figure 5.4. Both Plating and Stiffeners of the Bottom Plating have minimum yield stress of 315 Nt/mm<sup>2</sup>. It should be noted that "AH" denotes the structural elements of high tensile strength steel (315 Nt/mm<sup>2</sup>).

Panel	Stiffener Spacing (b)	Stiffeners ID No	Plate Thickness (t <sub>p</sub> )	Web (d <sub>w</sub> x t <sub>w</sub> )	Flange (b <sub>f</sub> x t <sub>f</sub> )	Aspect Ratio (a/b)	Plate Slenderness Ratio	Web Slenderness Ratio	
	(mm)	(-)	(mm)	(mm)	(mm)	(-)	(mm)	(mm)	
<b>B1</b>	850	<b>B1-15</b>	14 <sup>AH</sup>	381x10	125x19 <sup>AH</sup>	4.765	2.368	1.486	
		<b>B1-16</b>							
	675	<b>B1-17</b>							
<b>B2</b>	825	<b>B2-1</b>	14 /15.5 <sup>AH</sup>	381x10	125x19 <sup>AH</sup>	4.909	2.102	1.486	
		<b>B2-2</b>	14 <sup>AH</sup>				2.299		
		<b>B2-3</b>							
		<b>B2-4</b>							
		<b>B2-5</b>							
		<b>B2-6</b>	14 /14.5 <sup>AH</sup>				2.284		
		<b>B2-7</b>	14.5 <sup>AH</sup>						2.220
		<b>B2-8</b>							
		<b>B2-9</b>							
		<b>B2-10</b>	14 /14.5 <sup>AH</sup>				2.296		
		<b>B2-11</b>							
		<b>B2-12</b>	14 <sup>AH</sup>				2.299		
<b>B2-13</b>									

**Table 5.2.**Geometry properties of Bottom Plating Panels

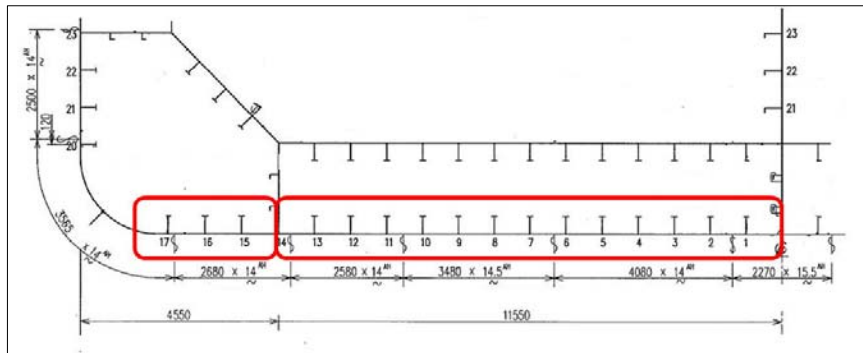


**Fig.5.4.** Bottom Plating Panels

### 5.3.2. Side Shell Panels

The side shell is divided in 5 panels (S1-S5) extending in height between the stringers of the side ballast tanks. As opposed to the bottom plating, the thickness of the side shell plating is identical along the panels, 14mm. The same applies for the steel type of the plates which is high tensile steel (315 Nt/mm<sup>2</sup>). The dimensions of the stiffeners though, differ substantially along the panels (refer to Figure 5.5) while the steel type is mild steel for panels S2-S5 (245 Nt/mm<sup>2</sup>) and high tensile steel for panel S1 (315 Nt/mm<sup>2</sup>). Geometry properties of the side shell plating panels are indicated in Table 5.3. The numbering of each stiffener along the panels follows the numbering shown in figure 5.5.

Panel	Stiffener Spacing (b)	Stiffeners ID No	Plate Thickness (t <sub>p</sub> )	Web (d <sub>w</sub> x t <sub>w</sub> )	Flange (b <sub>f</sub> x t <sub>f</sub> )	Aspect Ratio (a/b)	Plate Slenderness Ratio	Web Slenderness Ratio
	(mm)							
S1	715	S1-20	14 <sup>AH</sup>	331x10	125x19 <sup>AH</sup>	5.664	1.992	1.291
	850	S1-21						
		S1-22						
S2	850	S2-24	14 <sup>AH</sup>	384x10	125x16 <sup>MS</sup>	4.765	2.368	1.321
		S2-25		374x10				1.287
S3	850	S3-27	14 <sup>AH</sup>	334x10	125x16 <sup>MS</sup>	4.765	2.368	1.149
		S3-28		324x10				1.115
		S3-29		344x10	100x16 <sup>MS</sup>			1.183
		S3-30		344x10				
		S3-31		334x10				1.149
S4	850	S4-33	14 <sup>AH</sup>	294x10	100x16 <sup>MS</sup>	4.765	2.368	1,011
		S4-34		274x10				0.943
		S4-35		274x10				
S5	850	S5-37	14 <sup>AH</sup>	186x8	90x14 <sup>MS</sup>	4.765	2.368	0.800
	805	S5-38				5.031	2.243	

**Table 5.3.** Geometry properties of Side Shell panels

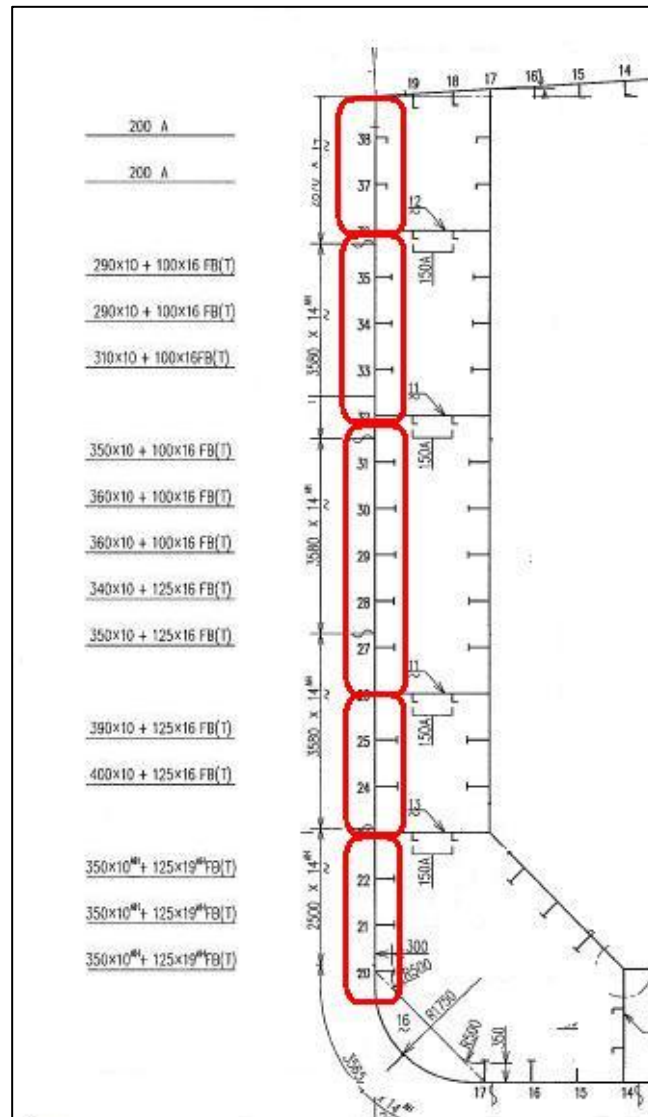


**Fig.5.5. Side Shell Panels**

### 5.3.3. Inner Bulkhead Panels

The inner bulkhead comprises of 4 panels (I1-I4) as shown in Figure 5.6. The thickness and the steel type of the inner bulkhead plating and stiffeners vary along the panels. Dimensions-steel type and geometry properties of the inner bulkhead panels are shown in Figure 5.6 and Table 5.4 respectively. The numbering of each stiffener along the panels follows the numbering shown in Figure 5.4. It should be noted that "AH" denotes the structural elements of high tensile strength steel.

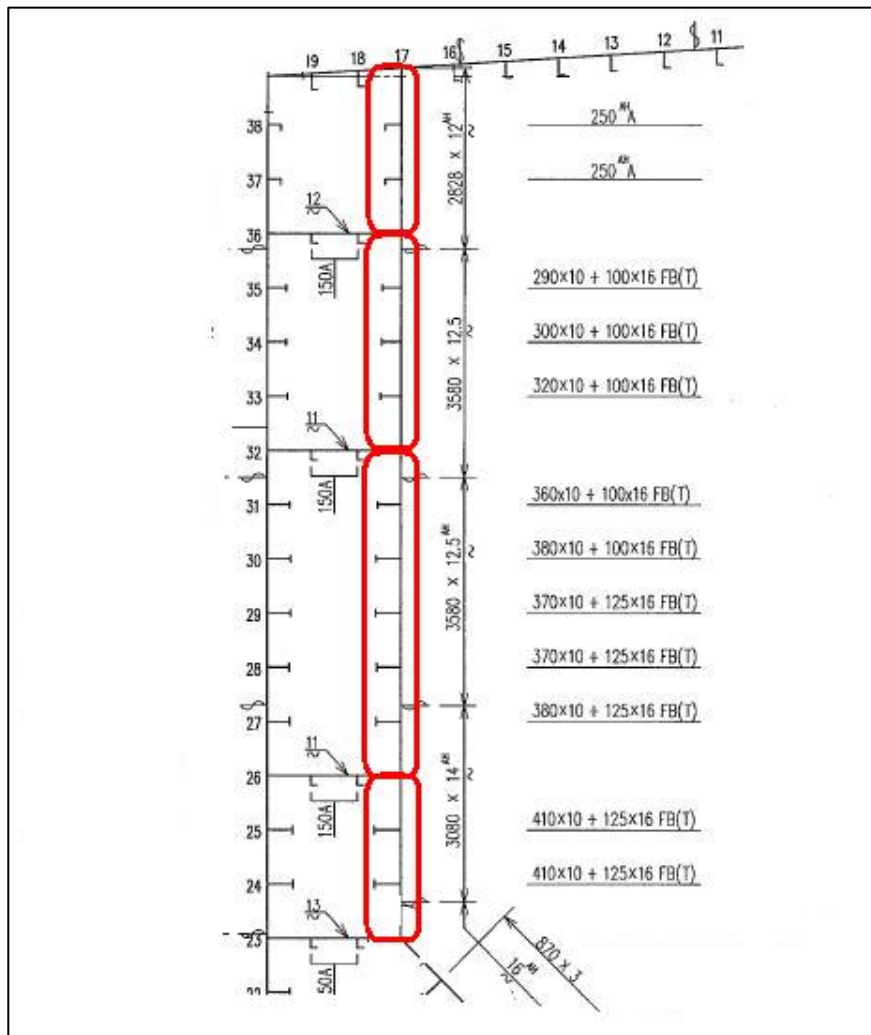


**Fig.5.6.** Inner Bulkhead Panels

Panel	Stiffener Spacing (b)	Stiffeners ID No	Plate Thickness ( $t_p$ )	Web ( $d_w \times t_w$ )	Flange ( $b_f \times t_f$ )	Aspect Ratio (a/b)	Plate Slenderness Ratio	Web Slenderness Ratio
	(mm)		(mm)	(mm)	(mm)		(mm)	(mm)
<b>I1</b>	850	<b>I1-24</b>	14 <sup>AH</sup> 16 <sup>AH</sup>	394x10	125x16 <sub>MS</sub>	4.765	2.312	1.335
		<b>I1-25</b>	14 <sup>AH</sup>				2.368	
<b>I2</b>	850	<b>I2-27</b>	12.5 <sup>AH</sup> 14 <sup>AH</sup>	364x10	125x16 <sub>MS</sub>	4.765	2.422	1.252
		<b>I2-28</b>	12.5 <sup>AH</sup>	354x10				100x16 <sub>MS</sub>
		<b>I2-29</b>		354x10	1.252			
		<b>I2-30</b>	364x10	1.183				
		<b>I2-31</b>	344x10					
<b>I3</b>	850	<b>I3-33</b>	12.5 <sup>MS</sup>	304x10	100x16 <sub>MS</sub>	4.765	2.653	1.046
		<b>I3-34</b>		284x10				0.977
		<b>I3-35</b>		274x10				0.943
<b>I4</b>	850	<b>I4-37</b>	12 <sup>AH</sup>	235x9	90x15 <sup>AH</sup>	4.661	2.763	1.019
	869.0	<b>I4-38</b>					2.825	

**Table 5.4.** Geometry properties of Inner Bulkhead Panels

### 5.3.4. CL Bulkhead Plating

The CL Bulkhead plating is divided in two (2) panels (CL1-CL2), the centre line girder and the remaining bulkhead. The centre line girder and stiffeners are of high tensile steel as opposed to the centre line bulkhead where the steel type varies significantly not only at the plate but at the stiffeners as well. Dimensions and geometry properties of the CL Bulkhead plating panels are shown in Figure 5.6 and Table 5.5 respectively. The numbering of each stiffener along the panels follows the numbering shown in figure 5.7. It should be noted that "AH" denotes the structural elements of high tensile strength steel.

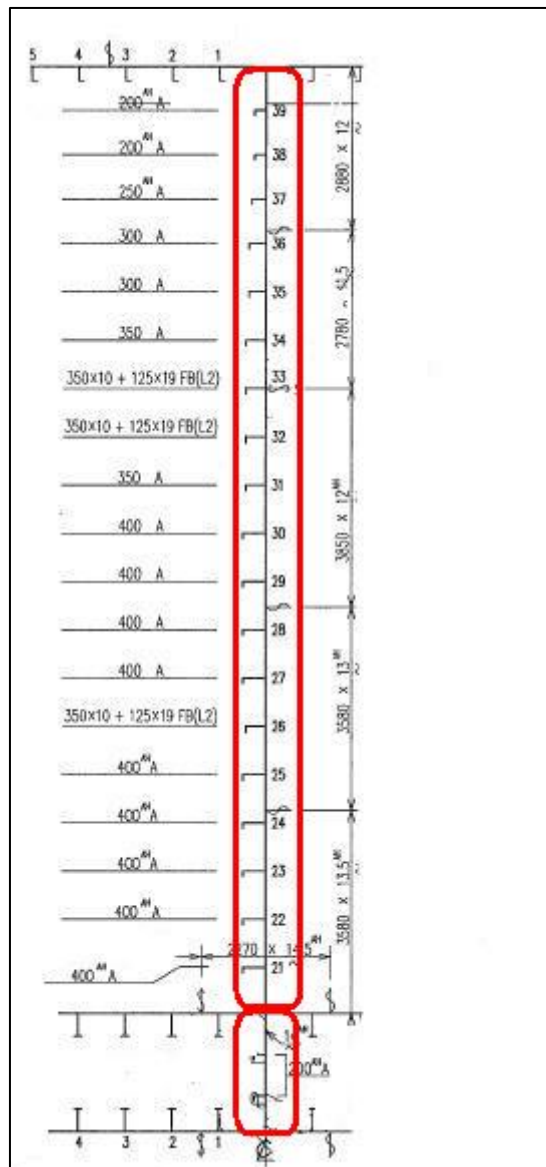


Fig.5.7. CL Bulkhead Panels

Panel	Stiffener Spacing (b)	Stiffeners ID No	Plate Thickness ( $t_p$ )	Web ( $d_w \times t_w$ )	Flange ( $b_f \times t_f$ )	Aspect Ratio (a/b)	Plate Slenderness Ratio	Web Slenderness Ratio	
	(mm)	(-)	(mm)	(mm)	(mm)	(-)	(mm)	(mm)	
<b>CL1</b>	850	<b>CL 1-1</b>	14 <sup>AH</sup>	186x8	90x14 <sup>AH</sup>	4.765	2.368	0.907	
		<b>CL 1-2</b>							
<b>CL2</b>	850	<b>CL 2-21</b>	13.5 <sup>AH</sup>	384 x 11.5	100x16 <sup>AH</sup>	4.765	4.880	2.398	1.303
		<b>CL 2-22</b>					2.456		
		<b>CL 2-23</b>					2.478		
		<b>CL 2-24</b>	13.5 <sup>AH</sup> 13 <sup>AH</sup>	331x10	125x19 <sup>MS</sup>		2.551	1.139	
		<b>CL 2-25</b>	13 <sup>AH</sup>						
		<b>CL 2-26</b>	13 <sup>AH</sup> 12 <sup>AH</sup>	384 x 11.5	100x16 <sup>MS</sup>		2.556	1.149	
		<b>CL 2-27</b>							
		<b>CL 2-28</b>							
		<b>CL 2-29</b>	12 <sup>AH</sup>	333x12	100x17 <sup>MS</sup>		2.763	0.955	
		<b>CL 2-30</b>							
		<b>CL 2-31</b>							
		<b>CL 2-32</b>	12 <sup>AH</sup> 11.5 <sup>MS</sup>	331x10	125x19 <sup>MS</sup>		2.661	1.139	
		<b>CL 2-33</b>							
		<b>CL 2-34</b>							
		<b>CL 2-35</b>	11.5 <sup>MS</sup>	333x12	100x17 <sup>MS</sup>		2.543	1.149	
	815	<b>CL 2-36</b>	11.5 <sup>MS</sup> 12 <sup>MS</sup>	284x10	90x16 <sup>MS</sup>	4.969	2.417	0.977	
	780	<b>CL 2-37</b>	12 <sup>MS</sup>	235x9	90x15 <sup>AH</sup>	5.192	2.236	1.019	
<b>CL 2-38</b>		186x8		90x14 <sup>AH</sup>	0.907				
775	<b>CL 2-39</b>				5.226	2.222			

**Table 5.5.** Geometry properties of CL Bulkhead Plating Panels

### 5.3.5. Main Deck Plating

The Inner Bulkhead Plating divides the Main Deck plating in two panels (M1-M2). At both panels the plate thickness and stiffener dimensions are identical, 13mm and 250x9/90x15. The same applies for the steel type of both plating and stiffeners which is of mild steel. The difference between the two panels is the stiffener spacing which is 703.83 mm and 825mm for panel M1 and M2 respectively. Main deck plating is depicted in Figure 5.8 and its geometry properties are summarised in Table 5.6.

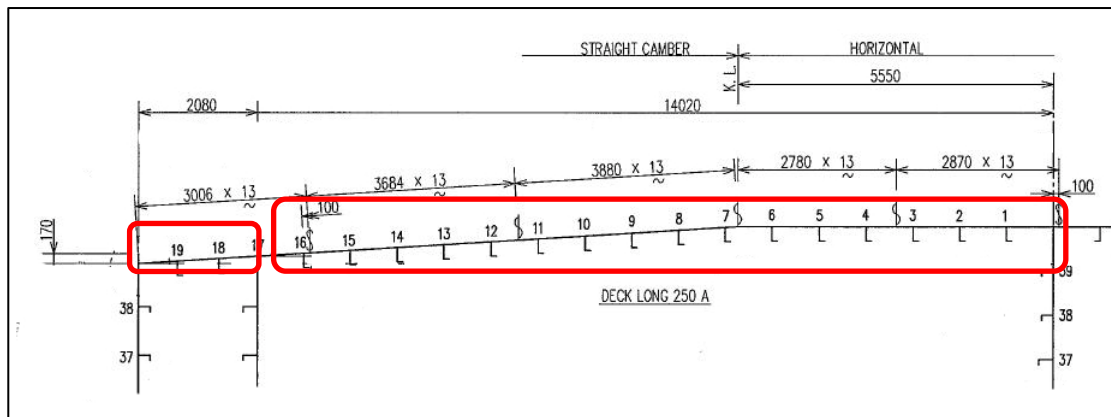


**Fig.5.8.** Main Deck Plating Panels

Panel	Stiffener Spacing (b)	Stiffeners ID No	Plate Thickness ( $t_p$ )	Web ( $d_w \times t_w$ )	Flange ( $b_f \times t_f$ )	Aspect Ratio (a/b)	Plate Slenderness Ratio	Web Slenderness Ratio
	(mm)		(mm)	(mm)	(mm)		(mm)	(mm)
<b>M1</b>	703.83	<b>M1-18</b>	13 <sup>MS</sup>	235x9	90x15 <sup>MS</sup>	5.754	1.863	0.898
		<b>M1-19</b>						
<b>M2</b>	825	<b>M2-1 to M2-15</b>	13 <sup>MS</sup>	235x9	90x15 <sup>MS</sup>	4.909	2.183	0.898
	822.5							

**Table 5.6.** Geometry properties of Main Deck Plating Panels

### 5.3.6. Inner Bottom Plating Panels

The Inner bottom plating forms a panel by itself. It has 14.5 and 16mm plate thickness and stiffener dimensions 400x10/125x22 as shown in Figure 5.9. The material type is high tensile steel (315 Nt/mm<sup>2</sup>).

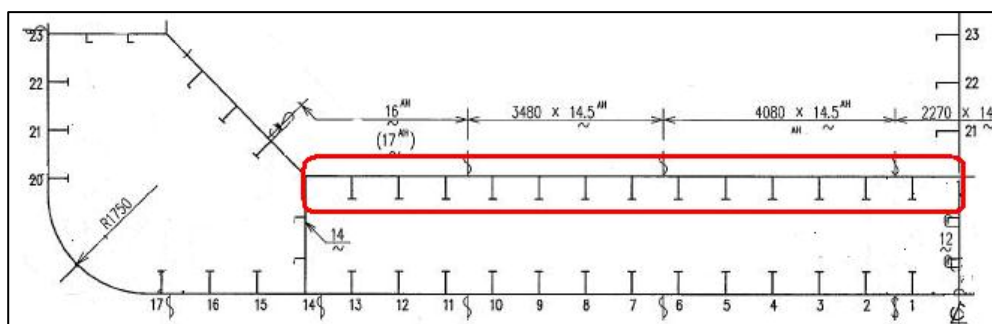


**Fig.5.9.** Inner Bottom Plating Panels

The geometry properties are summarised in Table 5.7.



Panel	Stiffener Spacing (b)	Stiffeners ID No	Plate Thickness ( $t_p$ )	Web ( $d_w \times t_w$ )	Flange ( $b_f \times t_f$ )	Aspect Ratio (a/b)	Plate Slenderness Ratio	Web Slenderness Ratio
	(mm)	(-)	(mm)	(mm)	(mm)	(-)	(mm)	(mm)
IB	825	IB-1	14.5 <sup>AH</sup>	378x10	125x22 <sup>AH</sup>	4.909	2.220	1.475
		IB-2						
		IB-3						
		IB-4						
		IB-5						
		IB-6						
		IB-7						
		IB-8						
		IB-9						
		IB-10						
		IB-11	14.5 <sup>AH</sup> 16 <sup>AH</sup>	2.019				
		IB-12 IB-13	16 <sup>AH</sup>	2.011				

**Table 5.7.** Geometry properties of Inner Bottom Plating Panels

### 5.3.7. Remaining panels

The remaining panels refer to hopper plating, stringers and bilge plating. Hopper plating & stiffeners and bilge plating are of steel with yield stress 315Nt/mm<sup>2</sup> while stringers & stiffeners are of mild steel. The dimensions and the geometry properties of these panels are as follows.

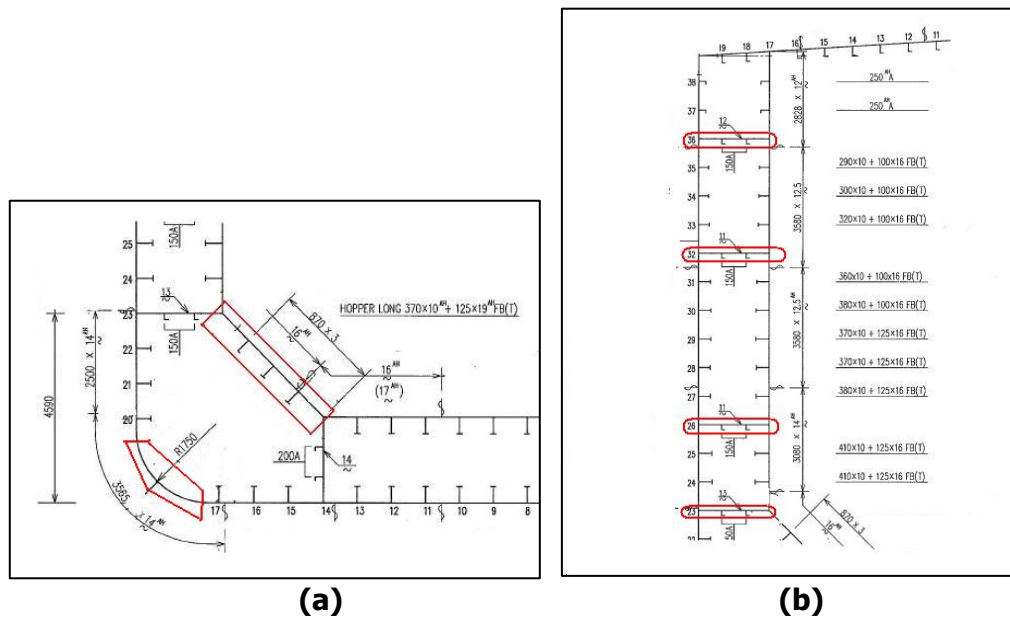


**Fig.5.10.** Remaining panels. (a) Hopper and Bilge Panel, (b) Stringers

Panel	Stiffener Spacing (b)	Stiffeners ID No	Plate Thickness ( $t_p$ )	Web ( $d_w \times t_w$ )	Flange ( $b_f \times t_f$ )	Aspect Ratio (a/b)	Plate Slenderness Ratio	Web Slenderness Ratio
	(mm)	(-)	(mm)	(mm)	(mm)	(-)	(mm)	(mm)
HP	870	HP-1	16 <sup>AH</sup>	351x10	125x19 <sup>AH</sup>	4.655	2.121	1.369
	890.76	HP-2				4.547	2.172	
ST1	702.50	ST1-18	13 <sup>MS</sup>	141x9	90x9 <sup>MS</sup>	5.754	1.859	0.539
		ST1-19						
ST2	702.50	ST2-18	11 <sup>MS</sup>	141x9	90x9 <sup>MS</sup>	5.754	2.197	0.539
		ST2-19						
ST3	702.50	ST3-18	11 <sup>MS</sup>	141x9	90x9 <sup>MS</sup>	5.754	2.197	0.539
		ST3-19						
ST4	702.50	ST4-18	12 <sup>MS</sup>	141x9	90x9 <sup>MS</sup>	5.754	2.014	0.539
		ST4-19						
BLG	-	BLG	14 <sup>HS</sup>	-	-	-	-	-

**Table 5.8.** Geometry properties of remaining panels

#### 5.4. Design bending moments

At this point it would be useful to make a reference to the CSR rule values of maximum expected still water and wave bending moments as well as to the permissible still water bending moments as per which the vessel operates.

The expected maximum still water and wave bending moments in way of the midship region as calculated in accordance with Common Structural Rules are presented in Table 5.9. The midship permissible still water bending moments in accordance with vessel's Loading Manual are indicated in Table 5.10.

Rule bending moments	Sagging Condition		Hogging Condition	
	(kNtm)	(tn m)	(kNtm)	(tn m)
Rule still water bending moment	926508	94445	1226250	68737
Rule wave Bending moment	1430541	145825	1297333	132246

**Table 5.9.** Maximum expected still water Bending Moments as per CSR

<b>Sagging Condition</b>		<b>Hogging Condition</b>	
<b>(kNtm)</b>	<b>(tn m)</b>	<b>(kNtm)</b>	<b>(tn m)</b>
549360	56000	1226250	125000

**Table 5.10.** Permissible still water Bending Moments as per vessel's Loading Manual

Considering the CSR Rule Still Water Bending Moment in Sagging Condition as **926508 kNt·m**, the Rule Wave Bending Moment as **1430541 kNt·m** and the load combination factors  $\gamma_s$  and  $\gamma_w$  as 1.1 and 1.2 respectively (refer to Figure 3.1), this leads to an expected maximum total bending moment of  **$2.643 \times 10^9$  Nt·m**.

## CHAPTER 6

# APPLICATION OF THE CSR INCREMENTAL-ITERATIVE APPROACH

### 6.1. General

This Chapter summarizes the application of the CSR Incremental-Iterative Approach used in the context of this study for the assessment of the Hull Girder Ultimate Strength of the double hull tanker presented at the previous chapter. All stages of the procedure are presented herewith including, but not limited, to the division of the midship-section into structural elements, the determination of the net scantlings, the calculation of the load end shortening curves and the presentation of any considerations/assumptions made. The results of the procedure will be compared to the results of the Finite Elements Approach in chapter 8.

### 6.2. Steps of Incremental – Iterative Approach

The Incremental – Iterative Approach is one of the new features of Common Structural Rules for the estimation of the hull girder ultimate bending capacity. It aims to determine the hull girder ultimate capacity by dividing the hull girder transverse section between two adjacent transverse webs into structural elements, which are considered to act independently of each other, and deriving the collapse behavior of each of these structural elements.

The sagging hull girder ultimate capacity of a hull girder section, is defined as the maximum value of the static non-linear bending moment-curvature relationship  $M-\kappa$  (refer to Figure 3.2) which represents the progressive collapse behaviour of the hull girder under vertical bending. At each step of the procedure, a curvature  $\mathbf{k}_i$  is imposed on the hull girder, the strain  $\boldsymbol{\varepsilon}_{ij}$  and corresponding stress  $\boldsymbol{\sigma}_{ij}$  acting on each structural element  $\mathbf{j}$  are determined, the new position of the neutral axis is recalculated until equilibrium is achieved and the bending moment  $\mathbf{M}_i$  corresponding to that equilibrium is recorded. The ultimate capacity is the peak value  $\mathbf{M}_u$  of the  $M_i-\kappa_i$  curve.

A detailed description of the method was given in Chapter 3. The following paragraphs describe the various steps of this procedure as applied in this study for the estimation of the double hull tanker's ultimate bending capacity.

### **6.2.1. Step 1 - Division of the Section into Structural Elements**

The first step of the Incremental Approach refers to the division of the midship section between two adjacent transverse webs (refer to Figure 6.1) into structural elements. The structural elements may comprise of longitudinal stiffeners with their attached plating (of breadth equal to the spacing of the stiffeners), hard corners or transversely stiffened panels. It should be noted that the bilge area, as per the CSR Rules, should be considered as a hard corner.

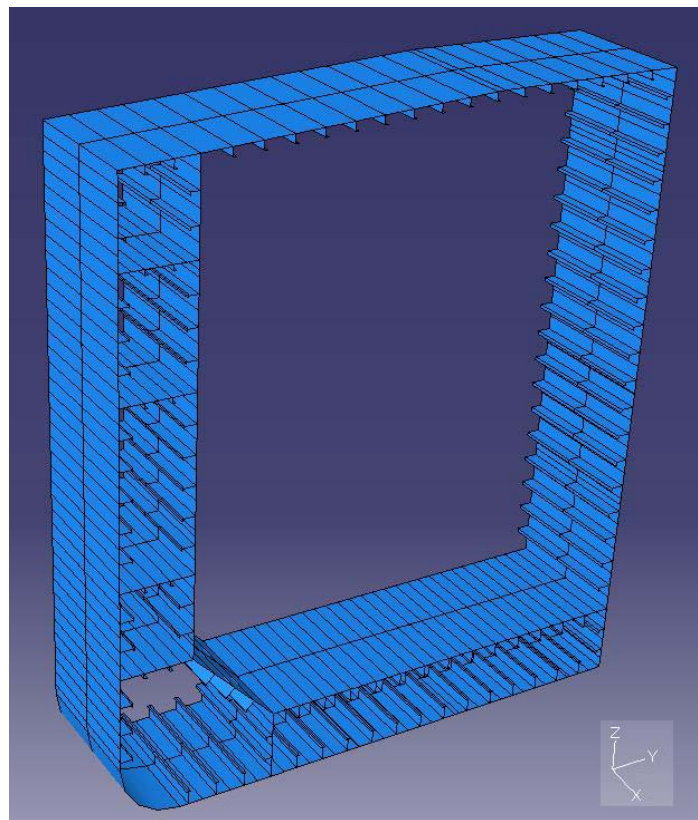


**Fig.6.1.**Midship section area of the tanker between the web frames

The division of the double hull tanker into structural elements is shown in Figure 6.2. As the midship section is longitudinally stiffened, this comprises of longitudinal stiffeners and hard corners.

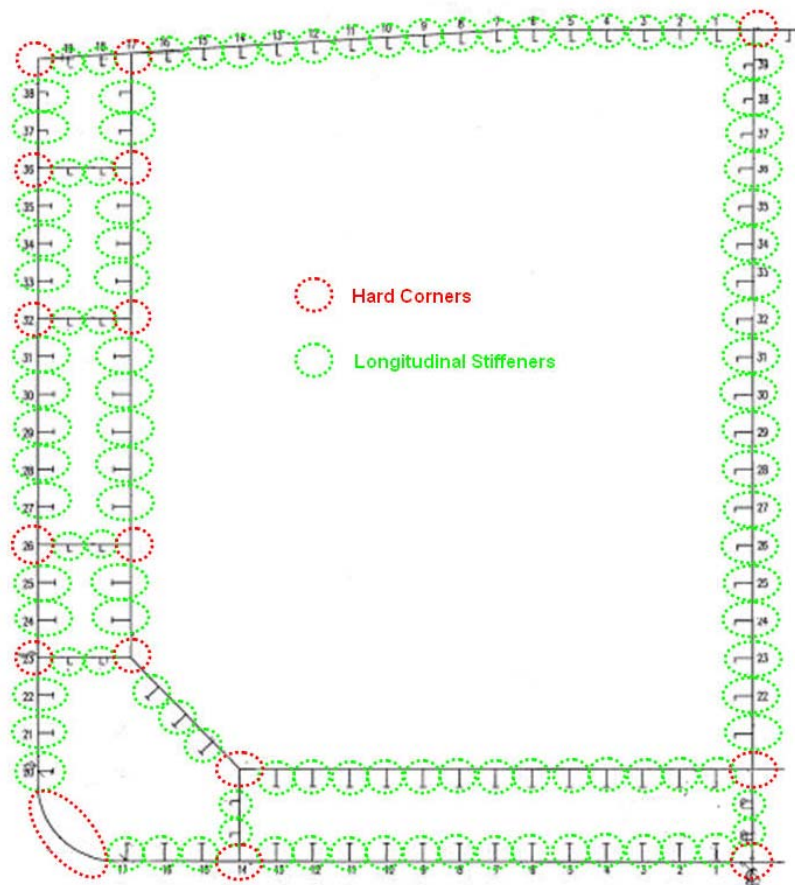


**Fig.6.2.** Division of the Double Hull Tanker into structural elements

### 6.2.2. Step 2 - Calculation of the Load-end Shortening Curves

In the next step the Load end Shortening curves of the structural elements are calculated taking into account that each structural element acts independently. At this point it should be highlighted that the Load end Shortening curves of all the structural elements are based on their net thickness.

This relates to the new net thickness approach adopted by the CSR as per which the assessment of hull girder scantlings is based on the overall global corrosion, by deducting half the local corrosion addition for all structural members simultaneously:

$$t_{net} = t_{grs} - 0.5 t_{cor}$$

The corrosion addition that should be deducted for the determination of the net scantlings, as defined by the CSR rules, is depicted in Figure 3.8. The application of the net thickness deduction for the double oil tanker of this study is illustrated in Figure 6.3 whereas the geometric characteristics of the longitudinal stiffeners taking into account the net scantlings are tabulated in Table 6.1.

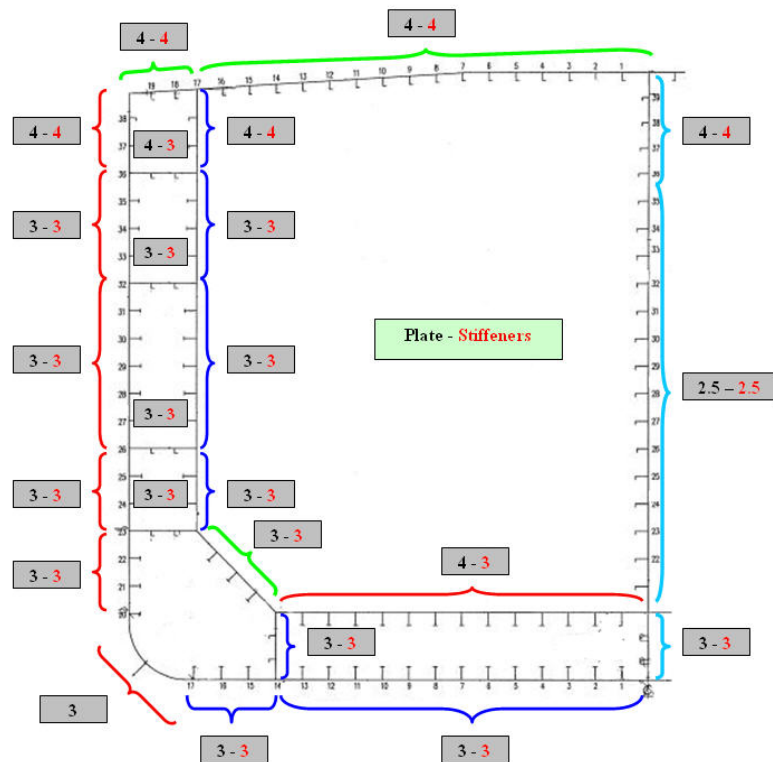


**Fig.6.3.** Corrosion addition accounted for the determination of the net scantlings

Having determined the net scantlings of the structural elements, the next step of the incremental-iterative approach is to derive the load end shortening curves. Under the assumptions that each structural element acts independently and that only the midship section between two adjacent transverse webs is taken into account, the CSR Rules have adopted certain formulas for the collapse behaviour of stiffened panels (refer to Chapter 3). These formulas consider all relevant failure modes for the individual structural elements, such as plate buckling, beam column buckling, torsional stiffener buckling and stiffener web buckling. It should be noted that the formulas proposed by CSR use the Euler Elastic Buckling Stress in conjunction with a correction due to plasticity, based on the well known Johnson-Ostenfeld formula (refer to figure 2.14).

Location	Panel	Structural Element	$\sigma_{yd}$ EQUIV	$\sigma_{yd}$ PLATE	$\sigma_{yd}$ STIFFENER	Plate Slenderness $b_p$	Web Slenderness $b_w$	$d_w/t_w$	As/A
Main Deck	M 2	M 2 - 1	245	245	245	2.580	1.155	33.57	0.24
		M 2 - 2	245	245	245	2.580	1.155	33.57	0.24
		M 2 - 3	245	245	245	2.580	1.155	33.57	0.24
		M 2 - 4	245	245	245	2.580	1.155	33.57	0.24
		M 2 - 5	245	245	245	2.580	1.155	33.57	0.24
		M 2 - 6	245	245	245	2.580	1.155	33.57	0.24
		M 2 - 7	245	245	245	2.585	1.155	33.57	0.24
		M 2 - 8	245	245	245	2.585	1.155	33.57	0.24
		M 2 - 9	245	245	245	2.585	1.155	33.57	0.24
		M 2 - 10	245	245	245	2.585	1.155	33.57	0.24
		M 2 - 11	245	245	245	2.585	1.155	33.57	0.24
		M 2 - 12	245	245	245	2.585	1.155	33.57	0.24
		M 2 - 13	245	245	245	2.585	1.155	33.57	0.24
		M 2 - 14	245	245	245	2.585	1.155	33.57	0.24
		M 2 - 15	245	245	245	2.585	1.155	33.57	0.24
	M 2 - 16	245	245	245	2.577	1.155	33.57	0.24	
	M 1	M 1 - 18	245	245	245	2.201	1.155	33.57	0.27
	M 1 - 19	245	245	245	2.201	1.155	33.57	0.27	
CL Bkhd	CL 2	CL 2 - 22	315	315	315	2.849	1.577	40.42	0.34
		CL 2 - 21	315	315	315	2.815	1.577	40.42	0.35
		CL 2 - 23	315	315	315	2.707	1.461	37.46	0.34
		CL 2 - 24	315	315	315	2.734	1.461	37.46	0.34
		CL 2 - 25	315	315	315	2.822	1.461	37.46	0.35
		CL 2 - 26	291.29	315	245	2.822	1.301	37.83	0.34
		CL 2 - 27	290.4	315	245	2.822	1.289	37.46	0.35
		CL 2 - 28	290.36	315	245	2.829	1.289	37.46	0.35
		CL 2 - 29	288.97	315	245	3.084	1.289	37.46	0.37
		CL 2 - 30	288.97	315	245	3.084	1.289	37.46	0.37
		CL 2 - 31	290.82	315	245	3.084	1.175	34.15	0.35
		CL 2 - 32	289.88	315	245	3.084	1.301	37.83	0.36
		CL 2 - 33	267.25	280	245	2.977	1.301	37.83	0.36
		CL 2 - 34	245	245	245	2.853	1.175	34.15	0.36
		CL 2 - 35	245	245	245	2.853	1.117	32.46	0.30
		CL 2 - 36	245	245	245	2.921	1.221	35.50	0.31
		CL 2 - 37	263.56	245	315	2.683	1.310	33.57	0.27
		CL 2 - 38	260.38	245	315	2.683	1.209	31.00	0.22
CL 2 - 39	260.46	245	315	2.666	1.209	31.00	0.22		
Inner Bkhd	14	14 - 38	315	315	315	3.390	1.310	33.57	0.24
		14 - 37	315	315	315	3.316	1.310	33.57	0.25
	13	13 - 35	245	245	245	2.658	1.109	32.24	0.29
		13 - 34	245	245	245	2.658	1.149	33.41	0.29
		13 - 33	245	245	245	2.658	1.230	35.76	0.30
	12	12 - 31	292.69	315	245	3.014	1.392	40.47	0.32
		12 - 30	292.11	315	245	3.014	1.473	42.82	0.33
		12 - 29	291.18	315	245	3.014	1.433	41.65	0.34
		12 - 28	291.18	315	245	3.014	1.433	41.65	0.34
		12 - 27	292.51	315	245	2.720	1.473	42.82	0.32
	11	11 - 25	292.11	315	245	2.653	1.595	46.35	0.33
		11 - 24	292.53	315	245	2.582	1.595	46.35	0.32

**Table 6.1.** Geometric properties of structural elements based on net scantlings



Location	Panel	Structural Element	$\sigma_{yd}$ EQUIV	$\sigma_{yd}$ PLATE	$\sigma_{yd}$ STIFFENER	Plate Slenderness $b_p$	Web Slenderness $b_w$	$d_w/t_w$	As/A
Side Shell	S 5	S 5 - 38	302.03	315	245	2.617	1.066	31.00	0.19
		S 5 - 37	302.6	315	245	2.763	1.066	31.00	0.18
	S 4	S 4 - 35	296.63	315	245	2.653	1.109	32.24	0.26
		S 4 - 34	296.63	315	245	2.653	1.109	32.24	0.26
	S 3	S 4 - 33	296.03	315	245	2.653	1.190	34.59	0.27
		S 3 - 31	294.87	315	245	2.653	1.352	39.29	0.29
		S 3 - 30	294.59	315	245	2.653	1.392	40.47	0.29
		S 3 - 29	294.59	315	245	2.653	1.392	40.47	0.29
		S 3 - 28	293.96	315	245	2.653	1.311	38.12	0.30
		S 3 - 27	293.69	315	245	2.653	1.352	39.29	0.30
	S 2	S 2 - 25	292.63	315	245	2.653	1.514	44.00	0.32
		S 2 - 24	292.37	315	245	2.653	1.554	45.18	0.32
	S 1	S 1 - 22	315	315	315	2.653	1.519	38.94	0.32
		S 1 - 21	315	315	315	2.653	1.519	38.94	0.32
		S 1 - 20	315	315	315	2.231	1.519	38.94	0.36
Hopper Plating	HP	HP - 1	315	315	315	2.341	1.611	41.29	0.29
		HP - 2	315	315	315	2.341	1.611	41.29	0.29
		HP - 3	315	315	315	2.396	1.611	41.29	0.29
Stringer 36	ST 4	ST 4 - 18	245	245	245	2.417	0.647	18.80	0.20
		ST 4 - 19	245	245	245	2.417	0.647	18.80	0.20
Stringer 32	ST 3	ST 3 - 18	245	245	245	2.544	0.647	18.80	0.21
		ST 3 - 19	245	245	245	2.544	0.647	18.80	0.21
Stringer 26	ST 2	ST 2 - 18	245	245	245	2.544	0.647	18.80	0.21
		ST 2 - 19	245	245	245	2.544	0.647	18.80	0.21
Stringer 23	ST 1	ST 1 - 18	245	245	245	2.102	0.647	18.80	0.18
		ST 1 - 19	245	245	245	2.102	0.647	18.80	0.18
Bottom	B 2	B 2 - 1	315	315	315	2.330	1.749	44.82	0.32
		B 2 - 2	315	315	315	2.575	1.749	44.82	0.34
		B 2 - 3	315	315	315	2.575	1.749	44.82	0.34
		B 2 - 4	315	315	315	2.575	1.749	44.82	0.34
		B 2 - 5	315	315	315	2.575	1.749	44.82	0.34
		B 2 - 6	315	315	315	2.556	1.749	44.82	0.34
		B 2 - 7	315	315	315	2.476	1.749	44.82	0.34
		B 2 - 8	315	315	315	2.476	1.749	44.82	0.34
		B 2 - 9	315	315	315	2.476	1.749	44.82	0.34
		B 2 - 10	315	315	315	2.476	1.749	44.82	0.34
		B 2 - 11	315	315	315	2.571	1.749	44.82	0.34
		B 2 - 12	315	315	315	2.575	1.749	44.82	0.34
	B 2 - 13	315	315	315	2.575	1.749	44.82	0.34	
	B 1	B 1 - 15	315	315	315	2.653	1.749	44.82	0.34
		B 1 - 16	315	315	315	2.653	1.749	44.82	0.34
B 1 - 17		315	315	315	2.107	1.749	44.82	0.39	
Inner Bottom	IB 1	IB 1 - 1	315	315	315	2.575	1.735	44.47	0.36
		IB 1 - 2	315	315	315	2.575	1.735	44.47	0.36
		IB 1 - 3	315	315	315	2.575	1.735	44.47	0.36
		IB 1 - 4	315	315	315	2.575	1.735	44.47	0.36
		IB 1 - 5	315	315	315	2.575	1.735	44.47	0.36
		IB 1 - 6	315	315	315	2.575	1.735	44.47	0.36
		IB 1 - 7	315	315	315	2.575	1.735	44.47	0.36
		IB 1 - 8	315	315	315	2.575	1.735	44.47	0.36
		IB 1 - 9	315	315	315	2.575	1.735	44.47	0.36
		IB 1 - 10	315	315	315	2.575	1.735	44.47	0.36
		IB 1 - 11	315	315	315	2.309	1.735	44.47	0.33
		IB 1 - 12	315	315	315	2.299	1.735	44.47	0.33
		IB 1 - 13	315	315	315	2.299	1.735	44.47	0.33
Side Girder	SG	SG - 1	245	245	245	1.865	0.984	28.62	0.22
		SG - 2	245	245	245	1.995	0.984	28.62	0.20
CL Girder	CL	CL - 1	245	245	245	1.865	0.984	28.62	0.22
		CL - 2	245	245	245	1.995	0.984	28.62	0.20

**Table 6.1 (cont.).** Geometric properties of structural elements based on net scantlings

As per the CSR procedure, the longitudinal stiffeners under compression are considered to fail because of beam column buckling, stiffener torsional buckling and stiffener web local buckling (refer to Table 3.1). Longitudinal stiffeners under tension as well as hard corners either under tension or under compression are regarded to have elastic, perfectly plastic failure (refer to Figure 3.6).

Due attention should be given to the fact that these formulas assume that the attached plate and the stiffener are of the same yield stress as well as that the thickness and yield stress within the attached plate remains the same. Nevertheless, in practice this is not always the case, as in the case of the double hull tanker used in this study. The International Association of the Classification Societies who has developed the CSR Rules retains an IACS-CSR Knowledge Centre to which the shipbuilding industry can refer for any necessary clarifications with regards to the implementation of the CSR Rules. All questions and answers are available on line at the IACS site ([www.iacs.co.org](http://www.iacs.co.org)). Based on the recommendations obtained by this CSR Knowledge Centre, the following procedure should be applied in such cases:

- **Different yield stress between the attached plate and the stiffener.**  
Where the yield stress of the plate and stiffener is not identical, two calculations should be carried out:
  - for the stiffener: by adding to the stiffener an attached plating of the same material as the one of the stiffener and determining the shortening curve and the stress  $\sigma$  to be applied to the stiffener.
  - for the attached plating: by adding a stiffener made of the same material as the one of the attached plating and determining the shortening curve and the stress  $\sigma$  to be applied to the attached plating.
- **Different thickness within the attached plate.** In such cases an average, over the area, thickness for the plate should be used.
- **Different thickness and yield stress within the attached plate.** An average, over the area, thickness and yield strength for the plate should be used.

The midship section scantlings of the double hull tanker used in this study have been presented in Chapter 5. As indicated, in most cases (except of the main deck plating and the bottom/ inner bottom plating) the yield stress of the stiffeners and attached plating are not identical. In such cases two load end shortening curves have been derived during the implementation of the Incremental-Iterative Approach, in accordance with above mentioned IACS recommendations:

- for the stiffener-plate combination of a yield stress equal to the yield stress of the plate, from which the stress acting on the plate has been derived.
- for the stiffener-plate combination of a yield stress equal to the yield stress of the stiffener, from which the stress acting on the stiffener has been derived.

In both cases all failure modes have been considered, bearing in mind that even in web local buckling and torsional buckling which refer mainly to the stiffeners buckling failure, result in (if not simultaneously) the plate failure since the plating is left practically with no support.

In cases where the thickness or yield stress fluctuates within the attached plate of the stiffeners, an equivalent, over the area, thickness or yield stress respectively has been used as follows:

$$t_{eq} = (t_1 \cdot L_1 + t_2 \cdot L_2) / (L_1 + L_2)$$
$$\sigma_{eq} = (\sigma_{yd1} \cdot A_1 + \sigma_{yd2} \cdot A_2) / (A_1 + A_2)$$

In order to evaluate the effect of using two load shortening curves in case of different yield stresses in the plate and stiffener, as per the IACS recommendation, two additional alternatives have been considered:

**A) Option A-Equivalent yield stress approach.** Using equivalent stress for the plate – stiffener combination, similar to the expression above and also given in Fig. 2.9.

**B) Option B-Applicable yield stress approach.** Using the plate yield stress or the stiffener yield stress dependent on the critical stress considered. More specifically, for the web local buckling mode the stiffener yield stress is used (equations 3.12, 3.13, 3.14), while for the beam column buckling failure the

equivalent yield stress (equations 3.3 & 3.4) is taken into account in the calculations. In case of the torsional buckling mode, the plate yield stress and the stiffener yield stress is used for the estimation of the ultimate strength of the attached plating ( $\sigma_{CP}$  - refer to equation 3.11) and torsional critical stress ( $\sigma_{c2}$  - refer to equation 3.9) respectively.

In the following Figures 6.4-6.6 the stress-strain curves are shown, as derived by using above mentioned considerations, for three different plate-stiffener combinations where the yield stresses of the plate and stiffener are not identical. For comparison reasons, the stress-strain curve computed by the FE analysis is also included. In all the cases reported below, the plate yield stress is  $315\text{Nt/mm}^2$ , whereas the stiffener yield stress is  $245\text{Nt/mm}^2$ . The critical buckling mode is also mentioned.

To enable the comparison of the IACS recommended approach (denoted by the brown curve) to the remaining approaches, the stress-strain curve of the IACS approach has been calculated as follows:

$$\sigma_{\text{IACS}} = (\sigma_{\text{plate}} \cdot A_{\text{plate}} + \sigma_{\text{stif}} \cdot A_{\text{stif}}) / (A_{\text{plate}} + A_{\text{stif}})$$

The figures also show with dotted lines the curves obtained when considering a uniform yield stress in the element, either that of the plating or the stiffener, as explained above.

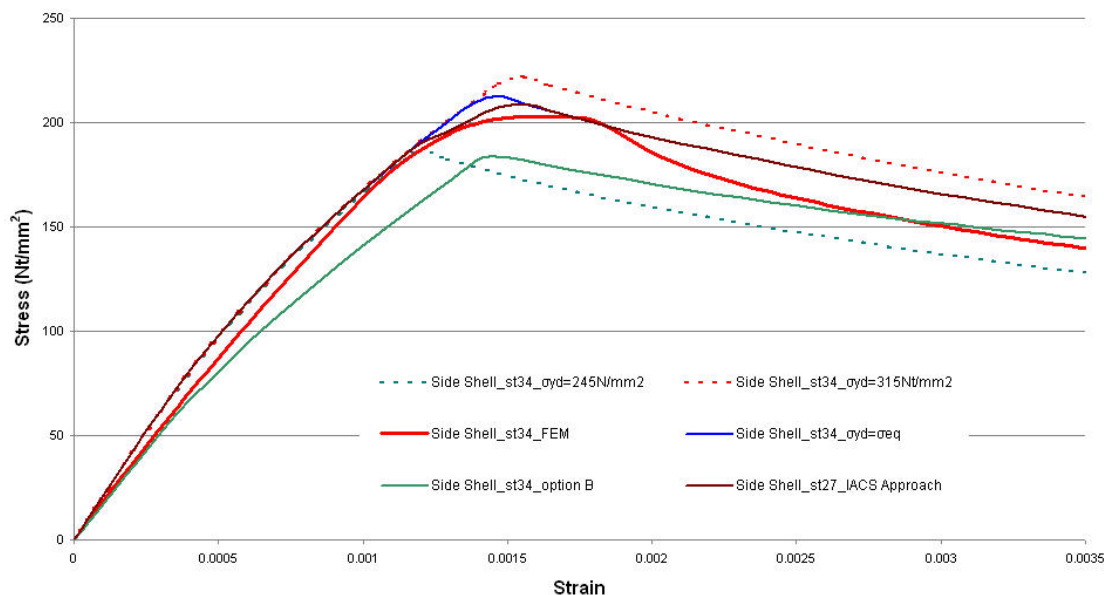


**Fig.6.4.** Side Shell Structural Element 34 (290x10/100x16) – Beam Column Buckling

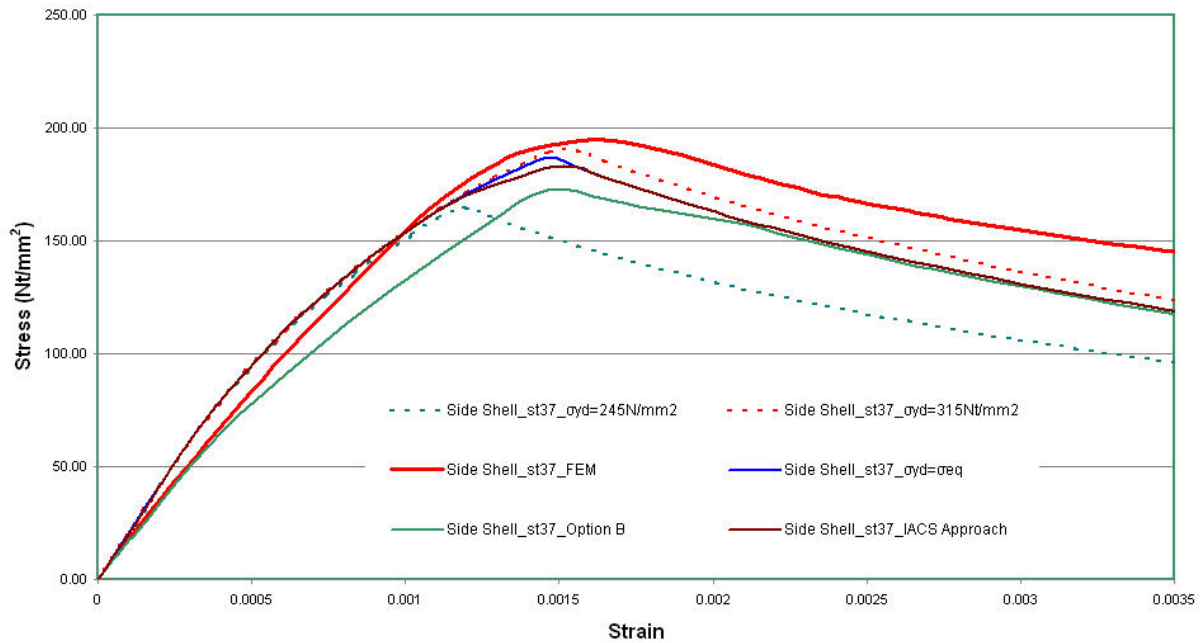


**Fig.6.5.** Side Shell Structural Element 37 (200x90x8/14) - Beam Column Buckling

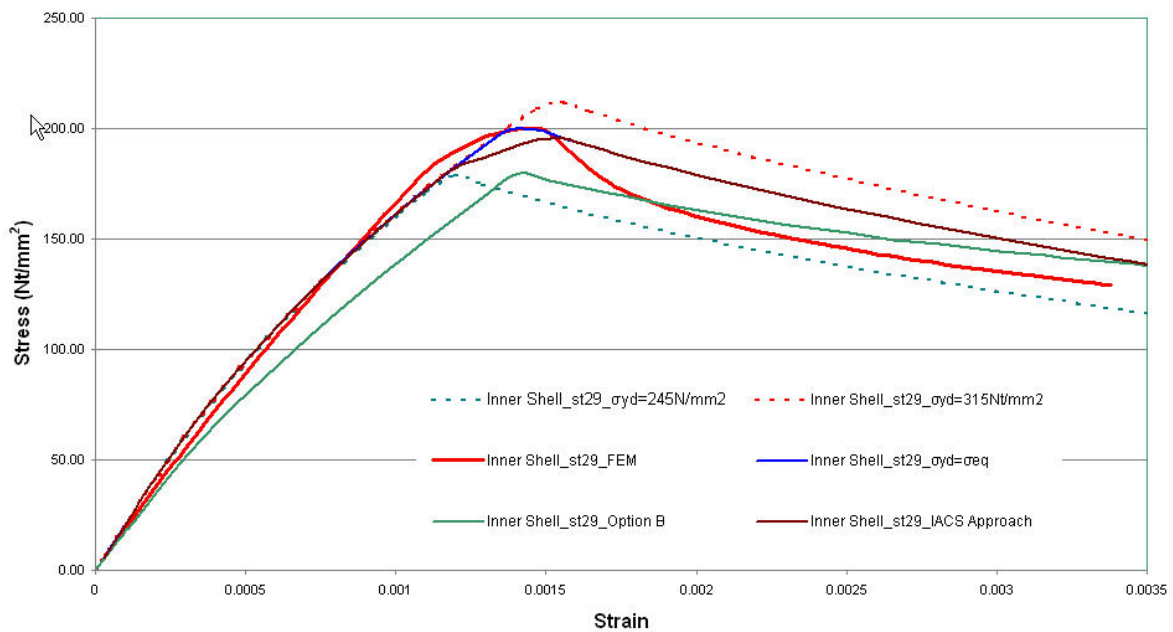


**Fig.6.6.** Inner Shell Structural Element 29 (370x10/125x16) - Torsional Buckling

It seems that from all the above three approaches, option B results in load end shortening curves that differ substantially from the ones derived by the finite element approach. Both the IACS recommended approach and the Equivalent yield

stress approach approximate better the ultimate limit state obtained from the FE analysis although there are marked differences in the post buckling regime.

Nevertheless, for comparison reasons the Incremental – Iterative Approach has been applied taking into account all the above mentioned alternatives.

### **6.2.3. Step 3 - Estimation of the curvature step size and initial position of the neutral axis**

For the estimation of the curvature increment size at each step, the expected maximum required curvature  $\kappa_F$  is estimated based on the vertical bending moment given by the linear elastic bending stress of yield in the deck ( $Z_{v-net50-dk} \sigma_{yd} 10^3$ ) or keel ( $Z_{v-net50-kl} \sigma_{yd} 10^3$ ), whichever is greater. The curvature increment size  $\Delta\kappa$  at each step is then taken as  $\kappa_F/300$ .

For this purpose, the midship section modulus of the double hull oil tanker in the deck and in the keel has been calculated in accordance with the provisions of CSR Rules. The calculation is detailed in Figure 6.7. The section modulus of the deck and the bottom was calculated at  $13808477 \text{ cm}^3$  and  $18722549 \text{ cm}^3$  respectively leading to a maximum vertical bending moment of 5.897.603 kNtm and a maximum expected curvature of:

$$\kappa_F = 5.9709 \times 10^{-4} \text{ m}^{-1}$$
$$\Delta\kappa = 1.99029 \times 10^{-6} \text{ m}^{-1}$$

The initial position of the neutral axis based on the linear elastic bending stress, as shown in Figure 6.7, has been calculated at:

$$Z_{NA-initial} = 7.683 \text{ m above Base Line}$$

**REQUIRED PARTICULARS**

LENGTH	171.69 (m) (0.97L <sub>wr</sub> )
BREADTH :	32.20 (m)
DEPTH	18.10 (m)
C <sub>b</sub> :	0.774

Minimum hull girder bending moment for seagoing operations amidships ,Section 7/2.1.2.1 for hogging and saqqing condition (kNm)	M <sub>sw hog</sub> =	926508.359
	M <sub>sw sag</sub> =	674305.1169

**REQUIRED SECTION MODULUS (according to CSR Rules for Oil Tankers and Section 8, Chapter 1 -Par. 1.2.2.2)**

**SMo = 0,9 · k · C<sub>wv</sub> · B · L<sup>2</sup> · (C<sub>b</sub>+0,7), (cm3)**

where :

L =	171.69
B =	32.20
C <sub>w</sub> =	9.297
C <sub>b</sub> =	0.774
k <sub>bottom</sub> =	0.7800
k <sub>deck</sub> =	0.9825
a =	190
σ <sub>bottom</sub> =	243.59
σ <sub>deck</sub> =	193.38
then :	

(wave coefficient as defined in Table 8.1.2)

(higher strength steel factor as defined in Section 6 / Par. 1.1.4)

(higher strength steel factor as defined in Section 6 / Par. 1.1.4)

(factor defining the perm. stress with regards to the legth range / design load combination)

(permissible stress, σ=a/k, as defined in Section 8/Table 8.1.3)

(permissible stress, σ=a/k, as defined in Section 8/Table 8.1.3)

If 150 ≤ L ≤ 300 m C<sub>w</sub> = 10.75 - ((300-L)/100)<sup>2.5</sup> C<sub>w</sub>= 9.30

If 300 < L < 350 m C<sub>w</sub> = 10.75 C<sub>w</sub>= --

If 350 ≤ L ≤ 500 m C<sub>w</sub> = 10.75 - ((L-350)/150)<sup>2.5</sup> C<sub>w</sub>= --

SMo =	11499600.76	(cm3) (deck)
SMo =	9129454.042	(cm3) (bottom)

**Wave bending moment amidships**

M <sub>w(+)</sub> = 0,19 · C <sub>w</sub> · B · L <sup>2</sup> · C <sub>b</sub> · 10 <sup>3</sup> kn·M =	1297333.01	kn <sup>3</sup> M	(hogging) (+)
M <sub>w(-)</sub> = -110 · C <sub>w</sub> · B · L <sup>2</sup> · (C <sub>b</sub> +0,7) kn·M =	-1430541.2	kn <sup>3</sup> M	(sagging) (-)

**Still water bending moment**

926508.359	kn <sup>3</sup> M	(hogging)
674305.117	kn <sup>3</sup> M	(sagging)

**Minimum required Section Modulus amidships**

SM <sub>deck</sub> =  M <sub>s</sub> +M <sub>w</sub>   · 10 <sup>3</sup> / σ, (cm <sup>3</sup> ) =	11499601	cm <sup>3</sup>	(hogging/deck)	3910536.751	cm <sup>3</sup>	(sagging/deck)
SM <sub>bottom</sub> =  M <sub>s</sub> +M <sub>w</sub>   · 10 <sup>3</sup> / σ, (cm <sup>3</sup> ) =	9129454.04	cm <sup>3</sup>	(hogging/bottom)	3104548.261	cm <sup>3</sup>	(sagging/bottom)

**Fig.6.7.** Calculation of the Midship Section Modulus

No	Description of Item	Pieces	Corrosion addition (mm)	Gross Dimensions (mm)		Net Dimensions (mm)		Area of Item (cm <sup>2</sup> )	Axis from B.L. (m)	Item's Moment (cm <sup>2</sup> *m)	Item's Inertia about B.L. (cm <sup>2</sup> *m <sup>2</sup> )	Item's Inertia about G (cm <sup>4</sup> )
			Thickness	Breadth	Height	Breadth <sub>net</sub>	Height <sub>net</sub>					
1	SIDE PLATING (14MM)	1.0	3.0	14	13890	13	13890	1736.25	8.6950	15096.69	131265.75	279148632.19
2	SIDE PLATING (14MM)-SHEER STRAKE	1.0	4.0	14	2460	12	2460	295.20	16.8700	4980.02	84013.00	1488693.60
3	BILGE PLATING	1.0	3.0	14	1750	13	1750	344.84	0.6359	219.29	139.45	1000258.63
4	BOTTOM PLATING (14MM)	1.0	3.0	5655	14	5655	13	706.88	0.0063	4.42	0.03	92.04
5	BOTTOM PLATING (14,5MM)	1.0	3.0	3480	15	3480	13	452.40	0.0065	2.94	0.02	63.71
6	BOTTOM PLATING (14MM)	1.0	3.0	4080	14	4080	13	510.00	0.0063	3.19	0.02	66.41
7	KEEL PLATE	0.5	3.0	2270	16	2270	14	158.90	0.0070	1.11	0.01	25.95
8	CENTER GIRDER	0.5	3.0	14	2080	13	2080	130.00	1.0400	135.20	140.61	468693.33
9	SIDE GIRDER	1.0	3.0	14	2080	13	2080	260.00	1.0400	270.40	281.22	937386.67
10	INNER BOTTOM PLATING (14,5MM)	1.0	4.0	8695	15	8695	13	1086.88	2.0863	2267.49	4730.56	141.52
11	INNER BOTTOM PLATING (16MM)	1.0	4.0	2855	16	2855	14	399.70	2.0870	834.17	1740.92	65.28
12	HOPPER PLATING (16MM)	1.0	3.0	3522	16	3522	15	510.62	3.3250	1702.91	5679.22	2680792.04
13	INNER SHELL PLATING (16MM)	1.0	3.0	570	16	570	15	82.65	4.8750	402.92	1964.23	14.48
14	INNER SHELL PLATING (14MM)	1.0	3.0	3080	14	3080	13	385.00	6.7000	2579.50	17282.65	50.13
15	INNER SHELL PLATING (12,5 MM)	1.0	3.0	7160	13	7160	11	787.60	11.8200	9309.43	110037.49	79.42
16	INNER SHELL PLATING (12 MM)	1.0	4.0	2588	12	2588	10	258.80	16.6940	4320.41	72124.88	21.57
17	INNER SHELL PLATING (12 MM)	1.0	3.0	240	12	240	11	25.20	18.1080	456.32	8263.07	2.32
18	STRINGER No 23	1.0	3.0	2080	13	2080	12	239.20	4.5958	1099.30	5052.12	26.36
19	STRINGER No 26	1.0	3.0	2080	11	2080	10	197.60	7.1448	1411.80	10086.98	14.86
20	STRINGER No 32	1.0	3.0	2080	11	2080	10	197.60	12.2448	2419.56	29626.94	14.86
21	STRINGER No 36	1.0	4.0	2080	12	2080	10	208.00	15.6450	3254.16	50911.33	17.33
22	DECK PLATE-CAMBER	1.0	4.0	10570	13	10570	11	1162.70	18.4305	21429.14	394949.81	117.24
23	DECK PLATE	1.0	4.0	5550	13	5550	11	610.50	18.7555	11450.23	214754.84	61.56
24	CL BLKHD PLATING (13,5MM)	0.5	2.5	3580	14	3580	12	219.28	3.8700	848.59	3284.06	27.42
25	CL BLKHD PLATING (13MM)	0.5	2.5	3580	13	3580	12	210.33	7.4500	1566.92	11673.56	24.20
26	CL BLKHD PLATING (12MM)	0.5	2.5	3850	12	3850	11	206.94	11.1650	2310.46	25796.25	19.93
27	CL BLKHD PLATING (11,5MM)	0.5	2.5	2125	12	2125	10	108.91	14.1525	1541.30	21813.19	9.53
28	CL BLKHD PLATING (11,5MM)	0.5	4.0	655	12	655	10	31.11	15.5425	483.57	7515.83	2.34
29	CL BLKHD PLATING (12 MM)	0.5	4.0	2880	12	2880	10	144.00	17.3100	2492.64	43147.60	12.00
30	SIDE LONGITUDINALS WEB (200A)	2.0	4.0	186	8	186	6	22.32	16.9150	377.54	6386.14	0.67
31	SIDE LONGITUDINALS FLANGE (200A)	2.0	4.0	14	90	12	90	21.60	16.8700	364.39	6147.29	145.80
32	SIDE LONGITUDINALS FLANGES (100X16)	6.0	3.0	16	100	15	100	87.00	12.2400	1064.88	13034.13	725.00
33	SIDE LONGITUDINALS WEB (290X10)	2.0	3.0	274	10	274	9	46.58	14.3650	669.12	9611.93	2.80
34	SIDE LONGITUDINALS WEB (310X10)	1.0	3.0	294	10	294	9	24.99	13.0900	327.12	4281.99	1.50
35	SIDE LONGITUDINALS WEB (350X10)	1.0	3.0	334	10	334	9	28.39	11.3900	323.36	3683.09	1.71
36	SIDE LONGITUDINALS WEB (360X10)	2.0	3.0	344	10	344	9	58.48	10.1150	591.53	5983.28	3.52
37	SIDE LONGITUDINALS FLANGES (125X16)	4.0	3.0	16	125	15	125	72.50	7.1400	517.65	3696.02	944.01
38	SIDE LONGITUDINALS WEB (340X10)	1.0	3.0	324	10	324	9	27.54	8.8400	243.45	2152.13	1.66
39	SIDE LONGITUDINALS WEB (350X10)	1.0	3.0	334	10	334	9	28.39	7.9900	226.84	1812.42	1.71
40	SIDE LONGITUDINALS WEB (390X10)	1.0	3.0	374	10	374	9	31.79	6.2900	199.96	1257.74	1.91
41	SIDE LONGITUDINALS WEB (400X10)	1.0	3.0	384	10	384	9	32.64	5.4400	177.56	965.94	1.97
42	SIDE LONGITUDINALS FLANGE (125X19)	3.0	3.0	19	125	18	125	65.63	2.8900	189.66	548.11	854.49
43	SIDE LONGITUDINALS WEB (350X10)	3.0	3.0	331	10	331	9	84.41	2.8900	243.93	704.96	5.08
44	INNER SHELL LONGITUDINALS WEB (250A)	2.0	4.0	235	9	235	7	32.90	16.9150	556.50	9413.26	1.34
45	INNER SHELL LONGITUDINALS FLANGE (250A)	2.0	4.0	15	90	13	90	23.40	16.8700	394.76	6659.57	157.95
46	INNER SHELL LONGITUDINALS FLANGES (100X16)	3.0	3.0	16	100	15	100	43.50	13.9400	606.39	8453.08	362.50
47	INNER SHELL LONGITUDINALS FLANGES (100X16)	2.0	3.0	16	100	15	100	29.00	10.9650	317.99	3486.71	241.67
48	INNER SHELL LONGITUDINALS WEB (290X10)	1.0	3.0	274	10	274	9	23.29	14.7900	344.46	5094.55	1.40
49	INNER SHELL LONGITUDINALS WEB (300X10)	1.0	3.0	284	10	284	9	24.14	13.9400	336.51	4690.97	1.45
50	INNER SHELL LONGITUDINALS WEB (320X10)	1.0	3.0	304	10	304	9	25.84	13.0900	338.25	4427.63	1.56
51	INNER SHELL LONGITUDINALS WEB (360X10)	1.0	3.0	344	10	344	9	29.24	11.3900	333.04	3793.37	1.76
52	INNER SHELL LONGITUDINALS WEB (380X10)	2.0	3.0	364	10	364	9	61.88	9.2650	573.32	5311.79	3.73
53	INNER SHELL LONGITUDINALS FLANGES (125X16)	3.0	3.0	16	125	15	125	54.38	8.8400	480.68	4249.17	708.01
54	INNER SHELL LONGITUDINALS FLANGES (125X16)	2.0	3.0	16	125	15	125	36.25	5.8650	212.61	1246.94	472.01
55	INNER SHELL LONGITUDINALS WEB (370X10)	2.0	3.0	354	10	354	9	60.18	9.2650	557.57	5165.86	3.62
56	INNER SHELL LONGITUDINALS WEB (410X10)	2.0	3.0	394	10	394	9	66.98	5.8650	392.84	2303.99	4.03



No	Description of Item	Pieces	Corrosion addition (mm)	Gross Dimensions (mm)		Net Dimensions (mm)		Area of Item	Axis from	Item's Moment	Item's Inertia	Item's Inertia		
			Thickness	Breadth	Height	Breadth <sub>net</sub>	Height <sub>net</sub>	(cm <sup>2</sup> )	B.L. (m)	(cm <sup>2</sup> *m)	about B.L. (cm <sup>2</sup> *m <sup>2</sup> )	about G (cm <sup>4</sup> )		
57	HOPPER LONGITUDINALS FLANGE (125X19)	3.0	3.0	19	125	18	125	65.63	3.3202	217.89	723.44	42724.61		
58	HOPPER LONGITUDINALS WEB (370X10)	3.0	3.0	351	10	351	9	89.51	3.3202	297.18	986.68	510551.44		
59	BOTTOM LONGITUDINALS WEB (400X10)	16.0	3.0	10	381	9	381	518.16	0.2032	105.30	21.40	62680.52		
60	BOTTOM LONGITUDINALS FLANGE (125X19)	16.0	3.0	125	19	125	18	350.00	0.4025	140.86	56.69	89.32		
61	INNER BOTTOM LONGITUDINALS WEB (400X10)	13.0	3.0	10	378	9	378	417.69	1.8910	789.85	1493.61	49734.35		
62	INNER BOTTOM LONGITUDINALS FLANGE (125X22)	13.0	3.0	125	22	125	21	333.13	1.6918	563.56	953.41	116.66		
63	SIDE GIRDER LONGITUDINALS WEB (200A)	2.0	3.0	186	8	186	7	24.18	0.9925	24.00	23.82	0.85		
64	SIDE GIRDER LONGITUDINALS FLANGE (200A)	2.0	3.0	14	90	13	90	22.50	0.9475	21.32	20.20	151.88		
65	CL GIRDER LONGITUDINALS WEB (200A)	1.0	3.0	186	8	186	7	12.09	0.9925	12.00	11.91	0.43		
66	CL GIRDER LONGITUDINALS FLANGE (200A)	1.0	3.0	14	90	13	90	11.25	0.9925	11.17	11.08	75.94		
67	DECK LONGITUDINALS WEB (250A) -CAMBER	12.0	4.0	9	235	7	235	197.40	18.3075	3613.90	66161.48	9084.51		
68	DECK LONGITUDINALS FLANGE (250A)-CAMBER	12.0	4.0	90	15	90	13	140.40	18.1835	2552.96	46421.81	19.77		
69	DECK LONGITUDINALS WEB (250A) -STRAIGHT	6.0	4.0	9	235	7	235	98.70	18.6325	1839.03	34265.68	4542.26		
70	DECK LONGITUDINALS FLANGE (250A)-STRAIGHT	6.0	4.0	90	15	90	13	70.20	18.5085	1299.30	24048.03	9.89		
71	CL BLKHD LONGITUDINALS WEB (200A)	1.0	4.0	186	8	186	6	11.16	17.5900	196.30	3452.99	0.33		
72	CL BLKHD LONGITUDINALS FLANGE (200A)	1.0	4.0	14	90	12	90	10.80	17.5450	189.49	3324.53	72.90		
73	CL BLKHD LONGITUDINALS WEB (250A)	0.5	4.0	235	9	235	7	8.23	16.4200	135.05	2217.59	0.34		
74	CL BLKHD LONGITUDINALS FLANGE (250A)	0.5	4.0	15	90	13	90	5.85	16.3750	95.79	1568.62	39.49		
75	CL BLKHD LONGITUDINALS WEB (300A)	0.5	4.0	284	10	284	8	11.36	15.6400	177.67	2778.77	0.61		
76	CL BLKHD LONGITUDINALS FLANGE (300A)	0.5	4.0	16	90	14	90	6.30	15.5950	98.25	1532.19	42.53		
77	CL BLKHD LONGITUDINALS WEB (300A)	0.5	2.5	284	10	284	9	12.43	14.7900	183.77	2717.90	0.79		
78	CL BLKHD LONGITUDINALS FLANGE (300A)	0.5	2.5	16	90	15	90	6.64	14.7450	97.87	1443.09	44.80		
79	CL BLKHD LONGITUDINALS WEB (350A)	1.0	2.5	333	11	333	10	32.47	12.6650	411.20	5207.86	2.57		
80	CL BLKHD LONGITUDINALS FLANGE (350A)	1.0	2.5	17	100	16	100	15.75	12.6150	198.69	2506.43	131.25		
81	CL BLKHD LONGITUDINALS WEB (350X10)	1.5	2.5	331	10	331	9	43.44	10.8233	470.21	5089.20	2.77		
82	CL BLKHD LONGITUDINALS FLANGE (125X19)	1.5	2.5	19	125	18	125	33.28	10.7608	358.13	3853.82	433.35		
83	CL BLKHD LONGITUDINALS WEB (400A)	2.0	2.5	384	12	384	10	78.72	9.2650	729.34	6757.34	6.89		
84	CL BLKHD LONGITUDINALS FLANGE (400A)	2.0	2.5	16	100	15	100	29.50	9.2150	271.84	2505.03	245.83		
85	CL BLKHD LONGITUDINALS WEB (400A)	2.5	2.5	384	12	384	10	98.40	4.5940	452.05	2076.72	8.62		
86	CL BLKHD LONGITUDINALS FLANGE (400A)	2.5	2.5	16	100	15	100	36.88	4.5440	167.56	761.39	307.29		
87	STRINGER 23 LONGITUDINALS WEB (150A)	2.0	3.0	9	141	8	141	21.15	4.5195	95.59	432.01	350.40		
88	STRINGER 23 LONGITUDINALS FLANGE (150A)	2.0	3.0	90	9	90	8	13.50	4.4453	60.01	266.76	0.63		
89	STRINGER 26 LONGITUDINALS WEB (150A)	2.0	3.0	9	141	8	141	21.15	7.0695	149.52	1057.03	350.40		
90	STRINGER 26 LONGITUDINALS FLANGE (150A)	2.0	3.0	90	9	90	8	13.50	6.9953	94.44	660.60	0.63		
91	STRINGER 32 LONGITUDINALS WEB (150A)	2.0	3.0	9	141	8	141	21.15	12.1695	257.38	3132.25	350.40		
92	STRINGER 32 LONGITUDINALS FLANGE (150A)	2.0	3.0	90	9	90	8	13.50	12.0953	163.29	1974.98	0.63		
93	STRINGER 36 LONGITUDINALS WEB (150A)	2.0	3.0	9	141	8	141	21.15	15.5695	329.29	5126.96	350.40		
94	STRINGER 36 LONGITUDINALS FLANGE (150A)	2.0	3.0	90	9	90	8	13.50	15.4953	209.19	3241.39	0.63		
								<b>1.55635</b>			<b>15740.91</b>	<b>120936.22</b>	<b>1619722.37</b>	<b>286412606.71</b>

Moulded Depth of vessel (cm)	<b>1810.0</b>	Total Area of Items (cm <sup>2</sup> )	<b>15741</b>
Moment of Inertia about B. L. (cm <sup>4</sup> )	<b>16483636342</b>	Moment of Inertia about Neutral axis (cm <sup>4</sup> )	<b>14 384 393 828</b>
Neutral axis from B.L. (cm)	<b>768.293</b>	Moment of Inertia about Decline (cm <sup>4</sup> )	<b>31 465 712 332</b>
Neutral axis from Decline (cm)	<b>1041.707</b>		
<b>Bottom Section Modulus (cm<sup>3</sup>)</b>	<b>18722549</b>	<b>Deck Section Modulus (cm<sup>3</sup>)</b>	<b>13808477</b>
205% OF REQUIRED SM <sub>0</sub>		120%	OF REQUIRED SM <sub>0</sub>
205% OF REQUIRED SM (+)		120%	OF REQUIRED SM (+)
603% OF REQUIRED SM (-)		353%	OF REQUIRED SM (-)
OK		OK	

#### 6.2.4. Steps 4 to 5 - Calculation of the neutral axis at each step

Steps 4 to 5 refer to a procedure which is iterative until the sum of the forces acting on all the hull girder's structural elements equals to zero and therefore the estimated stress distribution acting over the hull girder section is in equilibrium (refer to figure 3.5). For each structural element (denoted by the index  $j$ ), the strain corresponding to the curvature  $\kappa_i$ , is calculated as  $\epsilon_{ij} = \kappa_i (z_j - z_{NA-i})$ , the corresponding stress is derived by the end shortening curves obtained during step 2, while the (normal) force acting on the element is calculated as  $\sigma_j \cdot A_j$ . In sagging condition, which is the critical condition for tankers, structural elements above the neutral axis are under compression whereas structural elements below the neutral axis are under tension.

Not knowing in advance the position of the neutral axis at which the stress distribution is in equilibrium, the position of the new neutral axis is assumed to be at a certain position and the sum of the forces corresponding to that position are calculated. In the case where the sum of the forces is equal to zero the iterative loop is terminated and the neutral axis has been determined. In the opposite case, the position of the neutral axis is readjusted accordingly and the forces are recalculated.

This iterative procedure has been applied in this work using the software Excel. More specifically, a program has been developed which calculates for each step the stress-strain magnitudes acting on each structural element (longitudinal stiffener or hard corner) and corresponding to the applied curvature. Accordingly, the total force acting on the hull girder section is determined. Using the feature of Excel named "Goal seek", the position of the neutral axis at each step can be easily determined by setting as a "goal" to minimize the sum of forces acting on the hull girder section by repeatedly changing the position of the assumed neutral axis. This feature is shown below in Figure 6.8.

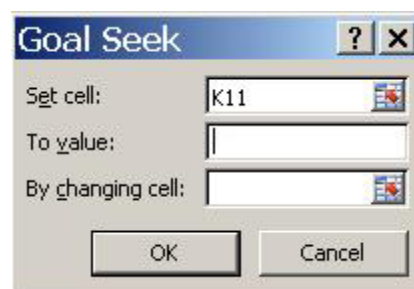


Fig.6.8. Feature "Goal seek" of software Excel

### 6.2.5. Step 6 - Calculation of the bending moment at each step

Having determined the position of the neutral axis for each step the corresponding bending moment is determined by summing the force contributions of all elements as follows:

$$M_i = 0.1 \sum \sigma_j A_j |z_j - z_{NA-i}|$$

where  $(z_j - z_{NA-i})$  is the distance of each structural element (with index j) from the neutral axis of step i under consideration.

### 6.2.6. Step 7 - Construction of the M-k Curve and the Ultimate Bending Capacity estimate

As described above, at each step the bending moment  $M_i$  corresponding to a curvature  $\kappa_i$  has been determined. The pair of values  $M_i$ -  $\kappa_i$  of each step define the M-k curve, the peak value of which represents the hull girder's ultimate bending capacity  $M_u$ .

## 6.3. Predominant Buckling modes obtained by CSR Approach

Prior to the presentation of the load end shortening curves, constructed using the CSR Formulas, it would be useful to make a reference to the predominant mode of failure in each structural element, as predicted by these formulas.

Table 6.2 summarizes a list of all structural elements that are under compression, at least at one step until the hull girder collapses (their position, at least in one step, is above the neutral axis). Structural elements not included in the table are either considered as hard corners or are always under tension and, therefore, their behavior is regarded as elastic-perfectly plastic resulting to an ultimate stress equal to their yield stress.

Location	Panel	Structural Element	Plate / Stiffener	Buckling mode 1: Min / 3: Max			$\sigma_{yd}$	$\sigma_u$	$\sigma_u/\sigma_{yd}$	$\epsilon_u/\epsilon_{yd}$
				1	2	3				
Main Deck	M 2	M 2 - 1	Both	Beam Column	Torsional	Web	245	172.74	0.705	1.012
		M 2 - 2	Both				245	172.74	0.705	1.012
		M 2 - 3	Both				245	172.74	0.705	1.012
		M 2 - 4	Both				245	172.74	0.705	1.012
		M 2 - 5	Both				245	172.74	0.705	1.012
		M 2 - 6	Both				245	172.74	0.705	1.012
		M 2 - 7	Both				245	172.55	0.704	1.012
		M 2 - 8	Both				245	172.55	0.704	1.012
		M 2 - 9	Both				245	172.55	0.704	1.012
		M 2 - 10	Both				245	172.55	0.704	1.012
		M 2 - 11	Both				245	172.55	0.704	1.012
		M 2 - 12	Both				245	172.55	0.704	1.012
		M 2 - 13	Both				245	172.55	0.704	1.012
		M 2 - 14	Both				245	172.55	0.704	1.012
		M 2 - 15	Both				245	172.55	0.704	1.012
	M 1	M 2 - 16	Both	245	172.85	0.706	1.012			
		M 1 - 18	Both	245	188.73	0.770	1.012			
		M 1 - 19	Both	245	188.73	0.770	1.012			
		CL 2 - 23	Both	315	225.59	0.716	1.024			
CL Blkh	CL 2	CL 2 - 24	Both	Torsional	Beam Column	Web	315	224.63	0.713	1.024
		CL 2 - 25	Both				315	221.60	0.704	1.024
		CL 2 - 26	Plate				315	226.51	0.719	1.024
		CL 2 - 26	Stiffener				245	188.86	0.771	1.012
		CL 2 - 27	Plate				315	221.60	0.704	1.024
		CL 2 - 27	Stiffener				245	185.98	0.759	1.012
		CL 2 - 28	Plate				315	221.37	0.703	1.024
		CL 2 - 28	Stiffener				245	185.80	0.758	1.012
		CL 2 - 29	Plate				315	213.57	0.678	1.024
		CL 2 - 29	Stiffener				245	179.49	0.733	1.012
		CL 2 - 30	Plate				315	213.57	0.678	1.024
		CL 2 - 30	Stiffener				245	179.49	0.733	1.012
		CL 2 - 31	Plate				315	214.72	0.682	1.024
		CL 2 - 31	Stiffener				245	179.97	0.735	1.012
		CL 2 - 32	Plate				315	219.10	0.696	1.024
		CL 2 - 32	Stiffener				245	182.70	0.746	1.012
		CL 2 - 33	Plate				280	199.65	0.713	1.019
		CL 2 - 33	Stiffener				245	181.16	0.739	1.012
		CL 2 - 34	Both				245	176.66	0.721	1.012
		CL 2 - 35	Both				245	174.03	0.710	1.012
		CL 2 - 36	Both				245	172.04	0.702	1.012
		CL 2 - 37	Plate				245	172.20	0.703	1.012
		CL 2 - 37	Stiffener				315	203.76	0.647	1.024
		CL 2 - 38	Plate				245	161.74	0.660	1.012
		CL 2 - 38	Stiffener				315	188.07	0.597	1.024
		CL 2 - 39	Plate				245	162.38	0.663	1.012
CL 2 - 39	Stiffener	315	188.86	0.600	1.024					

**Table 6.2.** Predominant Buckling Modes as per CSR Formulas

Location	Panel	Structural Element	Plate / Stiffener	Buckling mode 1: Min / 3: Max			$\sigma_{yd}$	$\sigma_u$	$\sigma_u/\sigma_{yd}$	$\epsilon_u/\epsilon_{yd}$		
				1	2	3						
Inner Bulkhead	I 4	I 4 - 38	Both	Beam Column	Torsional	Web	315	190.40	0.604	1.024		
		I 4 - 37	Both				315	193.12	0.613	1.024		
	I 3	I 3 - 35	Both	Torsional	Beam Column	Web	245	177.41	0.724	1.012		
		I 3 - 34	Both				245	177.12	0.723	1.012		
			I 3 - 33	Both				245	176.48	0.720	1.012	
	I 2		I 2 - 31	Plate	Torsional	Beam Column	Web	315	205.66	0.653	1.024	
			I 2 - 31	Stiffener				245	174.85	0.714	1.012	
			I 2 - 30	Plate				315	203.93	0.647	1.024	
			I 2 - 30	Stiffener				245	173.88	0.710	1.012	
			I 2 - 29	Plate				315	211.54	0.672	1.024	
			I 2 - 29	Stiffener				245	178.52	0.729	1.012	
			I 2 - 28	Plate				315	211.54	0.672	1.024	
			I 2 - 28	Stiffener				245	178.52	0.729	1.012	
			I 2 - 27	Plate				315	220.94	0.701	1.024	
			I 2 - 27	Stiffener				245	186.23	0.760	1.012	
	I 1		I 1 - 25	Plate	Torsional	Beam Column	Web	315	224.51	0.713	1.024	
			I 1 - 25	Stiffener				245	189.46	0.773	1.012	
			I 1 - 24	Plate				315	224.51	0.713	1.024	
			I 1 - 24	Stiffener				245	189.46	0.773	1.012	
	Side Shell	S 5	S 5 - 38	Plate	Beam Column	Torsional	Web	315	197.04	0.626	1.024	
			S 5 - 38	Stiffener				245	170.21	0.695	1.012	
			S 5 - 37	Plate				315	190.09	0.603	1.024	
			S 5 - 37	Stiffener				245	164.59	0.672	1.012	
S 4			S 4 - 35	Plate	Beam Column	Torsional	Web	315	221.90	0.704	1.024	
			S 4 - 35	Stiffener				245	186.40	0.761	1.012	
				S 4 - 34	Plate	Torsional	Beam Column	Web	315	221.90	0.704	1.024
				S 4 - 34	Stiffener				245	186.40	0.761	1.012
				S 4 - 33	Plate				315	222.60	0.707	1.024
				S 4 - 33	Stiffener				245	187.61	0.766	1.012
S 3			S 3 - 31	Plate	Torsional	Beam Column	Web	315	219.98	0.698	1.024	
			S 3 - 31	Stiffener				245	186.09	0.760	1.012	
			S 3 - 30	Plate				315	219.22	0.696	1.024	
			S 3 - 30	Stiffener				245	185.65	0.758	1.012	
			S 3 - 29	Plate				315	219.22	0.696	1.024	
			S 3 - 29	Stiffener				245	185.65	0.758	1.012	
			S 3 - 28	Plate				315	225.51	0.716	1.024	
			S 3 - 28	Stiffener				245	189.43	0.773	1.012	
			S 3 - 27	Plate				315	225.04	0.714	1.024	
			S 3 - 27	Stiffener				245	189.17	0.772	1.012	
S 2			S 2 - 25	Plate	Torsional	Beam Column	Web	315	222.92	0.708	1.024	
			S 2 - 25	Stiffener				245	187.94	0.767	1.012	
			S 2 - 24	Plate				315	222.32	0.706	1.024	
S 1			S 2 - 24	Stiffener				245	187.60	0.766	1.012	
	S 1 - 22		Both	315				226.35	0.719	1.024		
	S 1 - 21		Both	315				226.35	0.719	1.024		
Stringer 36	ST 4	S 1 - 20	Both				315	246.26	0.782	1.024		
Stringer 32	ST 3	ST 4 - 18	Both	Beam Column	Torsional	Web	245	148.79	0.607	1.012		
		ST 4 - 19	Both				245	148.79	0.607	1.012		
Stringer 26	ST 2	ST 3 - 18	Both	Beam Column	Torsional	Web	245	146.52	0.598	1.012		
		ST 3 - 19	Both				245	146.52	0.598	1.012		
		ST 2 - 18	Both				245	146.52	0.598	1.012		
		ST 2 - 19	Both				245	146.52	0.598	1.012		

**Table 6.2 (cont.).** Predominant Buckling Modes as per CSR Formulas

In table 6.2, Column 1 describes the plating to which the structural element corresponds (inner bulkhead, side shell etc), Columns 2 & 3 refer to the nomenclature of each stiffener, as presented in Figure 5.2, Column 4 denotes whether the corresponding results have been calculated in accordance with the yield stress of the plate or the stiffener ('both' means that the plate and stiffener are of the same yield stress), Columns 5-7 depict the buckling modes (1 and 3 refer to the buckling mode corresponding to the minimum and maximum stress respectively), whereas Columns 8,9 and 10 correspond to the structural element's yield stress, ultimate stress/yield stress ratio and ultimate strain/yield strain ratio respectively. The results indicated in Table 6.2 refer to IACS Approach.

The dimensions of each structural element were given in Chapter 5 whereas their geometric characteristics based on net scantlings are included in Table 6.1. As shown in above mentioned table, the predominant buckling modes of the structural elements, as per the CSR formulas, are either the torsional stiffener buckling or the beam-column buckling. This is dependent on the geometric properties of each structural element. It can be seen that structural elements with a predominant beam column buckling include all the longitudinal stiffeners of the Main deck ( $b_w=1.155$ ) and the stringers ( $b_w=0.647$ ), stiffeners 37-39 of the CL Bulkhead ( $b_w=1.209-1.310$ ), stiffeners 34-38 of Side Shell ( $b_w=1.066-1.109$ ) and stiffeners 37-38 of the Inner Bulkhead ( $b_w=1.310$ ). These structural elements have a web slenderness ratio lower than or equal to 1.310. All the remaining tabulated structural elements have a web slenderness ratio of 1.310-1.611 resulting in torsional column buckling (web height of 274mm and above). The load end shortening curves of these structural elements are presented in the following subsection.

Moreover, the ratio of the ultimate capacity to the yield stress for these structural elements seems to fluctuate from 0.598-0.773. It would be of great interest to compare the structural elements' ultimate capacity as derived by the CSR formulas to the one computed by FEA analysis described in Chapter 7. Such comparison are included in Chapter 8.

#### **6.4. Load End Shortening Curves of the Structural Elements**

At this point, the load end shortening curves of the structural elements as derived by the CSR Approach will be presented. This subsection presents a selection

of load end shortening curves obtained by the CSR IACS approach in order to demonstrate the effect of the structural element's geometric characteristics to their buckling behavior.

Figure 6.9 below shows the Load end Shortening Curves of the longitudinal stiffeners of the Main Deck (L 250x90x9/15) under compression. As shown, the critical stress for the Main Deck Stiffeners is the beam column buckling stress, which reaches the ultimate limit state at  $0.705 \sigma/\sigma_{yd}$  and  $1.012 \epsilon/\epsilon_{yd}$ .

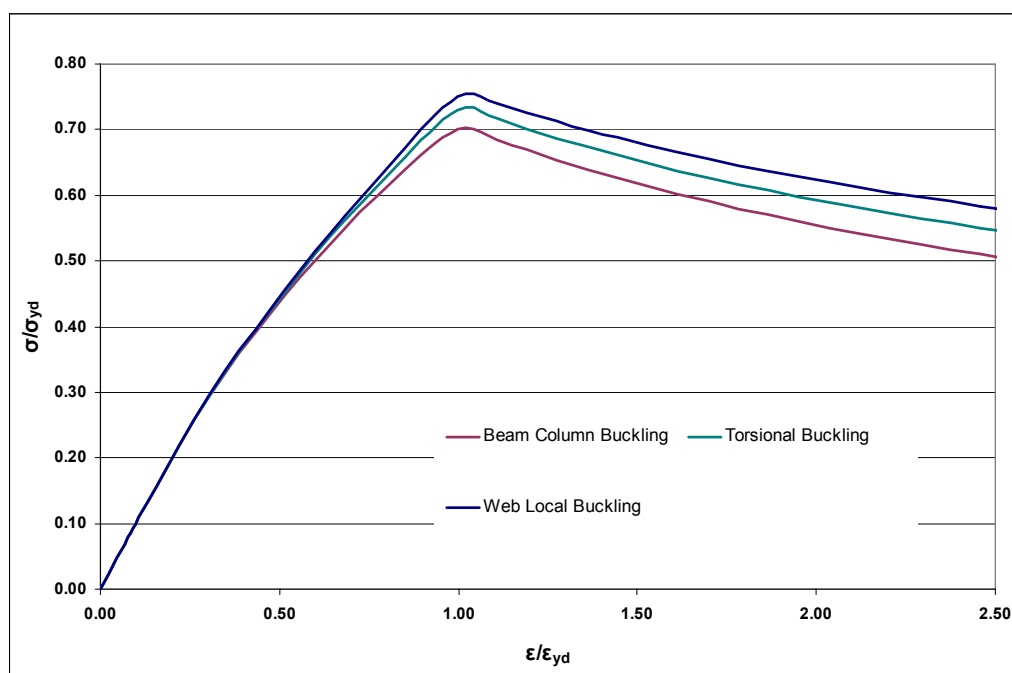


**Fig.6.9.** Load end shortening curves of Main Deck longitudinal stiffeners (L 250x90x9/15) under compression

As already mentioned, the buckling behaviour of a stiffener depends significantly on its geometric characteristics. Stiffeners of web slenderness ratio 0.647 to 1.310 and web height to web thickness ratio from 18.80 to 34.59 fail due to beam column buckling whereas stiffeners of web slenderness ratio 1.310 to 1.611 and web height to web thickness ratio from 35.76 to 46.35 fail due to torsional buckling. Figure 6.10 depicts the load end shortening curves of the Inner Shell Longitudinal Stiffener 33 (T 320x10/100x16) which is compared to the load end shortening curves of the same stiffener but with a decreased web height to 260mm (T 260x10/100x16). As shown by decreasing the web height the beam column buckling stress is decreased significantly whereas the torsional buckling stress is slightly increased (these are shown with dotted lines). As a result the beam column buckling stress becomes the critical stress as opposed to the torsional buckling

stress. The latter was the critical stress of the stiffener in the case of the greater web height.

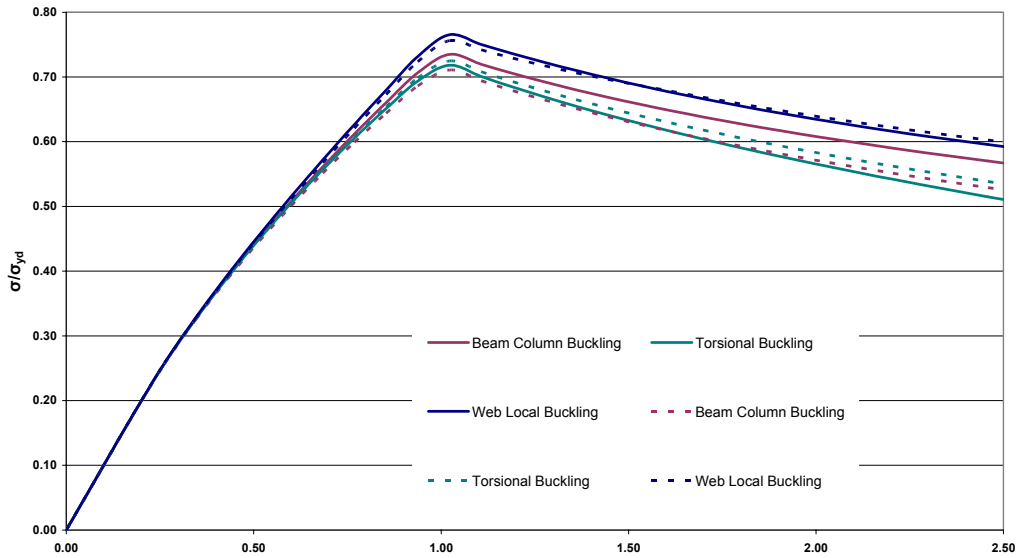


**Fig.6.10.** Load end shortening curves of  $\epsilon/\epsilon_{yd}$  Inner Shell Longitudinal Stiffener 33 (T 320x10/100x16) under compression

The above remark is also confirmed by the figures below in which the Load End Shortening Curves of CL Bulkhead Longitudinal Stiffener 37 (L 250x90x9/14) and Stiffener 36 (L 300x90x10/16) are shown.

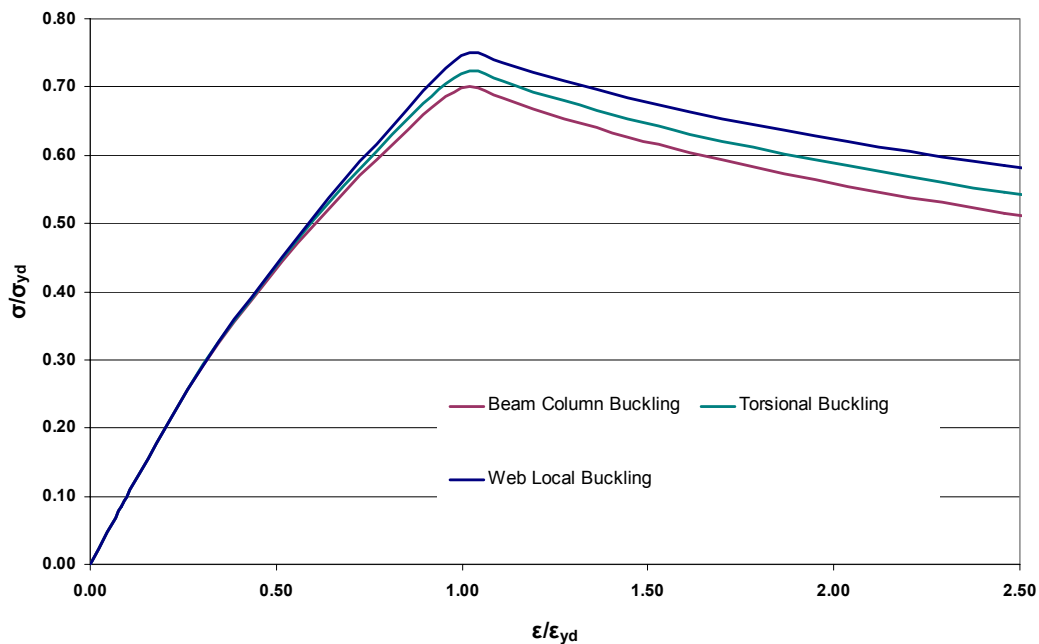


**Fig.6.11.** Load end shortening curves of CL Bulkhead Longitudinal Stiffener 37 (L 250x90x9/14) under compression



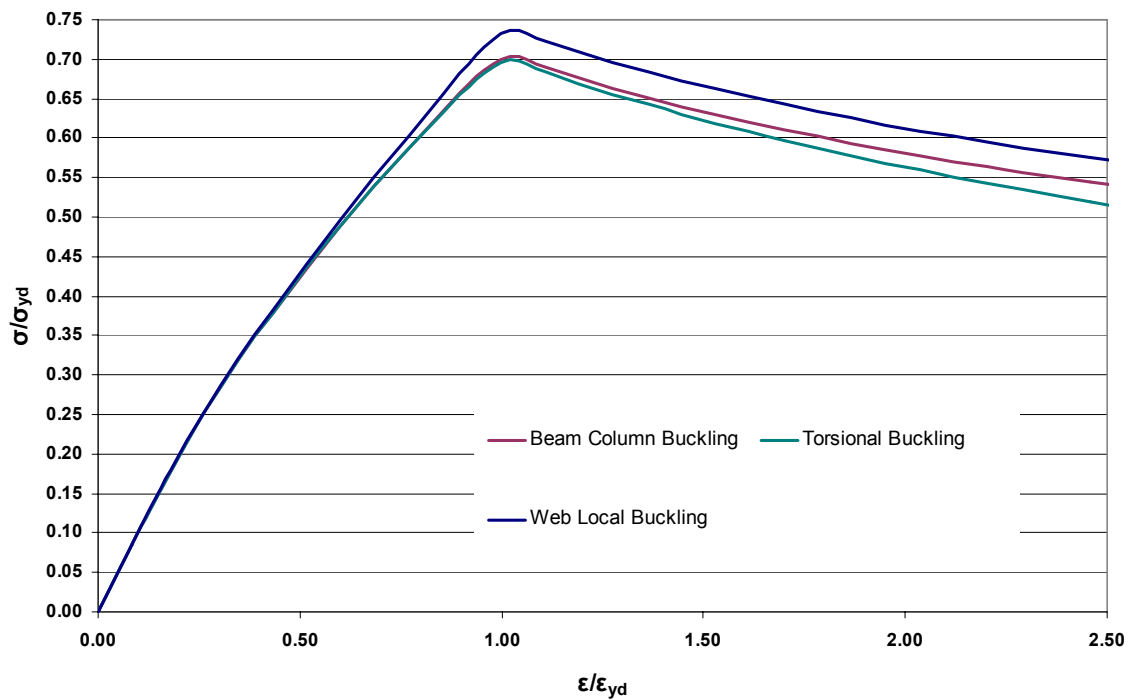


**Fig.6.12.** Load end shortening curves of CL Bulkhead Longitudinal Stiffener 36 (L 300x90x10/16) under compression

All the above end shortening curves correspond to structural elements under compression. Figure 6.13 depicts the stress-strain curve of the Inner Bottom Longitudinal 13 (T 400x10/125x22) under tension. It is clear that the CSR formulas for the structural elements under tension lead to an elastic-perfectly plastic behaviour.

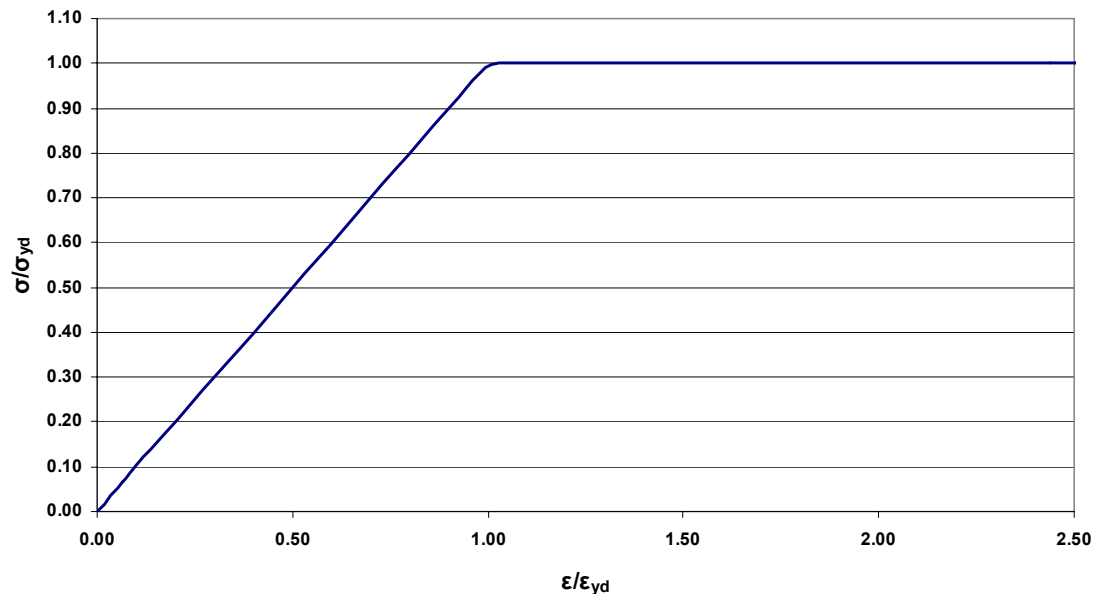


**Fig.6.13.** Load end shortening curves of Inner Bottom Longitudinal Stiffener 13 (T 400x10/125x22) under tension

We should emphasize here that the same elastic-perfectly plastic behaviour is obtained for hard corners either under tension or compression as shown in figures 6.14 and 6.15 respectively.

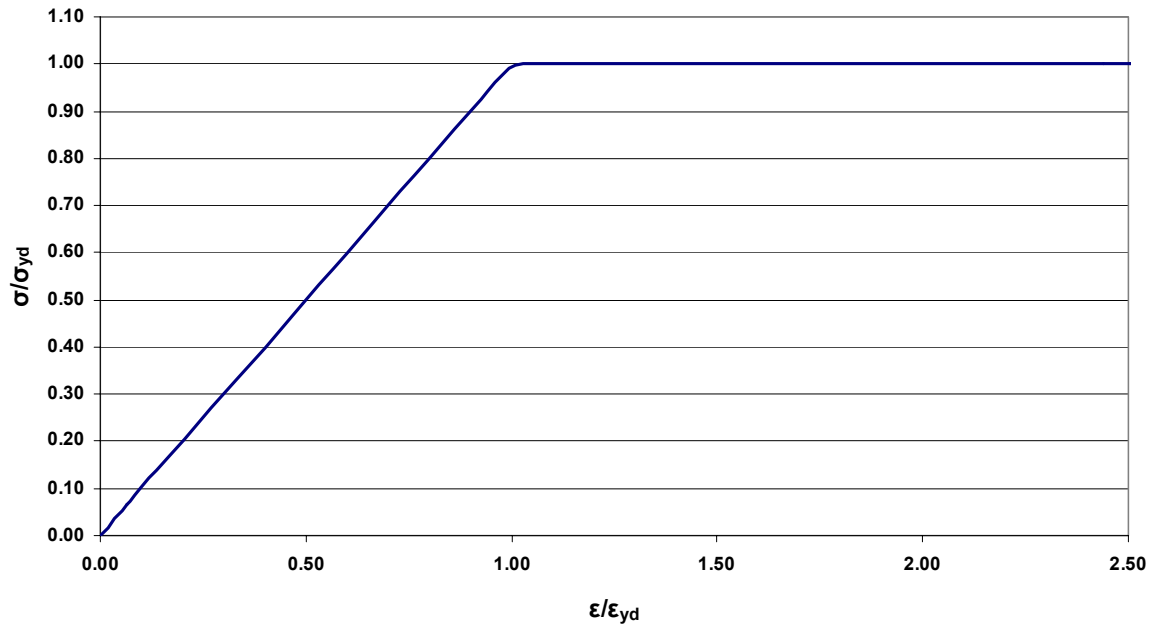


**Fig.6.14.** Load end shortening curves of Hard Corner Main Deck - CL Bulkhead under compression

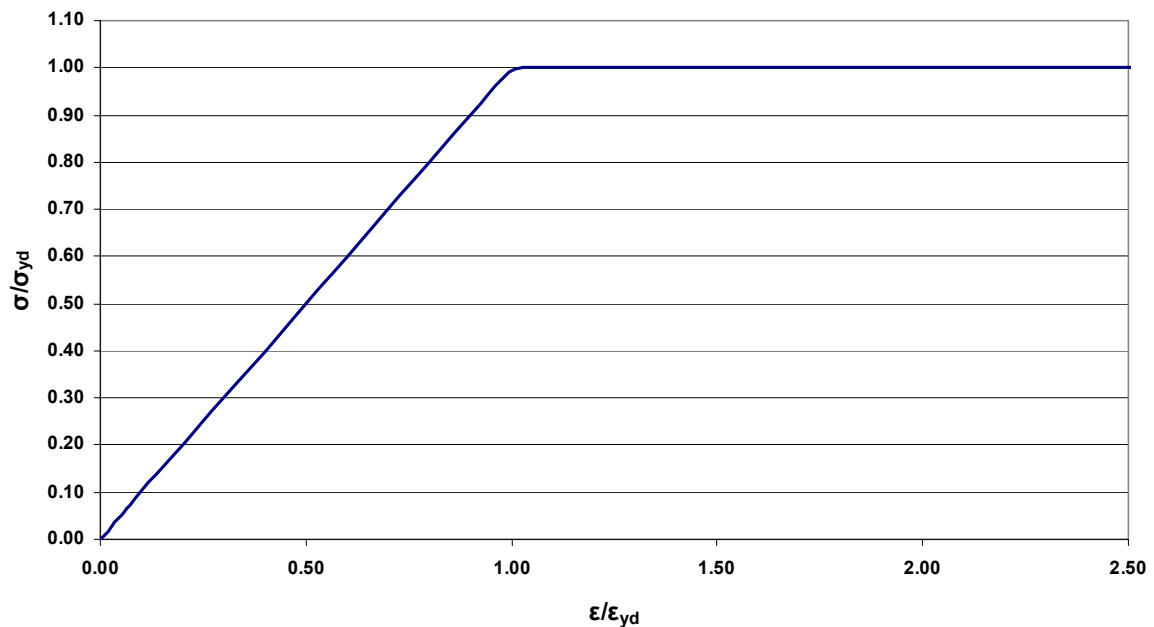


**Fig.6.15.** Load end shortening curves of Hard Corner Inner Bottom - CL Bulkhead under tension

## 6.5. Position of neutral axis versus imposed curvature

The position of the hull girder's neutral axis at each imposed curvature value in the sagging condition is shown in Figure 6.16. The results were obtained using the IACS recommended approach. As shown, the neutral axis position is reduced significantly with the increase of the curvature up to a certain curvature value beyond which the position of the neutral axis seems to be less affected.

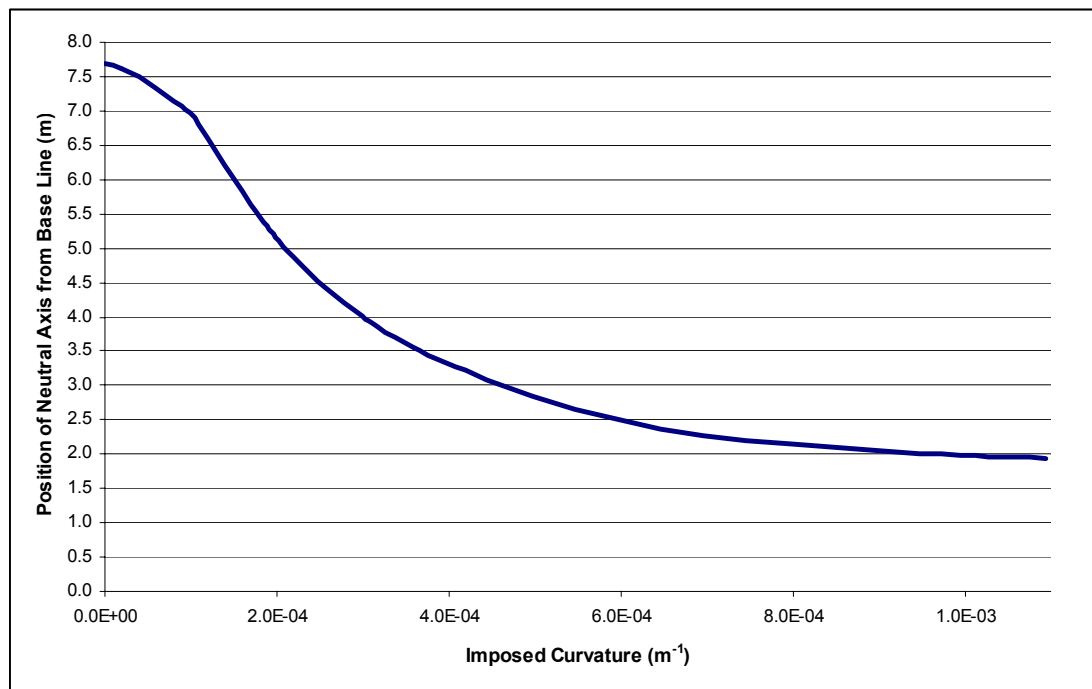


**Fig.6.16.** Position of neutral axis at each imposed curvature

## 6.6. Hull girder ultimate bending capacity

At this point the Hull Girder Vertical Bending Moment versus the imposed curvature curve is presented enabling us to determine not only the vertical hull girder bending moment capacity but also the structural elements that have collapsed prior the ultimate limit state. Figure 6.17 shows the M-k curve as derived by the CSR Incremental-Iterative Approach using the IACS Recommendation.

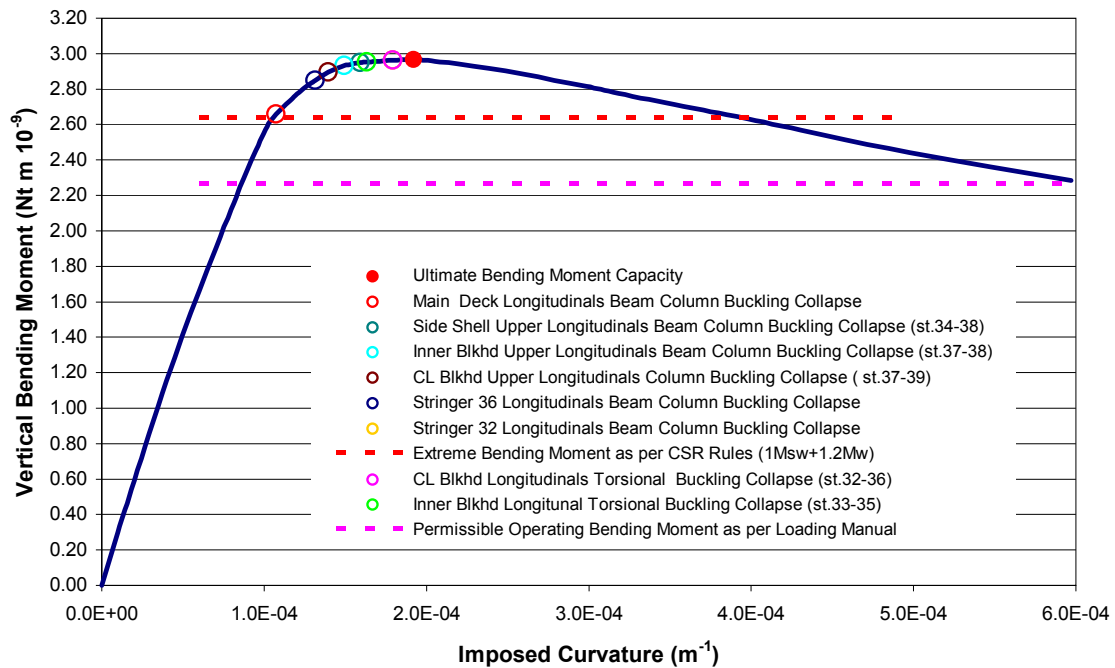


**Fig.6.17.** CSR Hull Girder Vertical Bending Moment - Imposed Curvature Curve

The ultimate bending capacity of the Double Hull Tanker is the peak value of the curve shown in above figure and corresponds to a bending moment of  **$2.968 \times 10^9$  Nt·m** and a curvature of  **$1.93 \times 10^{-4}$  m<sup>-1</sup>** occurring at step 97 of the incremental approach. The maximum extreme bending moment at which the vessel as per CSR Rules is expected to operate and is required to fulfil has been calculated in chapter 5 as  **$2.643 \times 10^9$  Nt·m** and is shown in the above figure with a red dotted line. Taking into account that the **design safety margin** can be derived by the difference of the ultimate bending capacity and the expected design extreme bending moment  $[(M_{UCSR} - M_{bIACS}) / M_{UCSR}]$ , in this case a **design safety margin of 11%** has been applied. We should note though, that CSR Rules introduce a safety factor  $\gamma_r$  in the estimation of the hull girder ultimate strength, due to uncertainties (refer to Figure 3.1) and equal to 1.1, providing for an extra safety margin.

Having the necessary information available by the vessel's loading manual it would be interesting to compare the permissible bending moment at which the vessel actually operates. The vessel's permissible still water bending moment as per the Loading Manual is at **549360 kNt·m** or  **$0.54936 \times 10^9$  Nt·m**. Considering the CSR extreme wave bending moment as **1 430 541 kNt·m** or  **$1.430541 \times 10^9$  Nt·m** (refer to Table 5.9) and the load combination factors  $\gamma_s$  and  $\gamma_w$  as 1.0 and 1.2

respectively (refer Figure 3.1), this leads to a permissible total bending moment of  **$2.266 \times 10^9$  Nt·m**. The permissible total bending moment is shown in the above figure by the pink dotted line.

Along the M-k curve, reference is made to the buckling failure mode of the hull girder's structural elements, which collapse before the hull girder reaches its ultimate limit state. Having obtained the ultimate limit state and collapse mode of the individual structural elements, as determined by the IACS load end shortening curves (refer to Table 6.2), and knowing the strain that is applied to each structural element at each imposed curvature by the Incremental-Iterative approach, it was possible to identify at which point of the M-k curve the structural elements collapse. We should point out though, that this is concluded under the assumption that each structural element acts independently which was one of the main assumptions of the Incremental-Iterative approach. For the candidate vessel used in this study, the main deck longitudinals are the first to collapse by beam column buckling. These longitudinals receive the greatest strain among the remaining stiffeners of the hull girder section as the distance of the neutral axis from the base line is decreased with the increase of the imposed curvature. The next to collapse are stringer 36 and upper CL Bulkhead longitudinals (st.37-39) again by beam column buckling failure. Then the collapse of the inner bulkhead longitudinals st.37-38 and st.33-35 takes place because of beam-column and torsional buckling failure respectively. Just before the ultimate limit state is reached, the CL Bulkhead longitudinals in the region of the vessel's mid depth (st.32-34) fail due to torsional buckling whereas the Stringer 32 longitudinals fails due to Beam Column Buckling.

The M-k curve in Fig.6.17 has been constructed based on the IACS approach with regards to the determination of the load end shortening curve of a plate-stiffener combination with a non identical yield stress. In order to evaluate the effect on the ultimate hull girder capacity of all the alternatives discussed previously, the M-k curve has been recalculated for both the Equivalent yield stress approach and the Applicable yield stress approach. All three M-k curves are presented in Figure 6.18 for comparison reasons.

At a first glance, it is obvious that the IACS approach provides the most conservative ultimate hull girder capacity as can be envisaged by comparing the individual load end shortening curves in section 6.4. It is somewhat surprising though

that all three approaches lead to small differences in the ultimate hull girder capacity, which is in contrast to the conclusions drawn by comparing the individual load end shortening curves corresponding to these approaches.

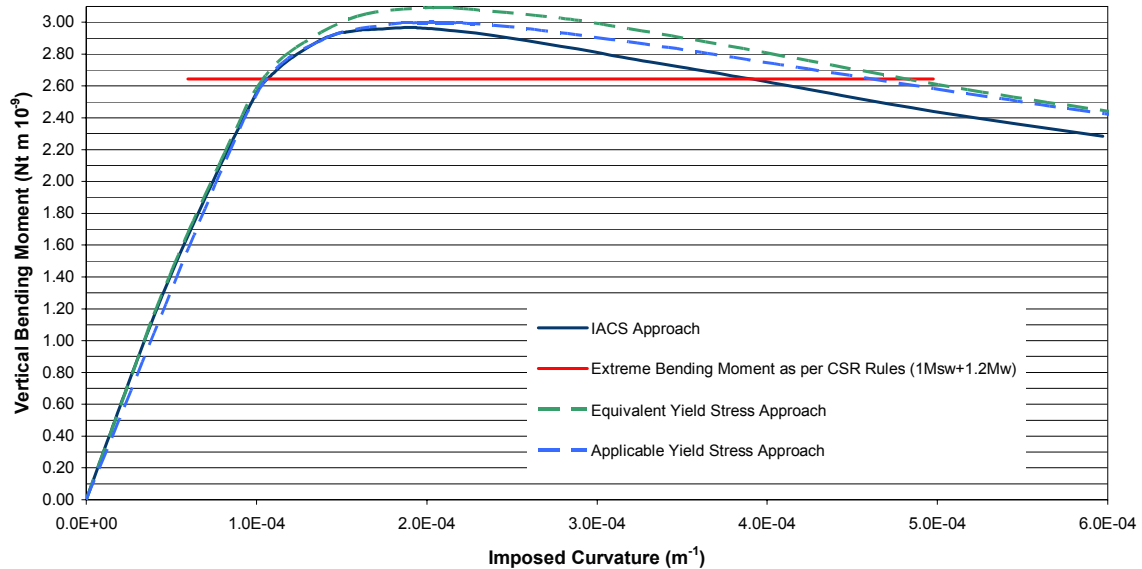


**Fig.6.18.** Hull Girder Vertical Bending Moment - Imposed Curvature Curve as per all alternative approaches

Nevertheless, by reviewing Table 6.1 in which the structural elements with different yield stresses in the plate and stiffener are shown, it can be seen that for the present vessel these correspond to 30% of the total hull girder section area. Moreover, they are placed in the mid depth area of the vessel and therefore the strain acting on these elements is relatively small. In this respect, they do not affect significantly the equilibrium of the total forces acting on the girder or the resulting bending moments as proven by the curves illustrated in above figure.

The Figure below presents the applied strain as a function of the distance from the base line for a series of imposed curvatures, which correspond to steps 5, 25, 51, 74, 86 and 97. The latter corresponds to the hull girder ultimate state in the case of the CSR-IACS approach.

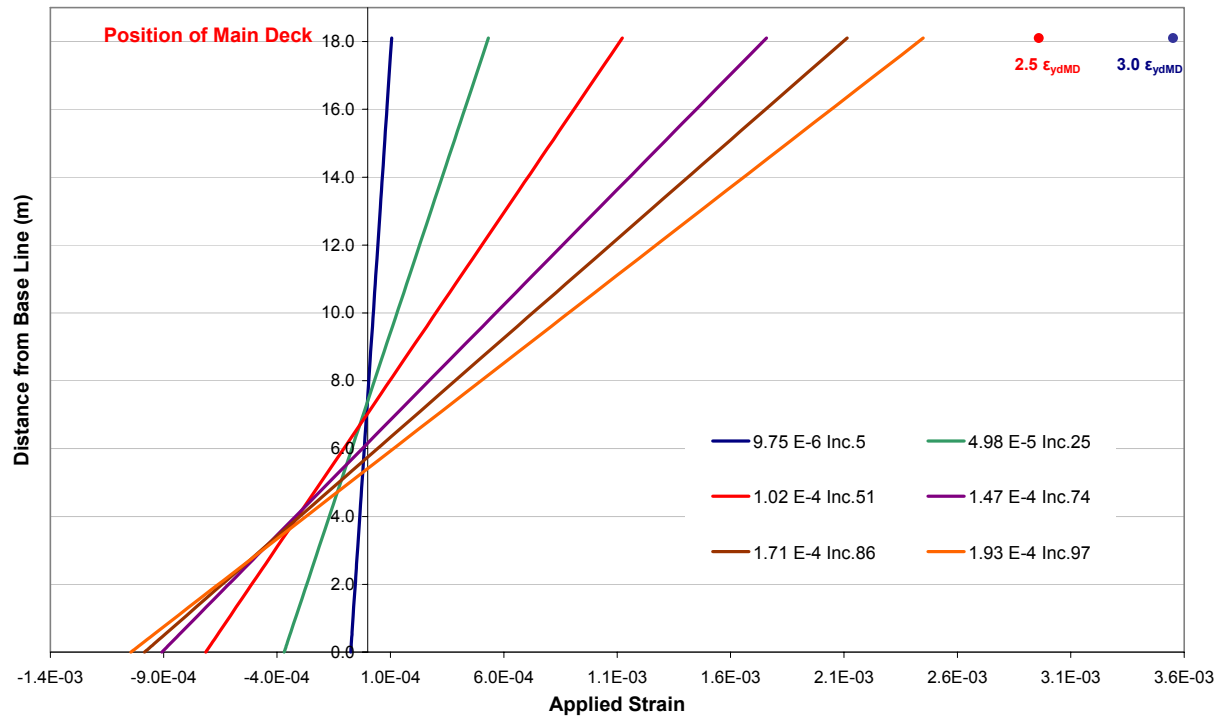


**Fig.6.19.** Applied Strain versus distance from Base Line and imposed curvature

Taking into account that the structural elements of non identical yield stress between plate and stiffener are placed approximately at 8m above base line, figure 6.19 demonstrates, as envisaged, that the strain applied on them is relatively small therefore their effect on the hull girder ultimate bending capacity is minimised.

In any case, it would be interesting to compare all three approaches to the finite element approach which will be presented in the following chapter.

## **CHAPTER 7**

### **FINITE ELEMENT APPROACH**

#### **7.1. General**

In addition to the Incremental - Iterative approach presented in the previous chapter and for the verification of same, a Finite Element Approach has been carried out for the determination of the tanker's Hull Girder's Ultimate Capacity. For this purpose, as already mentioned, the finite element code ABAQUS has been used. This Chapter describes the Finite Element approach used in the present work, outlines the assumptions made for the construction of the finite element models and describes the procedure used in the simulations and, finally, summarizes the results.

#### **7.2. Procedure of Finite Element Approach**

The Finite Element Approach used in the present dissertation thesis has the following objectives:

- the verification of the load end shortening curve formulas adopted by CSR for the collapse prediction of the hull girder structural elements (refer to chapter 3, Par.3.4.4.2).
- the comparison of the hull girder ultimate capacity, as calculated by the Incremental – Iterative Approach and the stress-strain formulas for each structural element proposed by CSR, to the hull girder ultimate capacity obtained from the Incremental – Iterative Approach in conjunction with the stress-strain curves computed via the Finite Element Approach.

The Finite Element Approach is based on the Incremental-Iterative Approach but with the stress-strain curves constructed in accordance with CSR Rules replaced by the corresponding stress-strain curves computed from FE Analysis. More specifically, all steps of the Incremental-Iterative Approach indicated by CSR Rules have been taken into account (refer to Chapter 3, Par.3.4.4.2 and Chapter 6, Par.6.2) with the exception of step 2 in which the corresponding structural element stress is calculated from the results of the FE Analysis.



The following paragraphs describe the assumptions made for the purpose of this study during the preprocessing of the adopted Finite Element models, the simulation process and the post processing of the results.

### **7.3. Preprocessing of the Finite Element Models**

It is self-explanatory, that a finite element analysis will only solve the mathematical problem, which is an idealization of the actual physical problem. Accordingly, any assumptions made during this idealisation will affect the solution of the mathematical model. For this reason it is of uppermost importance to discuss in detail the assumptions made during the pre-processing of the adopted finite element models prior to presenting the results of the simulation. These assumptions include, but are not limited to, the extent of the structural feature modelled, the size and type of the selected finite element, the boundary conditions applied, the model initial imperfections, the loading conditions, the materials, etc.

#### **7.3.1. Finite Element Structural Modeling**

During the Finite Element Approach, the longitudinally effective structure of the hull girder section has not been modelled as one piece including the entire hull girder section but has been modelled as separate stiffened and unstiffened panels of which it comprises. In this respect, the tanker midship section, as indicated in chapter 5 (refer to image 5.2), has been divided into nineteen (19) major stiffened and/or unstiffened panels which are considered to extend transversely between the adjacent primary support members (stringers, decks, girders or bulkheads, whichever is applicable) and longitudinally between the vessel's web frames.

At this point we should highlight that this is the structural modelling also proposed by the CSR Rules for the buckling assessment of the longitudinal strength of a tanker and the determination of the stiffened deck panel buckling capacity used in the estimation of the ultimate hull girder capacity, as per the CSR Single Step Method (refer to Chapter 3-Par.3.4.3). More specifically, Figure 7.1 depicts the longitudinal stiffened and/or unstiffened panels by which the CSR Rules require the longitudinally effective structure of the hull girder section to be modelled for the buckling strength assessment, whereas Table 7.1 summarizes their extent. "SP" denotes stiffened panel, while M1/M2 denote the applicable Method 1/Method 2 for

buckling strength assessment. Since it is outside the scope of this dissertation to make further reference to these methods, the reader should consult the CSR Rules.

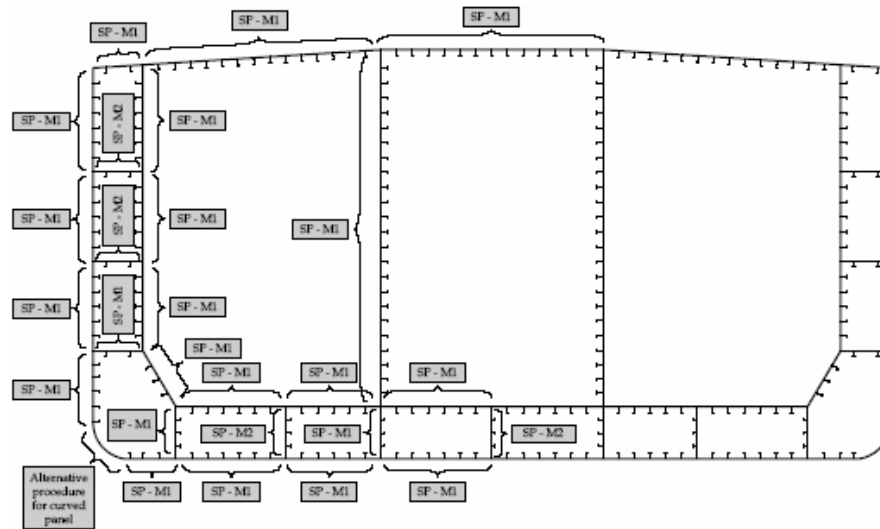


**Fig.7.1.** Stiffened and/or Unstiffened panels required by the CSR Rules for the modelling of the longitudinally effective hull girder structure and the buckling strength assessment

Structural Elements	Idealisation	Assessment method <sup>(1)</sup>	Normal panel definition <sup>(2)</sup>
<b>Longitudinal structure, see Figure D.5.1</b>			
Longitudinally stiffened panels Shell envelope Deck Inner hull Hopper tank side Longitudinal bulkheads Centreline bulkheads	Stiffened panel	Method 1	Length: between web frames Width: between primary support members (PSM) <sup>(2)</sup>
Double bottom longitudinal girders in line with longitudinal bulkhead or connected to hopper tank side	Stiffened panel	Method 1	Length: between web frames Width: full web depth
Web of horizontal girders in double side tank connected to hopper tank side	Stiffened panel	Method 1	Length: between web frames Width: full web depth
Web of double bottom longitudinal girders not in line with longitudinal bulkhead or not connected to hopper tank side	Stiffened panel	Method 2	Length: between web frames Width: full web depth
Web of horizontal girders in double side tank not connected to hopper tank side	Stiffened panel	Method 2	Length: between web frames Width: full web depth
Web of single skin longitudinal girders	Un-stiffened panel	Method 2	Between local stiffeners/face plate/PSM

**Table 7.1.** Stiffened and/or Unstiffened panels required by CSR Rules for the modelling of the longitudinally effective hull girder structure and the buckling strength assessment

Besides, as per CSR Rules, the ultimate strength of the hull girder section is to be calculated at a longitudinal section between two adjacent transverse web frames since the critical mode for tankers in sagging condition is generally the inter-frame buckling of deck structures. In view of the above, it seems that the modelling of the longitudinal extent between the vessel's web frames is adequate. The extent of the panels is illustrated in Figure 7.2.

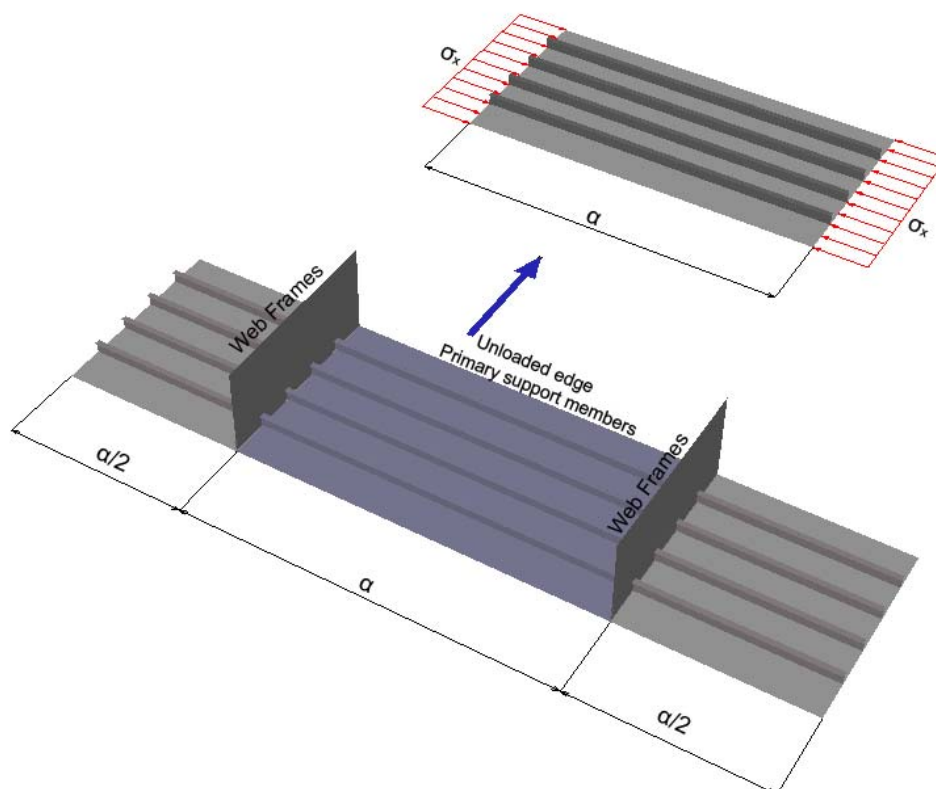
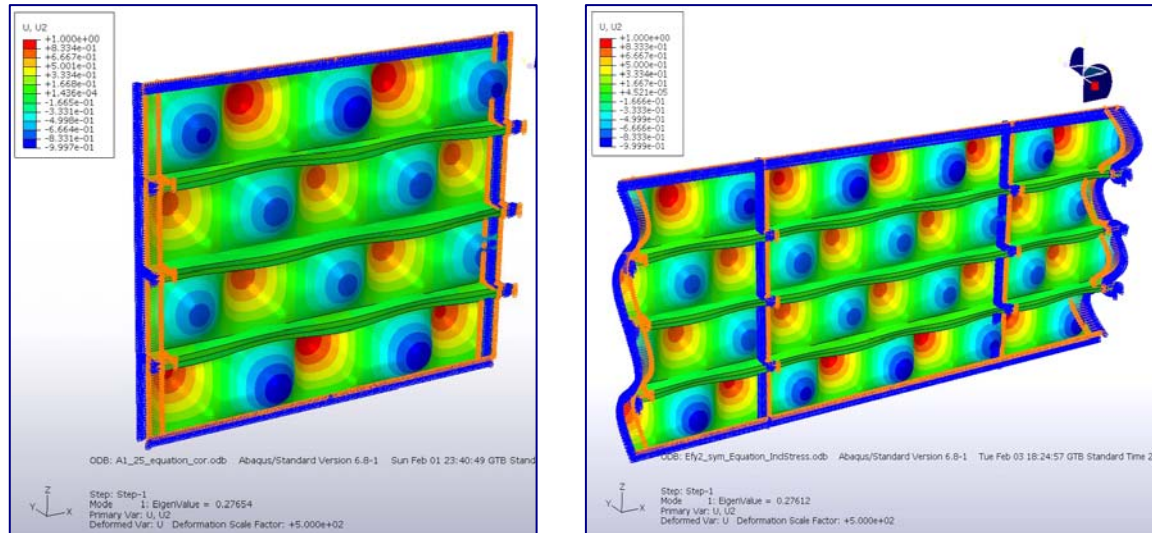


**Fig.7.2.** Extent of panels considered by Finite Element Approach

Nevertheless, in order to evaluate the effect of modelling the one-bay panel (a) instead of the two-bay panel ( $a/2+a+a/2$ ), buckling and non-linear static analysis has been performed for both alternatives at the Inner Bulkhead Panel, I3 (refer to Fig.5.2). Enabling the more effective evaluation of the resultant buckling modes the panel has been considered to be symmetric, therefore of uniform plate thickness and identical stiffener dimensions. Figure 7.3 depicts the buckling mode (displacement  $U_y$ ) of the symmetric I3 panel for both one-bay and two-bay panels.



(a)

(b)

**Fig.7.3.** Buckling Mode of I3 Symmetric Panel: **(a)** one-bay, **(b)** two-bays

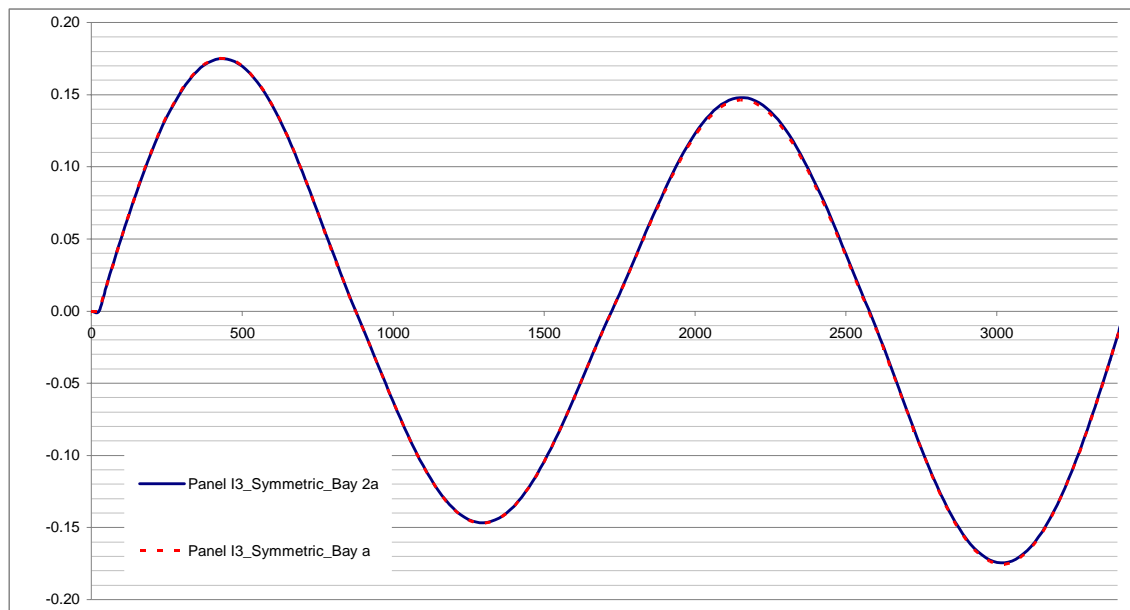


**Fig.7.4.** Normalised  $U_y$  displacement of the symmetric I3 Panel along a transverse edge

It can be seen that in both cases, the buckling analysis results in the prediction of similar buckling modes. In particular, 5 buckling waves are formed along the longitudinal edge between the web frames whereas 4 buckling waves are formed along the transverse edge. This is also confirmed by the plot of the normalised  $U_y$  displacement along the models' transverse (at mid span) and longitudinal edge (at distance  $s/2$  between stiffeners 34 and 35), shown in Figures 7.4 and 7.5 respectively.

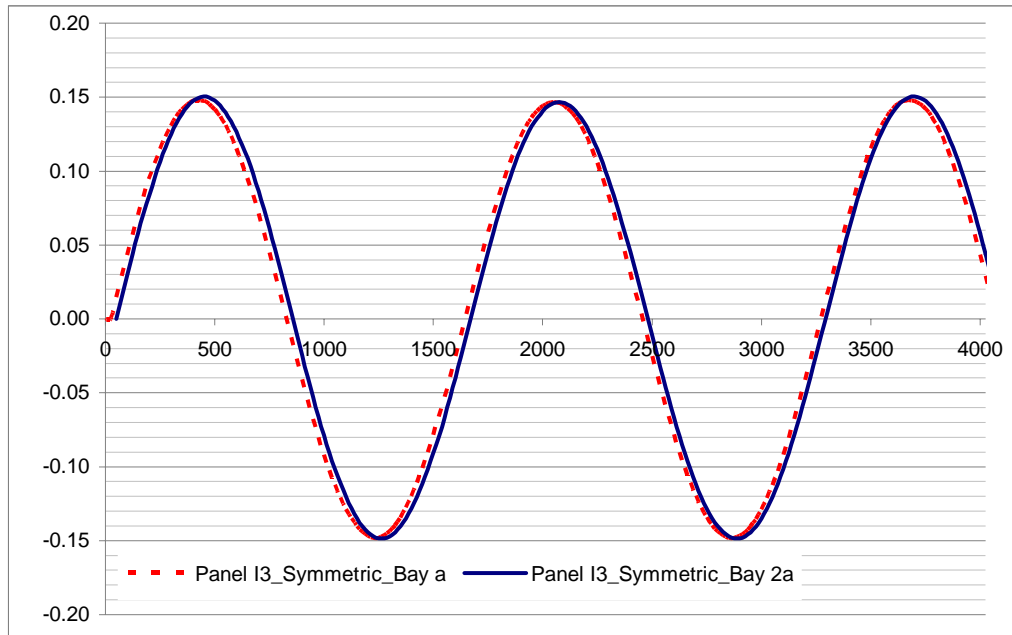


**Fig.7.5.** Normalised  $U_y$  displacement of the symmetric I3 Panel along a longitudinal edge

Using the illustrated buckling modes as an initial imperfection, a non linear static analysis has been performed for both alternatives, as mentioned above, enabling the calculation and comparison of the panels' load end shortening curves and ultimate limit strength. The resultant load end shortening curves are presented in Figure 7.6.

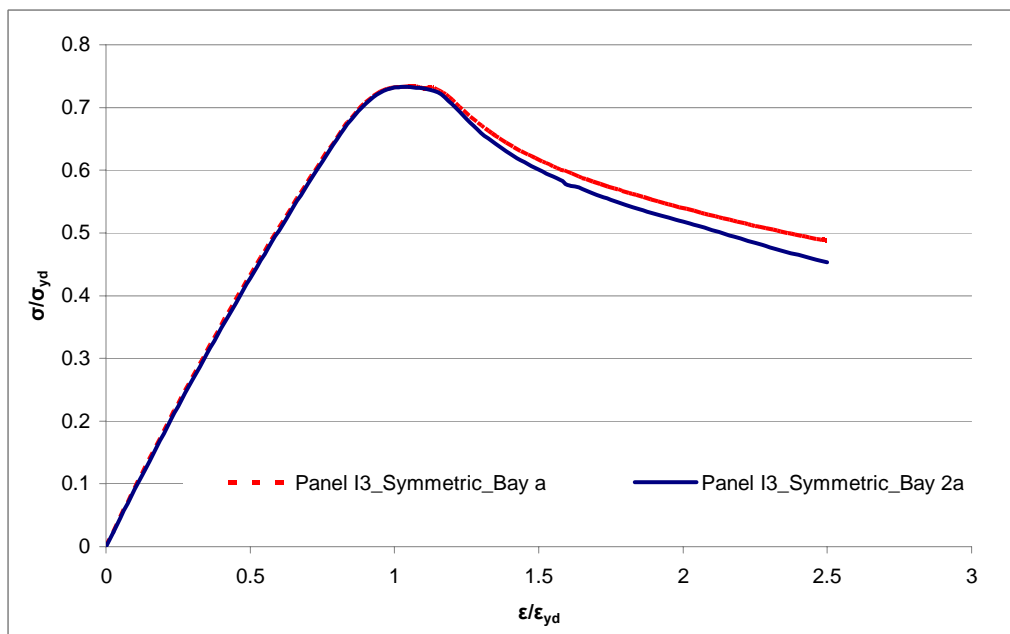


**Fig.7.6.** Load end shortening curves of I3 symmetric panel

As indicated in Figure 7.6, the ultimate limit strength of the one and two bay panel is identical and corresponds to  $\sigma/\sigma_{yd}$  and  $\varepsilon/\varepsilon_{yd}$  equal to 0.73 and 1.04 respectively. Slight differences are observed in the panels' behavior only during their subsequent collapse.

### **7.3.2. Type and Size of Finite Element**

As already mentioned in Chapter 4 - Par.4.4.1, the finite element used in this study is the general purpose shell element **S4**. In order to accurately capture the stresses on the inner and outer surfaces of the structure, Simpson's integration was used in the through thickness direction with seven section points.

The determination of an element size to be accounted for a finite element analysis depends on the specific structure and is subject to the respective computational cost and the accuracy/convergence of the results. Not knowing in advance the optimum mesh size, a mesh convergence analysis test is usually carried out enabling the determination of the optimum element size. For this purpose, a panel critical to the desired result should be taken into account.

In present study, the critical panels for the estimation of the ultimate hull girder capacity are the main deck panels. Therefore, panel M-1 has been chosen for the establishment of the mesh convergence analysis test. Bearing in mind CSR requirement that the element size is to be small enough to describe the buckling deflections and that a minimum of five elements across a half-buckling wave length is generally adequate, two different element sizes have been considered: 50mm and 25mm.

Figure 7.7 shows the mesh of panel M-1 when using 50mm element and the path to which the plot of the  $U_z$  displacement indicated in Figure 7.8 corresponds. Table 7.2 summarizes the required computational time for the non-linear analysis of the panel, the resultant ultimate limit state of the panel as well as the  $U_z$  displacement along the illustrated path at mid spacing of stiffeners.

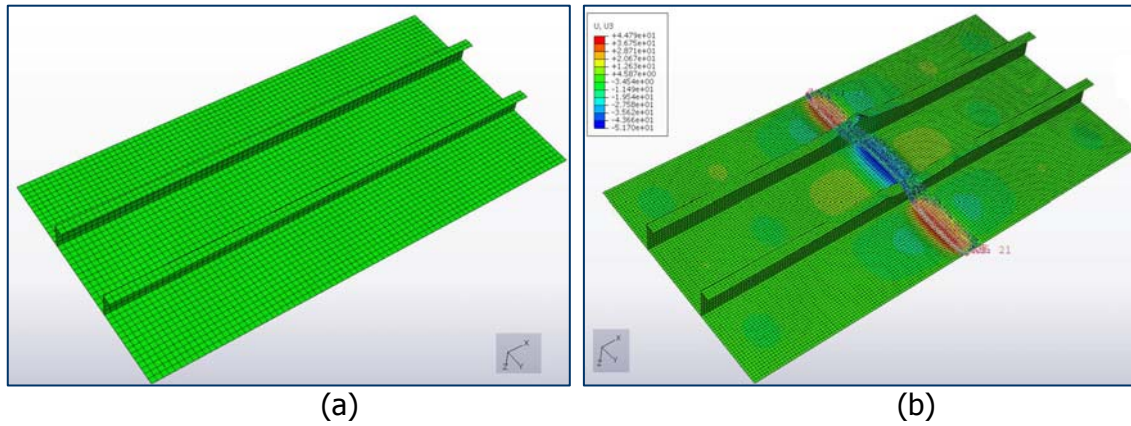


**Fig.7.7.** Panel M-1: (a) 50mm element mesh, (b) Path used for plotting of  $U_z$

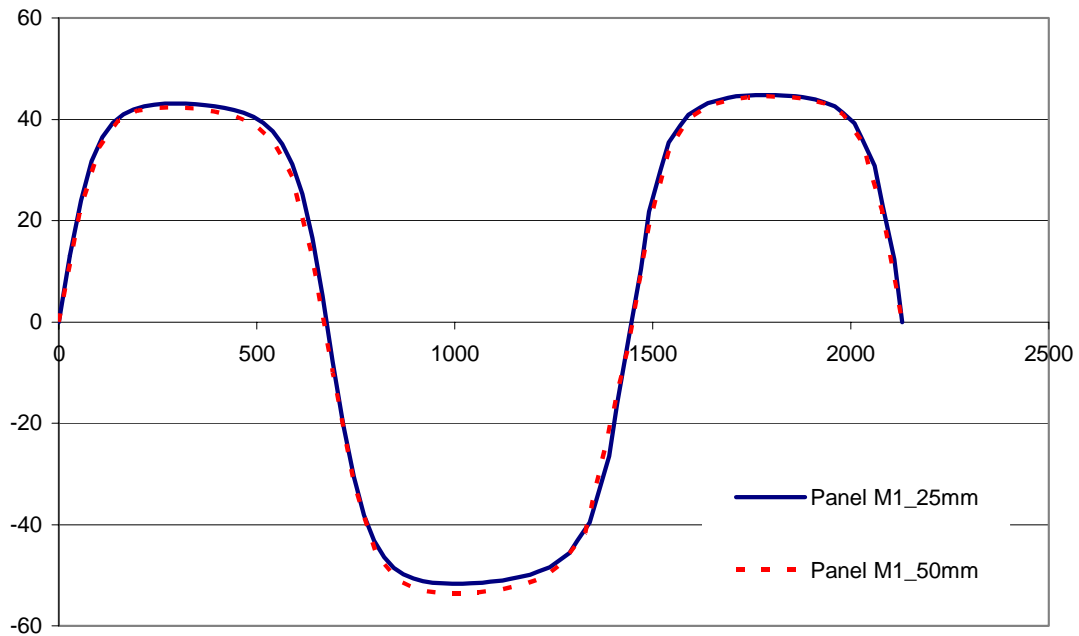


**Fig.7.8.** Panel M-1:Plot of  $U_z$  displacement along the path shown in Fig.7.7 (b).

As indicated by the tabulated results the ultimate limit state of the plate when 25mm and 50mm element size is used is close. The same applies for the plate's  $U_z$  displacement values as shown in Figure 7.8. Therefore, both the 25mm and 50mm element size have been considered to provide adequate accuracy.

		Element Size	
		25mm	50mm
Elements No	Plate	x direction: 162 y direction: 84	x direction: 81 y direction: 42
	Web	10	5
	Flange	4	2
Computational Time		0 hr 46 min	0 hr 20 min
Ultimate Limit State	$\varepsilon/\varepsilon_{yd}$	1.12	1.132
	$\sigma/\sigma_{yd}$	0.73516	0.737
Displacement $U_z$ (mm)	Y: 337.5	44.7902	44.5348
Displacement $U_z$ (mm)	Y: 1040	51.3462	53.3462
Displacement $U_z$ (mm)	Y: 1743.5	42.9504	42.117
Maximum Displacement	-	51.6978	53.5893

**Table 7.2.** Computational time/ Ultimate limit state /Plate  $U_z$  displacement of panel M1 for 25mm and 50mm element size

In view of the above, the 25mm element size has been used for most panels. Nevertheless, in cases of large panels, such as the CL Bulkhead (CL-2), Inner Bottom (IB-1), Bottom (B-2) and Main Deck Panels (M-2), a 50mm element size has been used instead, so as to minimize the computational cost.

### 7.3.3. Boundary Conditions

The application of boundary conditions that describe accurately the physical problem is of uppermost importance for the idealisation of the mathematical problem. The major influence of the boundary conditions stems from the conditions at the unloaded edges which are a consequence of the aspect ratio of the considered panel. With reference to Figure 7.9, plate F of aspect ratio equal to 1 can be considered as fully restrained since the closeness of the transverse girders does not allow lateral deflection (lateral deflection is not allowed - the edges remain undistorted), while plate A of aspect ratio much greater than 1 as constrained (lateral deflection is allowed-the edges are forced to remain straight).



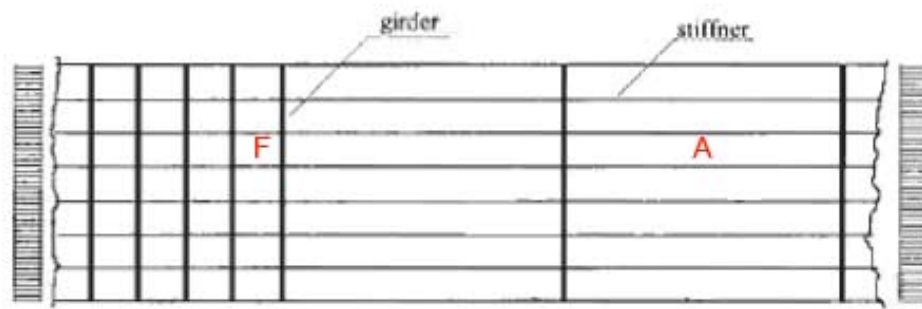


**Fig.7.9.** Boundary Conditions in way of unloaded edges

The panels of the considered midship section as indicated in Tables 5.2-5.8 are of aspect ratio 4.55-5.75 resulting to boundary conditions on the unloaded edge similar to panel A in Figure 7.9.

The following paragraphs indicate the boundary conditions considered for the finite element analysis of the panels referred to in paragraph 7.3.1. These boundary conditions for both horizontal (normal to x-y plane) and vertical (normal to x-z plane) panels of the midship section are summarized in Figure 7.11 and 7.12 respectively. The coordinate system is considered as illustrated in Figure 6.1. The x, y and z axis is regarded to be placed along the vessel's length, breadth and depth respectively.

### **7.3.3.1. Boundary Conditions along the unloaded edge of the panels**

The unloaded edge of all panels relates to the intersection of these panels to the adjacent primary support members as indicated in Figure 7.2. The primary support members are considered to simply support the plate of the panel at a direction perpendicular to the panel whereas, due to the adjoining structure, the corresponding panel edge is considered to remain straight and displace parallel to itself (as indicated by the arrow in Figure 7.2).

Let us consider the panel illustrated in Figure 7.10. The panel is considered to be simply supported along the edge AB in the z-direction (applicable in case of horizontal panels), leading to a displacement in the z-direction equal to zero:  $\mathbf{U}_z=0$ . This restraint in the z-displacement results in a restraint of the rotation about the y-axis:

$$\partial U_z / \partial x = 0 \rightarrow R_y = 0$$

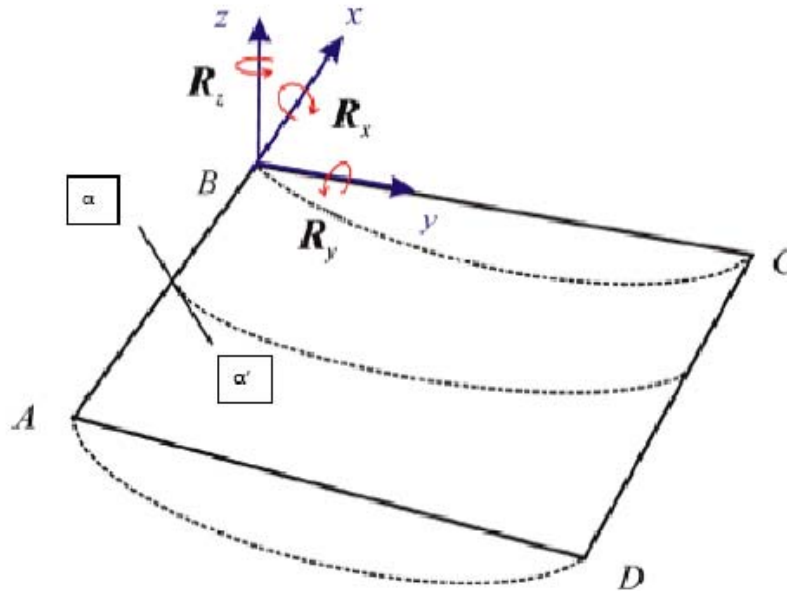


**Fig.7.10.** Panel for Illustration of simply support conditions

Similarly, in the case of perpendicular panels, the simply support condition is applied in the y-direction, resulting in the boundary conditions given in Table 7.3.

<b>Simply Support Conditions at unloaded edge</b>	
<b>Perpendicular Panels</b>	<b>Horizontal Panels</b>
$U_y = 0$	$U_z = 0$
$R_z = 0$	$R_y = 0$

**Table 7.3.** Simply Support Conditions at the unloaded edge of the panels

In order to simulate the requirement of the unloaded edge to remain straight and parallel to itself, all the nodes along the edge should have equal displacements (normal to the edge and in the plane of the panel). This can be expressed in ABAQUS with the help of the feature \*EQUATION in accordance to which the nodes specified are forced to move as per a linear equation set by the user.

More specifically the \*EQUATION option enables constraints between nodal degrees of freedom to be specified with linear equations of the following form:

$$A_1u_1 + A_2u_2 + \dots + A_nu_n = 0$$

where  $A_i$  is the coefficient associated with degree of freedom  $u_i$ .

Therefore by setting as equation  $u_{y1} - u_{y2} = 0$  and  $u_{z1} - u_{z2} = 0$  respectively for the horizontal (normal to x-y plane) and the perpendicular panels' (normal to x-z plane) of the midship section unloaded edge the desired requirement can be idealised accordingly:

<b>Additional Boundary Conditions at unloaded edge</b>	
<b>Perpendicular Panels</b>	<b>Horizontal Panels</b>
<b>Common <math>U_z</math></b>	<b>Common <math>U_y</math></b>

**Table 7.4.** Additional Boundary Support Conditions at unloaded edge

For example, in the case of an horizontal panel, the y-displacements ( $u_{y2}$ ) of all the unloaded edges' nodes (except of one) are connected to the y-displacement of the excluded node ( $u_{y1}$ ) via the equation  $u_{y1} - u_{y2} = 0$ , forcing the whole edge to remain straight and to displace parallel to itself.

### 7.3.3.2. Boundary Conditions along the panels' loaded edge

The loaded edge of the panels relate to the intersection of the panels to the web frames. As the midship section is longitudinally stiffened, the web frames act as primary support members and as a result they are considered to simply support the loaded plate edge of the considered panels at a direction perpendicular to the panels. It should be noted that the panel's loaded edge comprise of both the plate and the stiffeners' web and flange. In this respect, simply support conditions are also prescribed along the stiffeners' edge at a direction perpendicular to the stiffener's structural element considered, that is either the web or the flange.

These boundary conditions are summarized in Table 7.5 as follows:

Structural Element	Perpendicular Panels	Horizontal Panels
Plate	$U_y=0$	$U_z=0$
	$R_x=0$	$R_x=0$
Web	$U_z=0$	$U_y=0$
	$R_x=0$	$R_x=0$
Flange	$U_y=0$	$U_z=0$
	$R_x=0$	$R_x=0$

**Table 7.5.** Boundary Conditions in way of loaded edge of panels

All the above mentioned boundary conditions are illustrated in Figures 7.11 and 7.12 for horizontal and perpendicular panels respectively. These boundary conditions are applicable for panels of the midship section for which their longitudinal and transverse extent is defined by the web frames and the primary support members respectively. We should note that geometrical rotational restraint of the plate from the primary support members, that is rotation component  $R_y$  in case of horizontal panels, has been neglected in accordance with CSR Requirements.

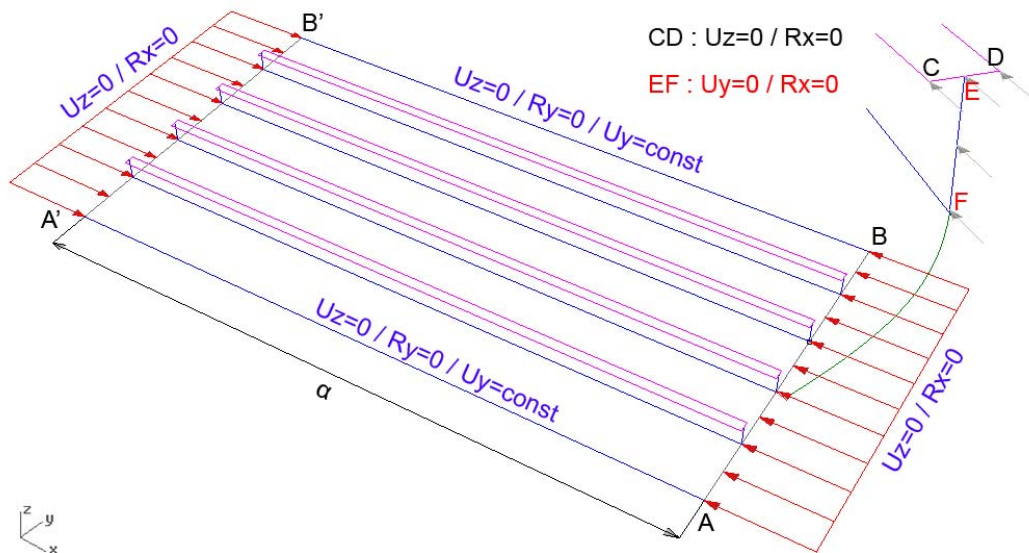


**Fig.7.11.** Boundary Conditions of hull girder section horizontal panels

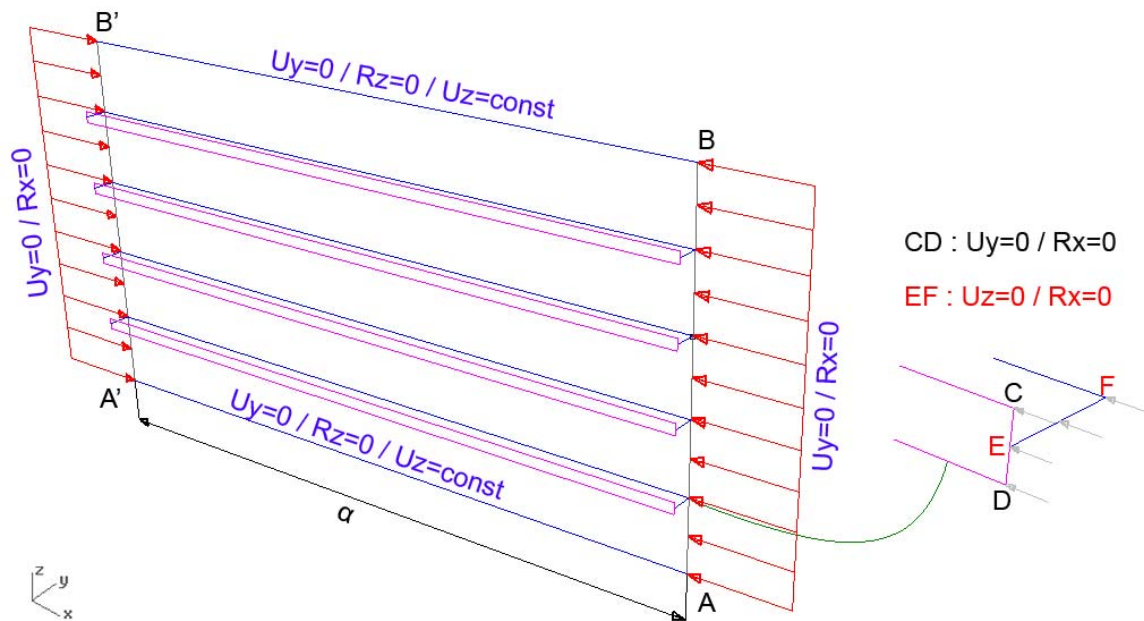


**Fig.7.12.** Boundary Conditions of hull girder section perpendicular panels

### 7.3.3.3. Boundary Conditions of panels that require special consideration

Due consideration should be given to the boundary conditions of the hopper plating panel, bilge plate and side shell – bottom panels adjacent to the bilge plating (panels S1 – B1 as per Figure 5.2).

These panels, except of the hopper plating panel, do not extend transversely up to the primary support members either at one transverse edge (panels S1 – B1) or both transverse edges (bilge plate panel, BLG). Therefore, the boundary conditions along the transverse edge and/or edges not extending up to the primary support members are slightly modified as indicated in Table 7.6. In these cases, such boundary conditions are applied so as to force the transverse edges to remain straight and to displace parallel to themselves. As mentioned above, this is achieved with the help of ABAQUS feature \*EQUATION.

Structural Panel	Transverse edge/edges not extending up to the primary support member
Bilge Plate (BLG)	Horizontal edge : Common $U_y$
	Perpendicular edge : Common $U_z$
Side Shell Panel (S1)	Common $U_z$
Bottom Panel (B1)	Common $U_y$

**Table 7.6.** Boundary condition in case of transverse edges not extending up to the primary support members

The hopper plating panel in the present study has been modelled without considering its angular position relative to the y-x plane (refer to Fig.6.1). In particular the panel has been considered as perpendicular (normal to the z-x plane) which at the transverse edges is simply supported both in the z and y direction. Taking into account that this panel is only under tension and therefore its behaviour is envisaged as perfectly plastic, it is considered that this approach will not have a significant effect on the results. The boundary conditions are illustrated in Fig.7.13.

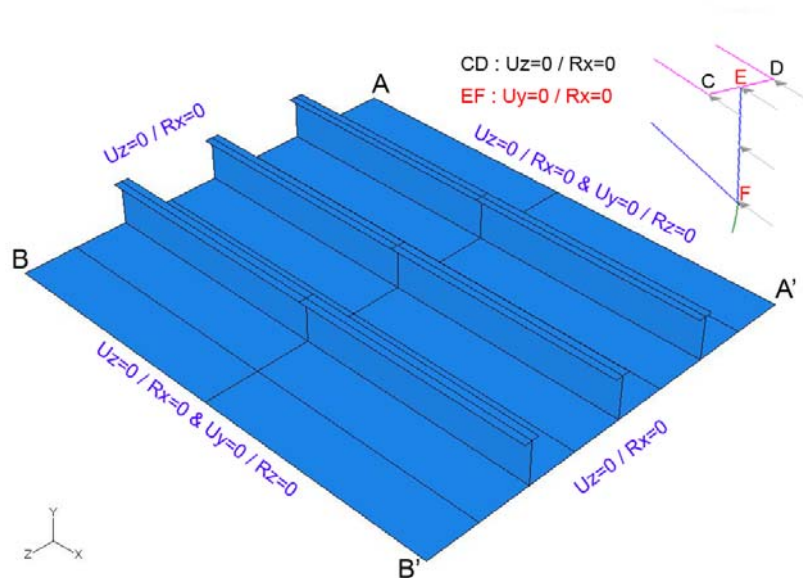


**Fig.7.13.**Boundary conditions of the hopper plating panel

### 7.3.4. Initial Imperfections

It is well recognised that initial imperfections existing in a stiffened panel affect the buckling behaviour and therefore the load shortening curves of same and should be taken into account when estimating its ultimate limit state.

In this respect, the CSR Rules require that appropriate initial imperfections are taken into account during FEA analysis. More specifically, the shape of the initial deflections is required to be such that the most critical failure modes are represented and triggered by the ensuing static analysis. In general, CSR Rules allow the lowest buckling eigen modes to be regarded as the critical failure modes.

At this point it should be noted that this is common practice when considering candidate initial imperfections. The initial imperfections are modelled in accordance with the considered structure's buckling modes, scaled by a factor equal to the maximum expected initial deflection.

This is the procedure also adopted in the present thesis. For this purpose, a buckling analysis of each panel has been performed prior to the non-linear static analysis enabling the determination of each panel's buckling modes. Having determined the buckling modes through an elastic buckling FE analysis, the initial imperfections were introduced in the FE model using the computed lowest eigenvalue (mode 1 has been used) which has been scaled using the maximum expected initial deflection. Moreover, the lowest buckling modes are frequently assumed to provide the most critical imperfections.

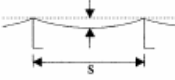
The maximum expected initial deflection  $w_o$  of each panel has been estimated by using the following widely applied Smith formula and taking into account average level of imperfections:

$$\frac{w_{opl}}{t} = \begin{cases} 0.025\beta^2 & \text{for slight level} \\ 0.1\beta^2 & \text{for average level} \\ 0.3\beta^2 & \text{for severe level} \end{cases}$$

where,  $\beta$  is the plate slenderness ratio of each panel.

We should highlight though that the CSR Rules for the Buckling Strength Assessment in conjunction with FEA Analysis, require the maximum values of the imperfections to be consistent with the IACS Shipbuilding and Quality Repair Standard, which specifies acceptance tolerance criteria for shipbuilding purposes.

Table 7.7 lists the tolerances for plate deflection between stiffeners while table 7.8 summarizes the maximum initial deflection taken into account for each panel in the present study. For comparison reasons the IACS Shipbuilding tolerances for deflection between stiffeners is also tabulated.

Item		Standard	Limit	Remarks
Shell plate	Parallel part (side & bottom shell)	4 mm	8 mm	
	Fore and aft part	5 mm		
Tank top plate	4 mm			
Bulkhead	Longl. Bulkhead Trans. Bulkhead Swash Bulkhead	6 mm		
Strength deck	Parallel part	4 mm	8 mm	
	Fore and aft part	6 mm	9 mm	
	Covered part	7 mm	9 mm	
Second deck	Bare part	6 mm	8 mm	
	Covered part	7 mm	9 mm	
Forecastle deck poop deck	Bare part	4 mm	8 mm	
	Covered part	6 mm	9 mm	
Super structure deck	Bare part	4 mm	6 mm	
	Covered part	7 mm	9 mm	
House wall	Outside wall	4 mm	6 mm	
	Inside wall	6 mm	8 mm	
	Covered part	7 mm	9 mm	
Interior member (web of girder, etc)		5 mm	7 mm	
Floor and girder in double bottom		5 mm	8 mm	

**Table 7.7.** Plate deflection tolerances between stiffeners as per IACS Shipbuilding and Quality Repair Standard



Location	Panel	Initial Deflections (mm)	IACS Shipbuilding tolerances for plate deflection between stiffeners	
			Standard (mm)	Limit (mm)
Main Deck	M 2	7.323	7	9
Main Deck	M 1	5.310	7	9
CL Blkhd	CL 2	8.144	6	8
Inner Bulkhead	I 4	10.995	6	8
Inner Bulkhead	I 3	7.774	6	8
Inner Bulkhead	I 2	8.884	6	8
Inner Bulkhead	I 1	7.818	6	8
Side Shell	S 5	8.144	4	8
Side Shell	S 4	7.818	4	8
Side Shell	S 3	7.818	4	8
Side Shell	S 2	7.818	4	8
Side Shell	S 1	8.796	4	8
Hopper Plating	HP	7.943	6	8
Stringer 36	ST 4	5.841	5	7
Stringer 32	ST 3	6.148	5	7
Stringer 26	ST 2	6.148	5	7
Stringer 23	ST 1	5.079	5	7
Bottom	B 2	8.286	4	8
Bottom	B 1	8.796	4	8
Inner Bottom	IB 1	8.286	4	8
Side Girder	SG	4.977	5	8
CL Girder	CL	6.399	5	8

**Table 7.8.** Initial Deflections accounted for the Finite Element Approach

As shown in Table 7.8 which includes the comparison of the considered deflections to the IACS Shipbuilding tolerances, the initial imperfection amplitudes specified here are in most cases consistent with the maximum tolerances allowed during shipbuilding.

At this point it would be interesting to demonstrate, as an example, the initial imperfections accounted for in the case of a specific panel. For this purpose, Panel M-1 of the Main Deck has been chosen (refer to Figure 5.2). The buckling mode of the main deck M1 panel used for the determination of its initial imperfections is depicted in Figure 7.14. More specifically, the figure demonstrates the magnitude of the displacement perpendicular to the plate ( $U_z$ ) along its length (at mid breadth) and its breadth (at mid span). In both cases the path along which the panel is sectioned, is indicated accordingly by a black line.

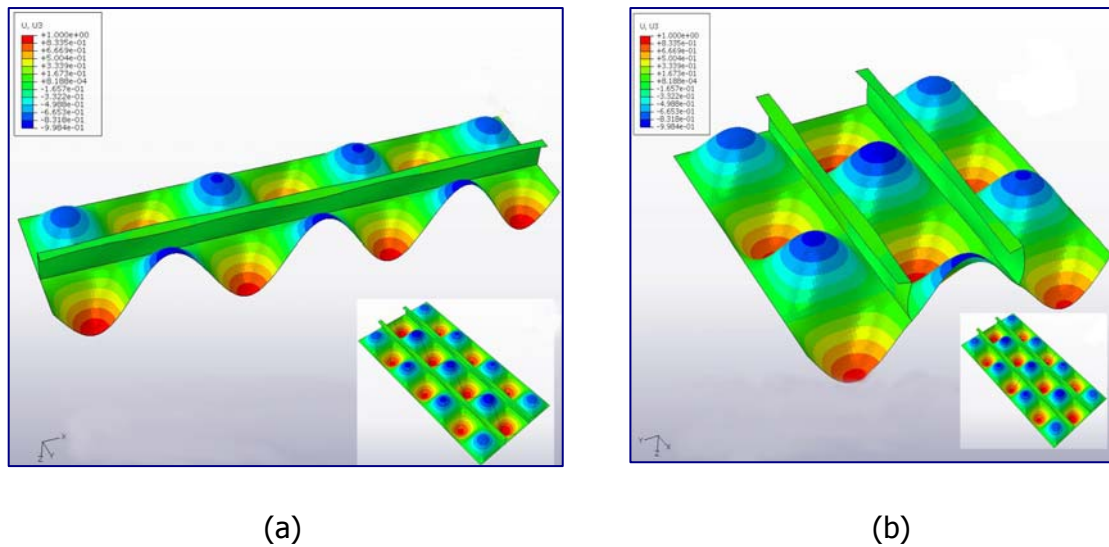


**Fig.7.14.** Buckling Mode of Panel M1. Normalised  $U_z$  displacement along **(a)** its length (mid breadth), **(b)** its breadth (mid span)

In order to have a clear indication of the magnitude of the initial imperfections applied not only on the plate but also on the stiffeners' flange and web, the plots of the normalized displacements perpendicular to the plate, the stiffeners' web as well as the flange are presented in the figures below.

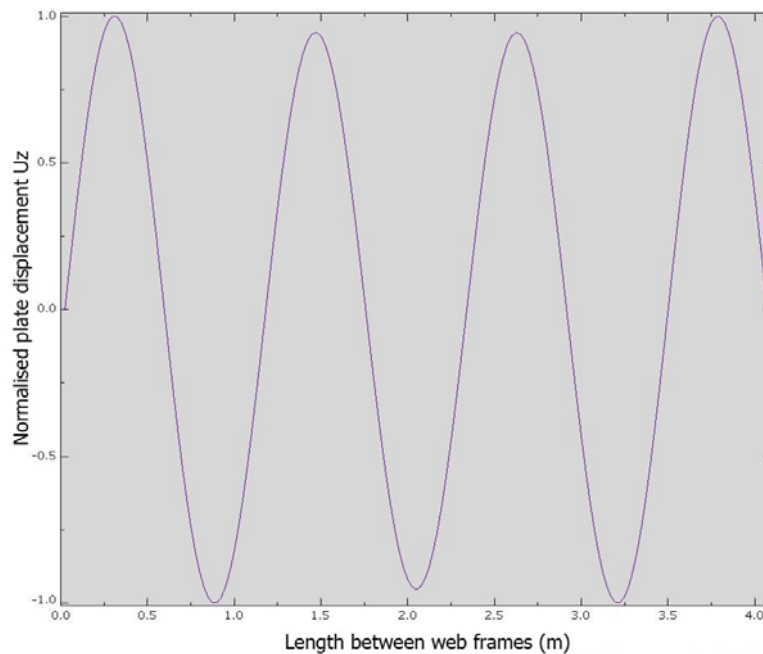


**Fig.7.15.** Panel M1: Plot of plate normalized  $U_z$  displacement along the plate's length (at mid-breadth)

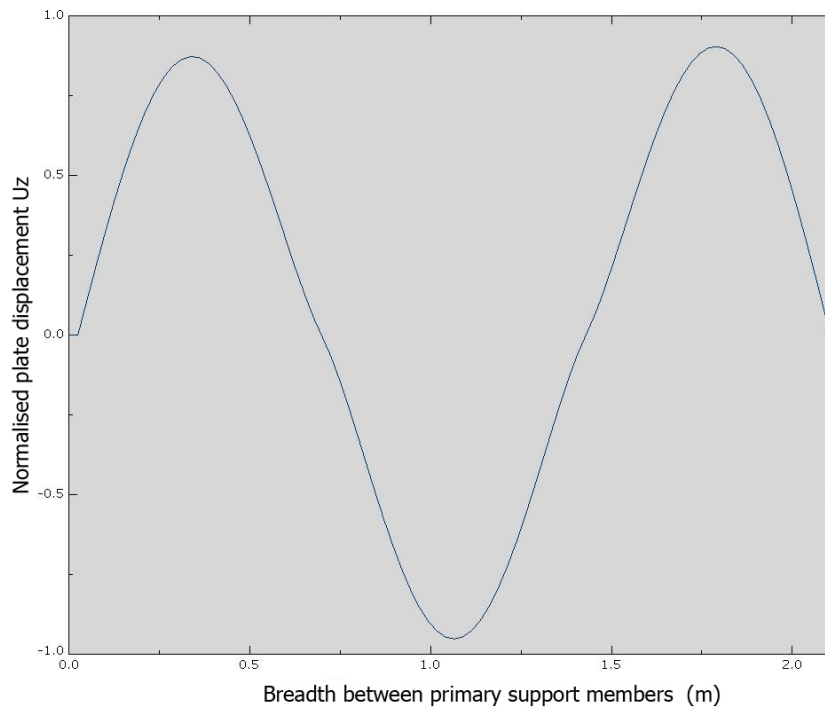


**Fig.7.16.** Panel M1: Plot of plate normalized  $U_z$  displacement along the plate's breadth (at mid span)

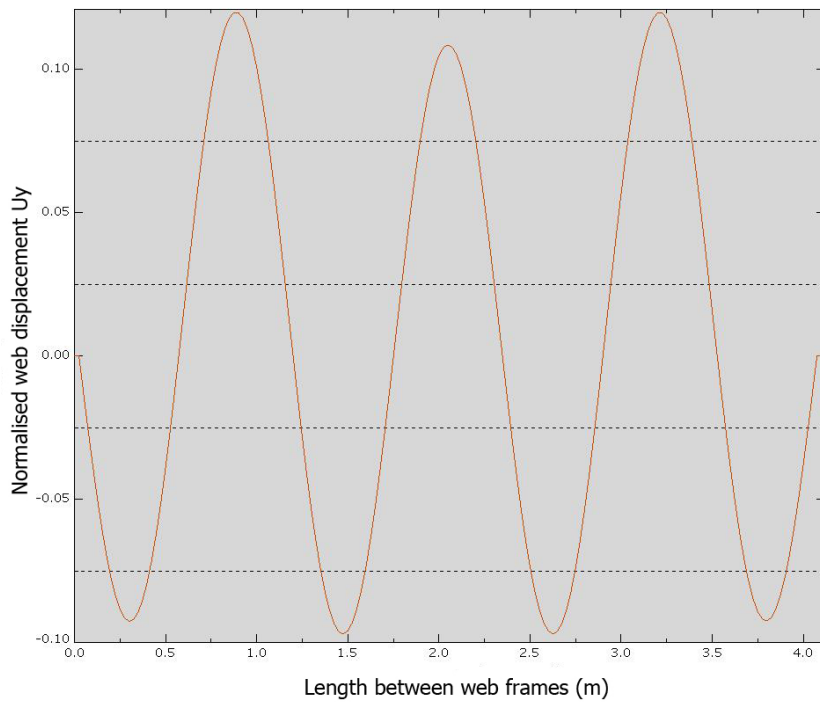


**Fig.7.17.** Panel M1: Plot of stiffener's web normalized  $U_y$  displacement along its length (at mid web height)

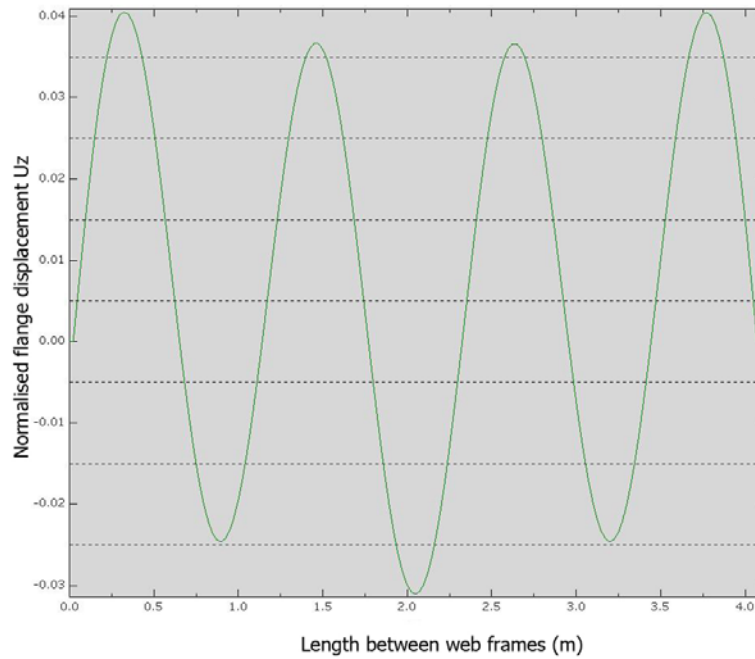


**Fig.7.18.** Panel M1: Plot of stiffener’s flange normalized  $U_z$  displacement along its length (at mid flange breadth)

By reviewing the above mentioned plots, it can be seen that 7 buckling waves occur along the plate’s and stiffeners’ web and flange length whereas 3 buckling waves occur along the plate’s breadth. The maximum magnitude of the plotted normalized displacements per each structural member of panel M1 are summarized in Table 7.9. Taking into account that as per Table 7.8 the scaling factor is 5.31, the considered applied imperfections can easily be derived.

		<b>Maximum Initial Deflections</b>	
		<b>Normalised values (-)</b>	
<b>Structural Member of Panel M1</b>	<b>Plate</b>	$U_z : 1.00$ <i>(x direction)</i>	
		$U_z : 0.98$ <i>(y direction)</i>	
	<b>Web</b>	$U_y : 0.14$	
	<b>Flange</b>	$U_z : 0.042$	

**Table 7.9.** Maximum Initial Deflections of Panel M1

Moreover, it should be noted that all above displacement plots seem to be symmetrical. Bearing in mind that the geometry of the panel itself is symmetric, we have a good indication of the effectiveness of the applied boundary conditions.

### **7.3.5. Loading conditions**

The scope of the Incremental-Iterative approach and of the Finite Element Approach used here is the determination of the load-end shortening curves of all structural panels that contribute to the vessel's longitudinal strength and therefore the prediction of their collapse behavior in order to estimate the entire hull girder section's limit state. The CSR Rules acknowledge that for the estimation of tankers' hull girder bending moment ultimate capacity in the sagging condition, only the vertical bending needs to be considered. The effects of shear force, torsional loading, horizontal bending moment and lateral pressure are neglected.

In order to simulate the effects of vertical bending moment on the structural panels during the adopted FE approach, only uniaxial stresses have been considered as illustrated in Figure 7.2. These uniaxial stresses have been imposed on the panels by means of enforced displacements  $U_x$  which were linearly increased as the analysis proceeded.

For this purpose, ABAQUS provides the possibility of multi-step loading of the model. The complete load history of the simulation is divided into a number of steps specified by the user which represent a period of "time" for which the response of the model to a particular set of loads and boundary conditions is calculated. The starting point for each general step is the deformed state at the end of the last general step. In the present work the loading is applied over a single step with an initial step representing the base state where the initial imperfection is introduced from the previous buckling analysis. Each step can be divided into several load increments. The user specifies the total "time" period of a step, the initial and minimum-maximum load increment size as well as the maximum load at the end of the step. The actual load incrementation is automatically controlled by ABAQUS according to the convergence rate of the Newton-Raphson method used to solve the nonlinear equilibrium equations (Section 4.6.1).

The maximum displacement  $u_x$  which was applied on each edge of the midship section structural panels has been calculated as follows:

$$U_{\text{applied}} = \epsilon_{\text{applied}} \cdot l/2$$

where,

$l$  the longitudinal extent of the panels which has been considered between the web frames (4050mm)

$\epsilon_{\text{applied}}$  the maximum applied strain in each panel which was dependent on the maximum imposed strain to each structural element during the application of the Incremental – Iterative Approach. In most panels  $\epsilon_{\text{applied}}$  was taken as  $2.5 \cdot \epsilon_{\text{yield}}$  whereas in some panels, especially in the region of the main deck, this was not adequate and was increased to  $4 \cdot \epsilon_{\text{yield}}$  (refer to Fig.6.19).

### 7.3.6. Materials properties

The behavior of the materials which were applied on the FE model was considered to be elastic-perfectly plastic, neglecting the effect of material strain-hardening, as depicted in Figure 7.19. The Young modulus, Poisson’s ratio and yield stress of the applied materials are indicated in Table 7.10.

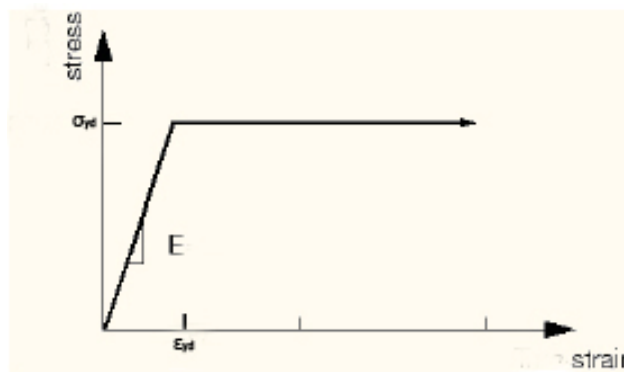


**Fig.7.19.** Elastic-perfectly plastic material behavior

Material	Yield stress (MPa)	Young Modulus (MPa)	Poisson Ratio
MS	245	207000	0.3
HS-32	315	207000	0.3

**Table 7.10.** Material properties

### **7.3.7. Net Thickness Approach**

As in the case of the Incremental-Iterative method, the CSR Net thickness approach has been adopted when applying the Finite Element Approach. In this respect, the net thicknesses of the plates and stiffeners per panel has been considered.

We should point out though, that as opposed to the Incremental-Iterative Approach where equivalent thickness and equivalent yield stress has been considered in cases where the plate thickness and the plate-stiffener yield stress was non identical, in the Finite Element Approach the panels have been modelled with their actual thickness and yield stress.

As a result, the FEA load end shortening curves of the individual structural elements can be compared to the ones derived by the three different approaches of the Incremental-Iterative method (refer to Par.6.2.2), enabling us to draw a conclusion on which approach best approximates the FEA results.

## **7.4. Simulation**

Having defined the mathematical idealisation of the actual physical problem, the next step of a finite element analysis is the choice of the type of analysis that will be performed. Taking into account that the hull structure, as most structures, has non linear response, non-linear analysis has been applied in the context of this study.

As already mentioned in Chapter 4, ABAQUS provides the possibility of performing Non-Linear Analysis by using either the Newton Raphson Method (Static Non Linear Analysis) or the Riks Method (Riks Non-Linear Analysis). The former is most commonly used whereas the latter is usually applied in cases where the static algorithm fails to converge, for example the unstable response depicted in Figure 4.10. Detailed description of both methods is provided in chapter 4.

In general, the application of the the Newton-Raphson Method was considered first in this work. In this respect, all panels' simulations have been carried out by using the Static Non Linear Analysis. Nevertheless, the simulation of panel M2 which corresponds to the Main Deck has been performed by the Riks method because when using the Newton Raphson Method the analysis could not be completed. It should be noted that among all panels, the Main Deck Panel is

subjected to the greatest strain, as the imposed curvature of the Hull girder increases. Taking into account that the Hull girder collapse, as per the Incremental-Iterative approach, corresponded to a curvature of  $\kappa_i=1.93 \times 10^{-4} \text{ m}^{-1}$  and that the applied strain is calculated as  $\epsilon_{ij} = \kappa_i \times (z_j - z_{NA-i})$ , we were drawn to the conclusion that the applied strain amplitude to yield strain ratio of the Main Deck Panel should be greater than 4. At such high levels of applied strain, the solution could not converge. More specifically, the Newton Raphson Method could not achieve equilibrium and the analysis was terminated.

## 7.5. Postprocessing

With the aim to calculate the Hull Girder Ultimate Strength of the Finite Element Approach and compare it to the one derived by the Incremental-Iterative Approach, the following paragraphs summarize the load end shortening curves and ultimate limit state of all panels, describe the method applied for the calculation of these load end shortening curves and present the calculated vertical bending moment versus curvature curve.

### 7.5.1. Stress-Strain Curves Calculation

To enable the estimation of the ultimate limit state of all panels, their load end shortening curves have been calculated using the axial stresses predicted by the FE Analysis.

The procedure adopted for the calculation of the stress-strain curves is as follows:

- **Output file of nodal axial – through thickness - stresses at the loaded edges.** Prior to the commencement of the FE Analysis the user can request certain variables of the structural response, corresponding to each load increment, to be saved in a data file. By requesting the output of the axial stresses at the loaded edges, a data file is created containing the axial nodal stresses during the entire load history. The nodal stress components are extrapolated from the integration points of the shell element and, accordingly, in the through thickness direction seven values per node are available, corresponding to the 7 section points used.



- **Calculation of the axial load intensities.** The axial stresses along each node in the through thickness direction are then integrated numerically using Simpson's first law to compute the axial load intensity,  $N_{xx}$ . In the case of a shell element with 7 section points in the through thickness direction, the following expression is used:

$$N'_{xx}{}^{(i)} = N_{xx} / t = (\sigma_1 + 4 \cdot \sigma_2 + 2 \cdot \sigma_3 + 4 \cdot \sigma_4 + 2 \cdot \sigma_5 + 4 \cdot \sigma_6 + \sigma_7) / 18$$

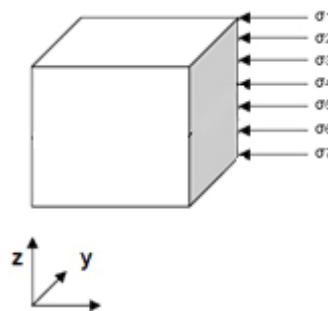


**Fig.7.20.** Stress components used to compute the axial stress intensity in the case of a shell element with 7 through thickness integration (section) points

- **Integration of load intensities over the plate/flange width and web height.** The axial load intensities are subsequently integrated numerically with respect to the y-axis over the width of the plate & flange, to compute the average axial stress over the plate section  $\sigma_p^{(i)}$  and flange section  $\sigma_f^{(i)}$ , and with respect to the z-axis over the height of the web to compute the average axial stress over the web section  $\sigma_w^{(i)}$ . The superscript (i) indicates the corresponding load increment at which the stress magnitude is computed.
- **Average axial stress over the loaded end section.** The total average axial stress over the loaded end of the stiffened plate at each time increment (i) is then obtained in accordance with the following expression:

$$\sigma_{xx}{}^{(i)} = (\sigma_p^{(i)} \cdot A_p + \sigma_w^{(i)} \cdot A_w + \sigma_f^{(i)} \cdot A_f) / (A_p + A_w + A_f)$$

The above mentioned procedure has been applied using the software "Matlab" and the program developed for this purpose by John Margaritis in the context of his dissertation [11].

## 7.5.2. Stress-strain curves of Structural Elements

With the procedure mentioned above, the load end shortening curves of all midship section structural elements have been calculated enabling their comparison to the ones derived by the CSR formulas and their usage for the estimation of the hull girder capacity. Such comparison is presented in Chapter 8.

This paragraph summarizes the ultimate limit state of all structural elements that at least in one stage during the hull girder collapse calculation are under compression (i.e. their position is above the position of the initial neutral axis). It should be noted that in the case of structural elements constructed from different materials, the yield stress is not uniform, and accordingly, an equivalent yield stress has been calculated as follows:

$$\sigma_{ydequiv} = (\sigma_{1yd} \cdot A_1 + \sigma_{2yd} \cdot A_2 + \dots + \sigma_{nyd} \cdot A_n) / (A_1 + A_2 + \dots + A_n)$$

In particular, for the calculation of the load end shortening curves of the hard corners which connect three adjoining panels, we should point out that they were not modeled as separate structural features. The stress distribution at their loaded ends were calculated by combining the stresses acting on the three adjoining panels. Let us consider the hard corner connecting stringer 36 (panel ST4) to the inner bulkhead (panels I4 and I3).

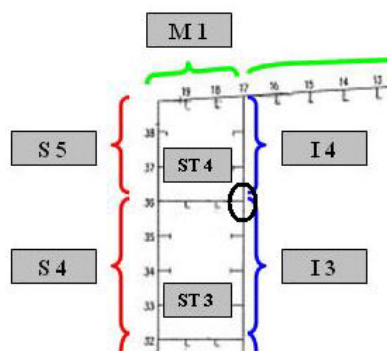


**Fig.7.21. Hard Corner between Stringer 36 and Inner Bulkhead**

Having modeled each of these panels separately the stress-strain curves of the hard corner have been calculated as follows:

$$\sigma_{HC} = (\sigma_{ST4} \cdot A_{ST4} + \sigma_{I4} \cdot A_{I4} + \sigma_{I3} \cdot A_{I3}) / (A_{ST4} + A_{I4} + A_{I3})$$

where  $\sigma_{ST4}$  ,  $\sigma_{I4}$  and  $\sigma_{I3}$  are the stresses in the adjoining panels integrated numerically over the respective cross section areas  $A_{ST4}$ ,  $A_{I4}$  and  $A_{I3}$  .

Table 7.11 includes the ultimate limit state characteristics of all the structural elements as derived by the FE approach, and in particular the strain ( $\epsilon_U$ ) and the stress ( $\sigma_U$ ) corresponding to the ultimate limit state of each structural element, the ratios  $\sigma_U/\sigma_{ydeq}$  and  $\epsilon_U/\epsilon_{ydeq}$ , as well as the ratio of the strain applied on the element at the time of the hull girder collapse ( $\epsilon_{HullColl}$ ) to its ultimate limit strain ( $\epsilon_U$ ).

LOCATION OF STRUCTURAL ELEMENT			YIELD STRESS		ULTIMATE LIMIT STATE PER STRUCTURAL ELEMENT					
Location	Panel	Structural Element	$\sigma_{yd}$ plate ( $Nt/mm^2$ )	$\sigma_{yd}$ stiffener ( $Nt/mm^2$ )	$\sigma_{yd eq}$ ( $Nt/mm^2$ )	$\epsilon_U$	$\sigma_U$ ( $Nt/mm^2$ )	$\epsilon_U/\epsilon_{yd}$	$\sigma_U/\sigma_{ydeq}$	$\epsilon_{HullColl}/\epsilon_U$
Main Deck	M 2	M 2 - 1	245	245	245	0.000995	186.54	0.84	0.761	2.7760
		M 2 - 2	245	245	245	0.000995	187.42	0.84	0.765	2.7760
		M 2 - 3	245	245	245	0.000995	185.05	0.84	0.755	2.7760
		M 2 - 4	245	245	245	0.001116	186.92	0.94	0.763	2.4743
		M 2 - 5	245	245	245	0.001131	189.03	0.96	0.772	2.4424
		M 2 - 6	245	245	245	0.001169	187.56	0.99	0.766	2.3613
		M 2 - 7	245	245	245	0.001228	187.87	1.04	0.767	2.2144
		M 2 - 8	245	245	245	0.001262	187.37	1.07	0.765	2.1548
		M 2 - 9	245	245	245	0.001228	187.03	1.04	0.763	2.2144
		M 2 - 10	245	245	245	0.001174	187.50	0.99	0.765	2.3151
		M 2 - 11	245	245	245	0.001140	188.04	0.96	0.768	2.3840
		M 2 - 12	245	245	245	0.001116	188.07	0.94	0.768	2.4359
		M 2 - 13	245	245	245	0.001106	185.88	0.93	0.759	2.4572
		M 2 - 14	245	245	245	0.001116	184.04	0.94	0.751	2.4359
		M 2 - 15	245	245	245	0.000990	186.39	0.84	0.761	2.7463
	M 2 - 16	245	245	245	0.000990	185.81	0.84	0.758	2.6738	
	M 1	M 1 - 18	245	245	245	0.001326	185.43	1.12	0.757	1.9871
	M 1 - 19	245	245	245	0.001326	185.30	1.12	0.756	1.9871	
CL Bulkhead	CL 2	CL 2 - 27	315	245	290	0.001418	215.69	1.01	0.743	0.3966
		CL 2 - 28	315	245	290	0.001418	214.11	1.01	0.737	0.5195
		CL 2 - 29	315	245	289	0.001418	211.18	1.02	0.731	0.6422
		CL 2 - 30	315	245	289	0.001418	210.64	1.02	0.729	0.7651
		CL 2 - 31	315	245	291	0.001477	210.69	1.05	0.724	0.8521
		CL 2 - 32	315	245	290	0.001418	209.20	1.01	0.722	1.0102
		CL 2 - 33	280	245	267	0.001309	195.64	1.01	0.732	1.2270
		CL 2 - 34	245	245	245	0.001363	183.21	1.15	0.748	1.3067
		CL 2 - 35	245	245	245	0.001309	173.15	1.11	0.707	1.4939
		CL 2 - 36	245	245	245	0.001201	176.24	1.01	0.719	1.7718
		CL 2 - 37	245	315	262	0.001006	184.88	0.79	0.705	2.2741
		CL 2 - 38	245	315	259	0.000960	184.81	0.77	0.713	2.5470
		CL 2 - 39	245	315	260	0.000955	185.70	0.76	0.713	2.7272
		Inner Bulkhead	I 4	I 4 - 38	315	315	315	0.001643	198.30	1.08
I 4 - 37	315			315	315	0.001583	205.12	1.04	0.651	1.4562
I 3	I 3 - 35		245	245	245	0.001243	173.25	1.05	0.707	1.5748
	I 3 - 34		245	245	245	0.001243	178.76	1.05	0.730	1.4346
	I 3 - 33		245	245	245	0.001243	177.10	1.05	0.723	1.2944
I 2	I 2 - 31		315	245	293	0.001454	182.66	1.03	0.624	0.8672
	I 2 - 30		315	245	292	0.001420	190.93	1.01	0.654	0.7651
	I 2 - 29		315	245	291	0.001454	199.98	1.03	0.687	0.6273
	I 2 - 28	315	245	291	0.001420	203.46	1.01	0.699	0.5195	
I 2 - 27	315	245	293	0.001386	211.38	0.98	0.723	0.4066		

**Table 7.11.** Ultimate Limit State characteristics of all structural elements under compression

As shown, the main deck panels (M1 & M2), the Stringer 36 panel (ST4) and the upper longitudinals of the CL Bulkhead (CL2: st.37-39) are the first to collapse before the hull girder collapses.

LOCATION OF STRUCTURAL ELEMENT			YIELD STRESS		ULTIMATE LIMIT STATE PER STRUCTURAL ELEMENT					
Location	Panel	Structural Element	$\sigma_{yd}$ plate (Nt/mm <sup>2</sup> )	$\sigma_{yd}$ stiffener (Nt/mm <sup>2</sup> )	$\sigma_{yd}$ eq (Nt/mm <sup>2</sup> )	$\epsilon_u$	$\sigma_u$ (Nt/mm <sup>2</sup> )	$\epsilon_u/\epsilon_{yd}$	$\sigma_u/\sigma_{ydeq}$	$\epsilon_{HullColl}/\epsilon_u$
Side Shell	S 5	S 5 - 38	315	245	302	0.001515	209.59	1.04	0.694	1.6404
		S 5 - 37	315	245	303	0.001623	194.78	1.11	0.644	1.4234
		S 4 - 35	315	245	297	0.001583	199.41	1.10	0.672	1.2381
	S 4	S 4 - 34	315	245	297	0.001623	203.02	1.13	0.684	1.0996
		S 4 - 33	315	245	296	0.001542	196.75	1.08	0.665	1.0445
		S 3 - 31	315	245	295	0.001488	193.27	1.04	0.655	0.8480
	S 3	S 3 - 30	315	245	295	0.001454	196.60	1.02	0.667	0.7478
		S 3 - 29	315	245	295	0.001522	198.64	1.07	0.674	0.5999
		S 3 - 28	315	245	294	0.001522	202.68	1.07	0.689	0.4851
S 3 - 27		315	245	294	0.001522	198.38	1.07	0.675	0.3705	
Stringer 36	ST 4	ST 4 - 18	245	245	245	0.001250	171.44	1.06	0.700	1.7027
		ST 4 - 19	245	245	245	0.001250	172.92	1.06	0.706	1.7027
Stringer 32	ST 3	ST 3 - 18	245	245	245	0.001302	162.50	1.10	0.663	1.0991
		ST 3 - 19	245	245	245	0.001302	163.78	1.10	0.668	1.0991
Hard Corner Inner Shell- Main Deck	M1 - I4 - M2	-	-	270	0.001400	153.57	1.08	0.570	1.8905	
Hard Corner Side Shell - Main Deck	S5 - M1	-	-	276	0.001407	189.28	1.05	0.685	1.8594	
Hard Corner CL Bikhd - Main Deck	CL2 - M2	-	-	245	0.000974	172.56	0.82	0.704	2.8251	
Hard Corner Inner Shell-Stringer 36	I4 - ST4 - I3	-	-	269	0.001491	159.32	1.15	0.591	1.4286	
Hard Corner Side Shell - Stringer 36	S5 - ST4 - S4	-	-	298	0.001623	161.56	1.13	0.542	1.3128	
Hard Corner Inner Shell-Stringer 32	I3 - ST3 - I2	-	-	271	0.001353	138.23	1.03	0.510	1.0606	
Hard Corner Side Shell - Stringer 32	S4 - ST3 - S3	-	-	299	0.001488	162.57	1.03	0.544	0.9641	

**Table 7.11 (cont).** Ultimate Limit State characteristics of all structural elements under compression

### 7.5.3. Ultimate Limit State Collapse of Panels under compression

At this point, it would be interesting to examine the deformed shape of the panels, as computed by the Finite Element Analysis, at their ultimate limit state. This will enable us to identify, as far as possible, the collapse mode of the structural elements of which each panel comprise and compare them to the collapse modes predicted by the Incremental-Approach and CSR Load end Shortening Curves.

Moreover, in order to obtain an idea of the hull girder section's deformed shape at its collapse, the deformed shape of the panels corresponding to the hull girder collapse will be presented.

The collapse mode of a stiffened panel under uniaxial compression is generally divided into overall buckling, beam column buckling, web local buckling or lateral-torsional buckling. In overall buckling, which can be initiated by beam column buckling, the ultimate strength of a stiffened panel is eventually reached by the formation of large yield regions inside the panel and/or the panel edges (Fig.2.4 b). Beam column buckling represents the collapse pattern at which the panel collapses by yielding along the plate-stiffener combination at mid-span (Fig.2.6), whereas in web local buckling and lateral torsional buckling, web local buckling and stiffener tripping occurs respectively (Fig.2.7-2.8). Further description of these modes is presented in Chapter 2.

It should be noted, that in practice the distinction of these modes is not always evident as in some cases they may interact or occur simultaneously.

### **7.5.3.1. Ultimate Limit State of Main Deck Panel M1**

Panel M1 is the part of the Main Deck which extends between the Side Shell and the Inner Shell (refer to Fig.5.2 and 5.8). During the Hull Girder Collapse, this is under compression and as the bending moment curvature increases, the compressive strain to which it is subjected becomes even greater.

The Axial Compressive Stress-Strain Curve of Panel M1 is shown in Fig.7.22. As indicated, its Ultimate Strength is as follows:

$$\sigma_{M1u} = 180.11 \text{ Nt/mm}^2$$

$$\sigma_{M1u} / \sigma_{yd \text{ equiv}} = 0.735$$

$$\epsilon_{M1u} / \epsilon_{yd \text{ equiv}} = 1.12$$

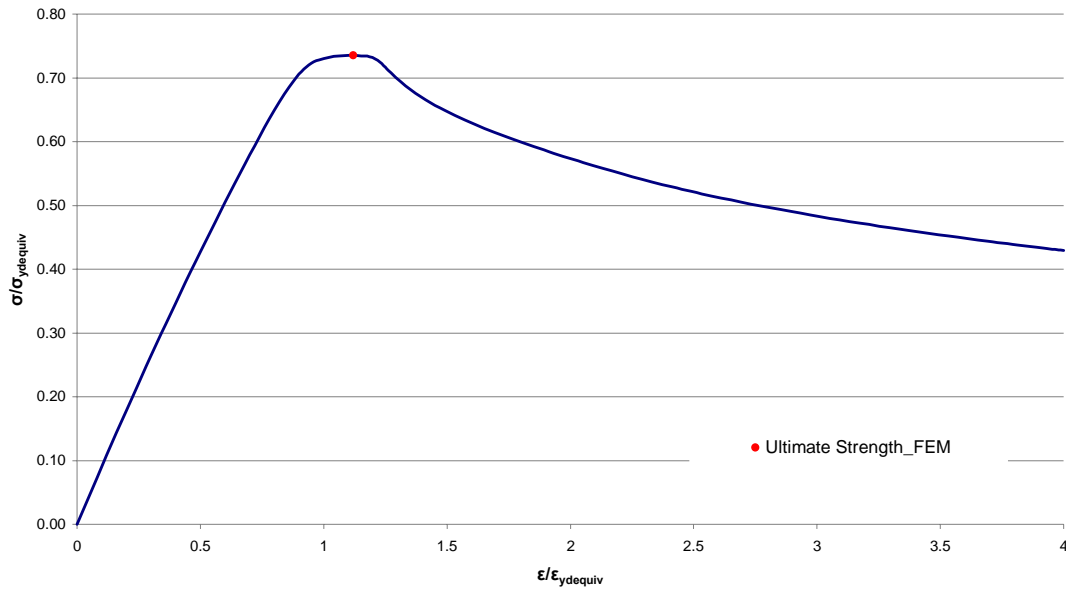


**Fig.7.22.** Axial compressive stress versus strain relationship of Panel M-1 obtained by FEA

The Figures below show the deformed shape of the panel corresponding to its ultimate limit strength. More specifically, both the magnitude of the displacement, i.e. the magnitude of the displacement vector, (Fig.7.23) as well as the displacement components perpendicular to the plate and the stiffeners' web (Fig.7.24),  $U_z$  and  $U_y$  respectively, are shown.

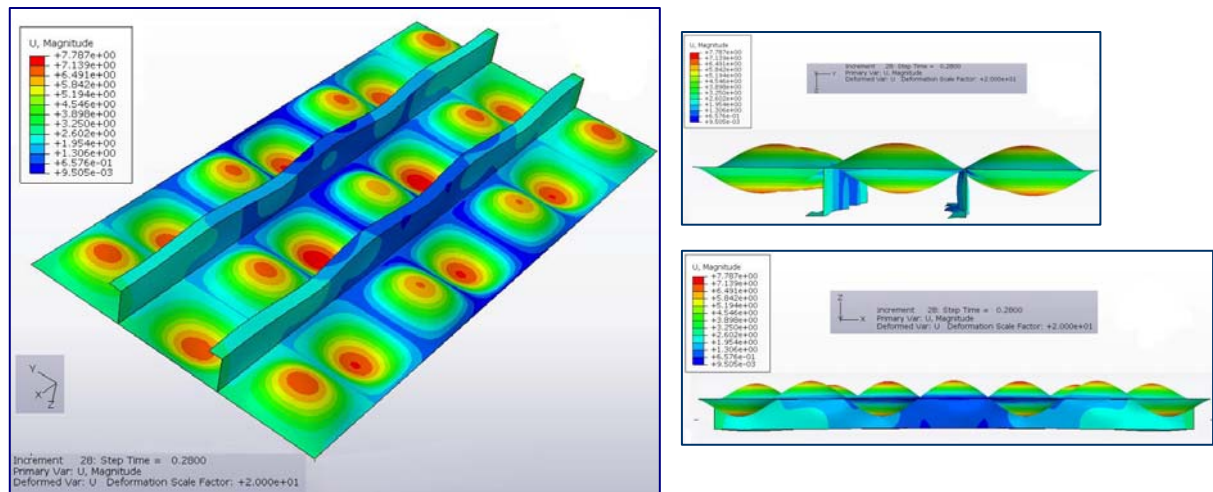
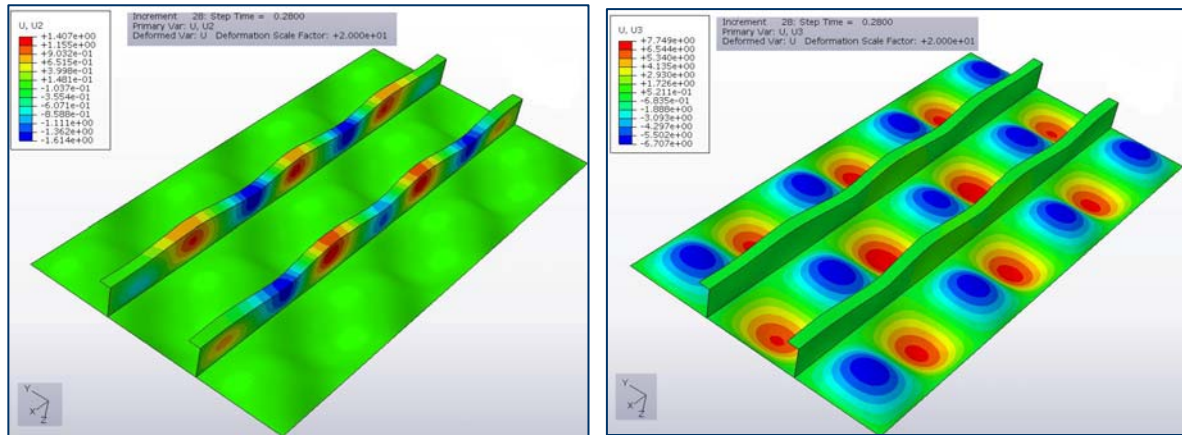


**Fig.7.23.** Deformed shape of Panel M-1 at its Ultimate Limit State– Magnitude of Displacement



(a)

(b)

**Fig.7.24.** Deformed shape of Panel M-1 at its Ultimate Limit State, **(a)**  $U_y$  Displacement, **(b)**  $U_z$  Displacement

By reviewing the deformation shape of Panel M-1 at its Ultimate Limit State, it can be seen that no significant tripping of the stiffener at its mid span has occurred. It seems that the collapse mode could be considered as a combination of beam-column and overall buckling collapse. This assumption is enhanced by the Von Mises Stress distribution shown in Fig.7.25 as per which the first occurrence of yield stress ( $245 \text{ Nt/mm}^2$ ) is shown at the plate-stiffener intersection in mid span. Bearing in mind that this is the failure mode of a beam column collapse (refer to Fig.2.4 b) and acknowledging that beam column collapse can lead to overall buckling collapse our assumption seems justified. The ULS is finally reached when a large yield region is formed in the plate-stiffener combination (refer to Fig.7.25.c).

At the time of the hull girder collapse (refer to Fig.7.25.d), it appears that tripping of the stiffeners at the mid span has occurred.

We should note that as far as the buckling mode of this panel is concerned, the CSR Formulas (refer to Table 6.2) are consistent with the FEA Analysis since in both cases beam-column buckling is considered as the critical mode.

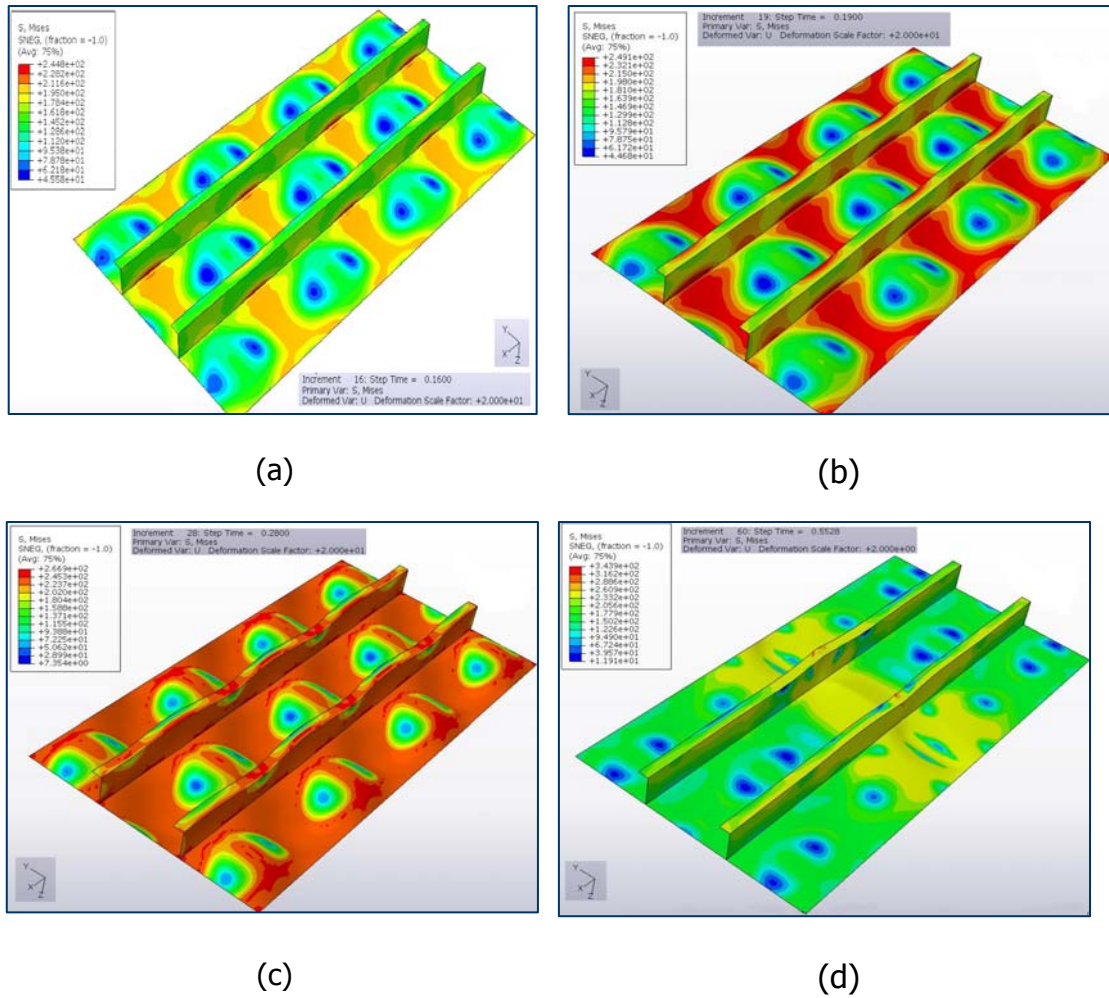


**Fig.7.25.** Von Mises Stress of Panel M-1 at (a)  $0.571 \epsilon_{M1u}$ , (b)  $0.679 \epsilon_{M1u}$ , (c)  $\sigma_{M1u}$ , (d) at Hull Girder Ultimate Limit State,  $1.987 \epsilon_{M1u}$

### 7.5.3.2. Ultimate Limit State of Main Deck Panel M2

Panel M2 refers to the remaining part of the Main deck extending from the Inner Shell to the CL Bulkhead (refer to Fig.5.2 and 5.8). The Axial Compressive Stress-Strain Curve of Panel M2 is shown in Fig.7.26. As indicated, its Ultimate Strength is as follows:

$$\sigma_{M2u} = 183.99 \text{ Nt/mm}^2$$

$$\sigma_{M2u} / \sigma_{yd \text{ equiv}} = 0.751$$

$$\epsilon_{M2u} / \epsilon_{yd \text{ equiv}} = 0.955$$



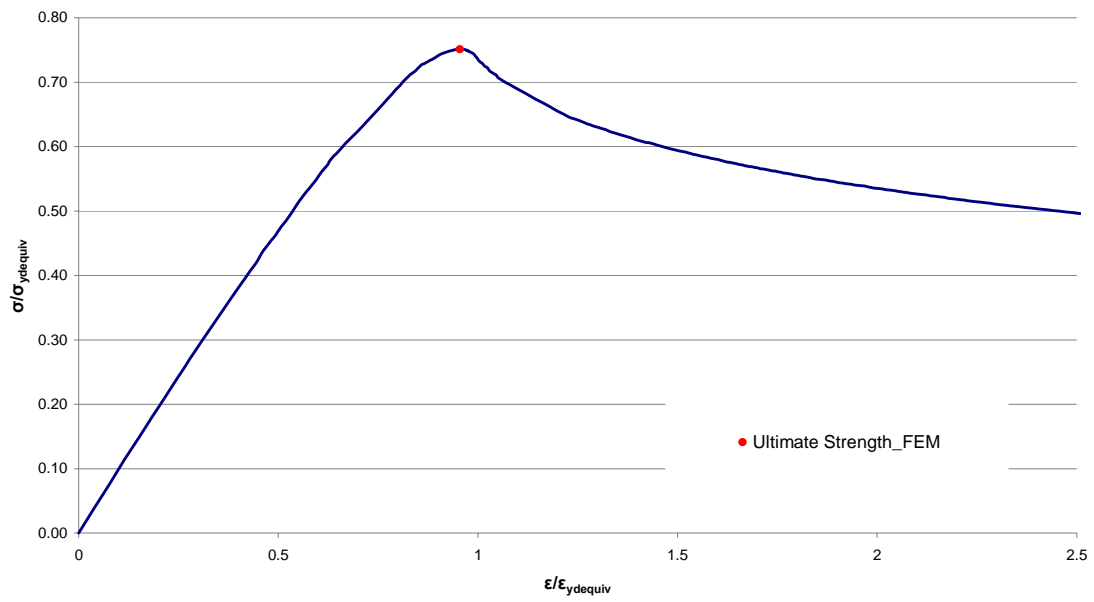


**Fig.7.26.** Axial compressive stress versus strain relationship of Panel M-2 obtained by FEA

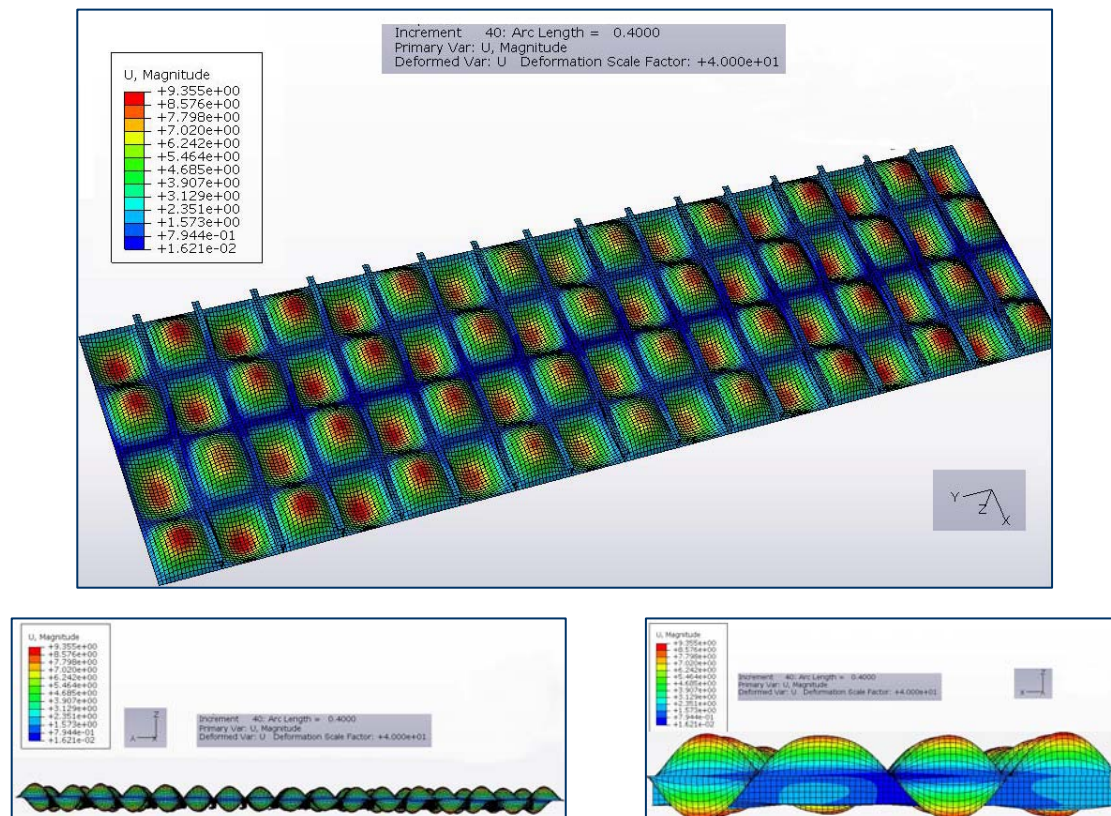
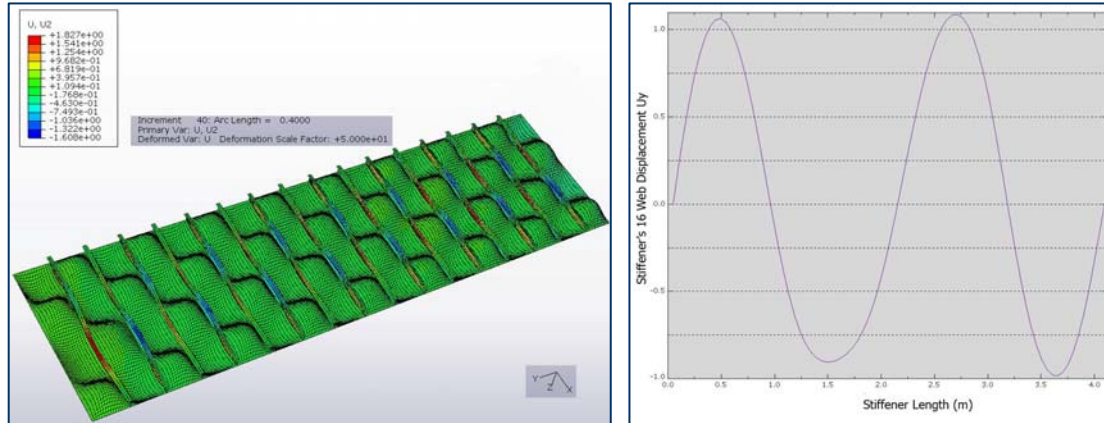


**Fig.7.27.** Deformed shape of Panel M-2 at its Ultimate Limit State,  $\sigma_{M2u}$  – Magnitude of Displacement

Figure 7.27. shows the displacement magnitude of the panel corresponding to its ultimate strength, whereas Figure 7.28 depicts the  $U_y$  displacement distribution in the panel and it's corresponding plot along the Stiffener's 16 web.



(a)

(b)

**Fig.7.28.** Deformed shape of Panel M-2 at its Ultimate Limit State, **(a)**  $U_y$  Displacement, **(b)** Plot of Stiffener's 16 web  $U_y$  Displacement

As in the case of panel M1, no significant tripping of the stiffeners at their mid span occurs. This can also be confirmed in Figure 7.28.b where the plot of the  $U_y$  displacement along the span of the stiffener web is presented. It can be seen that the  $U_y$  displacement is almost symmetric and no sudden increase of the displacement in the midspan region is observed that would insinuate that tripping failure is present.

In view of the above, we are drawn to the conclusion that the buckling collapse is a combination of beam-column and overall buckling which is in compliance to the CSR Formulas that predict that the critical collapse stress is the beam column buckling stress (refer to Table 6.2).

The Von Misses Stress of the panel at several stages up to the panel's collapse is indicated in Figure 7.29.

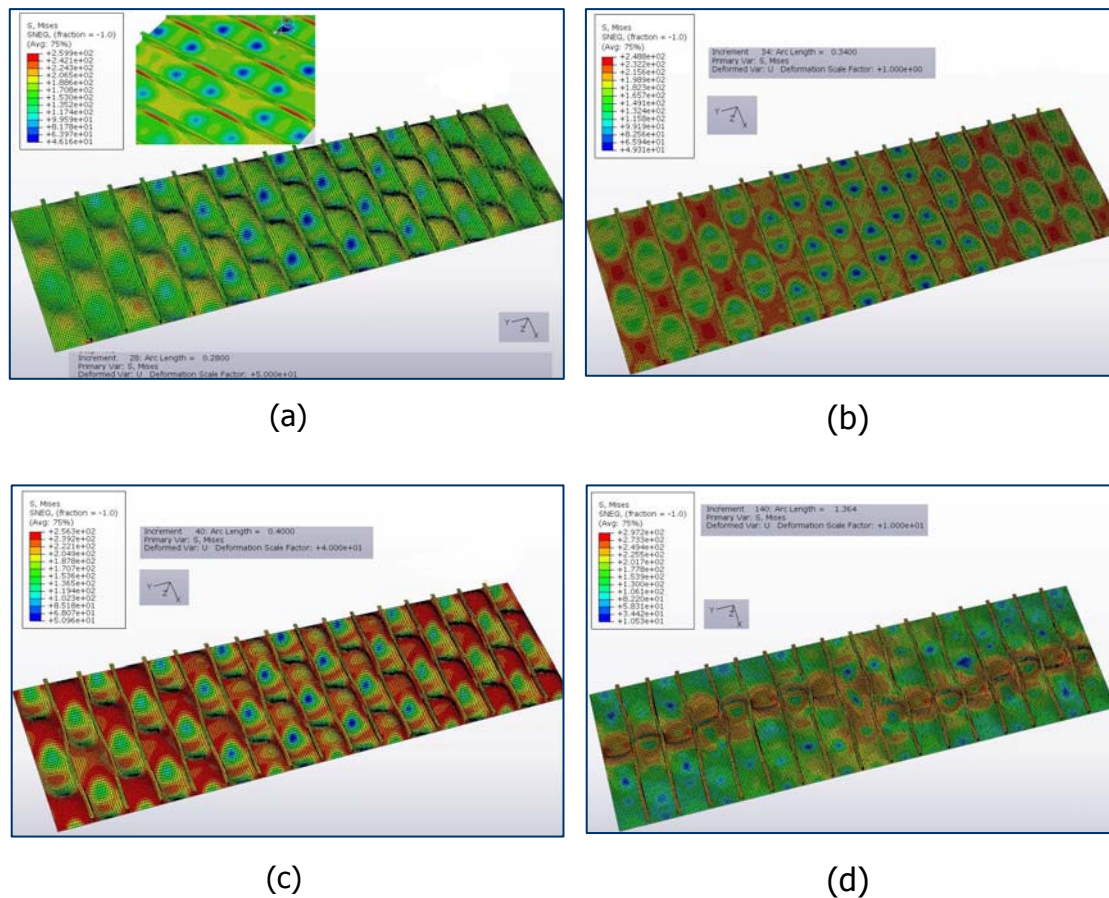


**Fig.7.29.** Von Mises Stress of Panel M-2 at **(a)**  $0.876 \epsilon_{M2Ur}$ , **(b)**  $0.931 \epsilon_{M2Ur}$ , **(c)**  $\sigma_{M2Ur}$ , **(d)** at Hull Girder Ultimate Limit State,  $2.405 \epsilon_{M2U}$

The first occurrence of yield stress ( $245 \text{ Nt/mm}^2$ ) takes place along the stiffeners-plate intersection at  $0.876 \sigma_{M2u}$ . At this point the plate behavior is still elastic except of certain isolated positions at the plates' edges where the yield stress has been reached. Subsequently, the yield region spreads especially in the vicinity of the panel's edges (Fig 7.29.b). Only until the yield region has spread both along the panel's edges and at mid breadth, is the Ultimate Limit State reached (Fig 7.29.c). At the time of the hull girder collapse severe buckling of the plate is observed.



It should be noted that at the time of the ultimate hull girder collapse, as indicated in Table 7.11, not all the longitudinal stiffeners of the depicted CL bulkhead have reached their ultimate limit state. More specifically at the time of the hull girder collapse, only the stiffeners of the upper part of the bulkhead (st.32-39) have reached their ultimate limit state, as opposed to the stiffeners of the lower part at which the ratio of the applied strain to their ultimate limit strain,  $\epsilon_{\text{HullColl}}/\epsilon_u$  varies between 0.40-0.85. Moreover, it seems that stiffeners 37-39 are the first to reach their ultimate state long before the collapse of the hull girder ( $\epsilon_u/\epsilon_{\text{HullColl}}=0.36-0.44$ ).

By reviewing Figures 7.30 (a) and 7.30 (b), it can be seen that large deformation in the plate takes place at the upper part of the Bulkhead, in the mid span region, as opposed to the lower part of the Bulkhead where the plate is deformed and increased tripping of the stiffeners is noticed. This is consistent to the yield stress of the various structural elements as in the upper part and lower part of the depicted CL Bulkhead panel, the yield stress of the plate-stiffener combination are  $245 \text{ Nt/mm}^2$ - $315 \text{ Nt/mm}^2$  and  $315 \text{ Nt/mm}^2$ - $245 \text{ Nt/mm}^2$  respectively.

This is also confirmed by the displacement component in the plate perpendicular to its plane,  $U_y$ , along the panel's height, shown in Figure 7.31.

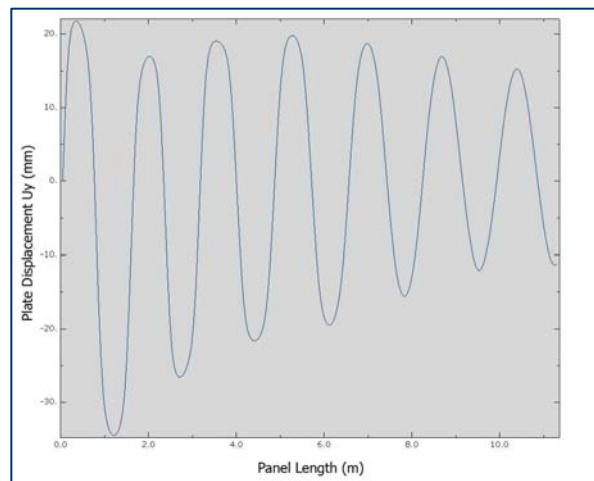


**Fig.7.31.** Plot of plate's  $U_y$  Displacement along its length at the time of the hull girder collapse



Regarding the collapse mode of the stiffeners, according to the CSR Load end Shortening Formulas, the 3 upper stiffeners (st. 37-39) reach their ultimate state by beam column collapse (refer to Table 6.2) whereas the remaining by torsional tripping. By reviewing the deformation shape of the panel (Figure 7.30), it seems that all stiffeners have failed due to torsional tipping. Nevertheless this figure does not correspond to the ultimate state of all stiffeners, as stiffeners 37-39 reach their ultimate state long before the collapse of the hull girder ( $\epsilon_u/\epsilon_{HullColl}=0.36-0.44$ ). Figures 7.32 (a) and 7.33 correspond to the deformation shape and the Von Mises distribution of the panel respectively at the time the stiffeners 37-39 have reached their ultimate strength.

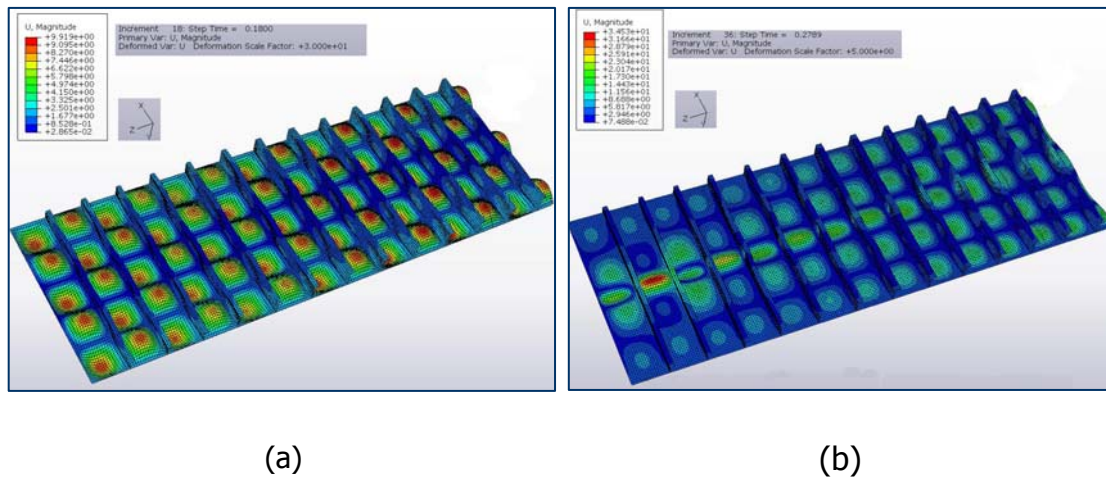


**Fig.7.32.** Displacement Magnitude of Panel CL2 above stiffener 27 at the time of **(a)** the Stiffeners' 37-39 Collapse,  $\epsilon_{CL2}/\epsilon_{HullColl}=0.40$ , **(b)** the Hull Girder Collapse,  $\epsilon_{CL2}/\epsilon_{HullColl}=1.00$

It can be seen that at the time the stiffeners 37-39 reach their ultimate state no tripping failure mode has occurred and that their failure is similar to that of the main deck stiffeners. This can be also confirmed in Figure 7.33 where no stiffener tripping is evident, and in the stiffener's 39  $U_z$  plot along it's length (Fig. 7.34) where there is a clear difference in the  $U_z$  distribution, oscillating at the time of the stiffener's collapse and exhibiting a distinct peak at the time of the Hull Girder Collapse.

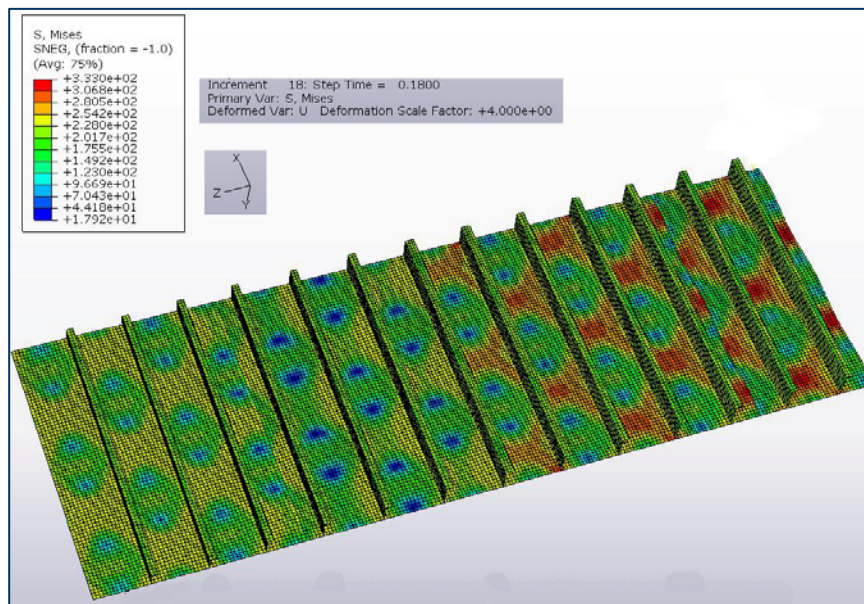


**Fig.7.33.** Von Mises Stress of Panel CL2 above stiffener 27 at the time of the Stiffeners' 37-39 Collapse,  $\epsilon_{CL2}/\epsilon_{HullColl} = 0.40$

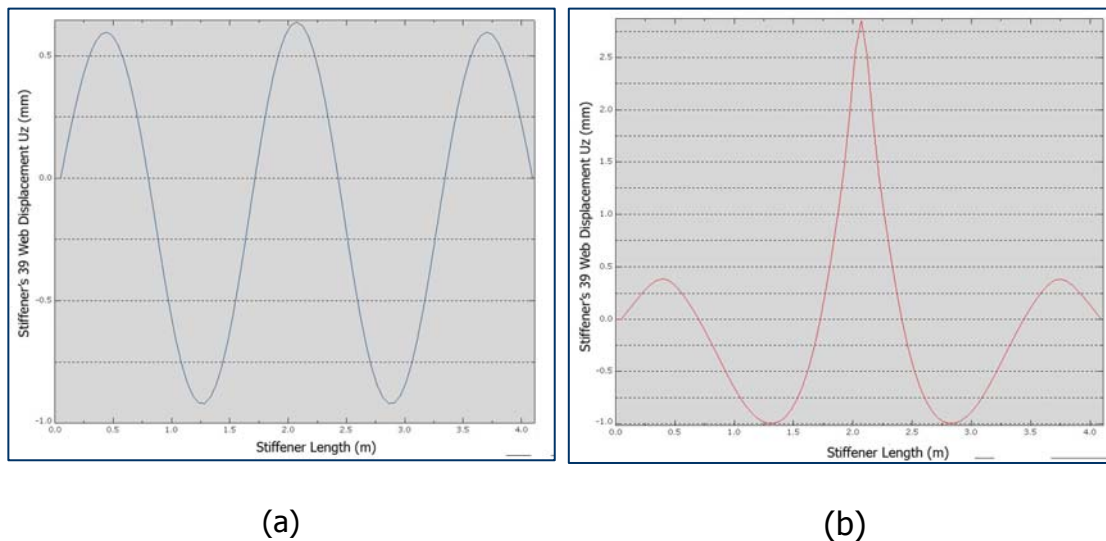


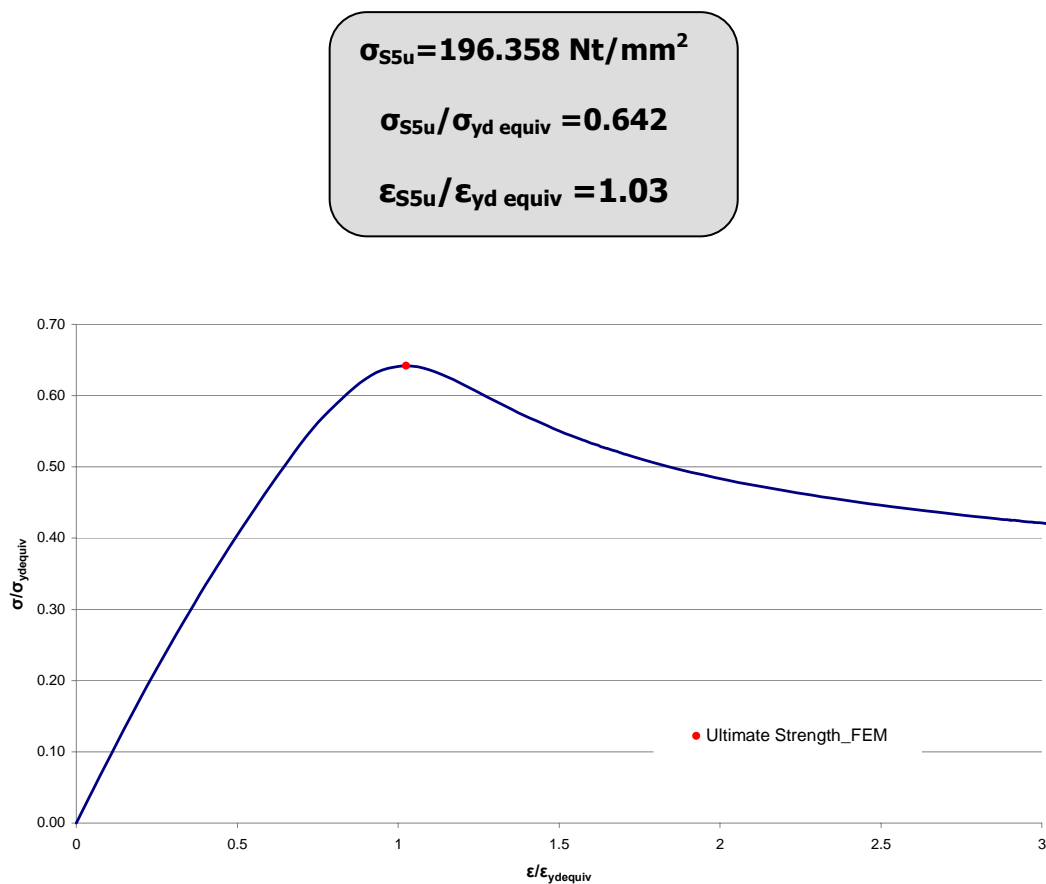
**Fig.7.34.** Plot of stiffener's 39  $U_z$  Displacement along its length at the time of (a) the stiffener's collapse, (b) the hull girder collapse

The remaining stiffeners fail due to torsional tripping (refer to Fig.7.30.b) as tripping is evident even at the time of the hull girder collapse, at which the applied strain to their ultimate strain  $\epsilon_{HullColl} / \epsilon_u$  corresponds to between 0.40-0.85.

### 7.5.3.4. Ultimate Limit State of Side Shell Panel S5

Side Shell Panel S5 refers to side shell that extends between Stringer 36 and the Main Deck (refer to Fig.5.2 and 5.5). This panel is always under compression and comprises of plate and stiffeners of yield stress equal to 315 Nt/mm<sup>2</sup> and 245 Nt/mm<sup>2</sup> respectively.

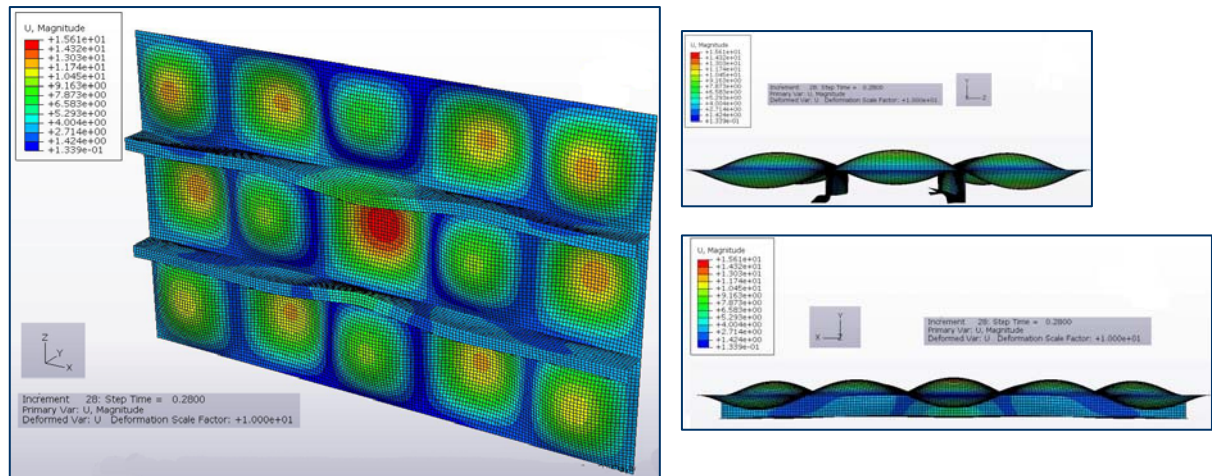
The Axial Compressive Stress-Strain Curve of Panel S5 is shown in Fig.7.35. As indicated, its Ultimate Strength is as follows:



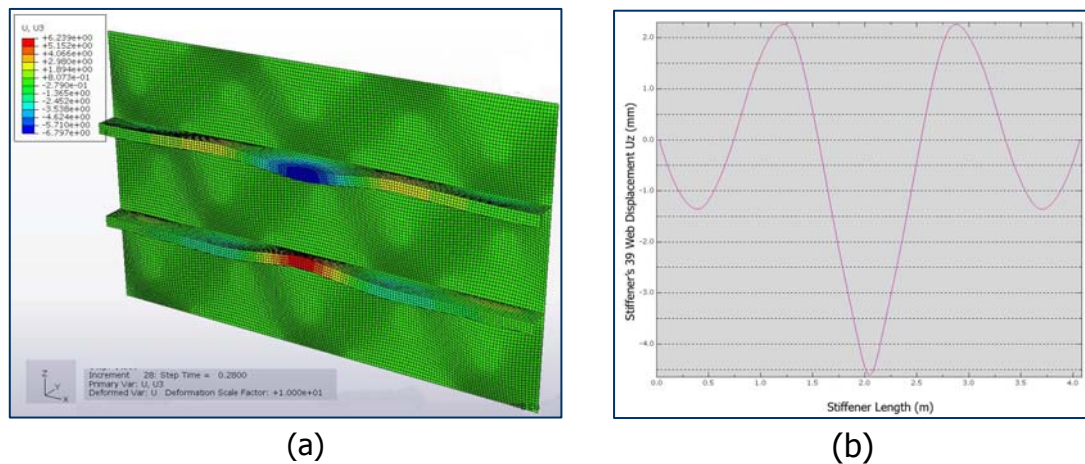
**Fig.7.35.** Axial compressive stress versus strain relationship of Panel S-5 obtained by FEA

Figure 7.36 demonstrates the magnitude displacement of the panel corresponding to its ultimate strength, whereas Figure 7.37 depicts the Uz displacement of the panel and the plot of same along the Stiffener's 39 web.





**Fig.7.36.** Deformed shape of Panel S-5 at its Ultimate Limit State– Magnitude of Displacement



**Fig.7.37.** Deformed shape of Panel S-5 at its Ultimate Limit State, **(a)**  $U_z$  Displacement, **(b)** Plot of Stiffener's 39 web  $U_z$  Displacement along its length

By reviewing above figures, it can easily be assumed that the failure mode of subject panel can be attributed to stiffener tripping. Nevertheless, this is inconsistent to the failure mode predicted by the CSR formulas (refer to Table 6.2), as per which the critical failure mode is beam column buckling. Taking into account that from all panels' deformed shapes presented so far with similar stiffener dimensions, this is the only case where the stiffeners have yield stress less than the plate, this discrepancy could be explained. As already mentioned the CSR Formulas account for identical yield stress between plate and stiffeners. In cases where the stiffeners' yield stress is less than the plate's it may be possible that the CSR formulas cannot capture the tripping failure of the stiffener. Further, all remaining midship section's

stiffeners of similar dimensions for which agreement of the two methods is observed, have a stiffener yield stress equal to or greater than the plate's.

The Von Mises Stress of the panel at several stages up to the panel's collapse is indicated in Figure 7.38.

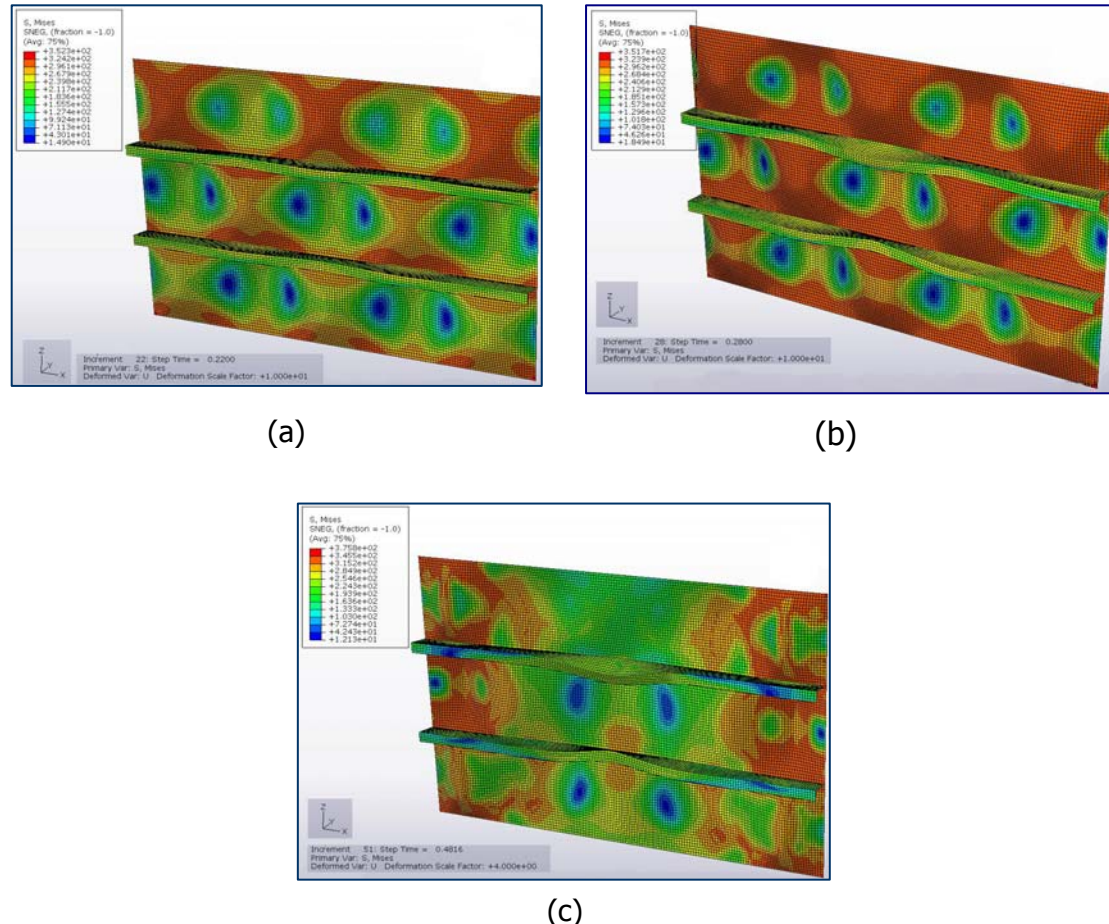


**Fig.7.38.** Von Mises Stress of Panel S-5 at **(a)**  $0.786 \epsilon_{S5u}$ , **(b)**  $1.0 \epsilon_{S5u}$ , **(c)** at Hull Girder Ultimate Limit State,  $1.573 \epsilon_{S5u}$

### 7.5.3.5. Inner Bulkhead Panel I2 and Side Shell Panel S3

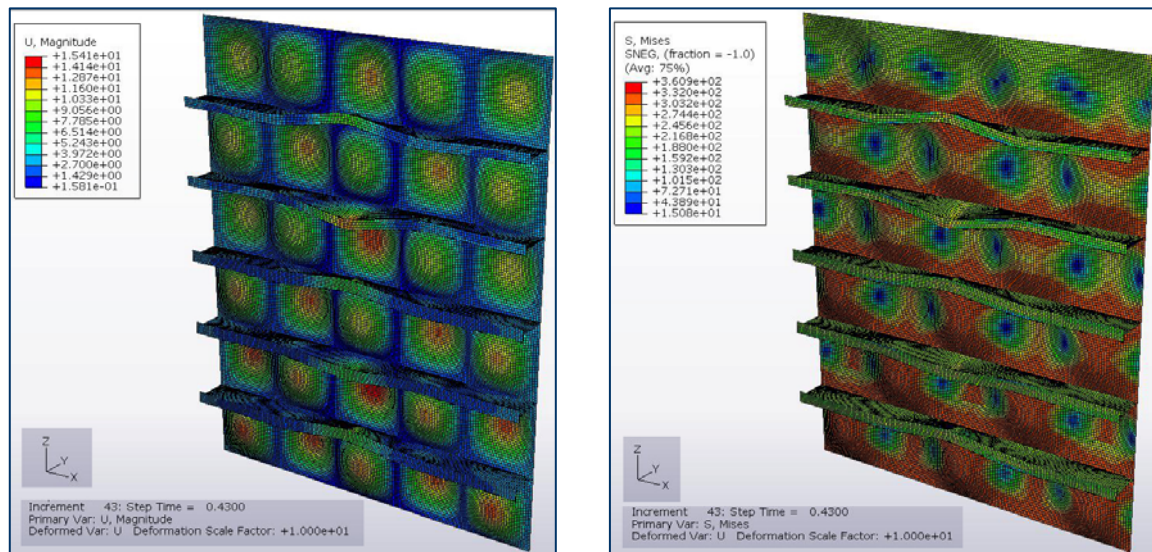
Inner Bulkhead Panel I2 and Side Shell S3 extend from Stringer 26 to 32 (refer to Figure 5.2). Most of the structural elements, of which the panel is comprised of, are constantly under compression since the initial neutral axis of the midship section lies 543 mm above stringer 26.

The corresponding Von Mises Stress and Magnitude of displacement distributions are shown in figures 7.39 and 7.40 below.

We should note that the stiffeners of panel I2 and S3 are shown to collapse by tripping. The asymmetry illustrated in the displacement magnitude distribution of



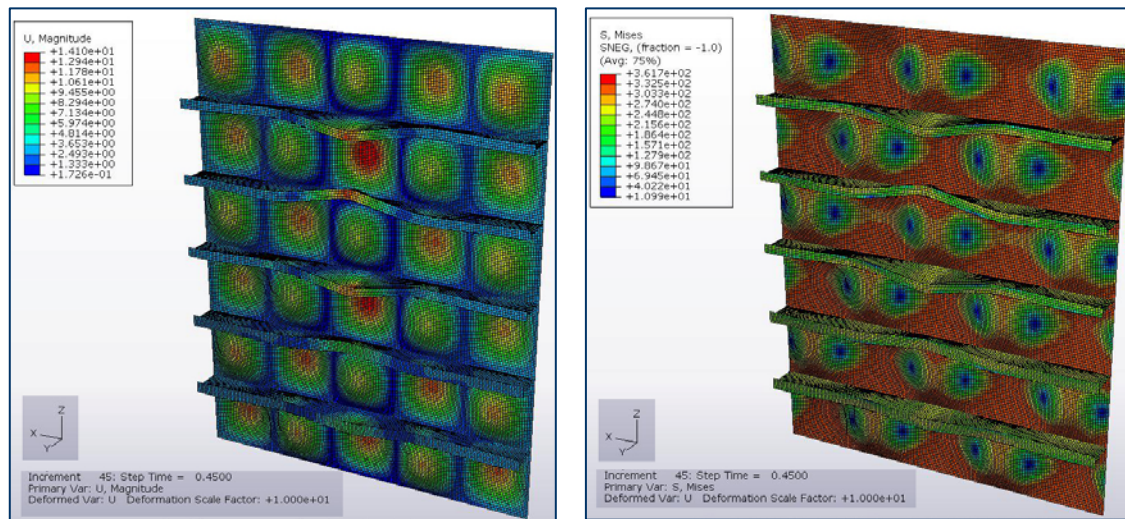
panel I2 along the Oz direction can be attributed to the difference in the yield stress of the inner bulkhead plating at its upper part.



(a)

(b)

**Fig.7.39.** Panel I2 at the time of its structural elements' collapse **(a)** Magnitude of Displacement, **(b)** Von Mises Stress Distribution



(a)

(b)

**Fig.7.40.** Panel S3 at the time of its structural elements' collapse **(a)** Magnitude of Displacement, **(b)** Von Mises Stress Distribution

### 7.5.3.6. Ultimate Limit State of remaining compressed Panels

In addition to the above, panels that are always under compression as the bending moment curvature of the hull girder increases are the Inner bulkhead panels, I4 (between Stringer 36 and Main Deck- Figure 5.2), I3 (between Stringer 36 and Stringer 32- Figure 5.2), the Stringer 36 and 32 Panels, as well as the Side Shell Panel S5 (between Stringer 36 and Main Deck- Figure 5.2).

In a similar way, as described above, the failure modes of these panels have been studied and have been found to be consistent with the failure modes predicted by the CSR formulas (refer to Table 6.2). The obtained results for these panels are not presented in the same detail as above in order to avoid repetition but for completeness are summarised below.

The axial compressive stress versus strain relationship of all the remaining panels subjected to compression are summarized below in Figures 7.41-7.45. The ultimate state characteristics of each panel and the longitudinal structural elements it consists of, are summarized in Table 7.12. Their Von Mises Stress Distribution as well as their deformed shape and displacement magnitude distribution corresponding to their ultimate limit state and at the time of the hull girder collapse are shown in Figures 7.51-7.55 and 7.46-7.50 respectively.

#### Axial compressive stress versus strain relationship

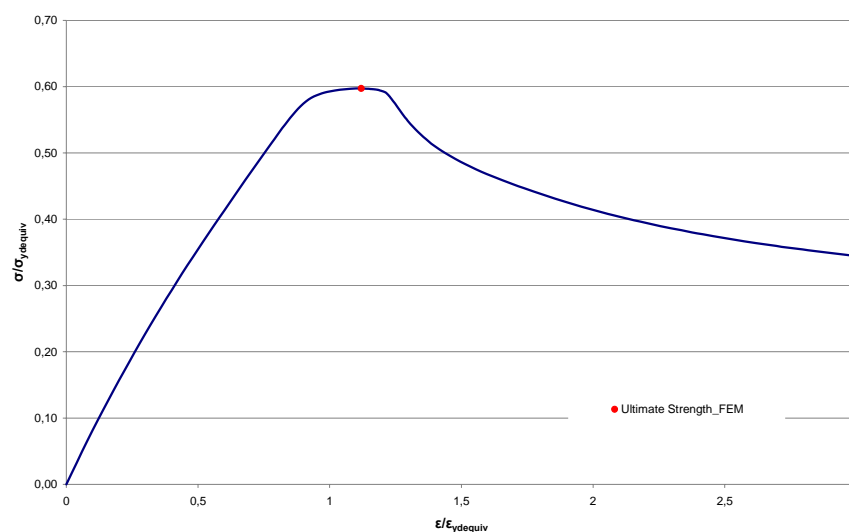


**Fig.7.41.** Axial compressive stress versus strain relationship of Panel I-4 obtained by FEA

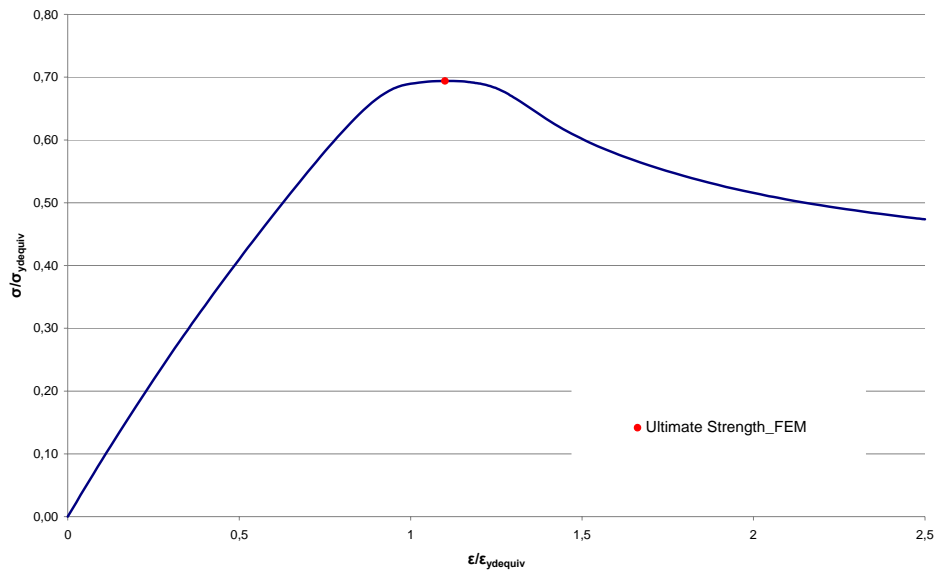


**Fig.7.42.** Axial compressive stress versus strain relationship of Panel I-3 obtained by FEA.

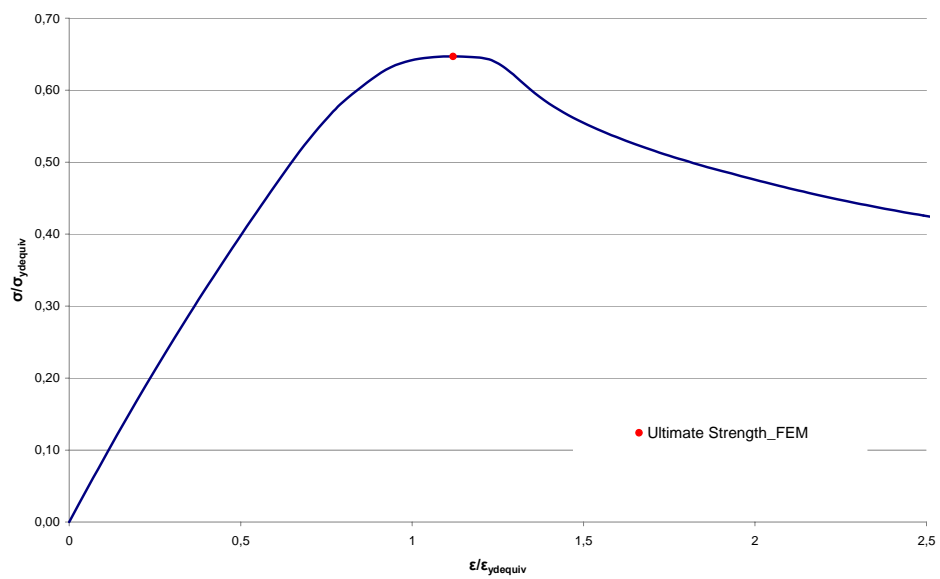


**Fig.7.43.** Axial compressive stress versus strain relationship of Panel S-4 by FEA

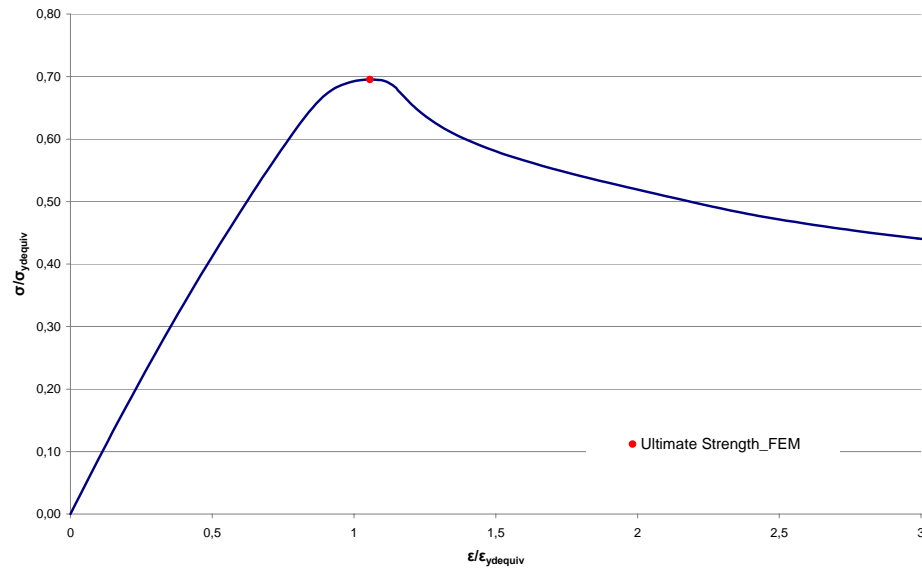


**Fig.7.44.** Axial compressive stress versus strain relationship of Panel ST-4 by FEA

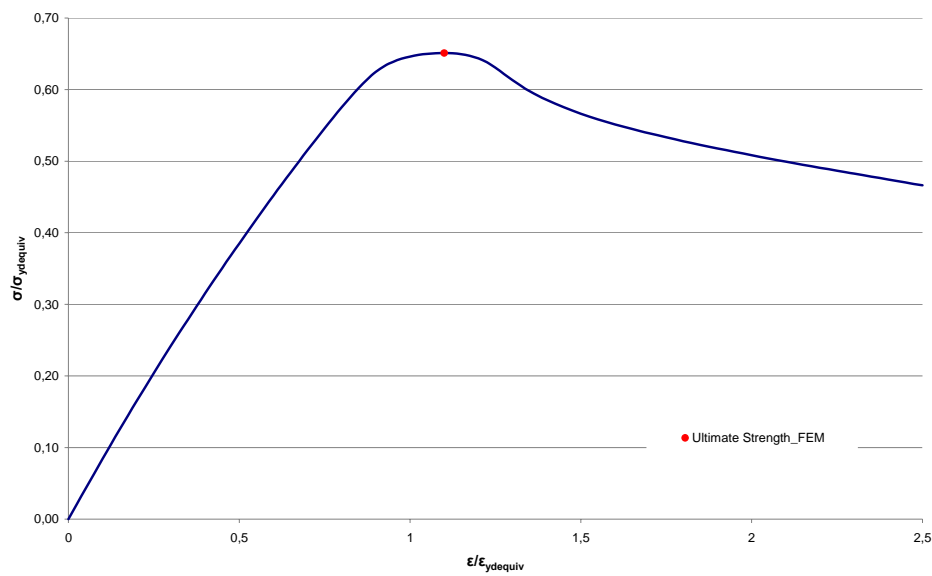


**Fig.7.45.** Axial compressive stress versus strain relationship of Panel ST-3 by FEA

As shown by the axial compressive stress-strain curves, the ultimate limit state of most panels occurs at a ratio of between 0.6-0.65  $\sigma_u/\sigma_{yd}$ , except of panel I3 and ST4 where a ratio of 0.70  $\sigma_u/\sigma_{yd}$  is attained .

**Deformed Shape - Magnitude of Displacement**

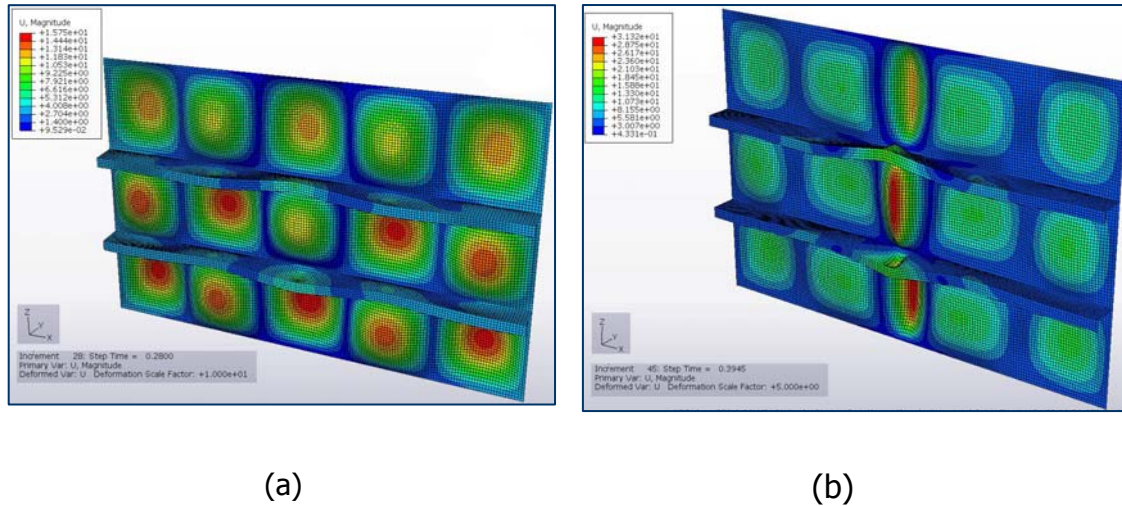


**Fig.7.46.** Deformed shape of Panel I4 - Magnitude of Displacement : (a) at its Ultimate Limit State,  $\epsilon_{I4u}$ , (b) at Hull Girder Collapse,  $1.391 \epsilon_{I4u}$

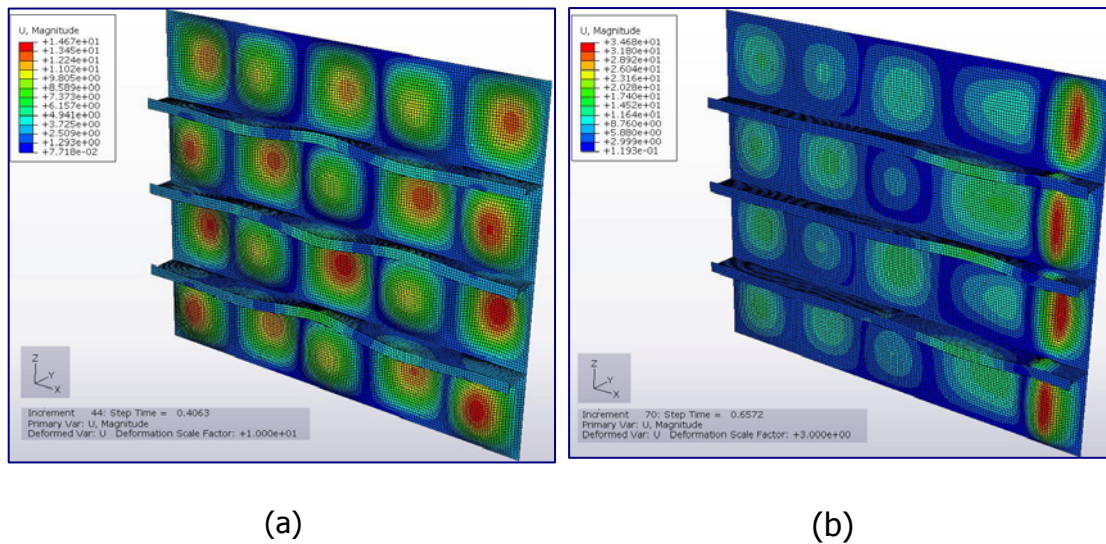


**Fig.7.47.** Deformed shape of Panel I3 - Magnitude of Displacement : (a) at its Ultimate Limit State,  $\epsilon_{I3u}$ , (b) at Hull Girder Collapse,  $1.369 \epsilon_{I3u}$

In Panel I4 and I3 plate and stiffeners are of the same yield stress, 315 Nt/mm<sup>2</sup> and 245 Nt/mm<sup>2</sup> respectively. In cases of panel I3 the failure mode at the time of its ultimate limit state can be assumed to be tripping of the stiffeners (Fig.7.47a). In Panel I4 the failure mode cannot be easily distinguished and could be



considered either beam column buckling or tripping of stiffeners (Fig.7.46a). Nevertheless, by also considering the stress distribution (Fig.7.51a) it becomes more clear that the failure mode is beam column buckling and/or overall buckling. At the time of the hull girder collapse, severe buckling of the plate and tripping of stiffeners is noticed at the midspan region of panel I4 (Fig.7.46b) as opposed to panel I3 (Fig.7.47b) where severe buckling occurs along the plate edge. We should note that the hull girder collapse corresponds to between 1.37-1.39 of their ultimate limit state.

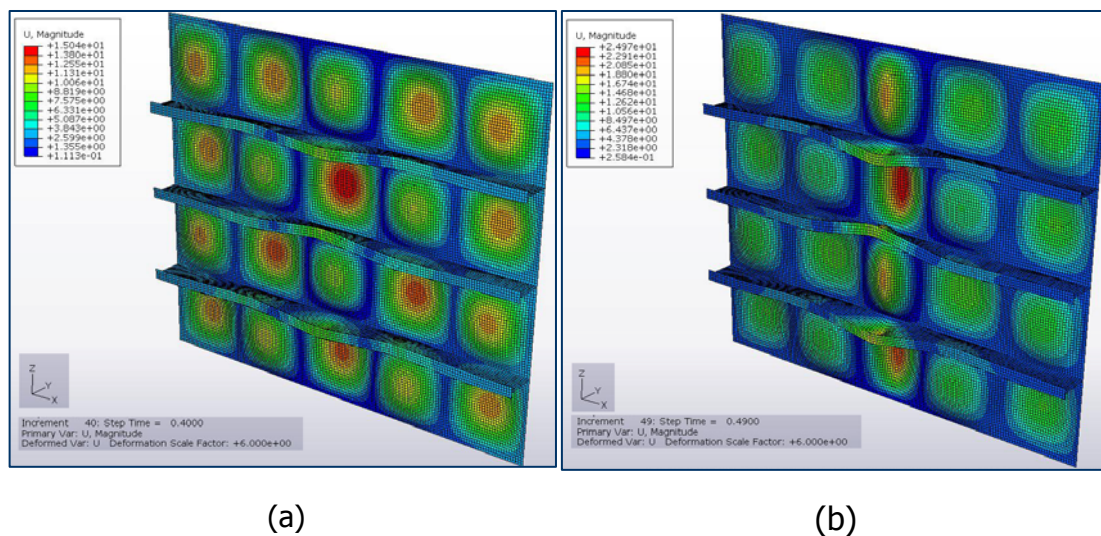


**Fig.7.48.** Deformed shape of Panel S4 - Magnitude of Displacement : (a) at its Ultimate Limit State,  $\epsilon_{S4u}$ , (b) at Hull Girder Collapse,  $1.098 \epsilon_{S4u}$

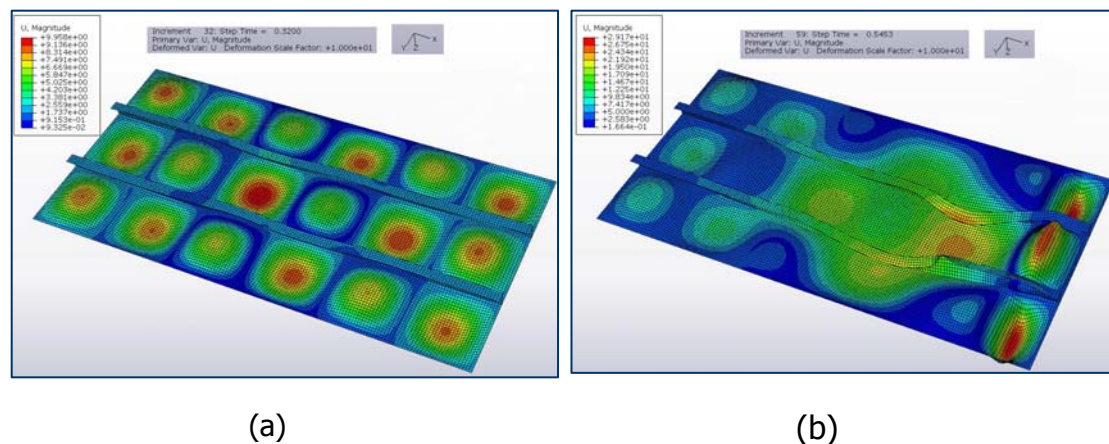
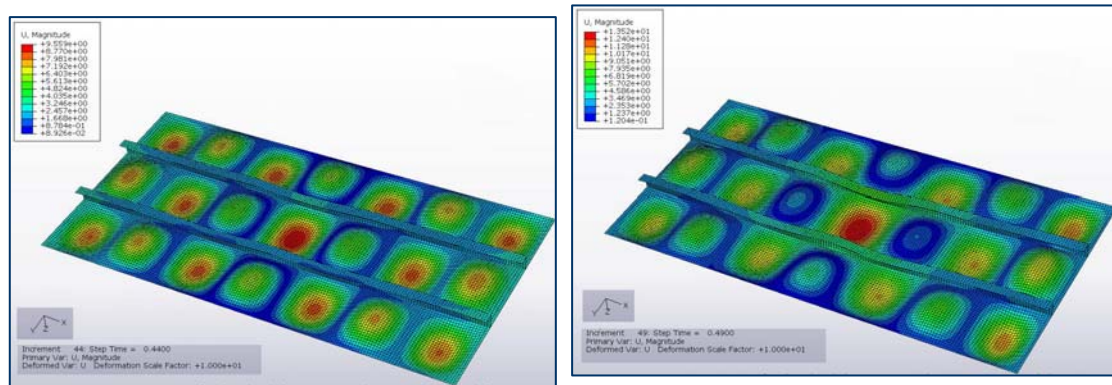


**Fig.7.49.** Deformed shape of Panel ST4 - Magnitude of Displacement : (a) at its Ultimate Limit State,  $\epsilon_{ST4u}$ , (b) at Hull Girder Collapse,  $1.703 \epsilon_{ST4u}$

Panel S4 collapses by tripping failure in contrast to panels ST4 and ST3 for which beam column buckling failure is observed.



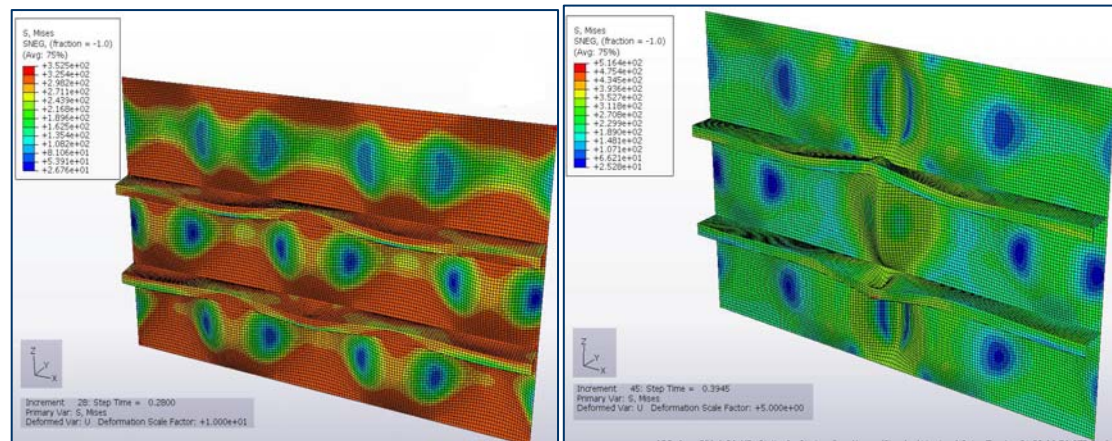


(a)

(b)

**Fig.7.50.** Deformed shape of Panel ST3 - Magnitude of Displacement : (a) at its Ultimate Limit State,  $\epsilon_{ST3Ur}$ , (b) at Hull Girder Collapse,  $1.099 \epsilon_{ST3u}$

Von Mises Stress Distribution



(a)

(b)

**Fig.7.51.** Von Mises Stress of Panel I4 : (a) at its Ultimate Limit State,  $\epsilon_{I4Ur}$ , (b) at Hull Girder Collapse,  $1.391 \epsilon_{I4u}$

By reviewing Figure 7.51a, significant differences can be noticed between the stress distribution of the upper and lower part of the plate of panel I4. This asymmetry is also evident in the deformed shape of same (Fig.7.46a) and can be attributed to the geometrical asymmetry of the plate (the upper plate width is greater). Moreover, as shown, the ultimate limit state of the panel is reached when a large yield area occurs in the plate-stiffener combination. This is also the case for all panels shown below (Fig.7.52-7.55 a).

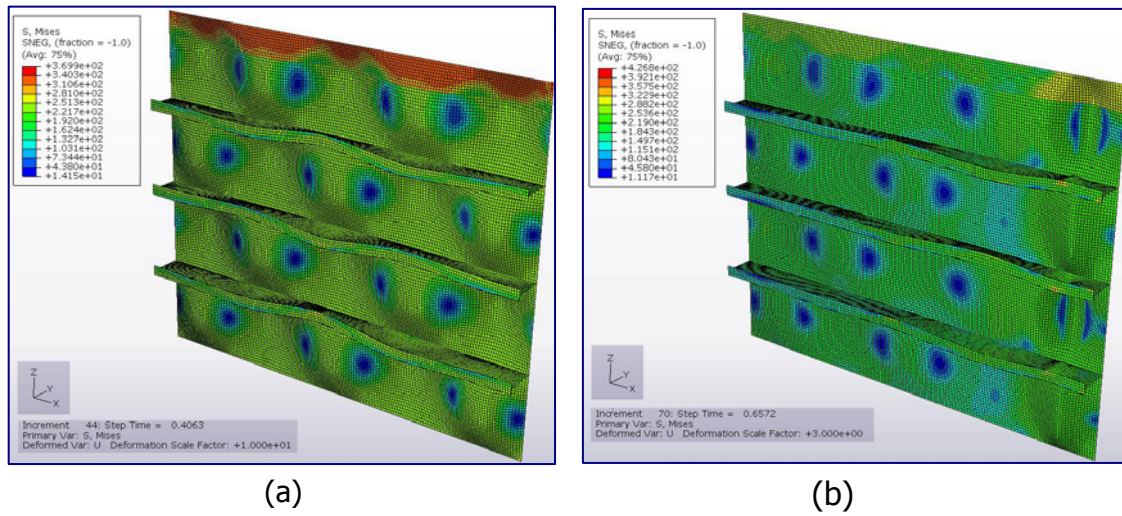


**Fig.7.52.** Von Mises Stress of Panel I3 : (a) at its Ultimate Limit State,  $\epsilon_{I3u}$ , (b) at Hull Girder Collapse,  $1.369 \epsilon_{I3u}$

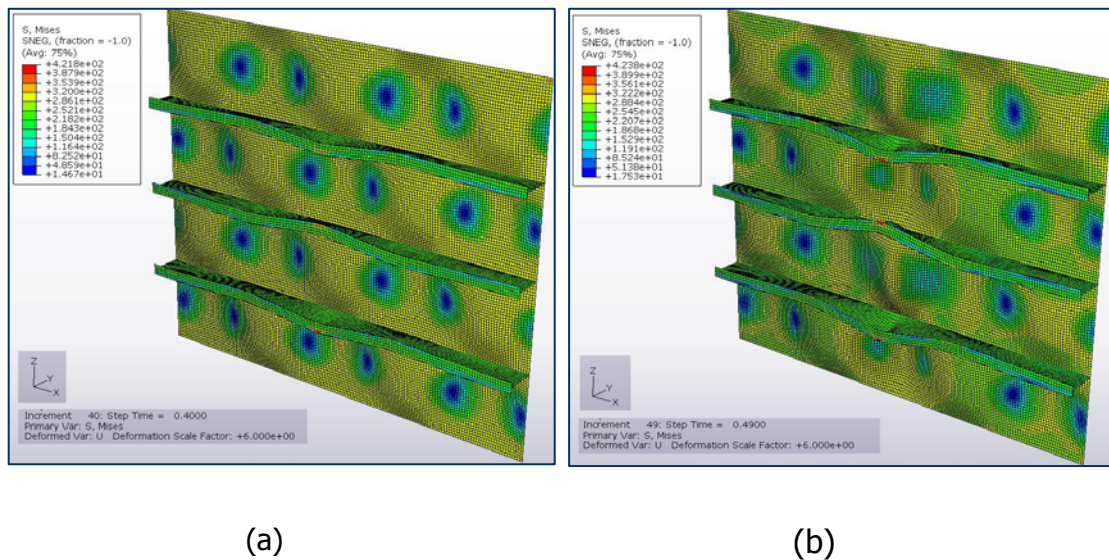


**Fig.7.53.** Von Mises Stress of Panel S4 : (a) at its Ultimate Limit State,  $\epsilon_{S4u}$ , (b) at Hull Girder Collapse,  $1.098 \epsilon_{S4u}$

Asymmetry is also noticed in the stress distribution of Panel I3 (Fig.7.52a), as 240mm of the panel's plate towards the deck region has a greater yield stress ( $315\text{Nt/mm}^2$ ).

Von Mises Stress Distribution (cont.)

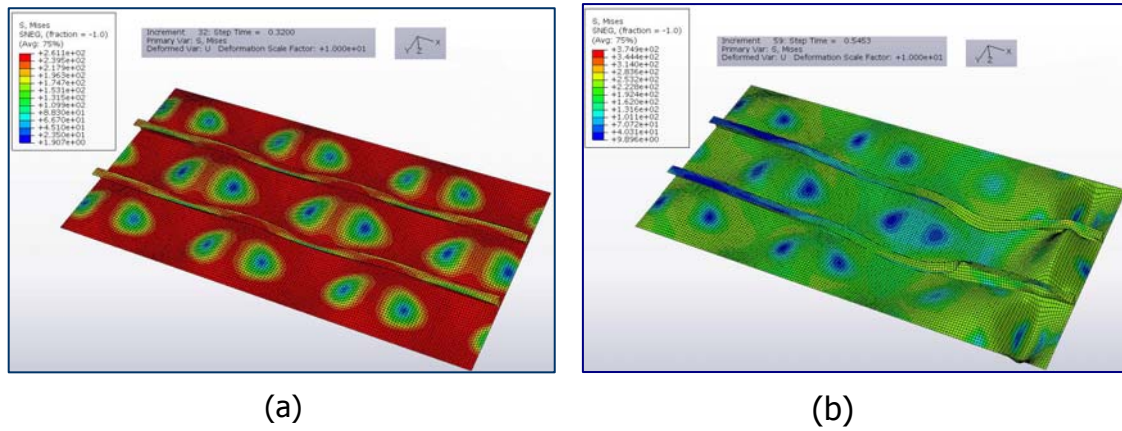


**Fig.7.54.** Von Mises Stress of Panel ST4 : (a) at its Ultimate Limit State,  $\epsilon_{ST4u}$ , (b) at Hull Girder Collapse,  $1.703 \epsilon_{ST4u}$

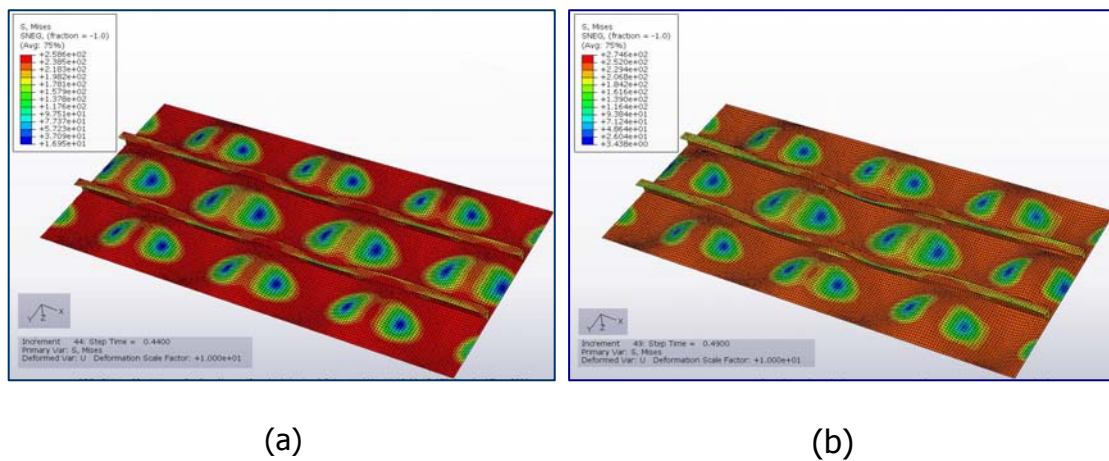


**Fig.7.55.** Von Mises Stress of Panel ST3 : (a) at its Ultimate Limit State,  $\epsilon_{ST3u}$ , (b) at Hull Girder Collapse,  $1.099 \epsilon_{ST3u}$



LOCATION OF LONGITUDINAL STIFFENER			YIELD STRESS		ULTIMATE LIMIT STATE PER LONGITUDINAL STIFFENER						ULTIMATE LIMIT STATE PER PANEL					
Location	Panel	Structural Element	$\sigma_{ydplate}$	$\sigma_{yd stiffener}$	$\sigma_{ydeq}$	$\epsilon_u$	$\sigma_u$	$\epsilon_u/\epsilon_{yd}$	$\sigma_u/\sigma_{ydeq}$	$\epsilon_{HullColl}/\epsilon_u$	$\sigma_{ydeq}$	$\epsilon_u$	$\sigma_u$	$\epsilon_u/\epsilon_{yd}$	$\sigma_u/\sigma_{ydeq}$	$\epsilon_{HullColl}/\epsilon_u$
Main Deck	M 2	M 2 - 1	245	245	245	0.000995	186.54	0.84	0.761	2.7760	245	0.001131	183.99	0.96	0.751	2.405
		M 2 - 2	245	245	245	0.000995	187.42	0.84	0.765	2.7760						
		M 2 - 3	245	245	245	0.000995	185.05	0.84	0.755	2.7760						
		M 2 - 4	245	245	245	0.001116	186.92	0.94	0.763	2.4743						
		M 2 - 5	245	245	245	0.001131	189.03	0.96	0.772	2.4424						
		M 2 - 6	245	245	245	0.001169	187.56	0.99	0.766	2.3613						
		M 2 - 7	245	245	245	0.001228	187.87	1.04	0.767	2.2144						
		M 2 - 8	245	245	245	0.001262	187.37	1.07	0.765	2.1548						
		M 2 - 9	245	245	245	0.001228	187.03	1.04	0.763	2.2144						
		M 2 - 10	245	245	245	0.001174	187.50	0.99	0.765	2.3151						
		M 2 - 11	245	245	245	0.001140	188.04	0.96	0.768	2.3840						
		M 2 - 12	245	245	245	0.001116	188.07	0.94	0.768	2.4359						
		M 2 - 13	245	245	245	0.001106	185.88	0.93	0.759	2.4572						
		M 2 - 14	245	245	245	0.001116	184.04	0.94	0.751	2.4359						
		M 2 - 15	245	245	245	0.000990	186.39	0.84	0.761	2.7463						
	M 2 - 16	245	245	245	0.000990	185.81	0.84	0.758	2.6738							
	M 1	M 1 - 18	245	245	245	0.001326	185.43	1.12	0.757	1.9871	245	0.001326	180.11	1.12	0.735	1.987
M 1	M 1 - 19	245	245	245	0.001326	185.30	1.12	0.756	1.9871							
Inner Bulkhead	I 4	I 4 - 38	315	315	315	0.001643	198.30	1.08	0.630	1.5083	315	0.001704	188.17	1.12	0.597	1.391
		I 4 - 37	315	315	315	0.001583	205.12	1.04	0.651	1.4562						
	I 3	I 3 - 35	245	245	245	0.001243	173.25	1.05	0.707	1.5748	245	0.001302	170.03	1.10	0.694	1.369
		I 3 - 34	245	245	245	0.001243	178.76	1.05	0.730	1.4346						
Side Shell	S 5	S 5 - 38	315	245	302	0.001515	209.59	1.04	0.694	1.6404	305.93	0.001515	196.36	1.03	0.642	1.573
		S 5 - 37	315	245	303	0.001623	194.78	1.11	0.644	1.4234						
	S 4	S 4 - 35	315	245	297	0.001583	199.41	1.10	0.672	1.2381	300.09	0.001623	194.16	1.12	0.647	1.098
		S 4 - 34	315	245	297	0.001623	203.02	1.13	0.684	1.0996						
S 4 - 33	315	245	296	0.001542	196.75	1.08	0.665	1.0445								
Stringer 36	ST 4	ST 4 - 18	245	245	245	0.001250	171.44	1.06	0.700	1.7027	245.00	0.001250	170.40	1.06	0.696	1.703
		ST 4 - 19	245	245	245	0.001250	172.92	1.06	0.706	1.7027						
Stringer 32	ST 3	ST 3 - 18	245	245	245	0.001302	162.50	1.10	0.663	1.0991	245.00	0.001302	159.52	1.10	0.651	1.099
		ST 3 - 19	245	245	245	0.001302	163.78	1.10	0.668	1.0991						

**Table 7.12.** Ultimate Limit State Characteristics of Panels constantly under Compression

#### **7.5.4. Deformed shape of Panels under Tension**

The panels of the Midship Section that as per the Finite Element Approach are always under tension before the Hull Girder reaches its Ultimate Limit State, include all panels extending below 5243mm above base line. This includes all the panels in the inner bottom and bottom shell plating, the hopper plating, the stringer 23 and the side and centre girder, as illustrated in Figure 7.66.

At the time of the hull girder collapse all these panels are still in the elastic region as detailed in Table 7.13, where their applied strain to the yield strain ratio is listed. More specifically, it can be seen that the applied strain at the hull girder collapse to their yield strain ratio varies from 0.09 to 0.80 depending on the position of the structural element considered.

POSITION OF STRUCTURAL ELEMENT			YIELD STRESS			APPLIED STRAIN TO YIELD STRAIN AT TIME OF HULL GIRDER COLLAPSE
Location	Panel	Structural Element	$\sigma_{yd}$ plate (Nt/mm <sup>2</sup> )	$\sigma_{yd}$ stiffener (Nt/mm <sup>2</sup> )	$\sigma_{yd}$ equivalent (Nt/mm <sup>2</sup> )	$\epsilon_{HullColl}/\epsilon_{yd}$
CL Blkh	CL 2	CL 2 - 23	315	315	315	-0,089
		CL 2 - 22	315	315	315	-0,203
		CL 2 - 21	315	315	315	-0,315
Side Shell	S 1	S 1 - 22	315	315	315	-0,202
		S 1 - 21	315	315	315	-0,317
		S 1 - 20	315	315	315	-0,422
Hopper Plating	HP	HP - 1	315	315	315	-0,301
		HP - 2	315	315	315	-0,301
		HP - 3	315	315	315	-0,176
Stringer 23	ST 1	ST 1 - 18	245	245	245	-0,115
		ST 1 - 19	245	245	245	-0,115
Bottom	B 2	B 2 - 1	315	315	315	-0,693
		B 2 - 2	315	315	315	-0,693
		B 2 - 3	315	315	315	-0,693
		B 2 - 4	315	315	315	-0,693
		B 2 - 5	315	315	315	-0,693
		B 2 - 6	315	315	315	-0,693
		B 2 - 7	315	315	315	-0,693
		B 2 - 8	315	315	315	-0,693
		B 2 - 9	315	315	315	-0,693
		B 2 - 10	315	315	315	-0,693
		B 2 - 11	315	315	315	-0,693
		B 2 - 12	315	315	315	-0,693
		B 2 - 13	315	315	315	-0,693
		B 1	B 1 - 15	315	315	315
B 1 - 16	315		315	315	-0,693	
B 1 - 17	315		315	315	-0,691	
Inner Bottom	IB 1	IB 1 - 1	315	315	315	-0,439
		IB 1 - 2	315	315	315	-0,439
		IB 1 - 3	315	315	315	-0,439
		IB 1 - 4	315	315	315	-0,439
		IB 1 - 5	315	315	315	-0,439
		IB 1 - 6	315	315	315	-0,439
		IB 1 - 7	315	315	315	-0,439
		IB 1 - 8	315	315	315	-0,439
		IB 1 - 9	315	315	315	-0,439
		IB 1 - 10	315	315	315	-0,439
		IB 1 - 11	315	315	315	-0,438
		IB 1 - 12	315	315	315	-0,438
		IB 1 - 13	315	315	315	-0,438
Side Girder	SG	SG - 1	245	245	245	-0,797
		SG - 2	245	245	245	-0,674
CL Girder	CL	CL - 1	315	315	315	-0,620
		CL - 2	315	315	315	-0,524
Bilge	BLG	-	-	315	-0,621	
Hard Corner Inner Shell-Stringer 23	-	-	-	299	-0,091	
Hard Corner Side Shell -Stringer 23	-	-	-	296	-0,093	
Hard Corner Side Girder-Bottom	-	-	-	296	-0,745	
Hard Corner Side Girder-Inner Bottom	-	-	-	296	-0,452	
Hard Corner CL Girder-Bottom	-	-	-	315	-0,697	
Hard Corner CL Girder-Inner Bottom	-	-	-	315	-0,424	

**Table 7.13.** Applied Strain to Panels' structural elements constantly under Tension at the time of the Hull Girder Collapse

As in the case of the panels under compression presented in the previous pages, the present section aims to give a short introduction of the deformed shapes of the panels and their Mises stress distribution at the time of the hull girder collapse. The displacement magnitude as well as the stress distribution of all panels under tension is shown in Figures 7.56 - 7.64.

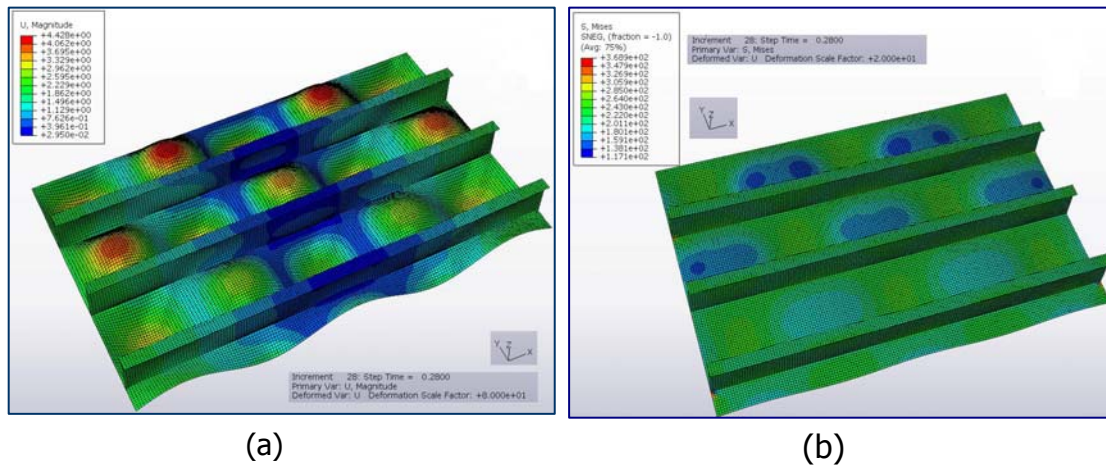


**Fig.7.56.** Panel B1 : (a) Displacement Magnitude, (b) Von Mises Stress Distribution at the time of the Hull Girder Collapse,  $\epsilon_{B1ap} = \epsilon_{Hullu}$

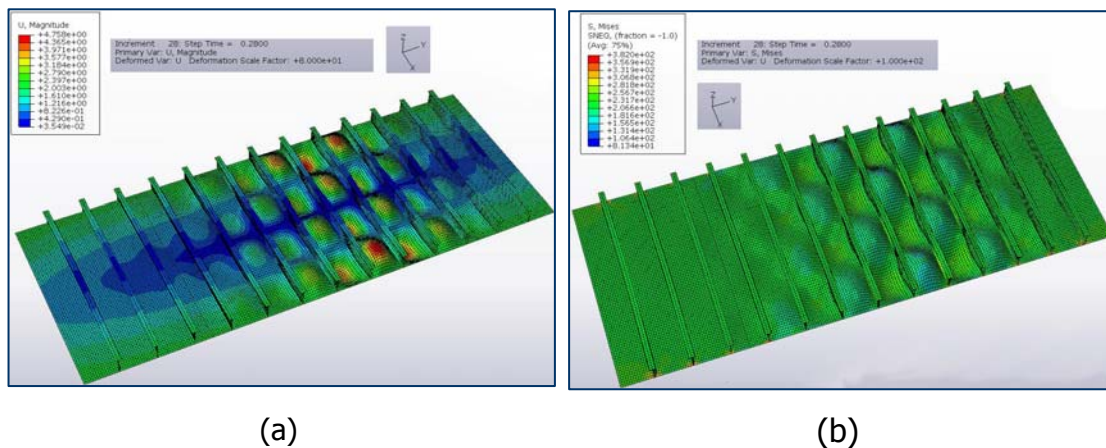
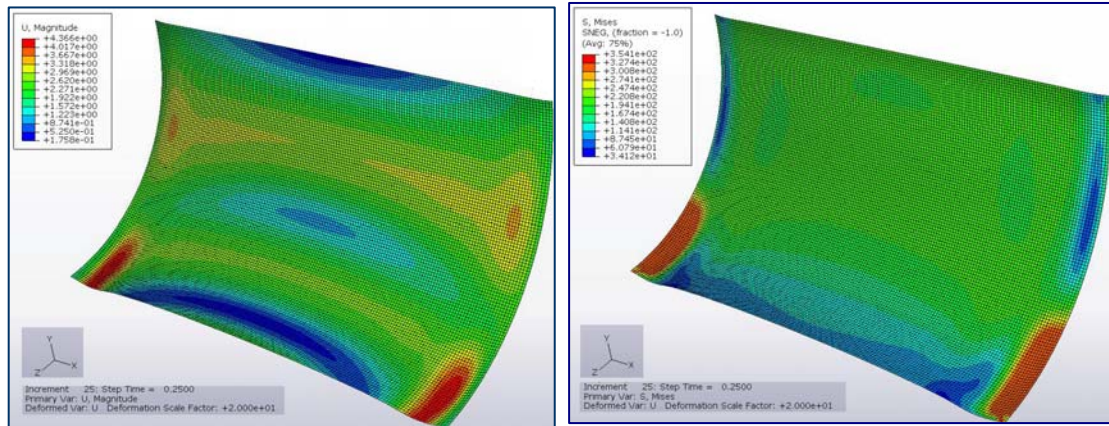


**Fig.7.57.** Panel B2 : (a) Displacement Magnitude, (b) Von Mises Stress Distribution at the time of the Hull Girder Collapse,  $\epsilon_{B2ap} = \epsilon_{Hullu}$

Both bottom panels have been subjected to buckling of the plate at the time of the hull girder collapse as depicted in above Figures. This can be attributed to the initial imperfections taken into account for the FE analysis.

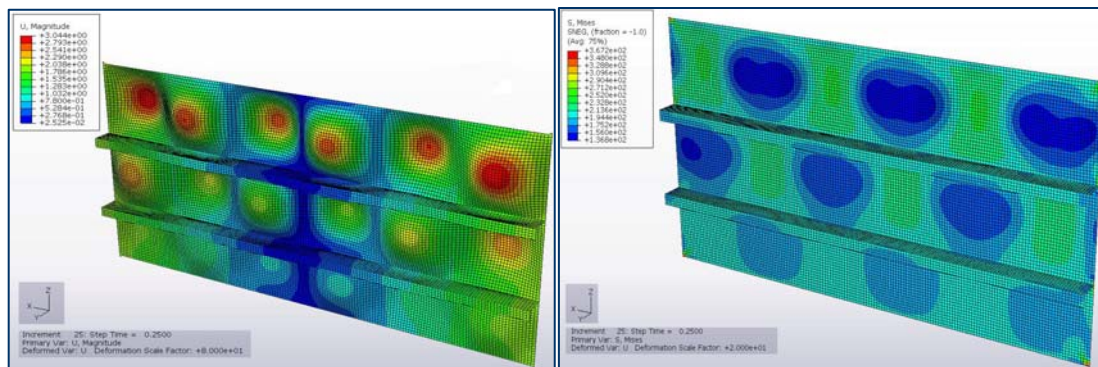
The bottom panels as well as all tensioned panels are in the elastic region at the time of the hull girder collapse as shown in the figures below.



(a)

(b)

**Fig.7.58.** Panel BLG : (a) Displacement Magnitude, (b) Von Mises Stress Distribution at the time of the Hull Girder Collapse,  $\epsilon_{BLGap} = \epsilon_{Hullu}$



(a)

(b)

**Fig.7.59.** Panel CL1 : (a) Displacement Magnitude, (b) Von Mises Stress Distribution at the time of the Hull Girder Collapse,  $\epsilon_{CL1ap} = \epsilon_{Hullu}$

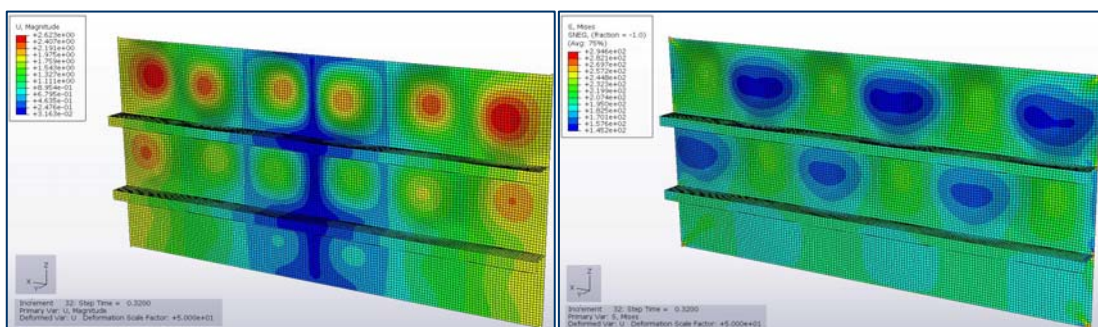
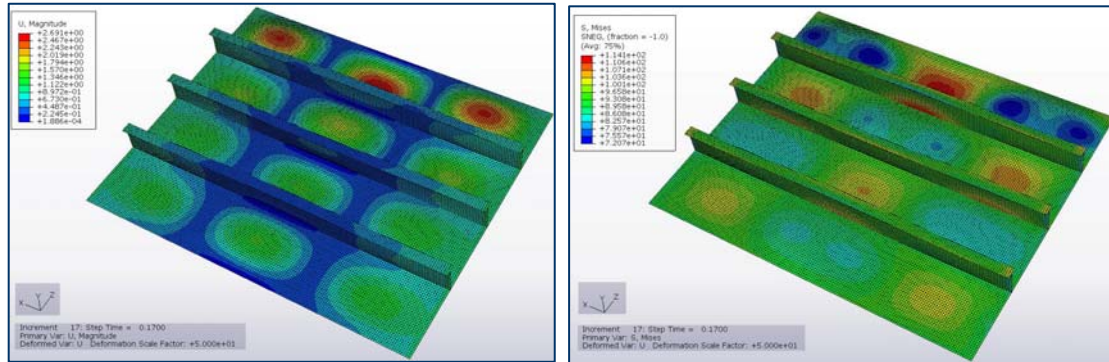


**Fig.7.60.** Panel SG : (a) Displacement Magnitude, (b) Von Mises Stress Distribution at the time of the Hull Girder Collapse,  $\epsilon_{SGap} = \epsilon_{Hullu}$



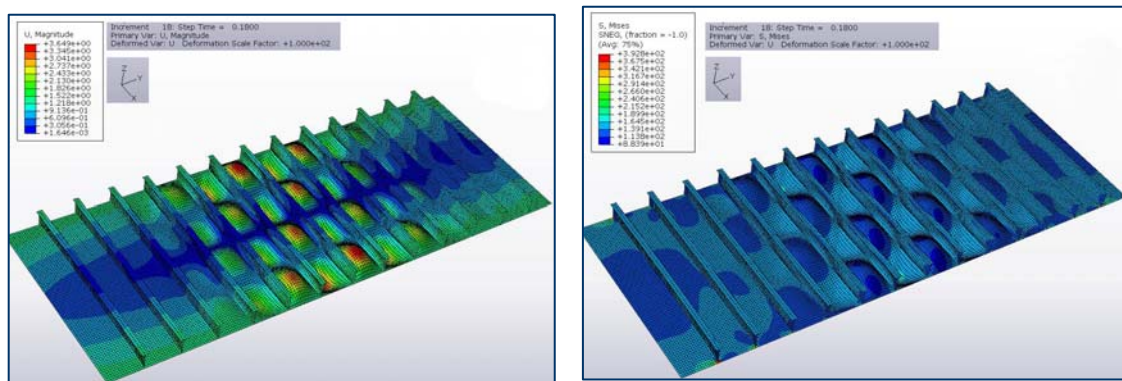
The deformation shape of CL Girder (CL1) and Side Girder (SG) panels are asymmetric due to the asymmetry in the stiffeners distance.



(a)

(b)

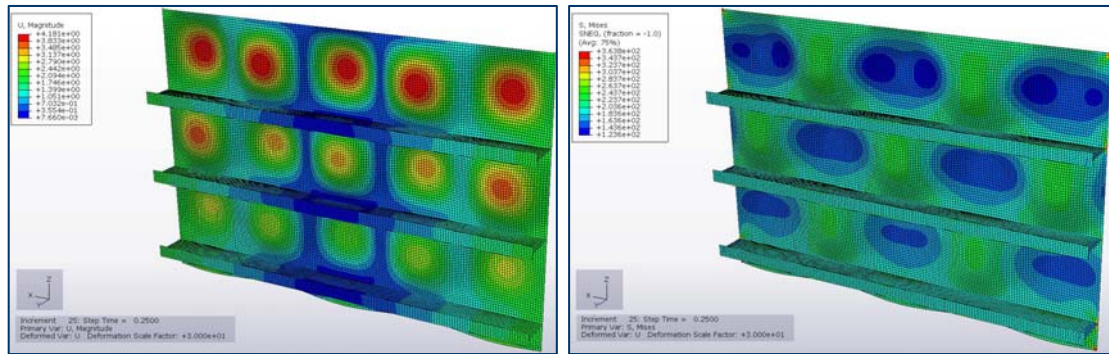
**Fig.7.61.** Panel HP : (a) Displacement Magnitude, (b) Von Mises Stress Distribution at the time of the Hull Girder Collapse,  $\epsilon_{HPap} = \epsilon_{Hullu}$



(a)

(b)

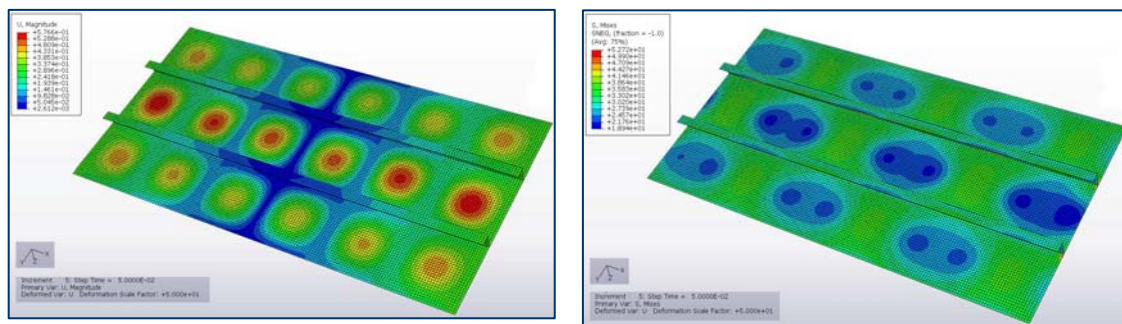
**Fig.7.62.** Panel IB1: (a) Displacement Magnitude, (b) Von Mises Stress Distribution at the time of the Hull Girder Collapse,  $\epsilon_{HPap} = \epsilon_{Hullu}$



(a)

(b)

**Fig.7.63.** Panel S1: (a) Displacement Magnitude, (b) Von Mises Stress Distribution at the time of the Hull Girder Collapse,  $\epsilon_{S1ap} = \epsilon_{Hullul}$



(a)

(b)

**Fig.7.64.** Panel ST1 : (a) Displacement Magnitude, (b) Von Mises Stress Distribution at the time of the Hull Girder Collapse,  $\epsilon_{ST1ap} = \epsilon_{Hullu}$

### 7.5.5. Panels in the region of the neutral axis

Structural elements that are positioned between the initial and final position of the hull girder neutral axis are initially under tension and subsequently under compression as the distance of the neutral axis from the base line decreases. These structural elements are listed in Table 7.14 below. The table also lists the strain levels to which these elements are being subjected at three stages during the hull girder collapse calculation and specifically at increment 1, increment 51 and increment 103 corresponding to the hull girder collapse. The negative sign denotes the tension strains whereas positive sign the compressive strains.

It can be seen that at these structural elements, as envisaged, the applied strain to yield strain ratio is very small, almost negligible. This is also confirmed in Figure 7.65 where the applied strain versus the position of the neutral axis is plotted for the structural elements CL 2 – 24, ST 2 – 18 and S 2 – 25. The graphs clearly show

the transition from tensile to compressive strain as the neutral axis shifts towards the base line.

Location	Structural Element	$\sigma_{yd}$ plate	$\sigma_{yd}$ stiffener	$\sigma_{yd}$ equivalent	$\epsilon_{appl} / \epsilon_{yd}$	$\epsilon_{appl} / \epsilon_{yd}$	$\epsilon_{appl} / \epsilon_{yd}$
					Inc.1	Inc.51	Inc.103
CL Blkhd	CL 2 - 24	315	315	315	-0.0028	-0.1054	0.0256
	CL 2 - 25	315	315	315	-0.0017	-0.0497	0.1404
	CL 2 - 26	315	245	291	-0.0006	0.0061	0.2751
Inner Bulkhead	I 1 - 25	315	245	292	-0.0018	-0.0533	0.1523
	I 1 - 24	315	245	292	-0.0030	-0.1132	0.0286
Side Shell	S 2 - 25	315	245	292	-0.0018	-0.0532	0.1520
	S 2 - 24	315	245	292	-0.0030	-0.1132	0.0286
Stringer 26	ST 2 - 18	245	245	245	-0.0007	0.0066	0.3256
	ST 2 - 19	245	245	245	-0.0007	0.0066	0.3256
Hard Corner Inner Shell- Stringer 26	-	-	-	298.8	-0.0006	0.0066	0.2696
Hard Corner Side Shell - Stringer 26	-	-	-	298.8	-0.0006	0.0066	0.2696

**Table 7.14.** Structural elements in way of the position of the neutral axis

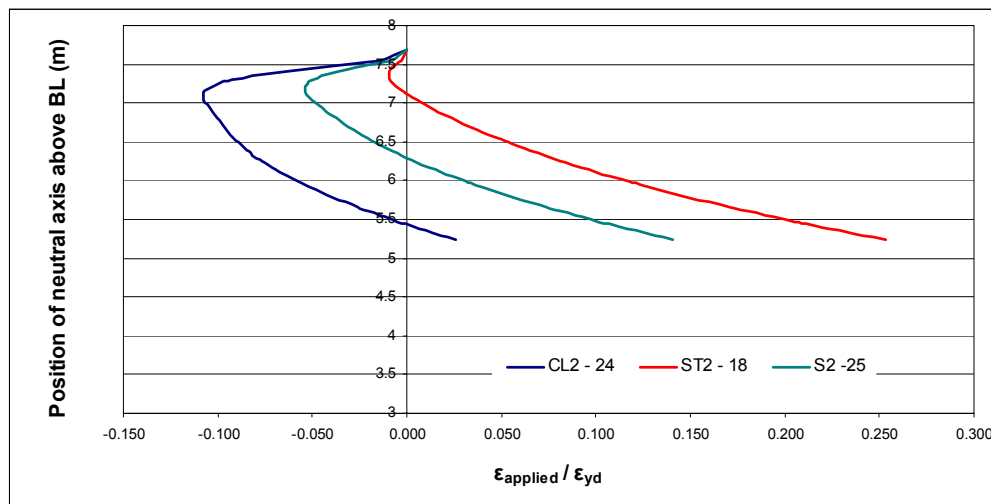


**Fig.7.65.** Applied strain/yield strain ratio versus position of neutral axis

Not knowing in advance the position of the neutral axis corresponding to each curvature, the applied strain to each element cannot be predicted. In this respect, as also proposed by the Incremental-Iterative approach the applicable stress for these elements have been derived by their compressive or tension stress-strain curves separately dependent on the strain considered.

### 7.5.6. Position of the neutral axis

As already mentioned, the position of the neutral axis at each step of the Incremental Iterative Approach is being calculated so as to achieve equilibrium of the forces acting on the Hull Girder. The initial position of the neutral axis as well as its position at the time of the Hull Girder Collapse is indicated in Figure 7.66. Initially the position of the neutral axis had been calculated at 7683mm. As shown in the figure below the position of the neutral axis computed by the Finite Element Approach at the time of the Hull Girder Ultimate Limit State is 5243mm.

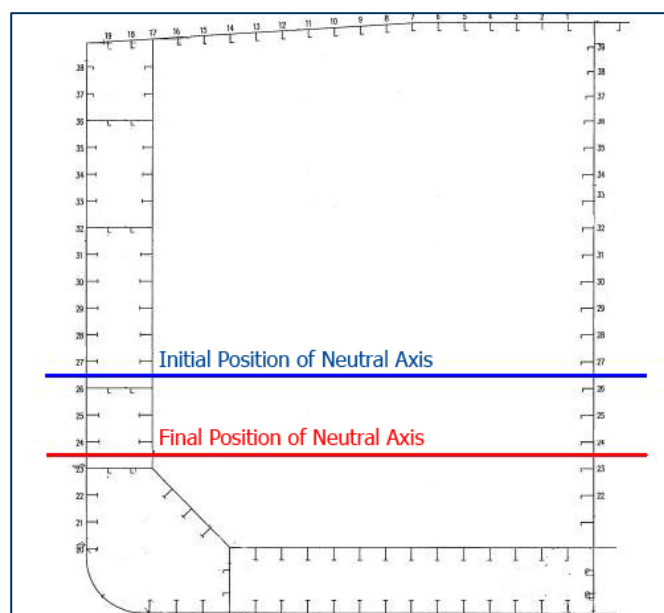


**Fig.7.66.** Illustration of initial and final position of the neutral axis

The change of the Neutral Axis position as the imposed curvature on the Hull girder increases is shown in Fig.7.67. With the increase of the imposed curvature, the distance of the hull girder neutral axis from base line is significantly decreased.

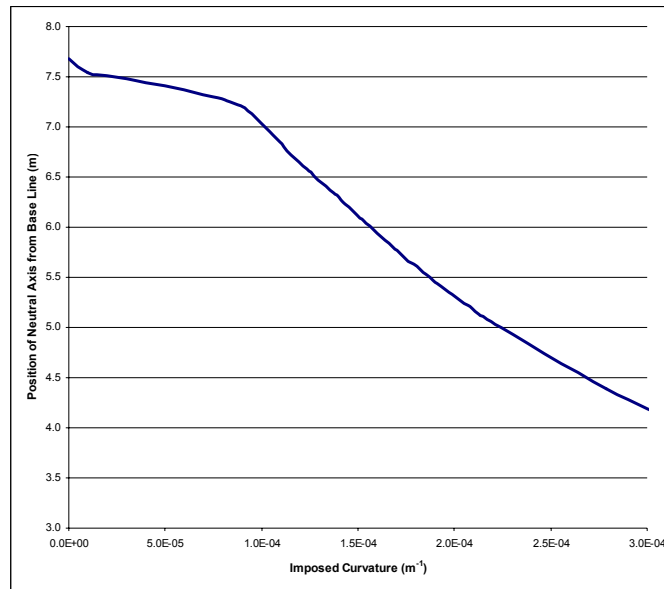


**Fig.7.67.** Position of neutral axis at each imposed curvature

### 7.5.7. Ultimate Hull Girder Limit State

By applying the Incremental – Iterative method with the use of the stress-strain curves computed by the Finite Element Approach, the Vertical Hull Girder Bending Moment curve as the imposed curvature increases can be derived. This is given in Figure 7.68.

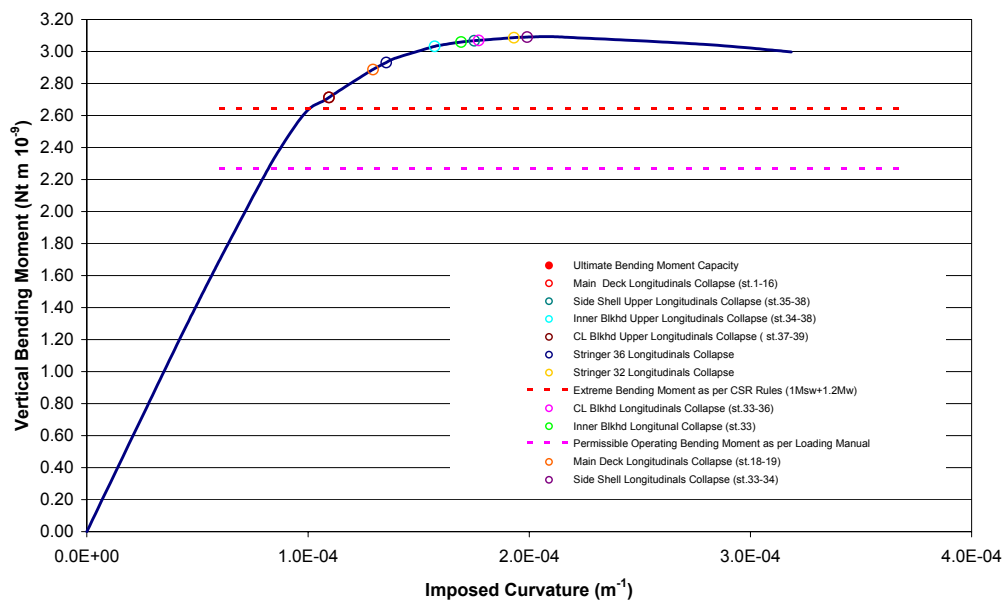


**Fig.7.68.** FEA Hull Girder Vertical Bending Moment - Imposed Curvature Curve

The FEA Hull Girder Ultimate Bending Capacity corresponds to the peak of M-k curve and specifically at a bending moment of  $3.093 \cdot 10^9$  Nt·m and a curvature of  $2.05 \cdot 10^{-4}$  m<sup>-1</sup> occurring at increment 103 of the incremental approach. The comparison of the resultant bending capacity of the two methods will be carried out in the next Chapter.

The extreme bending moment at which the vessel as per the CSR Rules is expected to operate, as well as the permissible total bending moment as which the vessel actually operates are demonstrated in above figure by red and pink dotted lines respectively. Reference for their calculation is made in Sub-section 6.6. Taking into account that the **design** ( $M_{uFE} - M_{bIACS} / M_{uFE}$ ) **and actual safety margin** ( $M_{uFE} - M_{perm} / M_{uFE}$ ) can be derived by the difference of the ultimate bending capacity to the expected design extreme bending moment and the actual permissible bending moment respectively, we obtain the following:

**Design Safety Margin: 14.5%**

**Actual Safety Margin: 26.7%**

We should note though, that CSR Rules account for a safety margin  $\gamma_r$  in the estimation of the hull girder ultimate strength due to uncertainties (refer to Figure 3.1) equal to 1.1. Therefore the permissible bending moment, as indicated in the vessel's loading manual should be compared to the corresponding ratio  $M_u / \gamma_r$ , here estimated as  $3.093 / 1.1$  or  $2.811 \text{ Nt m} \times 10^9$ , since the vessel's designers must have taken this safety ratio into account. In such case the actual safety margin considered becomes 19.5%  $\{[(M_{uFE} / \gamma_r) - M_{perm}] / (M_{uFE} / \gamma_r)\}$ .

Along the curve, reference is made to the imposing curvature at which each structural element collapses. It can be seen, that the main deck longitudinals and the CL bulkhead upper longitudinals (st.37-39) are the first to collapse, followed by the Inner Bulkhead (st.34-38 and st.33) & Side Shell upper longitudinals (st.35-38) and Stringer 36. The last to collapse are the Side shell longitudinals (st.33-34) at the mid depth and Stringer 32.

## **CHAPTER 8**

### **COMPARISON OF THE APPROACHES**

#### **8.1. General**

In previous chapters, Chapter 6 and Chapter 7, a detailed description has been provided of the methods applied in the context of the present study for the estimation of a double hull tanker's ultimate bending capacity. The results of each method have been presented separately. This chapter aims to compare the results of both methods and, in particular, the structural elements' load end shortening curves and ultimate limit strength as well as the calculated hull girder's Vertical Bending Moment – Imposed Curvature Curve and Ultimate Bending Capacity.

#### **8.2. Load End Shortening Curves of structural elements**

As already mentioned, the Incremental-Iterative approach aims to determine the hull girder ultimate capacity by dividing the hull girder transverse section between two adjacent transverse webs into structural elements which are considered to act independently of each other (refer to Figure 6.2), and to calculate the collapse behavior of each of these structural elements. The structural elements may comprise of longitudinal stiffeners with their attached plating (of breadth equal to the spacing of the stiffeners), hard corners or transversely stiffened panels. In the case of the double hull tanker used as a case study, the midship section has been divided into longitudinal stiffeners and hard corners.

For the determination of the elements' behavior, the CSR propose certain formulas, depending on the structural element considered (longitudinal stiffener or hard corner) and the uniaxial stresses to which it is subjected, compressive or tension stresses. The following subsections compare the Load end shortening curves of longitudinal stiffeners and hard corners, either under compression or tension, as derived by the Incremental-Iterative Approach and computed by the Finite Element Approach.

### **8.2.1. Longitudinal Stiffeners under uniaxial compression**

The CSR formulas for the estimation of the longitudinal stiffeners' collapse behavior under uniaxial compression, consider all relevant failure modes, such as beam column buckling, torsional stiffener buckling and stiffener web buckling (refer to figure 2.14). The load end shortening curve of each stiffener is then constructed using the minimum stress predicted for each of these failure modes.

Table 8.1 summarizes the critical failure mode of each longitudinal stiffener under compression of the tanker's midship section as predicted by the CSR Formulas and as indicated by the FE Analysis.

It can be seen that in general the failure modes of the two approaches are in agreement. Only in the case of the Side Shell Stiffeners in panels S-5 and S-4 (shown with grey colour) there is a discrepancy, with the CSR Formulas predicting beam column buckling whereas the FE Analysis indicates torsional buckling. Nevertheless, taking into account that in general, even with the help of FE Analysis, it is difficult to distinguish between these failure modes, as they interact and may occur simultaneously, this discrepancy is considered to be minor.

It should be noted though, as discussed previously, that this inconsistency can be attributed to the difference in yield stress between the stiffener and the plate and in particular to the fact that the stiffener yield stress is less than the plate's yield stress. Further, all remaining midship section's stiffeners of similar dimensions for which agreement of the two methods is observed, have a stiffener yield stress equal to or greater than the plate's. Moreover, the CSR Formulas in general account for identical yield stress between plate and stiffener. To account for this restriction, as per the IACS recommendation, two stress calculations are carried out, one for the plate-stiffener combination with yield stress equal to the plate's and one for the plate-stiffener combination with yield stress equal to the stiffener's.



LOCATION OF STRUCTURAL ELEMENT			INCREMENTAL APPROACH AS PER IACS APPROACH			FEA APPROACH	
Location	Panel	Structural Element	Plate / Stiffener	Buckling mode	$\sigma_{yd}$	Buckling mode	$\sigma_{yd}$ equiv
Main Deck	M 2	M 2 - 1	Both	Beam Column	245	Beam Column	245
		M 2 - 2	Both		245		245
		M 2 - 3	Both		245		245
		M 2 - 4	Both		245		245
		M 2 - 5	Both		245		245
		M 2 - 6	Both		245		245
		M 2 - 7	Both		245		245
		M 2 - 8	Both		245		245
		M 2 - 9	Both		245		245
		M 2 - 10	Both		245		245
		M 2 - 11	Both		245		245
		M 2 - 12	Both		245		245
		M 2 - 13	Both		245		245
		M 2 - 14	Both		245		245
		M 2 - 15	Both		245		245
		M 2 - 16	Both		245		245
	M 1	M 1 - 18	Both	Beam Column	245	Beam Column	245
		M 1 - 19	Both	Beam Column	245	Beam Column	245
	CL Bulkhead	CL 2	CL 2 - 27	Plate	Torsional	315	Torsional
Stiffener				245			
CL 2 - 28			Plate	Torsional	315	Torsional	290
			Stiffener		245		
CL 2 - 29			Plate	Torsional	315	Torsional	289
			Stiffener		245		
CL 2 - 30			Plate	Torsional	315	Torsional	289
			Stiffener		245		
CL 2 - 31			Plate	Torsional	315	Torsional	291
			Stiffener		245		
CL 2 - 32			Plate	Torsional	315	Torsional	290
			Stiffener		245		
CL 2 - 33			Plate	Torsional	280	Torsional	267
			Stiffener		245		
CL 2 - 34	Both	Torsional	245	Torsional	245		
CL 2 - 35	Both	Torsional	245	Torsional	245		
CL 2 - 36	Both	Torsional	245	Torsional	245		
CL 2 - 37	Plate	Beam Column	245	Beam Column	262		
	Stiffener		315				
CL 2 - 38	Plate	Beam Column	245	Beam Column	259		
	Stiffener		315				
CL 2 - 39	Plate	Beam Column	245	Beam Column	260		
	Stiffener		315				

**Table 8.1.** Comparison of the buckling failure and ULS modes of longitudinal stiffeners constantly under compression

LOCATION OF STRUCTURAL ELEMENT			INCREMENTAL APPROACH AS PER IACS APPROACH			FEA APPROACH	
Location	Panel	Structural Element	Plate / Stiffener	Buckling mode	$\sigma_{yd}$	Buckling mode	$\sigma_{yd}$ equiv
Inner Bulkhead	I 4	I 4 - 38	Both	Beam Column	315	Beam Column	315
		I 4 - 37	Both		315		315
	I 3	I 3 - 35	Both	Torsional	245	Torsional	245
		I 3 - 34	Both		245		245
		I 3 - 33	Both		245		245
	I 2	I 2 - 31	Plate	Torsional	315	Torsional	293
			Stiffener		245		
		I 2 - 30	Plate	Torsional	315	Torsional	292
			Stiffener		245		
		I 2 - 29	Plate	Torsional	315	Torsional	291
			Stiffener		245		
		I 2 - 28	Plate	Torsional	315	Torsional	291
			Stiffener		245		
		I 2 - 27	Plate	Torsional	315	Torsional	293
Stiffener	245						
Side Shell	S 5	S 5 - 38	Plate	Beam Column	315	Torsional	302
			Stiffener		245		
	S 5	S 5 - 37	Plate	Beam Column	315	Torsional	303
			Stiffener		245		
	S 4	S 4 - 35	Plate	Beam Column	315	Torsional	297
			Stiffener		245		
		S 4 - 34	Plate	Beam Column	315	Torsional	297
	Stiffener		245				
	S 4 - 33	Plate	Torsional	315	Torsional	296	
		Stiffener		245			
	S 3	S 3 - 31	Plate	Torsional	315	Torsional	295
			Stiffener		245		
		S 3 - 30	Plate	Torsional	315	Torsional	295
			Stiffener		245		
S 3 - 29		Plate	Torsional	315	Torsional	295	
		Stiffener		245			
S 3 - 28	Plate	Torsional	315	Torsional	294		
	Stiffener		245				
S 3 - 27	Plate	Torsional	315	Torsional	294		
	Stiffener		245				
Stringer 36	ST 4	ST 4 - 18	Both	Beam Column	245	Beam Column	245
		ST 4 - 19	Both		245		245
Stringer 32	ST 3	ST 3 - 18	Both	Beam Column	245	Beam Column	245
		ST 3 - 19	Both		245		245

**Table 8.1 (cont.).** Comparison of the buckling failure and ULS modes of longitudinal stiffeners constantly under compression

The ultimate limit state characteristics of all longitudinal stiffeners constantly under compression as derived by the FE Approach and the Incremental-Iterative Approach are given in Table 8.2. In the case of the Incremental-Iterative Approach, both the IACS and the Equivalent Yield Stress Approach referred to in paragraph 6.2.2 have been considered.

LOCATION OF STRUCTURAL ELEMENT			INCREMENTAL APPROACH AS PER IACS APPROACH						FEA APPROACH				INCREMENTAL APPROACH AS PER EQUIVALENT YIELD STRESS				COMPARISON		
Location	Panel	Structural Element	Plate / Stiffener	$\sigma_{yd}$	$\sigma_u$	$\sigma_u/\sigma_{yd}$	$\epsilon_u$	$\epsilon_u/\epsilon_{yd}$	$\sigma_{yd}$ equiv	$\sigma_u$	$\sigma_u/\sigma_{yde}$ equiv	$\epsilon_u/\epsilon_{yd}$ equiv	$\sigma_{yd}$ equiv	$\sigma_u$	$\sigma_u/\sigma_{yde}$ equiv	$\epsilon_u/\epsilon_{yd}$ equiv	$\sigma_{uIACSAppr} / \sigma_{uFEA}$	$\sigma_{uEquivAppr} / \sigma_{uFEA}$	$\sigma_{uEquivAppr} / \sigma_{uIACSAppr}$
Main Deck	M 2	M 2 - 1	Both	245	172.74	0.705	0.0012	1.012	245	186.54	0.761	0.840	245	172.74	0.705	1.012	0.93	0.93	1.00
		M 2 - 2	Both	245	172.74	0.705	0.0012	1.012	245	187.42	0.765	0.840	245	172.74	0.705	1.012	0.92	0.92	1.00
		M 2 - 3	Both	245	172.74	0.705	0.0012	1.012	245	185.05	0.755	0.840	245	172.74	0.705	1.012	0.93	0.93	1.00
		M 2 - 4	Both	245	172.74	0.705	0.0012	1.012	245	186.92	0.763	0.943	245	172.74	0.705	1.012	0.92	0.92	1.00
		M 2 - 5	Both	245	172.74	0.705	0.0012	1.012	245	189.03	0.772	0.955	245	172.74	0.705	1.012	0.91	0.91	1.00
		M 2 - 6	Both	245	172.74	0.705	0.0012	1.012	245	187.56	0.766	0.988	245	172.74	0.705	1.012	0.92	0.92	1.00
		M 2 - 7	Both	245	172.55	0.704	0.0012	1.012	245	187.87	0.767	1.037	245	172.55	0.704	1.012	0.92	0.92	1.00
		M 2 - 8	Both	245	172.55	0.704	0.0012	1.012	245	187.37	0.765	1.068	245	172.55	0.704	1.012	0.92	0.92	1.00
		M 2 - 9	Both	245	172.55	0.704	0.0012	1.012	245	187.03	0.763	1.037	245	172.55	0.704	1.012	0.92	0.92	1.00
		M 2 - 10	Both	245	172.55	0.704	0.0012	1.012	245	187.50	0.765	0.992	245	172.55	0.704	1.012	0.92	0.92	1.00
		M 2 - 11	Both	245	172.55	0.704	0.0012	1.012	245	188.04	0.768	0.963	245	172.55	0.704	1.012	0.92	0.92	1.00
		M 2 - 12	Both	245	172.55	0.704	0.0012	1.012	245	188.07	0.768	0.943	245	172.55	0.704	1.012	0.92	0.92	1.00
		M 2 - 13	Both	245	172.55	0.704	0.0012	1.012	245	185.88	0.759	0.935	245	172.55	0.704	1.012	0.93	0.93	1.00
		M 2 - 14	Both	245	172.55	0.704	0.0012	1.012	245	184.04	0.751	0.943	245	172.55	0.704	1.012	0.94	0.94	1.00
		M 2 - 15	Both	245	172.55	0.704	0.0012	1.012	245	186.39	0.761	0.836	245	172.55	0.704	1.012	0.93	0.93	1.00
		M 2 - 16	Both	245	172.85	0.706	0.0012	1.012	245	185.81	0.758	0.836	245	172.85	0.706	1.012	0.93	0.93	1.00
	M 1	M 1 - 18	Both	245	188.73	0.770	0.0012	1.012	245	185.43	0.757	1.120	245	188.73	0.770	1.012	1.02	1.02	1.00
	M 1 - 19	Both	245	188.73	0.770	0.0012	1.012	245	185.30	0.756	1.120	245	188.73	0.770	1.012	1.02	1.02	1.00	
	CL Bulkhead	CL 2	CL 2 - 27	Plate Stiffener	315 245	204.30	0.704	0.0016	1.024	290	215.69	0.743	1.010	290	208.45	0.718	0.982	0.95	0.97
CL 2 - 28			Plate Stiffener	315 245	204.05	0.703	0.0016	1.111	290	214.11	0.737	1.011	290	208.23	0.717	0.983	0.95	0.97	1.02
CL 2 - 29			Plate Stiffener	315 245	195.92	0.678	0.0016	1.116	289	211.18	0.731	1.015	289	200.99	0.696	0.987	0.93	0.95	1.03
CL 2 - 30			Plate Stiffener	315 245	195.92	0.678	0.0016	1.116	289	210.64	0.729	1.015	289	200.99	0.696	0.987	0.93	0.95	1.03
CL 2 - 31			Plate Stiffener	315 245	198.24	0.682	0.0016	1.109	291	210.69	0.724	1.051	291	201.80	0.694	0.981	0.94	0.96	1.02
CL 2 - 32			Plate Stiffener	315 245	201.63	0.696	0.0016	1.113	290	209.20	0.722	1.012	290	205.31	0.708	0.984	0.96	0.98	1.02
CL 2 - 33			Plate Stiffener	280 245	190.56	0.713	0.0014	1.067	287	195.64	0.732	1.014	287	193.56	0.724	0.998	0.97	0.99	1.02
CL 2 - 34			Both	245	176.66	0.721	0.0012	1.012	245	183.21	0.748	1.152	245	176.66	0.721	1.012	0.96	0.96	1.00
CL 2 - 35			Both	245	174.03	0.710	0.0012	1.012	245	173.15	0.707	1.108	245	174.03	0.710	1.012	1.01	1.01	1.00
CL 2 - 38			Both	245	172.04	0.702	0.0012	1.012	245	176.24	0.719	1.015	245	172.04	0.702	1.012	0.98	0.98	1.00
CL 2 - 37			Plate Stiffener	245 315	173.44	0.656	0.0012	0.941	262	184.88	0.705	0.793	262	181.17	0.687	1.012	0.94	0.96	1.04
CL 2 - 38			Plate Stiffener	245 315	183.06	0.626	0.0012	0.953	259	184.81	0.713	0.766	259	167.36	0.643	1.024	0.88	0.91	1.03
CL 2 - 39			Plate Stiffener	245 315	183.71	0.629	0.0012	0.952	260	185.70	0.713	0.759	260	168.08	0.645	1.024	0.88	0.91	1.03

**Table 8.2.** Comparison of the ultimate strength characteristics of longitudinal stiffeners constantly under compression

LOCATION OF STRUCTURAL ELEMENT			INCREMENTAL APPROACH AS PER IACS APPROACH						FEA APPROACH				INCREMENTAL APPROACH AS PER EQUIVALENT YIELD STRESS				COMPARISON		
Location	Panel	Structural Element	Plate / Stiffener	$\sigma_{yd}$	$\sigma_u$	$\sigma_u/\sigma_{yd}$	$\epsilon_u$	$\epsilon_u/\epsilon_{yd}$	$\sigma_{yd}$ equiv	$\sigma_u$	$\sigma_u/\sigma_{yde}$ equiv	$\epsilon_u/\epsilon_{yd}$ equiv	$\sigma_{yd}$ equiv	$\sigma_u$	$\sigma_u/\sigma_{yde}$ equiv	$\epsilon_u/\epsilon_{yd}$ equiv	$\sigma_{uIACSAppr}/\sigma_{uFEA}$	$\sigma_{uEquivAppr}/\sigma_{uFEA}$	$\sigma_{uEquivAppr}/\sigma_{uIACSAppr}$
Inner Bulkhead	14	14 - 38	Both	315	190.40	0.604	0.0016	1.024	315	198.30	0.630	1.080	315	190.40	0.604	1.024	0.96	0.96	1.00
		14 - 37	Both	315	193.12	0.613	0.0016	1.024	315	206.12	0.651	1.040	315	193.12	0.613	1.024	0.94	0.94	1.00
	13	13 - 35	Both	245	177.41	0.724	0.0012	1.012	245	173.25	0.707	1.050	245	177.41	0.724	1.012	1.02	1.02	1.00
		13 - 34	Both	245	177.12	0.723	0.0012	1.012	245	178.76	0.730	1.050	245	177.12	0.723	1.012	0.99	0.99	1.00
	12	13 - 33	Both	245	176.48	0.720	0.0012	1.012	245	177.10	0.723	1.050	245	176.48	0.720	1.012	1.00	1.00	1.00
		12 - 31	Plate	315	191.01	0.653	0.0016	1.102	293	182.66	0.624	1.028	293	195.19	0.667	1.038	1.05	1.07	1.02
		12 - 31	Stiffener	245															
		12 - 30	Plate	315	189.11	0.647	0.0016	1.104	292	190.93	0.654	1.006	292	193.62	0.663	0.977	0.99	1.01	1.02
		12 - 30	Stiffener	245															
		12 - 29	Plate	315	196.54	0.672	0.0016	1.108	291	199.98	0.687	1.034	291	199.61	0.686	0.980	0.98	1.00	1.02
		12 - 29	Stiffener	245															
		12 - 28	Plate	315	196.54	0.672	0.0016	1.108	291	203.46	0.699	1.010	291	199.61	0.686	0.980	0.98	0.98	1.02
		12 - 28	Stiffener	245															
		12 - 27	Plate	315	205.16	0.701	0.0016	1.103	293	211.38	0.723	0.981	293	209.11	0.715	1.039	0.97	0.99	1.02
12 - 27	Stiffener	245																	
Side Shell	S 5	5 - 38	Plate	315	188.93	0.626	0.0016	1.068	302	209.59	0.694	1.038	302	193.68	0.641	1.006	0.90	0.92	1.03
		5 - 37	Stiffener	245															
		5 - 37	Plate	315	182.61	0.603	0.0016	1.066	303	194.78	0.644	1.110	303	187.30	0.619	1.004	0.94	0.96	1.03
	5 - 37	Stiffener	245																
	S 4	4 - 35	Plate	315	208.96	0.704	0.0016	1.087	297	199.41	0.672	1.104	297	212.75	0.717	1.025	1.05	1.07	1.02
		4 - 34	Stiffener	245															
		4 - 33	Plate	315	209.20	0.707	0.0016	1.090	296	196.75	0.665	1.078	296	213.20	0.720	1.027	1.06	1.08	1.02
	4 - 33	Stiffener	245																
	S 3	3 - 31	Plate	315	205.92	0.698	0.0016	1.094	295	193.27	0.655	1.045	295	210.08	0.712	1.031	1.07	1.09	1.02
		3 - 31	Stiffener	245															
		3 - 30	Plate	315	205.02	0.696	0.0016	1.095	295	196.60	0.667	1.022	295	209.21	0.710	1.032	1.04	1.06	1.02
		3 - 30	Stiffener	245															
		3 - 29	Plate	315	205.02	0.696	0.0016	1.095	295	198.64	0.674	1.069	295	209.21	0.710	1.032	1.03	1.05	1.02
		3 - 29	Stiffener	245															
3 - 28	Plate	315	210.44	0.716	0.0016	1.097	294	202.68	0.689	1.072	294	214.30	0.729	1.034	1.04	1.06	1.02		
3 - 28	Stiffener	245																	
3 - 27	Plate	315	209.81	0.714	0.0016	1.098	294	198.38	0.675	1.073	294	213.70	0.728	1.035	1.06	1.08	1.02		
3 - 27	Stiffener	245																	
Stringer 36	ST 4	ST 4 - 18	Both	245	148.79	0.607	0.0012	1.012	245	171.44	0.700	1.056	245	148.79	0.607	1.012	0.87	0.87	1.00
Stringer 32		ST 3	ST 4 - 19	Both	245	148.79	0.607	0.0012	1.012	245	172.92	0.706	1.056	245	148.79	0.607	1.012	0.88	0.88
Stringer 32	ST 3	ST 3 - 18	Both	245	146.52	0.598	0.0012	1.012	245	162.60	0.663	1.100	245	146.52	0.598	1.012	0.89	0.89	1.00
Stringer 32		ST 3 - 19	Both	245	146.52	0.598	0.0012	1.012	245	163.78	0.668	1.100	245	146.52	0.598	1.012	0.89	0.89	1.00

**Table 8.2 (cont.).** Comparison of the ultimate strength characteristics of longitudinal stiffeners constantly under compression

By reviewing above table, it can be seen that the Equivalent Yield Stress Approach approximates better the resulting ultimate limit strength of the Finite Element Approach than the IACS Approach. The ratio of the ultimate limit strength of the Equivalent Yield stress approach to the IACS Approach ranges between 0.89-1.07 resulting to an approximate difference of 10%.

Moreover, it is noticed that the IACS Approach provides the most conservative results with respect to the ultimate limit strength of stiffeners.

In general, the greatest differences in the elements' Ultimate Limit State as per the CSR prediction and the FE Method have been found in the case of L-stiffeners (refer to the Main Deck Panels or Stringer Panels) and in the case of plate stiffener combinations with non identical yield stress (refer to panels I2, S5, S4,S3,etc). On the other hand, similar Ultimate Limit State has been found in the case of T stiffeners with identical yield stress in the attached plate and stiffener, with the ratio  $\sigma_{uIACS} / \sigma_{uFEA}$  ranging from 0.99-1.02 (refer to panel I3).

The above observations are also evident in the following figures, which depict the plot of the load end shortening curves for selected elements.

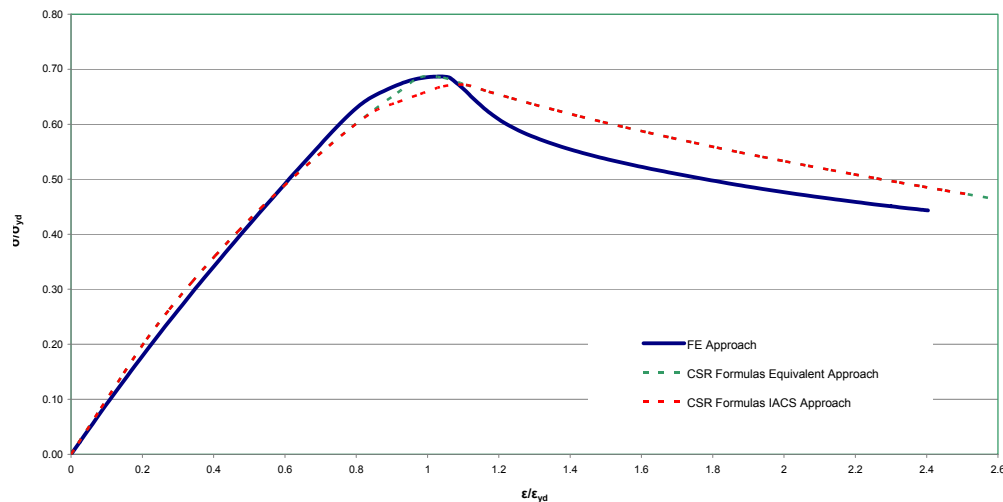
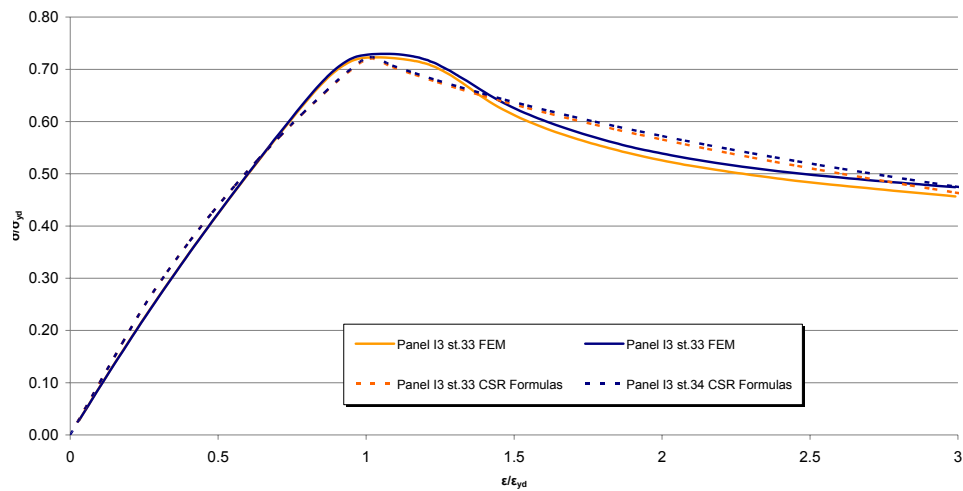
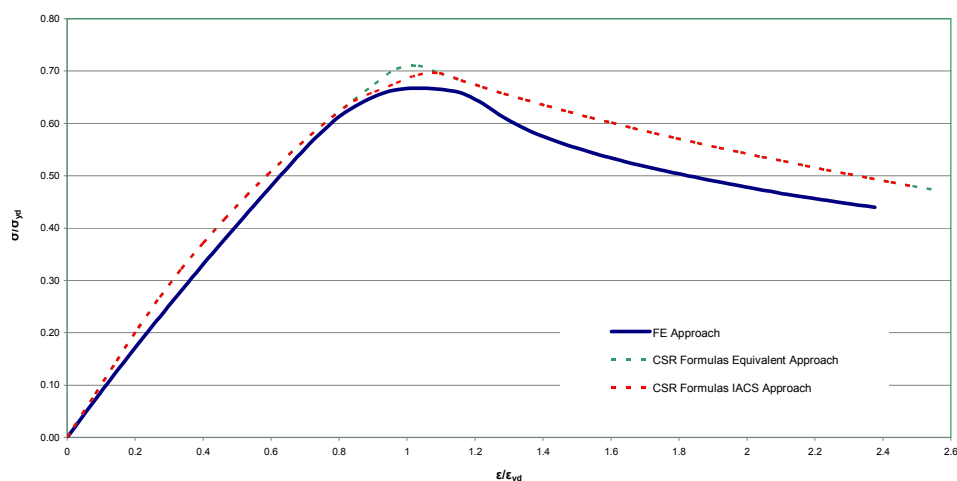


Fig.8.1. Load end Shortening Curves Comparison of Longitudinal Stiffener, I2-29



**Fig.8.2.** Load end Shortening Curves Comparison of Longitudinal Stiffener, I3-33

Both Inner Bulkhead Structural Elements, I2-29 and I3-33 are T-stiffeners. Nevertheless, the CSR Formulas approximate better the results of the FE Method in case of the latter element which, contrary to the former, has identical plate-stiffener yield stress. In both cases though, there are marked differences in the post buckling behavior. The difference in a structural element's response between CSR prediction and FE results in the case of elements with non identical plate-stiffener yield stress is also shown in below figures 8.3 and 8.4. These figures correspond to L-stiffeners.



**Fig.8.3.** Load end Shortening Curves Comparison of Longitudinal Stiffener, S4-30

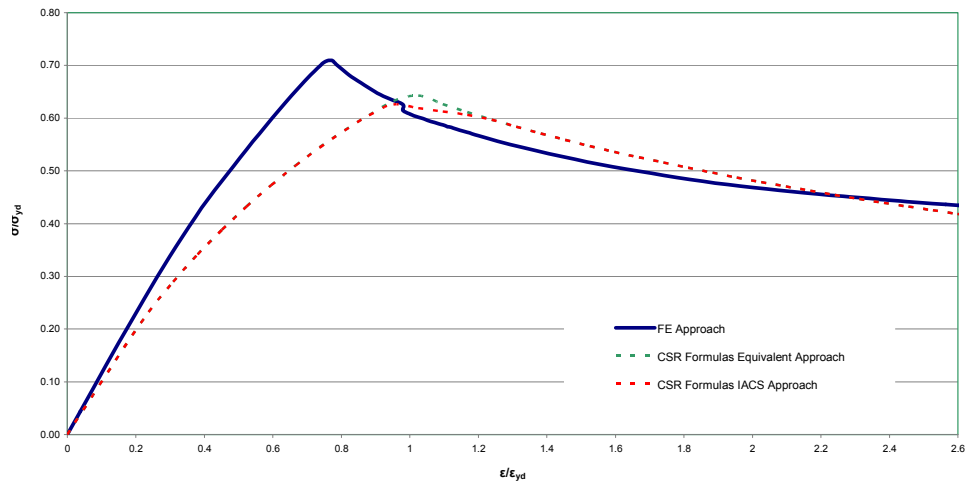


**Fig.8.4.** Load end Shortening Curves Comparison of Longitudinal Stiffener,CL2-38

The Load end shortening curves of a Main Deck structural element is shown in Figure 8.5. These are L-stiffened elements with plate-stiffener combinations with identical yield stress.

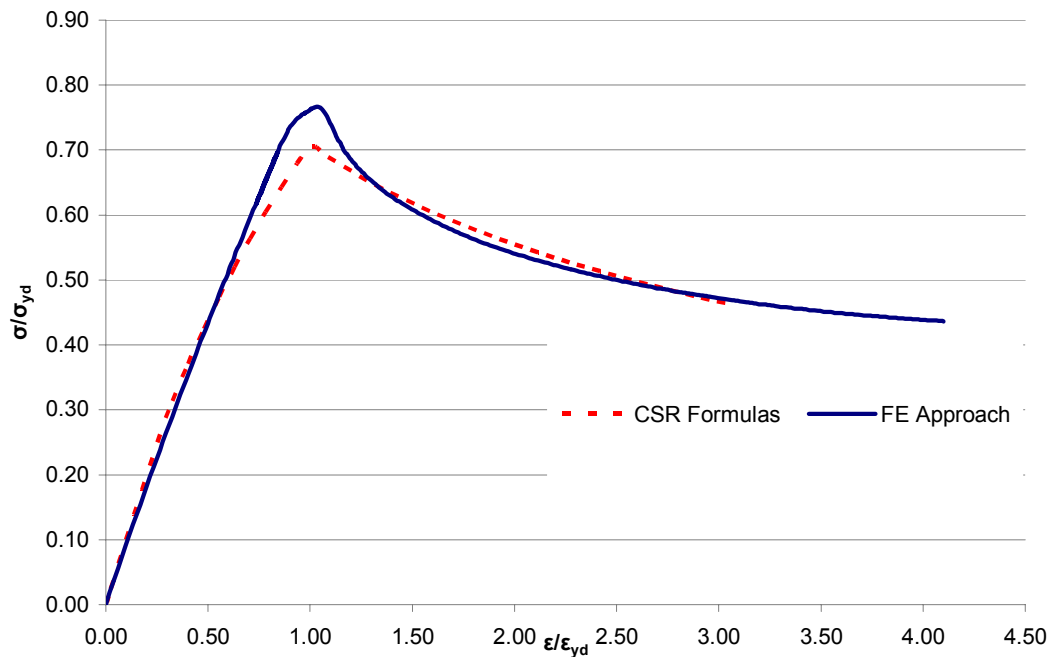


**Fig.8.5.** Load end Shortening Curves Comparison of Longitudinal Stiffener,M2-7

## 8.2.2. Longitudinal Stiffeners/Hard Corners under uniaxial tension

The CSR formulas for the behaviour of the structural elements under tension also assume elastic-perfectly plastic behaviour. The following show the stress-strain curves of three elements of the midship section constantly under tension, the bottom longitudinals B1-3, B1-4, B1-5 the side girder longitudinal SG-2 and the hard corner connecting the side shell to stringer 23. The stress-strain curves as derived by the FE Analysis are also plotted for comparison.

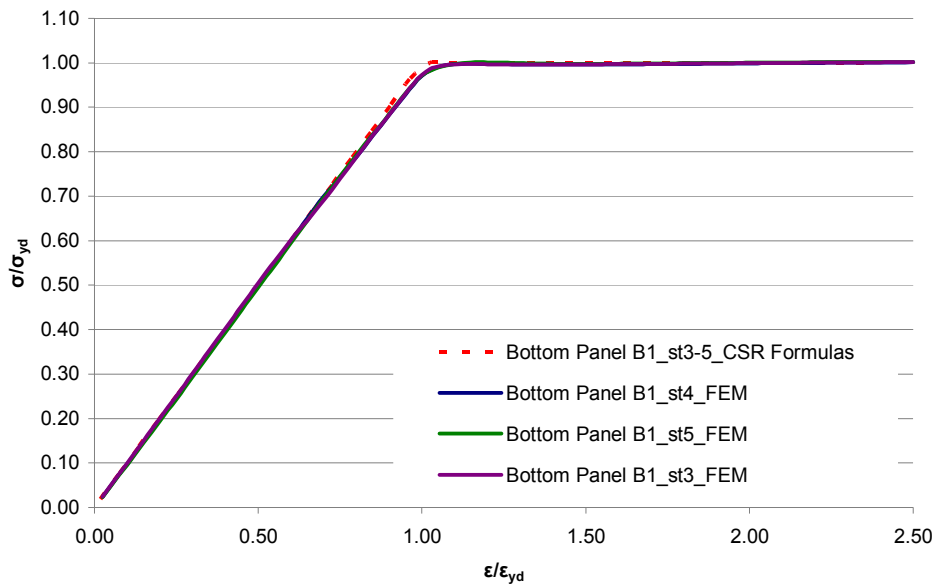


**Fig.8.6.** Bottom Longitudinals B1-3/ B1-4/ B1-5 under tension



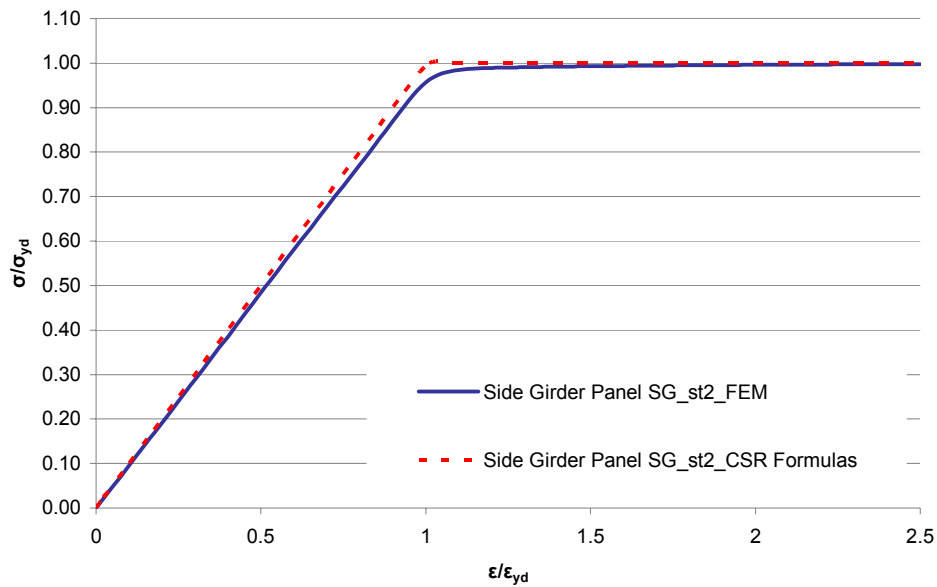


**Fig.8.7.** Side Girder Longitudinal SG-2 under tension

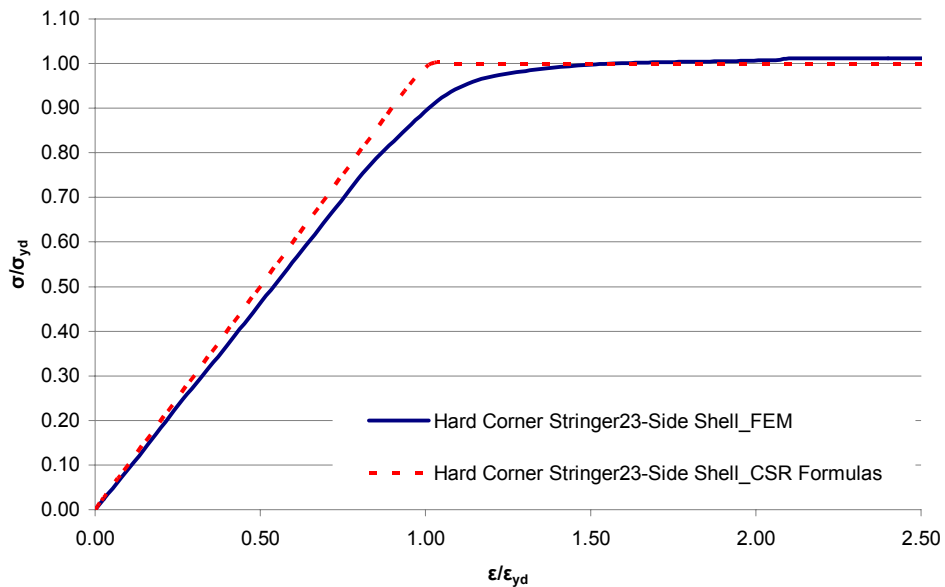


**Fig.8.8.** Hard corner connecting the side shell to stringer 23 under tension

As can be seen in the above figures, the strain-stress curves calculated by the two approaches in the case of elements under tension in general coincide. The curves obtained from the FE analysis also show an elastic-perfectly plastic behaviour, consistent with the material model specified, and a smoother transition which is attributed to the gradual spread of the plastic region in the structure.

The greatest deviation between CSR Formulas and FEA in case of elements under tension is observed for the hard corner (refer to Figure 8.8), where the element reaches the perfectly plastic yield stress value at a ratio, strain to yield strain, greater than 1.0.

### 8.2.3. Hard Corners under uniaxial compression

The CSR Formulas assume that the behavior of hard corners under compression is similar to their behavior under tension and, accordingly, an elastic-perfectly plastic stress-strain curve is obtained. Nevertheless, as shown in Figure 8.9, this is not the case as per the FE Approach. We should point out, however, that the hard corners were not modeled separately but the occurring stresses were calculated by combining the stresses acting on the corresponding adjoining panels (refer to Fig.7.21 & subsection 7.5.2).

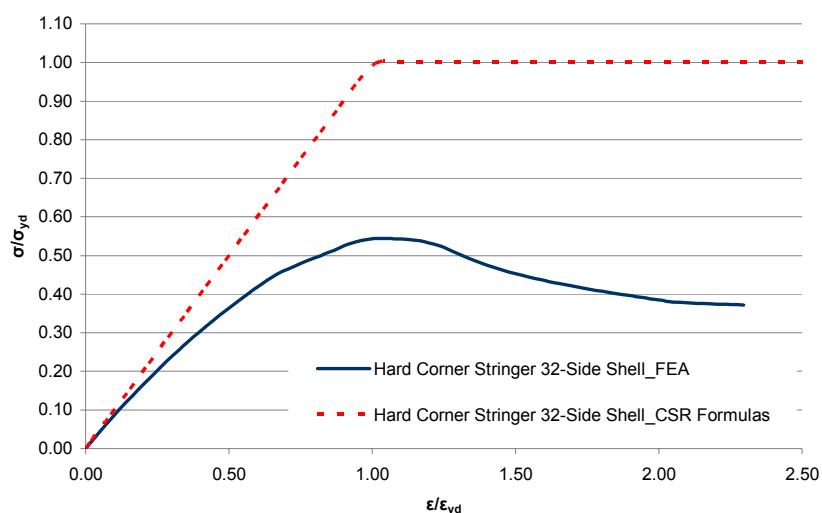


**Fig.8.9.** Hard corner connecting the main deck to CL Bulkhead under compression

Moreover, taking into account that the hard corners under compression represent only a very small part of the midship section, we can conclude that this discrepancy will have a small effect on the ultimate bending capacity, as will become evident in the following two subsections.

## 8.3. Position of Neutral Axis

At this point the predicted shift of the neutral axis as the curvature of the midship hull girder section increases will be compared. Figure 8.10 presents a plot of

the vertical position of the neutral axis, measured from the baseline, as a function of the applied curvature, as calculated by both the Incremental-Iterative and the Finite Element Approaches.

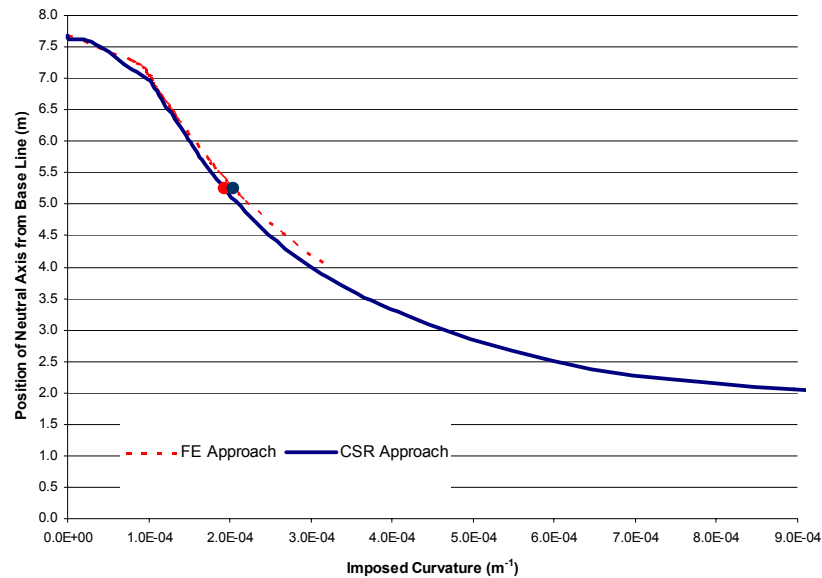


**Fig.8.10.** Position of neutral axis at each imposed curvature

The Finite Element Approach curve does not extend up to the curvature of  $9 \times 10^{-4}$ , as the Incremental-Iterative Approach, since due to the computational cost the Finite Element Analysis of most panels has been carried out for an applied displacement corresponding to a hull girder curvature of up to  $3.18 \times 10^{-4}$ . As shown in the above Figure, there is a slight difference between the two approaches in the position of the neutral axis at each imposed curvature increment, which is wider as the applied curvature increases.

At the time of the Hull Girder collapse, the neutral axis is placed at 5243 mm and 5257 mm corresponding to a curvature of  $2.05 \times 10^{-4}$  and  $1.93 \times 10^{-4}$ , according to the Finite Element and Incremental-Iterative Approaches respectively (this is shown in Figure 8.10 by the red and blue dots).

## 8.4. Vertical Bending Moment versus Imposed Curvature

The vertical bending moment versus the imposed curvature curves obtained by the two Approaches are presented in Figure 8.11. In the case of the Incremental-

Iterative Approach, all approaches mentioned in paragraph 6.2.2 for the case of plate - stiffener elements of non identical yield stress (Equivalent yield stress approach, Applicable yield stress approach and IACS approach) have been plotted for comparison reasons.

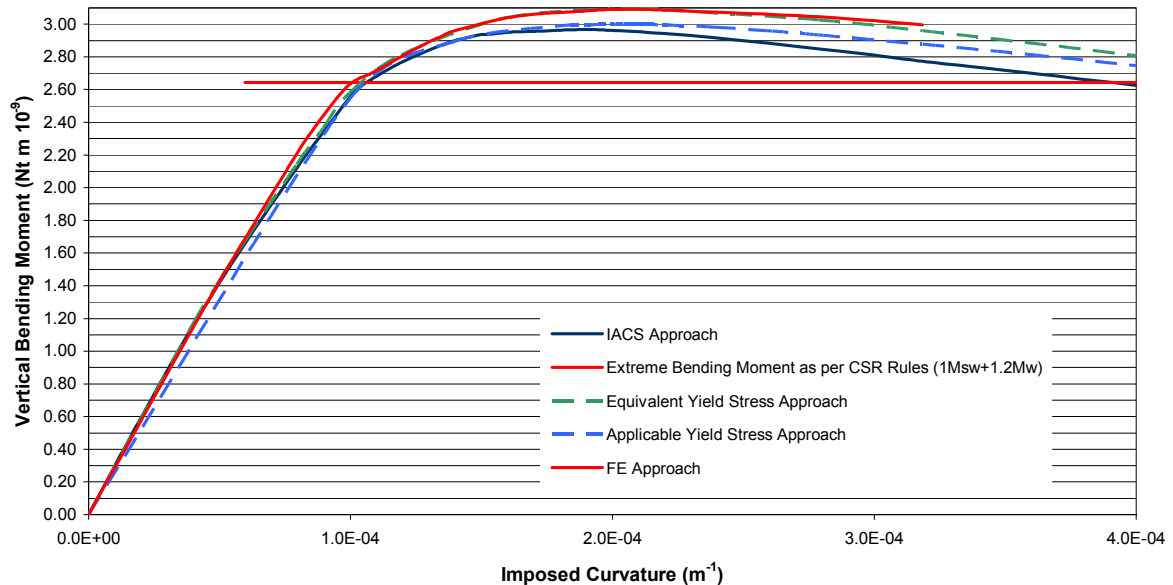


**Fig.8.11.** Comparison of M-k Curves of all applied approaches

At a first glance it is obvious that all approaches exhibit small deviations in the predicted ultimate bending capacity, as this varies within the range of **2.967-3.093×10<sup>9</sup> Nt·m**, resulting to a maximum difference of 4%.

Among the different approaches of the Incremental-Iterative Approach, applied in this study in view of the different yield stress in the plate and stiffener, the IACS Approach was found to be the most conservative. More specifically, the Applicable and Equivalent Yield Stress Approach result to a Hull Girder Ultimate Bending Capacity of **3.000×10<sup>9</sup> Nt·m** and **3.091×10<sup>9</sup> Nt·m** respectively, as opposed to the IACS Approach as per which the ultimate bending capacity is **2.967×10<sup>9</sup> Nt·m**.

As already mentioned in Chapter 6, it is somewhat surprising that the three different approaches of the Incremental-Iterative Approach lead to slight differences in the ultimate hull girder capacity, as this is in contrast to the conclusions drawn by comparing the load end shortening curves of some structural elements obtained by these approaches (refer to Figures 6.4-6.6). Nevertheless, by reviewing Table 6.1, in

which the structural elements of different yield stress in the plate and stiffener are listed, it can be concluded that for the present vessel these correspond to approximately 30% of the total hull girder section area. More importantly, the elements where the discrepancies are higher are placed in the mid depth region of the vessel and therefore the strain acting on these elements is relatively small, mostly corresponding to the linear part of the stress-strain response where the differences are smaller. In this respect, they do not affect significantly the equilibrium of the total forces acting on the girder or the resulting overall bending moments.

Surprisingly good similarity is found in the M-k Curve of the Incremental-Iterative Equivalent Yield Stress Approach and the Finite Element Approach. In fact these curves almost coincide, leading to identical Ultimate Hull Girder Capacity. In the case of the FE Approach the ultimate limit state occurs at  **$3.093 \times 10^9$  Nt·m** corresponding to a  **$2.05 \times 10^{-4} \text{ m}^{-1}$**  imposed curvature (increment 103). Identical limit state characteristics are obtained by the Incremental-Iterative Equivalent Yield Stress Approach as per which the ultimate limit state occurs at  **$3.0915 \times 10^9$  Nt·m** corresponding to a  **$2.05 \times 10^{-4} \text{ m}^{-1}$**  imposed curvature (also at increment 103). The greatest deviation of these two curves occurs at the imposed curvature range  $5.971 \times 10^{-5}$  to  $1.095 \times 10^{-4} \text{ m}^{-1}$  (Increments 30 to 55). In order to identify which structural elements contribute the most to the difference found in this range and to explain the close predictions of the ultimate limit state, the % percentage of absolute difference of the axial stresses, as computed by the FE Approach and the Equivalent-Yield Stress Approach, for the elements constantly under compression has been plotted in figure 8.12 for the increments 45 (curvature  $8.96 \times 10^{-5} \text{ m}^{-1}$ ) and 103 (curvature  $2.05 \times 10^{-4} \text{ m}^{-1}$ ).

At increment 45, as shown in Figure 8.12, the greatest difference in the axial stress computed by the two approaches is found on the Main Deck Longitudinals ( $\epsilon_{\text{Inc45}}/e_{\text{yd}}=0.82-0.87$ ), the Side Shell Longitudinals 28-33 ( $\epsilon_{\text{Inc45}}/e_{\text{yd}}=0.1-0.5$ ), the Inner Shell Longitudinals 29-31 ( $\epsilon_{\text{Inc45}}/e_{\text{yd}}=0.15-0.26$ ), and the CL Bulkhead Longitudinals 37-39 ( $\epsilon_{\text{Inc45}}/e_{\text{yd}}=0.7-0.76$ ). The percentage stress differences for these structural elements reach on average the 10-22% level at increment 45, as opposed to increment 103 where they are much lower, reaching a maximum of 6%. It should

be noted that these elements correspond to either L stiffeners or T stiffeners with non identical yield stress in the plate-stiffener combination.

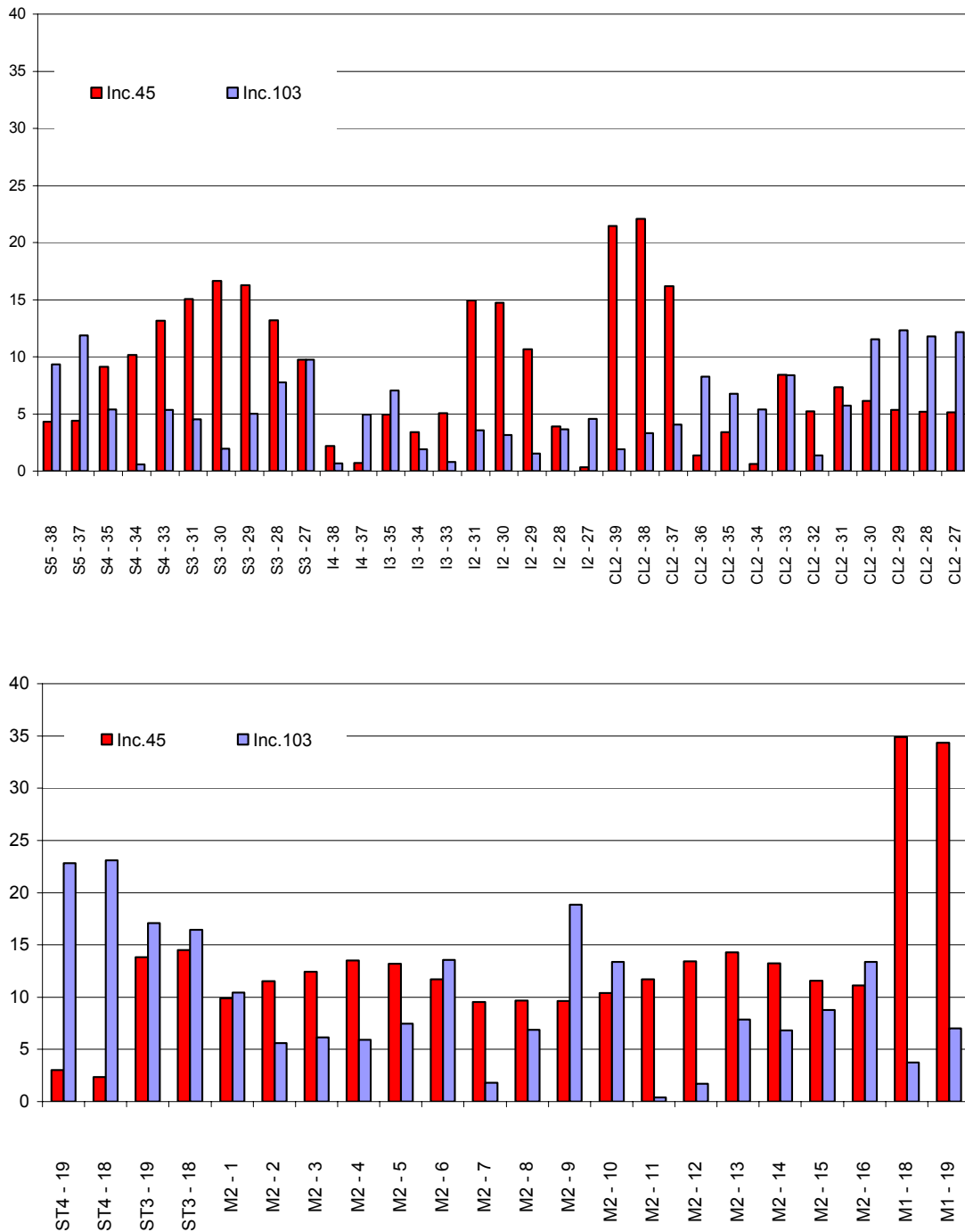


**Fig.8.12.** Percentage of absolute difference in stress response of structural elements under compression at Increment 45 and Increment 103

Let us consider a typical structural element of the Main Deck L type Longitudinals, for example M2-7. The applied strain to yield strain ratio in this element at increments 45 and 103 is  $\varepsilon/\varepsilon_{yd}=0.85$  and  $\varepsilon/\varepsilon_{yd}=2.30$  respectively. Figure 8.5 shows that increment 45 ( $\varepsilon/\varepsilon_{yd}=0.85$ ) corresponds just before the ultimate limit state of the stiffener with the two approaches exhibiting substantial differences in the response of the stiffener (refer also to Figure 8.12). Nevertheless at the time of the hull girder collapse ( $\varepsilon/\varepsilon_{yd}=2.30$ ), which corresponds to the post buckling behaviour of the element, the differences of the two approaches are small.

The same conclusion can be reached in the case of the CL Bulkhead stiffener, CL2-38. Figure 8.4 shows that the response of this stiffener as computed by the FE analysis differs substantially at increment 45 ( $\varepsilon/\varepsilon_{yd}=0.71$ ) from the CSR Formulas prediction, whereas at increment 103 ( $\varepsilon/\varepsilon_{yd}=1.95$ ), which corresponds to its post buckling behaviour, these differences are almost negligible.

Similar observations can also be made for the remaining structural elements shown in Fig. 8.12 by reviewing their stress-strain response and taking into account their applied yield to strain ratio at the time of the hull girder collapse. It should also be noted that as per Figure 8.12 the smaller differences in applied stress between the two approaches is found in case of Inner Bulkhead stiffeners, I2-33, I2-34 and I2-35 which are T-stiffeners with identical yield stress for the plate-stiffener combination. Moreover, at increment 103, in only a few elements the axial stress computed by the FE analysis differs more than 8% from the CSR prediction. Moreover this 8% deviation in the computed axial stress is counterbalanced since although in most elements the FE analysis provides less conservative results (ST4-19, ST4-18, ST3-18, ST3-19, M2-9 to M2-12, CL2-27 to CL2-31, S5-38 and S5-37), for the remaining elements more conservative results are obtained. The result is a very close ULS prediction for the hull girder bending moment

For structural elements under tension the two approaches estimate a similar stress-strain response and the differences in axial stress in most cases does not exceed 2%.

In view of the above we are drawn to the conclusion that in general the FE Method and the CSR formulas provide different stress-strain response in case of L stiffeners or T stiffeners with non identical yield stress for the plate-stiffener

combination. Nevertheless, because of their position in the midship section of the tanker used in this study, their applied strain is such that these differences affect mostly the M-k curve before the ultimate limit state is reached, that is for an imposed curvature in the range  $5.971 \times 10^{-5}$  to  $1.095 \times 10^{-4} \text{ m}^{-1}$  (refer to Figure 8.11) and less in the region of the Ultimate Limit State.

The resulting ultimate hull girder capacity of all approaches are summarised in Table 8.3. Comparison is made to the vessel's maximum bending capacity as predicted by IACS and the permissible bending capacity as referred to in vessel's loading manual in order to obtain the design and actual safety margin respectively.

	COMPARISON OF CSR TO FEM APPROACH		COMPARISON OF IACS REQUIRED CAPACITY TO ULTIMATE CAPACITY			COMPARISON OF LOADING MANUAL'S PERMISSIBLE BENDING MOMENT TO ULTIMATE CAPACITY		
	$M_{U_{CSR}}$ (Ntm * 10 <sup>9</sup> )	$M_{U_{CSR}}/M_{U_{FEA}}$	$M_{bIACS}$ (Ntm * 10 <sup>9</sup> )	$M_u/M_{bIACS}$	Design Margin (%)	$M_{perm}$ (Ntm * 10 <sup>9</sup> )	$M_u/M_{perm}$	Actual Margin (%)
IACS Approach	2.967	0.959	2.643	1.123	10.92	2.266	1.309	23.63
Equivalent Yield Stress Approach	3.091	1.000		1.170	14.51		1.364	26.70
Applicable Yield Stress Approach	3.000	0.970		1.135	11.90		1.324	24.47
Finite Element Approach	3.093	1.000		1.170	14.55		1.365	26.74

**Table 8.3.** Comparison of Hull Girder's Ultimate Limit State Characteristics of all Approaches

As shown in above table, the Ultimate Hull Girder Capacity ratio of IACS Approach to FE Approach equals to 0.96, leading to a variation of the two methods of 4%. Moreover, taking into account all approaches the design margin and actual margin varies from 11-14.5% ( $(M_u - M_{bIACS})/M_u$ ) and 24-27% ( $(M_u - M_{perm})/M_u$ ) respectively.

We should note though, that CSR Rules account for a safety margin  $\gamma_r$  in the estimation of the hull girder ultimate strength due to uncertainties (refer to Figure 3.1) equal to 1.1. Therefore the permissible bending moment, as indicated in the vessel's loading manual should be compared to the corresponding ratio  $M_u/\gamma_r$ , here estimated as  $2.967/1.1$  or  $2.697 \text{ Nt m} \times 10^9$ , since the vessel's designers must have taken this safety ratio into account. In such case the actual safety margin considered becomes 16%.



## **8.5. The Tanker Ultimate Hull Girder Capacity as per the CSR and other methods reported in the literature**

For the ultimate limit strength assessment of tankers' hull girder section, three studies [1,3,9] are available providing comparison of the resultant ultimate hull girder capacity between the CSR Incremental-Iterative approach and the employed methods, mainly ISUM (ALPS/HULL) and ANSYS/FEM. All three studies refer to a hypothetical Aframax type double hull oil tanker.

The conclusion of these studies was that the CSR Incremental-Iterative approach agrees well with the ANSYS/FEM or ALPS/HULL methods providing minor differences in the ultimate hull girder prediction under sagging. A 5% difference has been found in the resultant ultimate hull girder capacity as per CSR/Incremental-Iterative and ANSYS/FE method with the former surprisingly being less conservative. This discrepancy is in accord with the difference of 4% found here (for the IACS recommended approach), although clearly the CSR methodology is more conservative. The design safety margin as per CSR/Incremental-Iterative and ANSYS/FE method was reported in [3] to be 10% ( $M_{uCSR} - M_{bIACS} / M_{uCSR}$ ) and 5.2% ( $M_{uFE} - M_{bIACS} / M_{uFE}$ ) respectively whereas the difference between the ALPS/HULL and the ANSYS/FE method was 2.7% ( $M_{uALPS} / M_{uFE}$ ).

These studies also indicate the differences in the prediction of the various methods in the case of Hogging Condition. The safety margin in the case of Hogging condition compared to the ultimate limit state as per ANSYS/FE method was found to be 40% ( $M_{uFE} - M_{bIACS} / M_{uFE}$ ), whereas the CSR/Incremental-Iterative method was found to overestimate the ultimate hogging capacity by 15.6% ( $M_{uCSR} / M_{uFE}$ ).

## **CHAPTER 9**

### **DISCUSSION**

The International Association of Classification Societies, recognizing the fact that the ultimate limit state approach is a more rational basis for the design and strength assessment of the hull girder, has incorporated in its newly developed Common Structural Rules methods for the estimation of the Hull Girder Ultimate Bending Capacity. One of the methods adopted by IACS for the Hull Girder Ultimate Strength Assessment is the Incremental –Iterative Approach which is a multi-step method based on the estimation of the Hull Girder Bending Moment – Imposed Curvature (M-k) relationship.

This dissertation initially presented the application of the CSR-IACS Incremental – Iterative Approach to a double hull tanker and, subsequently, examined the accuracy of the estimated M-k response by introducing an alternative procedure which couples the Incremental-Iterative Approach with FE analysis. In the so called, Finite Element Approach, the stress-strain response of the individual structural elements, comprising the hull girder section, is calculated using nonlinear FE instead of the simplified design formulae proposed by CSR. The load end shortening curves, failure modes and ultimate limit states of the hull girder's stiffened panels, as calculated by both methods, have been analyzed and the resulting comparisons have been presented. Moreover, the hull girder section ultimate bending capacity computed by both approaches has been compared.

The concluding remarks for the above mentioned study are outlined in the following paragraphs:

- The CSR formulas for the estimation of structural elements' load end shortening curves assume that the plate and stiffener are of identical yield stress as well as that the thickness and yield stress of the attached plating is the same.
- In the case of the plate-stiffener combination with different yield stress two separate calculations are recommended by IACS, which are not included in the CSR Rules as discussed in subsection 6.2.2, to calculate the stress acting on the

plate and stiffener respectively. The estimated stress-strain response of each structural element has been compared here with those obtained assuming an equivalent yield stress for the whole unit (the Equivalent yield stress approach) and also using a separate yield stress for the plate and stiffener, according to the failure mode and critical stress considered (the Applicable yield stress approach)

- The effect of the above three options, concerning the yield stress definition, on the individual element's stress-strain response has been examined, Figures 6.4-6.6, and in general the IACS recommended and Equivalent yield stress approaches give closer estimates. Among these three options, the Equivalent Yield Stress Approach approximated better the FE calculated response, as determined from FE analysis of the multi-stiffener panels subjected to uniaxial compression. As shown in Table 8.2, the calculated ratio  $\sigma_{uEQIV} / \sigma_{uFEA}$  ranged from 0.89 to 1.12.
- In particular, concerning the stress-strain response of the constituent structural elements as calculated by the CSR formulas (in all three options) and the FE analysis, we should note that significant differences were observed in case of L-stiffeners (refer to Main Deck Panels, Stringer Panels, CL Bulkhead Panels) and in case of plate-stiffener combinations of non identical yield stress (refer to panels I2, S5, S4, S3, etc). On the other hand, close estimates have been found in the case of T stiffeners of identical yield stress in the attached plate and stiffener, with the ratio  $\sigma_{uIACS} / \sigma_{uFEA}$  ranging from 0.99-1.02 (e.g. refer to panel I3).
- The buckling failure modes of the structural elements under uniaxial compression as predicted by the CSR Rules are in reasonable agreement with those found in the FE analysis, although it is sometime difficult to clearly distinguish these in a simulation when one or more modes may closely interact (refer to Table 8.1). Some discrepancies were particularly observed in the case of certain elements with plate and web slenderness ratios within the range 2.62-2.76 and 1.07-1.11 respectively.
- Regarding the effect of the three yield stress options on the subsequent Incremental-Iterative Approach and the resultant Ultimate Bending Moment - Curvature Relationship of the specific vessel, it was observed that this was

small (a maximum of 4% deviation), with the IACS recommended procedure being the most conservative.

- The Incremental-Iterative Approach, with the equivalent yield stress used in conjunction with the CSR formulas, was found to give a Bending Moment - Curvature Relationship very close to that obtained through the FE Approach. In fact the ultimate limit state of the two curves is indeed very close (refer to Fig.8.10) despite differences in the stress-strain response of the individual structural elements mentioned above. Taking into account their position in the midship section of the tanker, their applied strain is such that these differences affect mostly the M-k curve before the ultimate limit state is reached.
- The design margin (ultimate hull girder strength versus IACS required bending capacity) of all approaches varies from 11-14.5%.

## **CHAPTER 10**

### **CONCLUDING REMARKS**

The Finite Element Approach, introduced in the present work as an alternative method for the calculation of the ultimate hull girder bending capacity in conjunction with the Incremental-Iterative procedure proposed in the CSR Rules, leads to a small, that is 4%, or negligible difference from that obtained with the Incremental-Iterative Approach and the CSR simplified design formula for the prediction of failure in the individual structural elements.

The above results clearly suggest that the additional effort and time involved in the application of the Finite Element Approach does not justify its use when the gain in accuracy is only 4%. Although this result is valuable in providing further verification to the CSR Rules methodology, we should note that higher differences were found in the stress-strain response and ultimate limit state of individual structural elements. Accordingly, the much closer agreement in the ultimate hull girder bending capacity is partly attributed to the "averaging" involved in the bending moment calculation, that is higher estimates in some elements were balanced by underestimates in others. Also, structural elements with marked differences in their stress-strain response were positioned at the midship section of the candidate tanker and, accordingly, had a smaller influence on the ultimate hull girder capacity.

We should also emphasize that the agreement in the predicted results can be also attributed to the fact that the two methods applied are not independent. The Finite Element Approach is based on the Incremental-Iterative procedure of the CSR Rules, and as such the assumptions and limitations of the latter are also built in the alternative method used here. Accordingly, the assumption that the structural elements/panels act independently, the simplified technique used to calculate the vertical shift in the position of the neutral axis etc, were also present in the applied Finite Element Approach.

Therefore, in order to arrive to a more accurate conclusion on this matter a nonlinear Finite element Analysis of the whole midship section should be carried out, enabling the determination of the new neutral axis at each imposed curvature and

the calculation of the corresponding bending moment. This will determine the influence of the structural modeling, the coupling of the constituent panels and the applied loading conditions on the Bending Moment-Imposed Curvature relationship and of course on the hull girder bending moment capacity. It should be emphasized here that to calculate the shift of the neutral axis and subsequently to apply the curvature with respect to its new position is difficult to combine with a nonlinear FE analysis of the whole midship section. This is because the FE nonlinear algorithm has to be interrupted at each load increment in order to calculate the new neutral axis from the acting axial stress distribution, and then to restart the solution process by imposing the next curvature increment with respect to the updated position of the neutral axis. Although it is mentioned in one or two publications in the literature [3] that the shift of the neutral axis has been taken into account in the nonlinear FE analysis of a midship section, no details of the implementation are actually given.

## REFERENCES

[1] Jang, B.S., Suh, Y.S., Paik, J.K., Seo, J.K., Kim, B.J., "Ultimate Limit State Assessment of Tankers considering Common Structural Rules", TSCF 2007 Shipbuilders Meeting, 2007.

[2] Paik, J.K., Kim, B.J., Seo, J.K., "Methods for ultimate limit state assessment of ships and ship-shaped offshore structures: Part II stiffened panels", *Ocean Engineering*, **Vol. 35:271-280**, 2008.

[3] Paik, J.K., Kim, B.J., Seo, J.K., "Methods for ultimate limit state assessment of ships and ship-shaped offshore structures: Part III hull girders", *Ocean Engineering*, **Vol. 35:281-286**, 2008.

[4] Ozguc, O, Das, P.K., Barltrop, N, "The new simple design equations for the ultimate compressive strength of imperfect stiffened plates", *Ocean Engineering*, **Vol.34: 970-986**, 2007.

[5] Ozguc, O, Das, P.K., Barltrop, N, "A comparative study on the structural integrity of single and double side skin bulk carriers under collision damage", *Marine Structures*, **Vol.18: 511-547**, 2005.

[6] Parunova, J.K., Soaresb, C.G., "Effects of Common Structural Rules on hull-girder reliability of an Aframax oil tanker", *Reliability Engineering and System Safety*, **Vol.93: 1317-1327**, 2008.

[7] Amlashi, K.K, Moan, T., "Ultimate strength analysis of a bulk carrier hull girder under alternate hold loading condition – A case study Part 1: Nonlinear finite element modelling and ultimate hull girder capacity", *Marine Structures*, **Vol:1-26**, 2008.

[8] Yao, T., "Hull girder strength", *Marine Structures*, **Vol.16: 1-13**, 2003.

[9] Paik, J.K., "Ultimate limit state performance of oil tanker structures designed by IACS common structural rules", *Thin-Walled Structures*, **Vol.45: 1022-1034**, 2007.

[10] Hughes, O.F, Ghosh, B., Chen, Y., "Improved prediction of simultaneous local and overall buckling of stiffened panels", *Thin-Walled Structures*, **Vol.42: 827-856**, 2004.

[11] Margariths, J., "Elasto-plastic behaviour of cracked stiffened panels under uniaxial compression", Dissertation, NTUA , 2007.

[12] Paik, J.K., Thayamballi, A.K., "Ultimate Limit State Design of Steel-Plated Structures", *John Wiley & Sons, Chichester, UK*, 2003.

[13] Rawson, K.J., Tupper, E.C., "Basic Ship Theory", *Butterworth-Heinemann*, Fifth Edition, 2001.

- [14] Tupper, E.C., "Introduction to Naval Architecture", *Butterworth-Heinemann*, Third Edition, 1996.
- [15] Yong B., "Marine Structural Design", *Elsevier*, First Edition, 2003.
- [16] Eyres, D.J., "Ship Construction", *Butterworth-Heinemann*, Fifth Edition, 2001.
- [17] Liu, G.R., Quek, S. S., "The Finite Element Method: A Practical Course", *Butterworth-Heinemann*, First Edition, 2003.
- [18] Bathe, K.J., "The Finite Element Procedures", *Prentice-Hall*, First Edition, 1996.
- [19] Abaqus, "Analysis User's Manual", *Simulia*, **Vol. II: Analysis**, Version 6.8.
- [20] Abaqus, "Analysis User's Manual", *Simulia*, **Vol. IV: Elements**, Version 6.8.
- [21] Abaqus, "Getting Started with ABAQUS/Standard", *Simulia*, Version 6.8.
- [22] IACS, Common Structural Rules for Double Hull Oil Tankers, International Association of Classification Societies.



# **APPENDIX A**

*(Midship Section Plan)*

